

IDENTIFICATION AND CHARACTERIZATION OF NOVEL KINASES
THAT REGULATE BRCA1 EXPRESSION AND FUNCTION

BY

Copyright 2010
Wenjia Wang
B.S., University of Kansas, 2004

Submitted to the graduate degree program in Pathology and Laboratory Medicine and the
Graduate Faculty of the University of Kansas Medical Center
in partial fulfillment of the requirements for the degree of
Doctor of Philosophy.

Committee members

Chairperson, Roy Jensen, M.D.

Patrick Fields, Ph.D.

Ossama Tawfik, M.D., Ph.D.

Charlotte Vines, Ph.D.

Jay Vivian, Ph.D.

Date defended: _____

The Dissertation Committee for Wenjia Wang certifies
that this is the approved version of the following dissertation:

IDENTIFICATION AND CHARACTERIZATION OF NOVEL KINASES
THAT REGULATE BRCA1 EXPRESSION AND FUNCTION

Committee

Chairperson, Roy Jensen, M.D.

Patrick Fields, Ph.D.

Ossama Tawfik, M.D., Ph.D.

Charlotte Vines, Ph.D.

Jay Vivian, Ph.D.

Date approved: _____

DEDICATION

To my mom, my sister Wennie, and Ken for encouraging me to never give up
as well as in remembrance of my dad who has always been an inspiration.

ACKNOWLEDGEMENTS

There are so many people I want to thank for helping me to reach this milestone in my education and in my life. I would like to start with my mentor, Dr. Roy Jensen, who has provided me an invaluable opportunity to learn and to grow, both in my understanding of what it takes to become successful in research as well as about myself. He has given me the freedom to explore different avenues and to persevere despite the setbacks. I would like to express my gratitude to Dr. Lisa Harlan-Williams, who took me under her wing and has been there every step of the way to provide words of wisdom, encouragement, and guidance. She has always been there with either an answer or a way to find the answer and has always taken the time to help me prepare for presentations and to provide feedback on anything I have written. Thank you for your friendship and support through the ups and downs, both relating to my project and everyday life. I would also like to thank Dr. Easwari Kumaraswamy for her advice and help with learning new molecular biology techniques. Additionally, the other members of our lab have made this process both enjoyable and rewarding. Many thanks to Shane Stecklein for sharing his expertise in various cell and molecular biology techniques as well as artistic skill, for all of our stimulating conversations, and especially his funny stories. Many thanks to Jeff Overton, Vamsee Chaguturu, and Laura Augustine for always taking the time to listen and to help whenever I have needed it. We have shared many laughs and lunches throughout my time in the lab. I would be remiss if I did not thank everyone in our lab for helping me prepare for my comprehensive exam by dedicating at least one hour every week to quiz me over anything related to cancer biology, especially Lisa who spent extra time to quiz me one-on-one.

I would like to also thank everyone in my comprehensive exam and dissertation committees, Drs. Patrick Fields, Linheng Li, Ossama Tawfik, Charlotte Vines, and Jay Vivian, who have offered many helpful suggestions and feedback throughout the years. I am also grateful to the MD/PhD program, especially Dr. Joseph Bast, Dr. Timothy Fields, and Janice Fletcher, as well as the Department of Pathology and Laboratory Medicine, especially Dr. Michael Soares and Mayshell-Ann Sinclair for their help and support.

I would also like to express my appreciation to Drs. Charlotte Vines, Patrick Fields, David Albertini, George Vielhauer, and Michael Soares for allowing me to use their laboratory equipment (fluorescence microscope, confocal microscope, and qRT-PCR instrument) that we did not have in our lab. Additionally, I would like to thank Dr. Joyce Slusser and the flow cytometry core for all of their help with data acquisition and analysis on the LSRII, FACSCalibur, and LSC.

Finally, I would like to express my deepest appreciation to my family. To my mom and sister, who have always been my biggest supporters and have believed in me every step of the way even when I had my doubts. In memory of my dad, who inspired me to pursue research in cancer biology. To Ken, whose constant encouragement, patience, and love have been a wonderful addition to my life.

ABSTRACT

Transcriptional and functional regulation of the breast cancer susceptibility gene 1 (*BRCA1*) in the pathogenesis of sporadic breast cancers is poorly understood. We developed a functional assay, which assesses the ability of BRCA1 to localize to sites of DNA damage and form ionizing radiation-induced foci (IRIF), to screen a kinase siRNA library and thirty-two potential positive regulators of BRCA1 were identified. Subsequent validation resulted in fourteen kinases that consistently diminished BRCA1 IRIF. Secondary screening assays for three selected kinases determined whether siRNA-mediated knockdown of the kinases caused an expression or function defect of BRCA1. Repair capacity and cell survival after DNA damage were characterized following siRNA-mediated knockdown of these three kinases. Our long term goal is to describe signaling pathways that explain how the identified kinases are able to regulate BRCA1. This knowledge could potentially translate into a novel therapeutic approach for sporadic breast cancers expressing low levels of BRCA1.

LIST OF FIGURES AND TABLES

Chapter I. INTRODUCTION

Figure 1: Schematic diagram of the <i>BRCA1</i> gene	3
Figure 2: Schematic diagram of the 1863 amino acid BRCA1 phosphoprotein.....	6
Figure 3: Schematic diagram showing sites of BRCA1 protein phosphorylation.....	9
Figure 4: Schematic of BRCA1 functions	11
Figure 5: MMTV-BRCA1 transgenic constructs.....	13
Figure 6: Tumor specific survival for MMTV-BRCA1 transgenic lines	14
Figure 7: BRCA1 in homology-directed repair of double-strand breaks	18
Figure 8: The biogenesis of miRNAs and siRNAs.....	20

Chapter II. IDENTIFY AND VALIDATE POTENTIAL REGULATORY KINASES OF BRCA1 EXPRESSION AND FUNCTION

Figure 1: Staining optimization for BRCA1 IRIF following IR.....	43
Figure 2: Effect of IR on BRCA1 IRIF formation.....	45
Figure 3: Cell cycle analysis to determine the dose of IR and time post-IR to stain for BRCA1 IRIF	49
Figure 4: Cell cycle analysis to determine the time point following serum release to expose cells to IR	51
Figure 5: Cell cycle analysis to determine the time point following serum release and exposure to IR to stain for BRCA1 IRIF	54

Figure 6: Comparison of BRCA1 IRIF formation in synchronized vs. semisynchronized MCF7 cells	56
Figure 7: Analysis to determine the effect of Neg and BRCA1 siRNAs following cell synchronization and exposure to IR on cell cycle	58
Table 1: Representative data of siRNA-mediated knockdown by chemical transfection with siPORT NeoFX.....	63
Table 2: Representative data of siRNA-mediated knockdown by chemical transfection with siPORT Amine (Ambion), XtremeGENE (Roche), and Lipofectamine 2000 (Invitrogen).....	65
Figure 8: A FAM-labeled siRNA (green) was used to monitor transfection efficiency by chemical transfection with siPORT NeoFX	67
Table 3: Representative data of siRNA-mediated knockdown following transfection by electroporation	70
Figure 9: A vector pmaxGFP (green) was used to monitor transfection efficiency following transfection by electroporation	72
Figure 10: Analysis of GAPDH mRNA levels by qRT-PCR following transfection by electroporation	74
Figure 11: Analysis of BRCA1 mRNA levels by qRT-PCR following transfection by electroporation	76
Figure 12: Representative fluorescence images of MCF7 cells following transfection by electroporation	78
Figure 13: Analysis of BRCA1 mRNA levels by qRT-PCR following chemical transfection with RNAiMAX.....	81

Figure 14: Analysis of BRCA1 protein levels by Western blot following chemical transfection with RNAiMAX.....	83
Figure 15: Analysis of BRCA1 IRIF formation by the LSC following chemical transfection with RNAiMAX.....	85
Figure 16: BRCA1 functional assay workflow and analysis of potential kinase regulators	89
Figure 17: Representative data from the kinase siRNA library screen.....	91
Figure 18: Effect of siRNA-mediated knockdown of kinases from the Ambion <i>Silencer</i> ® Kinase siRNA Library on BRCA1 IRIF formation	94
Table 4: List of 32 kinase hits identified from the kinase siRNA library.....	96
Figure 19: BRCA1 IRIF formation analysis performed in triplicate with three siRNAs targeting the indicated putative kinase regulator – set 1	99
Figure 20: BRCA1 IRIF formation analysis performed in triplicate with three siRNAs targeting the indicated putative kinase regulator – set 2	101
Figure 21: BRCA1 IRIF formation analysis performed in triplicate with three siRNAs targeting the indicated putative kinase regulator – set 3	103
Figure 22: BRCA1 IRIF formation analysis performed in triplicate with three siRNAs targeting the indicated putative kinase regulator – combined analysis.....	108

Chapter III. EVALUATE THE EFFECT OF siRNA-MEDIATED KNOCKDOWN OF LEAD KINASES ON BRCA1 mRNA LEVELS AS WELL AS ON BOTH TARGET AND BRCA1 PROTEIN LEVELS

Figure 1: Effect of siRNA-mediated knockdown of kinases on BRCA1 mRNA levels	118
Figure 2: Effect of siRNA-mediated knockdown of MAP3K1 on BRCA1 protein levels.....	121

Figure 3: Effect of siRNA-mediated knockdown of FGFR2 on BRCA1 protein levels	123
Figure 4: Effect of siRNA-mediated knockdown of HCK on BRCA1 protein levels.....	126
Figure 5: Validation of siRNA-mediated knockdown of HCK siRNAs.....	128
Chapter IV. EVALUATE THE EFFECT OF KINASE KNOCKDOWN ON THE ABILITY OF CELLS TO RESPOND TO DNA DAMAGE	
Figure 1: Schematic of the DR-GFP reporter plasmid and DSB repair mechanisms.....	137
Figure 2: Schematic of the DSB repair assay workflow.....	140
Figure 3: Efficiency of HDR in HeLa cells compared to MCF7 cells.....	141
Figure 4: HeLa cells with stably integrated DR-GFP have decreased total repair capacity following siRNA-mediated knockdown of MAP3K1	144
Figure 5: HeLa cells with stably integrated DR-GFP have decreased total repair capacity following siRNA-mediated knockdown of FGFR2.....	146
Figure 6: HeLa cells with stably integrated DR-GFP have decreased total repair capacity following siRNA-mediated knockdown of HCK	148
Figure 7: HeLa cells with stably integrated DR-GFP have normal levels of NHEJ following siRNA-mediated knockdown of MAP3K1	150
Figure 8: HeLa cells with stably integrated DR-GFP have normal levels of NHEJ following siRNA-mediated knockdown of FGFR2	152
Figure 9: HeLa cells with stably integrated DR-GFP have normal levels of NHEJ following siRNA-mediated knockdown of HCK.....	154
Figure 10: HDR is compromised in HeLa cells stably expressing DR-GFP following siRNA- mediated knockdown of MAP3K1 and expression of the I-SceI expression vector	156

Figure 11: HDR is compromised in HeLa cells stably expressing DR-GFP following siRNA-mediated knockdown of FGFR2 and expression of the I-SceI expression vector158

Figure 12: HDR is compromised in HeLa cells stably expressing DR-GFP following siRNA-mediated knockdown of HCK and expression of the I-SceI expression vector160

Figure 13: Schematic of the clonogenic assay workflow165

Figure 14: Knockdown of HCK sensitizes cells to ionizing radiation to a level similar to that of BRCA1166

Figure 15: Knockdown of either MAP3K1 does not sensitize cells to ionizing radiation168

Figure 16: Knockdown of either FGFR2 does not sensitize cells to ionizing radiation170

Chapter V. SIGNIFICANCE AND PERSPECTIVE

Figure 1: Schematic of the two isoforms of HCK176

LIST OF ABBREVIATIONS

BRCA1 – breast cancer susceptibility gene 1

DNA – deoxyribonucleic acid

RNA – ribonucleic acid

DSBs – double-strand breaks

IR – ionizing radiation

IRIF – ionizing radiation-induced foci

qRT-PCR – quantitative real-time polymerase chain reaction

siRNA – small interfering RNA

Nbr1 – neighbor of BRCA1 gene 1

NBR2 – neighbor of BRCA1 gene 2

ERE – estrogen response element

AP-1 – activator protein-1 (Jun/Fos)

IP – immunoprecipitation

PRR – positive regulatory region

POU – Pit-Oct-Unc

Rb – retinoblastoma

TGF- β 1 – transforming growth factor β 1

CREB – cAMP response element-binding

Id4 – inhibitor of DNA binding 4, dominant negative helix-loop-helix

HMGA1 – high mobility group AT-hook 1

BRCT – BRCA1 C-terminus

NLS – nuclear localization signal or sequence

ATF1 – activating transcription factor 1

ZBRK1 – zinc finger and BRCA1-interacting protein with a KRAB (Kruppel-associated box) domain 1

STAT1/3/5 – signal transducer and activator of transcription 1/3/5

HDAC – histone deacetylase

CtIP – CtBP-interacting protein

BARD1 – BRCA1 associated RING (really interesting new gene) domain 1

BRCA2 – breast cancer susceptibility gene 2

HDR – homology-directed repair

BASC – BRCA1-associated gene surveillance complex

MSH2/6 – mutS homolog 2/6 (E. coli)

MLH1 – mutL homolog 1 (E. coli)

ATM - ataxia telangiectasia mutated

BLM – Bloom syndrome, RecQ helicase-like

MRN - MRE-RAD50-NBS1

BAP1 – BRCA1 associated protein 1 (ubiquitin carboxy-terminal hydrolase)

GADD45 – growth arrest and DNA-damage inducible

UTR – untranslated region

mRNA – messenger RNA

PI3K/Akt – phosphatidylinositol 3-kinase/protein kinase B

CDK1/2/4/6 – cyclin-dependent kinase 1/2/4/6

CK1/2 – creatine kinase 1/2

NEK6 – NIMA (never in mitosis gene a)-related kinase 6

PKA – protein kinase A

GSK3 – glycogen synthase kinase 3

EGF – epidermal growth factor

ATR – ATM and Rad-3-related

SILAC – stable isotope labeling with amino acids in cell culture

MMTV – mouse mammary tumor virus

LTR – long terminal repeat

DMBA – 7,12-dimethylbenzanthracene

NHEJ – non-homologous end joining

SSBs – single-strand breaks

NER – nucleotide excision repair

NBS – Nijmegen breakage syndrome

dsDNA – double-stranded DNA

MMR – mismatch repair

BER – base excision repair

PARP – poly (ADP-ribose) polymerase

DNA-PK – DNA-dependent protein kinase

53BP1 – p53 binding protein 1

MDC1 – mediator of DNA damage checkpoint 1

Ubc13 – E2 ubiquitin conjugating enzyme

Rnf8 – ring finger protein 8

Rnf168 – ring finger protein 168

Rap80 (UIMC1) – receptor-associated protein 80 (ubiquitin interaction motif containing 1)

Abraxas (CCDC98) – (coiled-coil domain containing 98)

Brc36/45 – BRCA1/BRCA2-containing complex subunit 36/45

ssDNA – single-strand DNA

PALB2 – partner and localizer of BRCA2

BACH1 (BRIP1, FANCI) – BRCA1-associated C-terminal helicase (BRCA1-interacting protein 1, Fanconi anemia, complementation group J)

MERIT40 (NBA1) – mediator of Rap80 interactions and targeting 40 kD (new component of the BRCA1 A complex)

TOPBP1 – topoisomerase (DNA) II binding protein 1

RNAi – RNA interference

PTGS – post-transcriptional gene silencing

dsRNA – double-strand RNA

shRNAs – short hairpin RNAs

shRNA-mirs – shRNA in a microRNA context

RISC – RNA-induced silencing complex

LSC – laser scanning cytometer

FBS – fetal bovine serum

RT – room temperature

PI – propidium iodide

GAPDH – glyceraldehyde-3-phosphate dehydrogenase

OBF – optimal balance factor

β -ME – β -mercaptoethanol

UNG – uracil-N-glycosylase

cDNA – complementary DNA

BSA – bovine serum albumin

SDS-PAGE – sodium dodecyl sulfate polyacrylamide gel electrophoresis

PVDF – polyvinylidene fluoride

mAb – monoclonal antibody

pAb – polyclonal antibody

GAM-HRP – goat anti-mouse IgG, HRP-linked

ErbB2/HER2 – human epidermal growth factor receptor 2

MAP3K1 – mitogen-activated protein kinase kinase kinase 1

HCK – hemopoietic cell kinase

FGFR2 – fibroblast growth factor receptor 2

PI4KA – phosphatidylinositol 4-kinase, catalytic, alpha

PLK3 – polo-like kinase 3

EGFR – epidermal growth factor receptor

SAM – S-adenosylmethionine

PLC γ – phospholipase C gamma

MAPK – mitogen-activated protein kinase

ERK1/2 – extracellular signal-regulated kinase 1/2

JNK/SAPK – c-Jun NH₂-terminal kinase/stress-activated protein kinase

SNPs – single nucleotide polymorphisms

SH2 – Src-homology 2

SH3 – Src-homology 3

ER – estrogen receptor

PR – progesterone receptor

TABLE OF CONTENTS

TITLE PAGE.....	i
ACCEPTANCE PAGE.....	ii
DEDICATION.....	iii
ACKNOWLEDGEMENTS.....	iv
ABSTRACT.....	vi
LIST OF FIGURES AND TABLES.....	vii
LIST OF ABBREVIATIONS.....	xii
TABLE OF CONTENTS.....	xviii

Chapter I. INTRODUCTION

Breast Cancer and BRCA1	1
BRCA1: Gene, Protein and Functions	2
The <i>BRCA1</i> gene.....	2
The BRCA1 protein and its functions.....	5
BRCA1 in DNA Damage Repair	15
Use of RNAi in Functional Studies	19
Summary/Specific Aims	22

Chapter II. IDENTIFY AND VALIDATE POTENTIAL REGULATORY KINASES OF BRCA1 EXPRESSION AND FUNCTION

Introduction.....	24
Materials and Methods.....	26

Cells	26
Immunofluorescence Staining	26
Cell Cycle Analyses	29
siRNA Transfection Optimization	31
Kinase siRNA Library and Plate Description	39
Kinase siRNA Library Screen and Validation	40
Results and Discussion	41
Studies to Optimize BRCA1 Functional Assay	41
Immunofluorescence Staining	41
Cell Cycle Analyses	47
siRNA Transfection Optimization	60
Kinase siRNA Library Screen and Validation	87
Ranking of Lead Kinases	107
Conclusions	107
Chapter III. EVALUATE THE EFFECT OF siRNA-MEDIATED KNOCKDOWN OF LEAD KINASES ON BRCA1 mRNA LEVELS AS WELL AS ON BOTH TARGET AND BRCA1 PROTEIN LEVELS	
Introduction	111
Materials and Methods	111
Chemical Transfection of siRNAs with RNAiMAX	111
Isolation of Total RNA from Cells	112
Quantitative Real-Time PCR (qRT-PCR)	113
Isolation of Total Protein from Cells	115

Western Blot Analysis	115
Results and Discussion	117
Effect of siRNA-Mediated Knockdown of Lead Kinases on BRCA1 mRNA Levels	117
Effect of siRNA-Mediated Knockdown of Lead Kinases on BRCA1 and Target Protein Levels	120
Conclusions.....	125
Chapter IV. EVALUATE THE EFFECT OF KINASE KNOCKDOWN ON THE ABILITY OF CELLS TO RESPOND TO DNA DAMAGE	
Introduction.....	131
Materials and Methods.....	133
DSB Repair Assay	133
Extraction of Genomic DNA	134
I-SceI and BcgI Restriction Enzyme Digest	135
Purification of PCR Products.....	135
Clonogenic Assay	135
Results and Discussion	136
DSB Repair Assay to Assess DNA Repair Capacity.....	136
Clonogenic Assay to Assess Sensitivity to Ionizing Radiation	163
Conclusions.....	172
Chapter V. SIGNIFICANCE AND FUTURE DIRECTIONS	
Potential Role of Lead Kinase in Regulating BRCA1 Expression and Function.....	173
Significance and Future Directions.....	179

Perspective	181
REFERENCES	183
CURRICULUM VITAE.....	208

CHAPTER I

INTRODUCTION

Breast Cancer and BRCA1

Breast cancer is the most commonly diagnosed non-cutaneous cancer and the second leading cause of mortality after lung cancer in women in the United States. In 2009, the American Cancer Society estimated that 254,650 new cases of invasive and *in situ* breast cancer will be diagnosed. One of the major genes associated with an increased risk for breast cancer is the breast cancer susceptibility gene 1 (*BRCA1*). Familial breast cancers account for about ten percent of all breast cancer cases, of which about half are due to germ-line mutations in *BRCA1* (Easton et al., 1993; Miki et al., 1994). The vast majority of breast cancer cases, however, are considered sporadic and have not been linked to mutations in *BRCA1* (Xu and Solomon, 1996). Instead, 30-40% of these cases demonstrate a decreased expression of *BRCA1* (Mueller and Roskelley, 2003; Thompson et al., 1995), which translates to approximately 80,000 newly diagnosed cases in 2009. The mechanism for this decreased expression is not well-defined. There is evidence that promoter methylation (Catteau et al., 1999; Rice et al., 1998) and protein degradation (Blagosklonny et al., 1999; Choudhury et al., 2004) may play a role, but neither is sufficient to account for all breast cancer cases. Much of the current BRCA1 literature focuses on its involvement in various cellular processes including cell-cycle progression, DNA damage repair, centrosome duplication, transcriptional regulation of downstream target genes, and mammary stem cell differentiation (Liu et al., 2008; Starita and Parvin, 2003; Welch et al., 2000). These functions are based on its interactions with various molecules that have well-established functions, such as RAD51 in DNA damage repair (Scully et al., 1997c) and RNA

polymerase II in transcriptional regulation (Atalay et al., 2002; Scully et al., 1997a). Thus, the role of BRCA1 is quite ubiquitous and the potential for widespread consequences when BRCA1 is not adequately expressed is significant. This thesis outlines the studies performed in the development of a BRCA1 functional assay to identify novel kinase regulators of BRCA1 expression and function that can serve as potential candidates for drug development.

BRCA1: Gene, Protein and Functions

The *BRCA1* gene: Clusters of familial breast cancer cases suggested the possibility of heritable germ-line mutations in genes that would increase the risk for developing breast cancer and eventually led to the discovery of *BRCA1* (Weber et al., 1994). *BRCA1* was mapped to chromosome 17q21 in 1990 by Hall and colleagues (Hall et al., 1990) from genetic linkage analysis of breast cancer families and then cloned in 1994 by Miki and colleagues (Miki et al., 1994). The human *BRCA1* gene can be transcribed from two alternative promoters, α or β (**Figure 1**). The α promoter is the minimal bidirectional promoter that is situated head-to-head with Nbr1 (neighbor of BRCA1 gene 1) in the mouse or NBR2 in the human and has shown a quasi-reciprocal expression pattern (Dimitrov et al., 2001). The β promoter is unique to humans and contains the estrogen response element (ERE) (Xu et al., 1995; Xu et al., 1997). It may be possible that estrogen plays a role in *BRCA1* expression because ER α can either bind the AP-1 domain in the α *BRCA1* promoter or the ERE in the β *BRCA1* promoter (Jeffy et al., 2005). Based on sequence analysis, immunoprecipitation (IP), and other approaches, additional cis-elements have been proposed within the minimal bidirectional promoter that regulate *BRCA1* expression. For example, the GA-binding protein α/β , a member of the ETS family of transcription factors, binds to three tandem ETS factor-binding domains, or RIBS element, of the

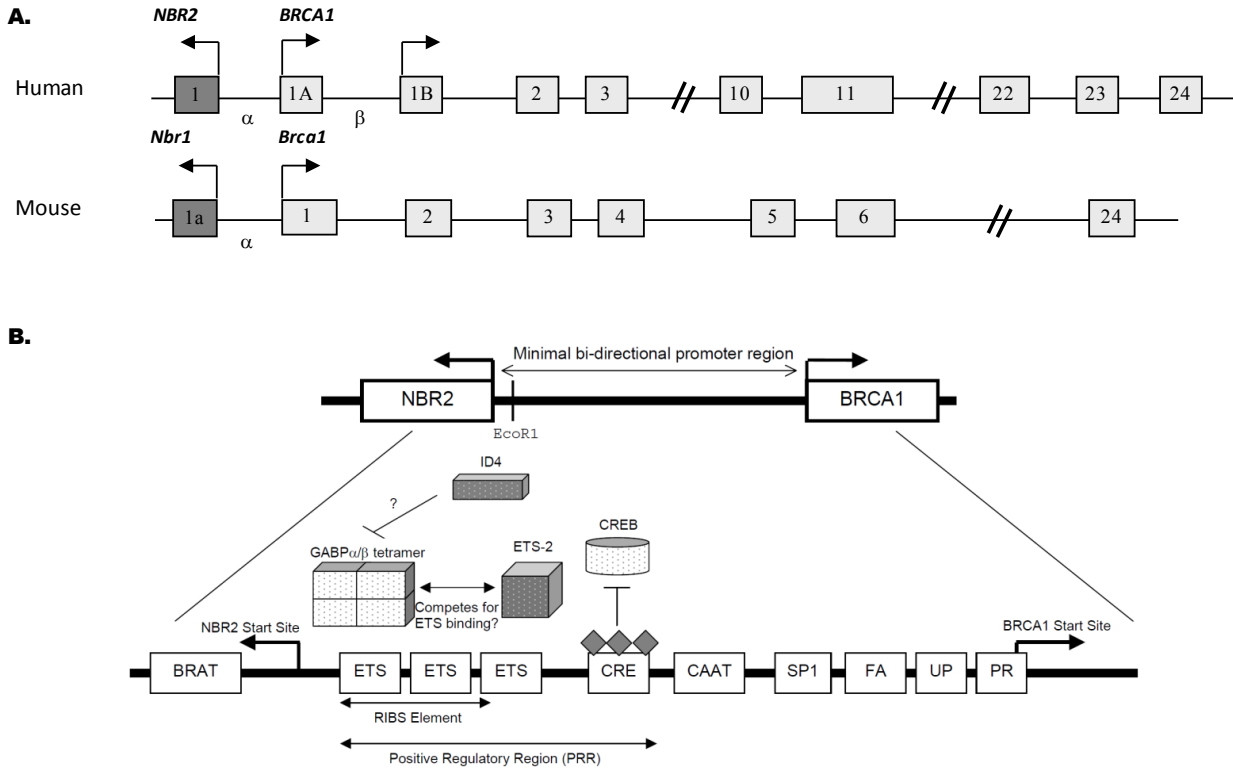


Figure 1: Schematic diagram of the *BRCA1* gene. Panel A shows a comparative map of human *BRCA1* and mouse *Brca1*. *BRCA1* is an 81-kb tumor suppressor gene located on chromosome 17q21 that encodes a 7.8 kb transcript with 24 exons. Human *BRCA1* contains two alternative promoters, α and β . Panel B depicts the human α promoter of *BRCA1* and characterized functional sites that regulate *BRCA1* expression. The α promoter is the minimal bidirectional promoter that is situated head-to-head with *NBR2* and contains tissue-specific transcriptional activity (McCoy et al., 2003).

positive regulatory region (PRR) and induces transcription of *BRCA1* (Atlas et al., 2000). Alternatively, ETS-2, another member of the ETS family of transcription factors, which also binds the RIBS element, represses *BRCA1* transcription (Baker et al., 2003). A member of the POU (Pit-Oct-Unc) family of transcription factors, Brn-3b, has also been shown to repress *BRCA1* expression (Budhram-Mahadeo et al., 1999). *BRCA1* expression has also been shown to be positively regulated by E2F1 at a conserved site while being repressed by Rb-E2F complexes (Wang et al., 2000a), E2F6 (Oberley et al., 2003), and p53 (Arizti et al., 2000). Rb has also been shown to be activated by TGF- β 1 to repress *BRCA1* expression (Satterwhite et al., 2000). Additionally, a potential CREB site was identified, which leads to constitutive *BRCA1* promoter expression that can be affected by CpG methylation (Atlas et al., 2001; Mancini et al., 1998). There is also Id4, a member of the helix-loop-helix family of transcription factors, that acts as a negative regulator of *BRCA1* expression (Beger et al., 2001). Regulatory elements have also been identified in the non-coding regions of the gene that can modulate expression (Suen and Goss, 2001; Wardrop and Brown, 2005). Structural genes such as HMGA1 have also been shown to negatively regulate *BRCA1* expression (Baldassarre et al., 2003). The 81-kb *BRCA1* encodes a 7.8 kb transcript that subsequently undergoes alternative splicing to produce the full-length BRCA1 or other splice variants (Miki et al., 1994). At least 12 distinct BRCA1 splice variants have been identified, of which 11 maintain the original open reading frame (Orban and Olah, 2003). However, only the full length, the $\Delta(9,10)$, the $\Delta(11q)$, and the $\Delta(9,10,11q)$ variants are believed to be predominantly expressed in various tissues. A variant lacking most of exon 11 localized BRCA1 to the cytoplasm, which identified two nuclear localization sequences (NLS1 and NLS2) (Lu et al., 1996; Thakur et al., 1997). Cells transfected with the $\Delta(11q)$ variant showed increased levels of apoptosis (Shao et al., 1996). BRCA1 splice variants have been

shown to exhibit both overlapping and distinct functions, including cell cycle regulation and transcriptional transactivation (McEachern et al., 2003; Wang et al., 1997). Therefore, epigenetics, long-range DNA associations, alternative promoters, cis- and trans-elements, and splice variants are just some of the ways *BRCA1* expression has been found to be regulated.

The BRCA1 protein and its functions: The predominant protein product is an 1863 amino acid phosphoprotein that contains several important functional domains (**Figure 2**), including a RING domain at the N-terminus, Exon 11, and two tandem BRCT domains at the C-terminus (Miki et al., 1994). Exon 11 is the largest exon in *BRCA1* and is known to contain two nuclear localization signals (NLS), which are required along with the N-terminus RING domain of *BRCA1* for nuclear localization of *BRCA1* (Fabbro et al., 2002). Each of these regions is involved in protein-protein interactions that are important for the various functions of *BRCA1* (**Figure 2**). For example, *BRCA1* has been shown to interact with ATF1 (transcription factor) at the RING domain (Houvras et al., 2000); ZBRK1 (transcription factor) (Zheng et al., 2000), STAT1 (transcriptional activation) (Ouchi et al., 2000), and SWI/SNF (chromatin remodeling complex) (Bochar et al., 2000) at Exon 11; RNA polymerase II (transcription) (Scully et al., 1997a) via RNA helicase A (Anderson et al., 1998), HDAC 1 and 2 (histone deacetylation) (Yarden and Brody, 1999), and CtIP (transcriptional co-repressor) (Yu et al., 1998) at the BRCT domain; c-Myc (transcription factor) at the N-terminus and exon 11 (Wang et al., 1998); CBP/p300 (transcriptional co-activator) at the RING and BRCT domains (Pao et al., 2000); and p53 (transcription factor) with Exon 11 and BRCT domain (Chai et al., 1999), all of which affect the function of *BRCA1* in transcriptional regulation of downstream targets. *BRCA1* has also been shown to interact with BARD1 (ubiquitylation) at the RING domain that confers the

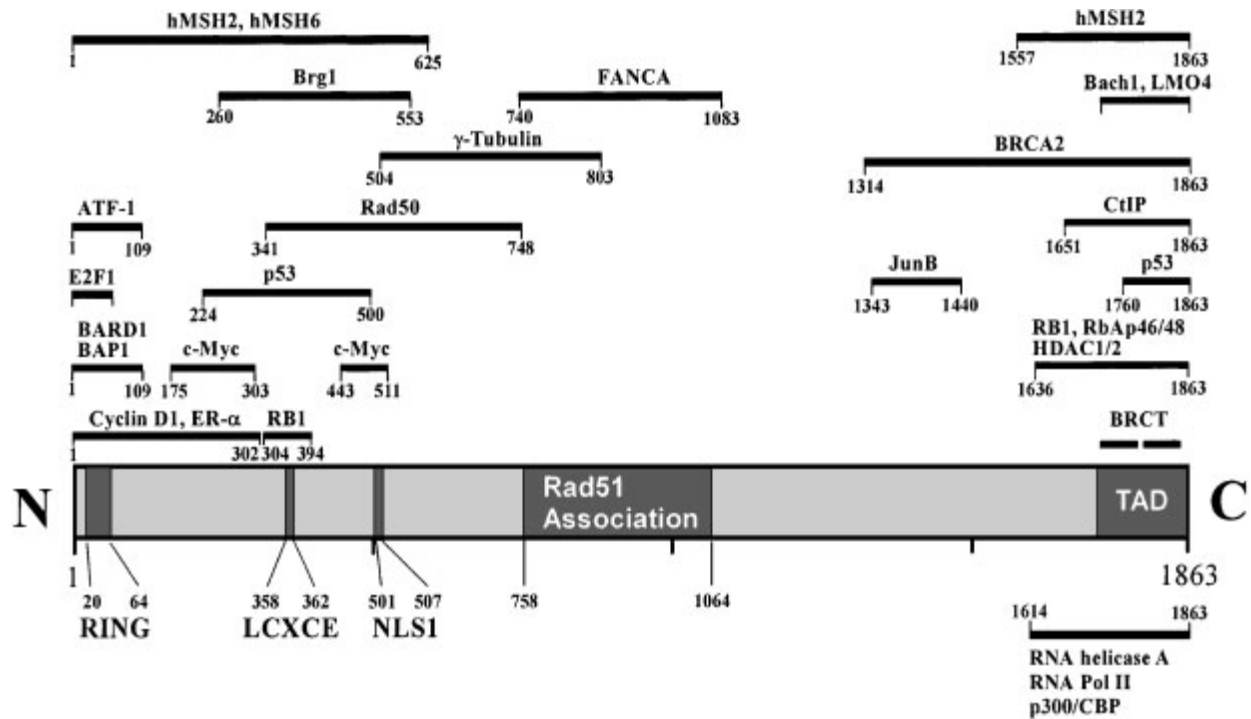


Figure 2: Schematic diagram of the 1863 amino acid BRCA1 phosphoprotein. The BRCA1 protein is characterized by several important functional domains, including a RING domain near the amino-terminus, two tandem copies of the BRCT motif at the carboxy-terminus, and two nuclear localization signals (NLS1 and NLS2) within exon 11. BRCA1 functions have been identified via protein-protein interactions with other proteins at these domains (Rosen et al., 2003).

function of BRCA1 as an E3 ubiquitin ligase (Baer and Ludwig, 2002; Polanowska et al., 2006; Wu et al., 1996). The interactions of BRCA1 with RAD51 (DSB repair) (Scully et al., 1997c) and RAD50 (DSB repair) (Zhong et al., 1999) at Exon 11, with BRCA2 (DSB repair) (Zhong et al., 1999) at its BRCT domain of BRCA1, and with H2AX (signals DNA damage) (Paull et al., 2000) are important for the role of BRCA1 to function in DNA damage repair. Association of BRCA1 with Rad51 was the first evidence for a role of BRCA1 in homology-directed repair (HDR). BRCA1 can form a complex called BASC (BRCA1-associated gene surveillance complex), which is a collection of proteins that serves as a DNA damage sensor and includes tumor suppressors and DNA repair proteins MSH2, MSH6, MLH1, ATM, BLM, and the MRN protein complex (Wang et al., 2000b). BRCA1 can also form a complex with the centrosome to affect chromosome segregation (Hsu and White, 1998). Other protein-protein interactions that contribute to BRCA1 function are BAP1 (deubiquitylation) with the RING domain of BRCA1 (Jensen et al., 1998) and pRB (cell cycle regulator) with Exon 11 and BRCT domain (Aprelikova et al., 1999) in cell growth; and GADD45 in apoptosis (Harkin et al., 1999). Thus, in cases of sporadic breast cancer with decreased expression of BRCA1, the consequences could be far-reaching.

The 3' and 5' UTRs have been shown to regulate BRCA1 mRNA stability and translation efficiency, respectively (Saunus et al., 2007; Signori et al., 2001). In addition, heregulin β 1-induced activation of PI3K/Akt increases nuclear localization of BRCA1 to enable its various functions (Hinton et al., 2007). It has been suggested that a defect in nuclear import of BRCA1 may play a role in tumorigenesis (Chen et al., 1996a; Fabbro et al., 2002). BRCA1 protein can be regulated by phosphorylation, sumoylation, ubiquitylation and proteasomal degradation, and glycosylation (Blagosklonny et al., 1999; Choudhury et al., 2004; Cortez et al., 1999; Galanty et

al., 2009; Jensen et al., 1996; Morris et al., 2009). BRCA1 expression is also regulated in a cell cycle-dependent manner (Chen et al., 1996b; Gudas et al., 1996). It is low during G₀ and G₁ phases, increases as cells enter the S phase and progress through the G₂ and M phases before falling to low levels again. This regulation may be due to the E2F binding sites within the promoter region of BRCA1 that can mediate transcriptional activation by E2F1 and repression by Rb (Vaughn et al., 1996; Wang et al., 2000a). BRCA1 is stabilized as cells enter mitosis by heterodimeric interaction with BARD1 (Baer and Ludwig, 2002; Polanowska et al., 2006; Wu et al., 1996). After mitosis, BRCA1 is ubiquitinated and degraded by the proteasome (Choudhury et al., 2004). This change in expression of BRCA1 is also accompanied by hyperphosphorylation of BRCA1 as cells enter the S phase in response to DNA replication blocks (Thomas et al., 1997). Furthermore, phosphorylation of BRCA1 by kinases is a critical step in directing its various functions. Several kinases have been identified that phosphorylate BRCA1 to direct its various functions (**Figure 3**). Phosphorylation at S308 by Aurora-A is involved in the regulation of G₂ to M transition (Ouchi et al., 2004). Phosphorylation at T509 by Akt1 is involved in nuclear localization and transcriptional activity of BRCA1 (Hinton et al., 2007). Phosphorylation of S632 by CDK4 inhibits the ability of BRCA1 to be recruited to particular promoters (Kehn et al., 2007). Phosphorylation of S988 by Chk2 regulates DNA double-strand break repair (Zhang et al., 2004) and subcellular localization (Okada and Ouchi, 2003). Phosphorylation of S1143 and S1280 target BRCA1 to nuclear foci following alkylative DNA damage (Au and Henderson, 2007). Phosphorylation at multiple residues including S1189, S1423, S1457, S1497, S1524 by ATM regulates the DNA damage response to double-strand breaks (Cortez et al., 1999). Phosphorylation of S1423 by ATM is important for the G₂/M checkpoint (Xu et al., 2001). Phosphorylation of S1211, S1218, S1336 by CK2; of S1212 by NEK6; of S1497 by PKA,

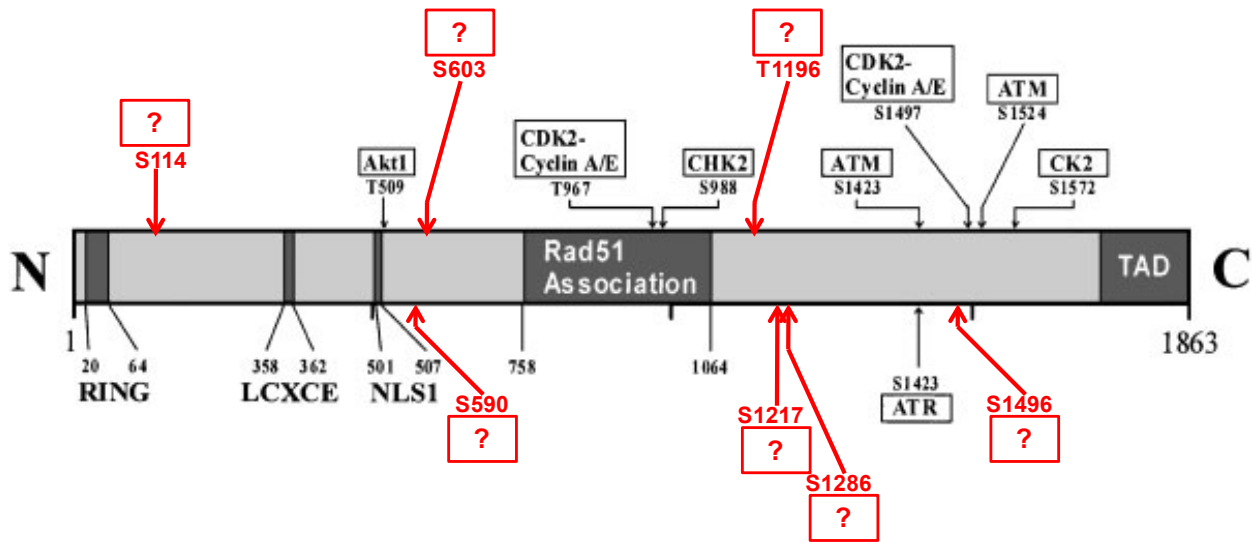


Figure 3: Schematic diagram showing sites of BRCA1 protein phosphorylation. BRCA1 functions depend on both expression and phosphorylation. Known kinases and their corresponding phosphorylation sites are depicted in black while orphan phosphorylation sites are depicted in red (adapted from Rosen et al., 2003).

CDK2, and CDK1; of S1499 by CK1 and GSK3; and of S1217 and S1496 following epidermal growth factor (EGF) stimulation have also been studied (Olsen et al., 2006; Ruffner et al., 1999). Phosphorylation of S1239, S1245, S1330, S1336, S1342, S1466, T1720 by ATM/ATR were identified following a proteomic analysis using antibodies to phospho-SQ or phospho-TQ sites combined with peptide IP and SILAC (stable isotope labeling with amino acids in cell culture) (Matsuoka et al., 2007). Phosphorylation of S1387 by ATM regulates S-phase checkpoint after ionizing radiation (Xu et al., 2002). Large-scale proteomic studies have been used to identify various phosphorylation sites of BRCA1 following a stimulus, such as exposure to ionizing radiation or stimulation with EGF (Matsuoka et al., 2007; Olsen et al., 2006). However, many of these identified phosphorylation sites have no known associated kinase(s), including S114, S590, S603, T1196, Y1202, S1217, S1286, and S1496 (Blom et al., 1999). New signaling pathways involving BRCA1 may be evaluated by identifying the kinases that phosphorylate these putative sites.

A variety of approaches have been used to understand the role of BRCA1 in genetic instability and tumorigenesis. These approaches include antisense RNA to selectively reduce BRCA1 mRNA levels (Rao et al., 1996; Thompson et al., 1995) and using BRCA1-defective cell lines, such as HCC1937, which has no functional BRCA1 due to a frameshift mutation (inserted C at nucleotide 5382) that leads to a truncated protein (Abbott et al., 1999; Tomlinson et al., 1998), Cre-loxP to selectively disrupt BRCA1 in mammary epithelium (Xu et al., 1999), and transgenic mice to overexpress wild-type BRCA1 (Hoshino et al., 2007). Through these studies, it has been determined that loss of BRCA1 results in defective DNA damage repair, attenuated cell cycle checkpoints, abnormal centrosome duplication, impaired growth arrest and apoptosis, resulting in genetic instability and tumor formation (Deng and Scott, 2000) (**Figure 4**). The

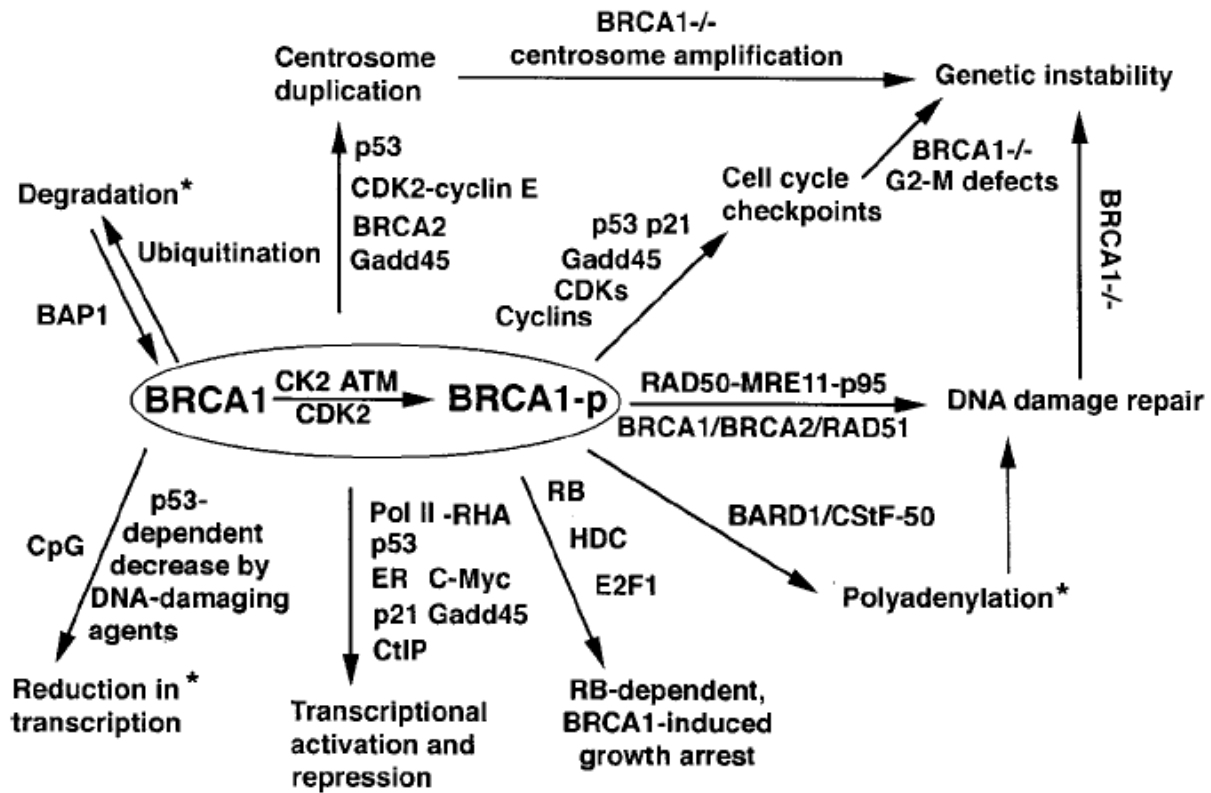


Figure 4: Schematic of BRCA1 functions. BRCA1 has a variety of critical functions, including DNA damage repair, cell cycle checkpoint control, and transcriptional regulation of downstream target genes, that are dependent on both expression and phosphorylation of BRCA1 (Deng and Brodie, 2000).

induction of BRCA1 synthesis that occurs near the G1/S boundary (Chen et al., 1996b), the association of BRCA1 with RNA polymerase II (Scully et al., 1997a), and the subsequent localization with repair proteins following DNA damage (Paull et al., 2000; Polanowska et al., 2006; Wang et al., 2000b; Wu et al., 1996; Zhong et al., 1999) suggest a major role of BRCA1 in genome surveillance. As the cell replicates its DNA in S phase, phosphorylated BRCA1 can be recruited to areas of replication error. The same occurs when DNA is damaged via other mechanisms, such as ionizing radiation (IR) (Thomas et al., 1997). Additionally, our lab developed transgenic mice to overexpress wild-type human BRCA1 and BRCA1 mutant (BRCA1sv (70 amino acid N-terminal deletion) and BRCA1t340 (BRCA1 C-terminal truncation)) proteins, under the control of the mouse mammary tumor virus (MMTV) LTR promoter (**Figure 5**). Differential survival curves or Kaplan-Meier plots were established after challenging the transgenic mice and nontransgenic control to the carcinogen 7,12-dimethylbenzanthracene (DMBA). Wild-type human BRCA1 (blue curve) has a protective effect against tumor development or death as seen by the delayed onset compared to the nontransgenic (purple curve) while the BRCA1sv mutants (green curve) exhibit a more rapid onset of tumor development and accelerated mortality (**Figure 6**). The BRCA1t340 (yellow curve) had no effect on mammary tumor incidence or survival compared to the nontransgenic. Therefore, the BRCA1 construct lacking the N-terminus predisposed the mammary gland to tumor development while wild-type BRCA1 protected the mammary gland from tumor development. These observations are specific to mammary tumors since there is no difference in survival when looking at other tumor types (Hoshino et al., 2007). These methods have proven effective in identifying the functional importance of BRCA1; however, they fail to explain how BRCA1 expression is regulated.

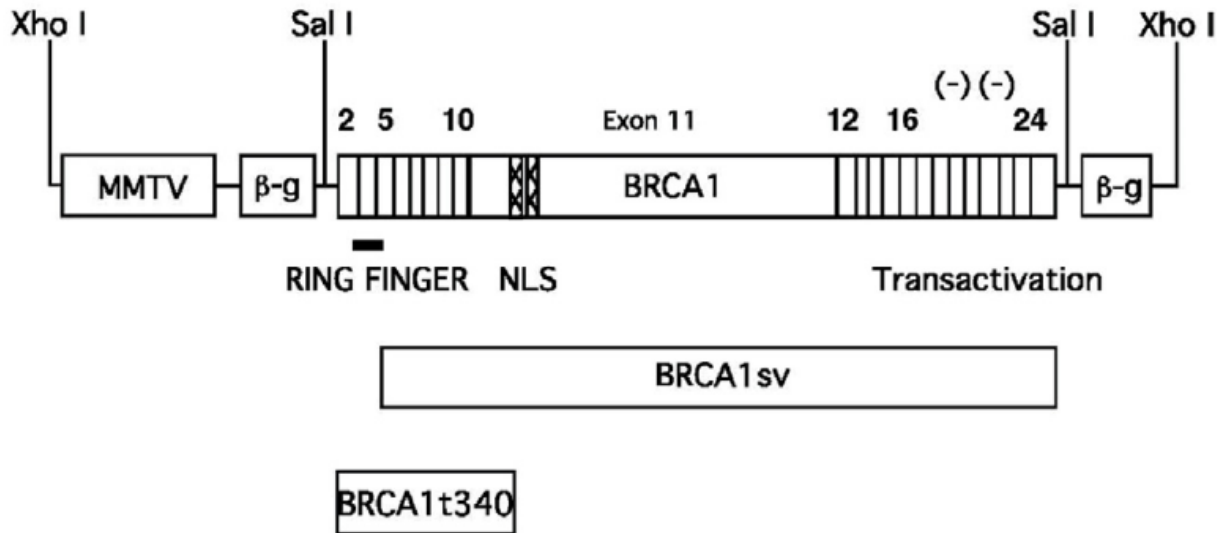


Figure 5: MMTV-BRCA1 transgenic constructs. Schematic of the wild type human BRCA1, BRCA1sv (70 amino acid N-terminus deletion), and BRCA1 t340 (BRCA1 C-terminal truncation) cDNAs used to generate transgenic mice to overexpress the respective proteins under the control of the mouse mammary tumor virus (MMTV)-LTR promoter. The bar indicates the N-terminal RING domain, the hatched region corresponds to the nuclear localization signals, and the (-) designates the negatively charged BRCT domains (Hoshino et al., 2007).

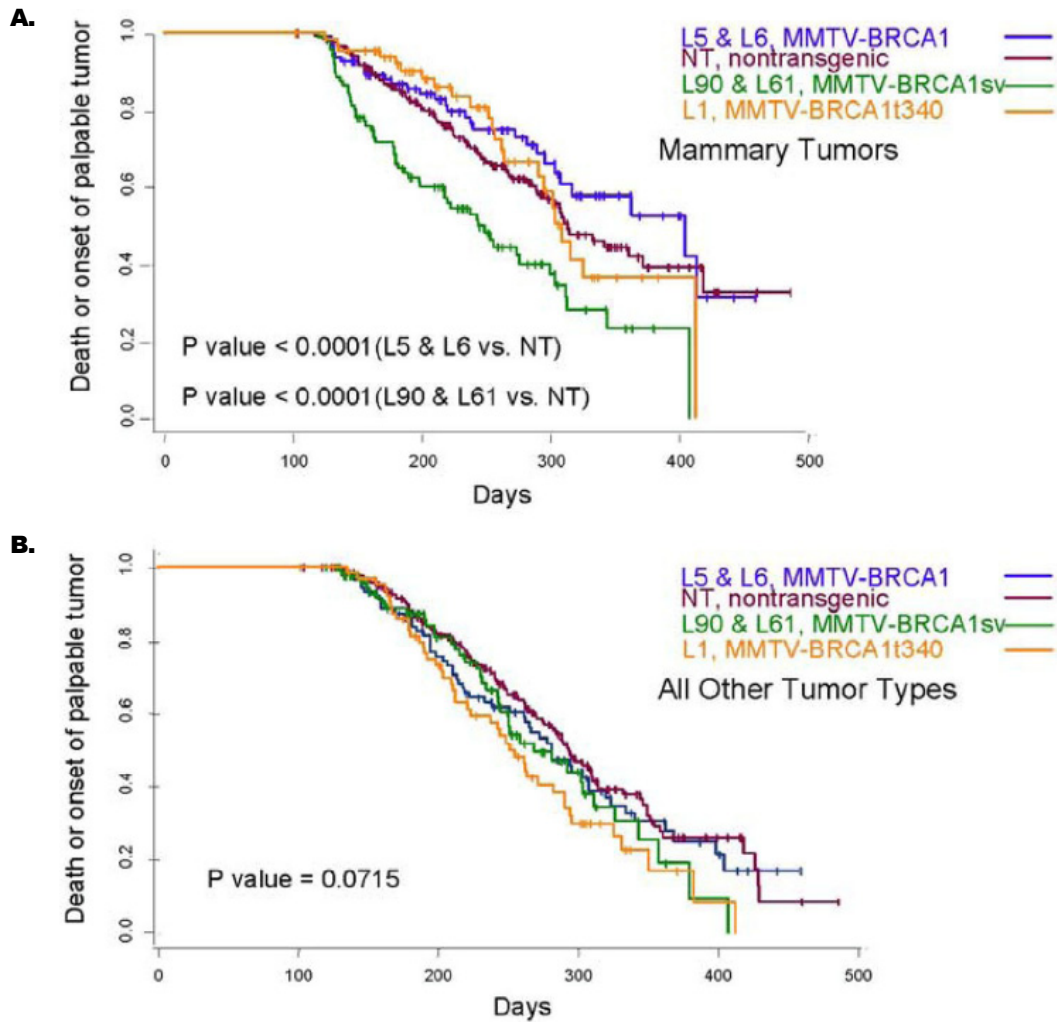


Figure 6: Tumor specific survival for MMTV-BRCA1 transgenic lines. Panel A shows a Kaplan-Meier curve plotting tumor-free survival from mammary tumors for mice treated with the carcinogen 7,12-dimethylbenzanthracene (DMBA). Panel B depicts a Kaplan-Meier curve plotting tumor-free survival from all other tumor types for mice treated with DMBA. L5 & L6 = MMTV-BRCA1 mice (n=95), NT = nontransgenic mice (n=205), L90 & L61 = MMTV-BRCA1sv mice (n=97), L1 = MMTV-BRCA1t340 female (line 2 F58) (Hoshino et al., 2007).

BRCA1 in DNA Damage Repair

BRCA1 is involved in DNA repair by homology-directed repair (HDR) and non-homologous end joining (NHEJ) (Snouwaert et al., 1999; Zhong et al., 2002). These repair pathways encompass a network of proteins that act as sensors, mediators, and effectors to recognize and repair DNA damage as well as to activate cell cycle checkpoints (Iliakis et al., 2003; Yarden et al., 2002; Zhou and Elledge, 2000). This ensures that a cell with DNA damage such as single-strand breaks (SSBs) and double-strand breaks (DSBs) does not undergo division until it can be repaired. If the damage cannot be repaired, the cell undergoes apoptosis, or programmed cell death, to ensure the integrity of the DNA. Intact DNA damage repair systems are critical to maintain genomic stability and prevent tumorigenesis, as demonstrated by studies of patients with inherited defects in DNA-repair genes, such as xeroderma pigmentosum (defect in nucleotide excision repair (NER)), Nijmegen breakage syndrome (defect in *NBS* and processing of double-stranded DNA (dsDNA) breaks), ataxia telangiectasia (defect in *ATM* and HDR of dsDNA breaks), and familial breast and ovarian cancers (defect in *BRCA1* or *BRCA2* and HDR of dsDNA breaks) (Thompson and Schild, 2002). DNA damage can result from endogenous biochemical processes (e.g., depurination, deamination, oxidation) and exogenous carcinogens (e.g., radiation, alkylating agents, heterocyclic amines). Cells employ a variety of mechanisms to repair DNA damage, including mismatch repair (MMR) enzymes that recognize normal but misincorporated nucleotides and other enzymes that detoxify (e.g., glutathione-S-transferase) or remove DNA adducts (e.g., O⁶-methylguanine DNA methyltransferase). Additionally, base excision repair (BER) recognizes chemically altered bases caused by endogenous sources, NER recognizes helix-distorting adducts from exogenous sources, HDR of dsDNA breaks utilizes the undamaged, homologous DNA sequence to direct repair, and the

more error-prone NHEJ results in fusion of two dsDNA ends (van Gent et al., 2001). One anti-cancer treatment approach takes advantage of the failure of DNA damage repair. Poly (ADP-ribose) polymerase (PARP) is an enzyme that participates in BER, a mechanism that cancer cells with mutations in *BRCA1* or *BRCA2* depend on to repair their DNA damage. These cancer cells become hypersensitive to chemotherapy and radiation when PARP inhibitors are given to prevent repair by this mechanism as well (Martin et al., 2008).

Ionizing radiation (IR) results in DSBs, which are believed to be the most severe type of DNA damage that can be repaired by high-fidelity homologous recombination (Khanna and Jackson, 2001). BASC and DNA-PK serve as sensors for DNA damage by phosphorylating the histone variant H2AX (γ -H2AX) on S139, an early step in the response to DSBs (Paull et al., 2000; Stiff et al., 2004; Wang et al., 2000b). 53BP1 and MDC1 are then recruited to γ -H2AX to further activate ATM, which phosphorylates a variety of downstream targets, including BRCA1 (Cao et al., 2009; Lou et al., 2003; Stucki et al., 2005; Wang et al., 2002). Additionally, the Ubc13/Rnf8 and Rnf168 ubiquitin ligases polyubiquitylate γ -H2AX to recruit the Rap80/Abraxas/Brcal/Brc36 complex (Chen et al., 2006; Kim et al., 2007a; Kim et al., 2007b; Liu et al., 2007; Shao et al., 2009a; Sobhian et al., 2007; Wang and Elledge, 2007; Wang et al., 2007; Yan et al., 2007). A BRCA1/CtIP/MRN interaction then enables conversion of DSBs to single-strand DNA (ssDNA), which allows strand invasion via Rad51 into the homologous chromosome (Baumann et al., 1996; Chen et al., 2008; Gravel et al., 2008; Nimonkar et al., 2008; Zhong et al., 1999). Rad51 is recruited via its interaction with BRCA2, which associates with BRCA1 via PALB2 and functions in the Fanconi anemia pathway (Nakanishi et al., 2005; Sy et al., 2009; Wang, 2007; Zhang et al., 2009). Subsequent DNA synthesis and ligation

complete the repair. These results demonstrate a central role for BRCA1 in coordinating formation of various complexes required for DNA damage repair (**Figure 7**).

BRCA1 is a key component of a variety of macrocomplexes that are involved in DNA damage repair. BRCA1 interacts with phosphorylated Abraxas, BACH1, and CtIP as distinct macrocomplexes that are mediated through BRCA1 BRCT domain (Cantor et al., 2001; Wang et al., 2007; Yu et al., 1998). The complex consisting of BRCA1, Abraxas (CCDC98), RAP80 (UIMC1), BRCC36, BRCC45 and MERIT40 (NBA1) enable the targeting of BRCA1 to DSBs and has been shown to be involved in G2/M checkpoint control (Chen et al., 2006; Feng et al., 2009; Kim et al., 2007a; Kim et al., 2007b; Liu et al., 2007; Shao et al., 2009b; Sobhian et al., 2007; Wang et al., 2009; Wang et al., 2007). The complex consisting of BRCA1, BACH1, and TOPBP1 is involved in the G1-S and intra-S checkpoint (Cantor et al., 2001; Greenberg et al., 2006; Xu et al., 2001; Xu et al., 2002). The complex of BRCA1, CtIP, and MRN directs DNA resection and facilitates G2-M checkpoint control (Chen et al., 2008; Yun and Hiom, 2009).

The presence of repair proteins at DSBs can be visualized as distinct, punctate ionizing radiation-induced foci (IRIF) by immunofluorescence (Scully et al., 1997b). γ -H2AX and 53BP1 foci have been shown to form within minutes in response to IR while BRCA1 may take hours (Paull et al., 2000). This technique has been used extensively to examine the recruitment and interaction of these DNA damage repair proteins (Bekker-Jensen et al., 2006; Scully et al., 1997b). Dysregulation in the pathway often results in altered IRIF formation. Therefore, BRCA1 IRIF formation can be used to assess the effect of dysregulation on BRCA1 expression and function.

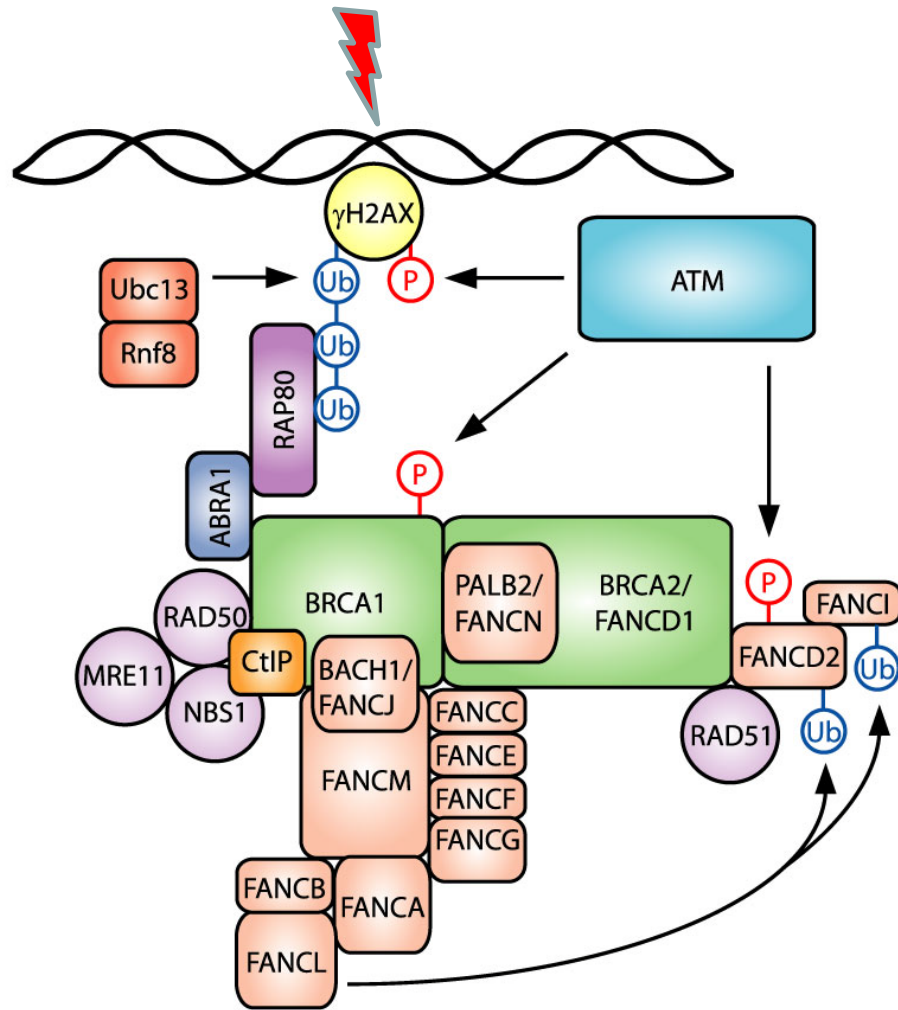


Illustration by Shane Stecklein

Figure 7: BRCA1 in homology-directed repair of double-strand breaks. DNA repair is initiated when surveillance proteins recognize DSBs caused by ionizing radiation. Phosphorylation of H2AX (γ -H2AX) by ATM and polyubiquitylation of γ -H2AX by Ubc13/Rnf8 result in activation and recruitment of BRCA1 to DSBs. BRCA1 then acts as the central scaffold that brings together the required proteins involved in repairing the DSB.

Use of RNAi in Functional Studies

Since the completion of the human genome project, RNA interference (RNAi) has become a powerful genetic tool to evaluate loss-of-function and has been modified for high-throughput screening (Echeverri and Perrimon, 2006; Moffat and Sabatini, 2006). Its role in post-transcriptional gene silencing (PTGS) was explored following the observation that a pigment-producing gene introduced into petunias suppressed expression of both the exogenous and endogenous gene (Napoli et al., 1990). Fire and colleagues made the discovery that PTGS was mediated by double-strand RNA (dsRNA) (Fire et al., 1998). Small interfering RNAs (siRNAs) and short hairpin RNAs (shRNAs) or shRNA in a microRNA context (shRNA-mirs) can be used to mediate knockdown of gene expression. siRNAs are short double-stranded RNAs that are 19-22 bp in length. They are introduced into target cells by transfection to cause transient knockdown of a target gene. shRNA and shRNA-mir constructs can be packaged into a virus and transduced into target cells to cause stable integration and expression of the shRNA or shRNA-mir (Hannon and Rossi, 2004). shRNAs are produced as a single-stranded RNA of 50-70 bp in length that forms a stem-loop structure. shRNAs exit the nucleus and are cleaved by DICER and assembled into the RNA-induced silencing complex (RISC) to mediate knockdown in a sequence specific manner (Bernstein et al., 2001; Hammond et al., 2000; Yi et al., 2003). shRNA-mirs are produced as a single-stranded RNA that forms a dsRNA hairpin molecule called the primary polyadenylated miRNA (pri-miRNA) of 70-90 bp in length, which is cleaved by Drosha to form the miRNA precursor (pre-miRNA) (Lee et al., 2003; Lee et al., 2002). The pre-miRNA is actively transported out of the nucleus by exportin-5, cleaved by DICER, and assembled into RISC to mediate knockdown (Bernstein et al., 2001; Hammond et al., 2000; Lund et al., 2004; Yi et al., 2003) (**Figure 8**). siRNA-mediated knockdown was the chosen method because transient

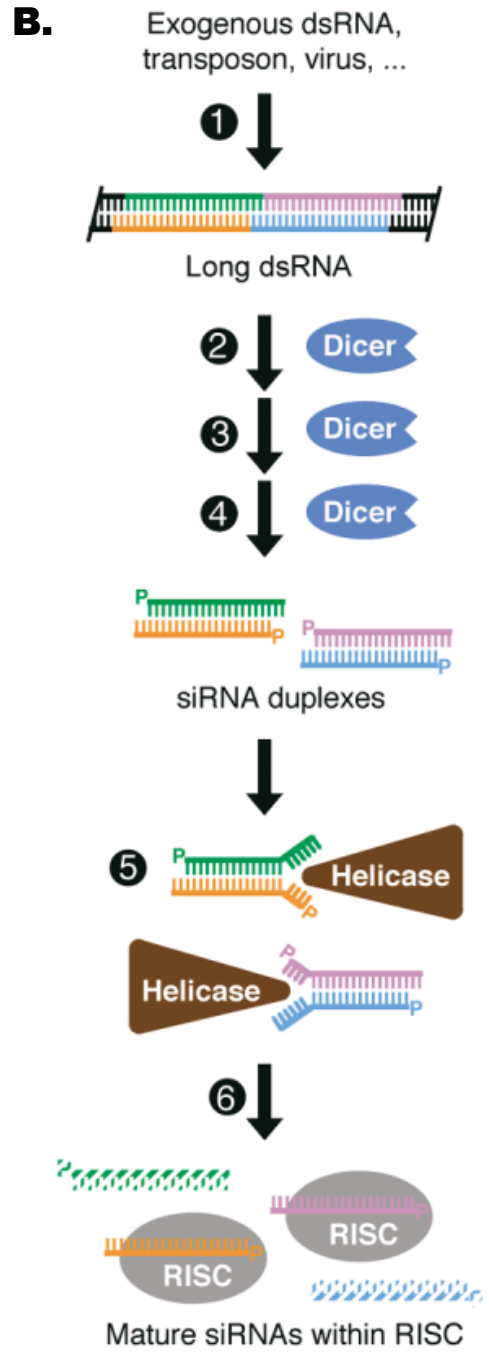
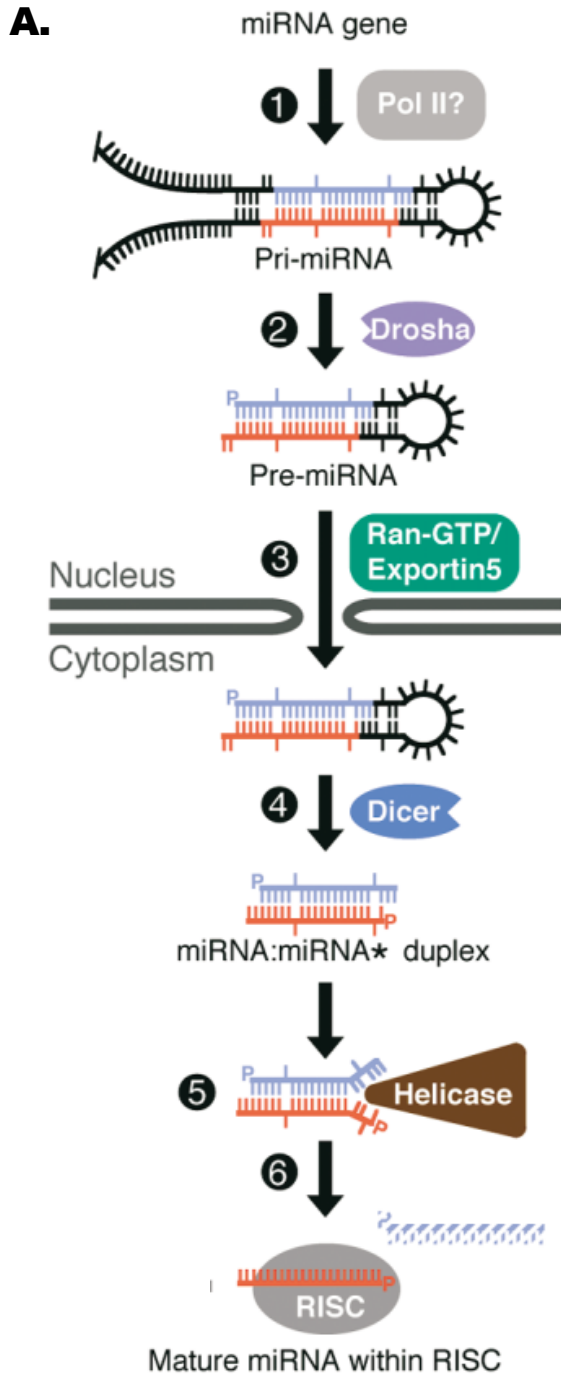


Figure 8: The biogenesis of miRNAs and siRNAs. Panel A depicts the steps and players necessary for proper biogenesis of miRNAs. A dsRNA hairpin molecule called the pri-miRNA is produced following transcription of the miRNA gene (step 1). The Drosha RNase III endonuclease cleaves both strands of the stem to form the pre-miRNA (step 2). The pre-miRNA is actively transported from the nucleus to the cytoplasm by Ran-GRP and exportin-5 (step 3). The Dicer RNase III endonuclease cleaves off the loop to form the miRNA:miRNA* duplex (step 4). A helicase enzyme (not yet identified) unwinds the duplex (step 5) and miRNA is loaded onto the ribonucleoprotein complex RISC while mirRNA* is degraded (step 6). The mature miRNA within RISC then targets mRNAs from loci unrelated to the miRNA gene and mediates either mRNA cleavage or translational repression. Panel B depicts the steps and players necessary for proper biogenesis of siRNAs. A long dsRNA is either artificially introduced into the target cell or naturally produced (step 1) and is processed by Dicer into many siRNAs that are 19-22 bp in length (steps 2-4). A helicase enzyme (not yet identified) unwinds the siRNA duplexes (step 5) and the single-stranded RNA is loaded onto RISC (step 6). The mature siRNA within RISC then targets mRNAs from the same (or similar) loci to and mediates mRNA cleavage (Bartel, 2004).

knockdown can be achieved in a relatively short period of time, siRNAs are titratable, and customizable siRNA libraries are available. This approach was used to develop a systematic functional analysis of BRCA1 expression and function by selectively silencing kinases and observing BRCA1 IRIF phenotype.

Summary/Specific Aims

Transcriptional and functional regulation of the breast cancer susceptibility gene 1 (*BRCA1*) in the pathogenesis of sporadic breast cancers is poorly understood. About 90% of all breast cancers are considered sporadic in origin, and 30-40% of these cases exhibit decreased expression of BRCA1 in the absence of mutations at its genetic locus. Loss of BRCA1 accelerates growth of tumor cells, while expression of BRCA1 leads to growth arrest and apoptosis. Additionally, our lab has demonstrated that overexpression of wild-type BRCA1 delays tumor formation following mutagen exposure. These observations support further examination of the regulatory pathways of BRCA1 to restore its expression and function. Our hypothesis is that an increase in BRCA1 expression enhances DNA repair capacity and protects cells against chemical and physical mutagens, resulting in delayed or decreased tumor onset.

To identify potential regulators of BRCA1, a functional assay was developed based on the role of BRCA1 in DNA damage repair. BRCA1 acts as a central scaffold that assembles a complex of repair proteins to sites of double-strand breaks (DSBs) following exposure to ionizing radiation (IR). Immunostaining for BRCA1 reveals these repair sites as punctate ionizing radiation–induced foci (IRIF). The ability of BRCA1 to localize to DSBs depends on both its expression and phosphorylation status. The use of siRNAs enables the transient knockdown of a specific target and assessment of downstream effects of that knockdown. The

effect of siRNAs against kinases was evaluated on BRCA1 IRIF formation because 1) phosphorylation of BRCA1 regulates many of its functions, 2) bioinformatics provides BRCA1 phosphorylation sites where the kinase involved is unknown, 3) kinases play key roles in signaling pathways that influence gene expression or phosphorylation status, and 4) kinases are druggable targets. Chapter 2 will describe the development of the BRCA1 functional assay, including the iterative process by which each step of the assay was optimized, as well as the implementation of the BRCA1 functional assay to screen an Ambion *Silencer*® Kinase siRNA library. Additionally, the rationale and process for identifying and validating potential regulators of BRCA1 expression and function will be explained. Chapter 3 will evaluate the effect of siRNA-mediated knockdown of three lead kinases on BRCA1 mRNA levels as well as on both target and BRCA1 protein levels. Chapter 4 will further assess the effect of kinase knockdown on the ability of cells to repair by HDR or NHEJ and the functional consequence to cell proliferation following DNA damage. Finally, Chapter 5 will review the significance and potential impact of these results to our understanding of the pathogenesis of sporadic breast cancers expressing low levels of BRCA1.

CHAPTER II

IDENTIFY AND VALIDATE POTENTIAL REGULATORY KINASES OF BRCA1 EXPRESSION AND FUNCTION

Introduction

Localization of DNA repair proteins at sites of DNA damage follows a spatiotemporal pattern that can be visualized easily as ionizing radiation-induced foci (IRIF) using immunofluorescence (Bekker-Jensen et al., 2006; Scully et al., 1997). Following ionizing radiation (IR), BRCA1 foci formation increases both in number and size, peaking within 3-8 hours and resolving by 24 hours (Paull et al., 2000). Dysregulation at any point of BRCA1 expression and function could manifest as an altered IRIF phenotype. Therefore, the BRCA1 IRIF assay was used to measure the effect of siRNA-mediated knockdown of kinases on BRCA1 expression and function in MCF7 cells. To do so, chemically synthesized siRNAs were used because they are amenable to high content analysis in a timely manner and can be customized to target a particular class of genes. The effect of siRNAs against kinases was evaluated because they are involved in signaling pathways that can influence gene expression or protein function and are commonly dysregulated in cancer. For example, in response to DNA damage, ATM and ATR kinases phosphorylate various downstream target proteins, including BRCA1, which localizes to DSBs and serves as a central scaffold in the recruitment of associated repair proteins to facilitate DNA damage repair, as well as CHK1 and CHK2 to activate cell cycle checkpoints (Iliakis et al., 2003; Tibbetts et al., 2000; Zhou and Elledge, 2000). Assay development involved designing a workflow that included siRNA transfection, exposure to ionizing radiation, fixation/permeabilization and immunostaining of cells, as well as data collection and analysis.

Kinase siRNAs were introduced into MCF7 cells via chemical transfection to maximize target knockdown and to minimize cytotoxicity. MCF7 cells were chosen because they represent a mammary cell line derived from the most common subtype of invasive breast carcinoma and are widely used and well-documented as *in vitro* models of breast tumors (Lacroix and Leclercq, 2004). Various experimental parameters were evaluated, including determining serum concentration, transfection reagents, and antibodies as well as establishing an optimal dose of IR, an optimal time following IR to stain for BRCA1, appropriate assay controls, fixation/permeabilization reagents and conditions, and imaging parameters. The laser scanning cytometer (LSC) is an emerging technology with automated imaging and analysis capabilities that provide quantitative information about BRCA1 IRIF. Use of the LSC enabled a standardized analysis based on mean fluorescence intensity. Once assay optimization was complete, 289 kinases from an Ambion *Silencer*® Kinase siRNA Library were screened. The kinase siRNA library is composed of a diverse array of kinases from each of the major groups, including AGC (containing PKA, PKG, PKC families), CAMK (calcium/calmodulin-dependent protein kinase), CK1 (Casein kinase 1), CMGC (containing CDK, MAPK, GSK3, CLK families), STE (homologs of yeast Sterile 7, Sterile 11, Sterile 20 kinases), TK (tyrosine kinase), and TKL (tyrosine kinase-like). Three individual siRNAs targeting each kinase were assessed for their ability to alter BRCA1 IRIF formation. Thirty-two kinase hits were identified based on BRCA1 IRIF expression relative to the assay controls. The list of thirty-two was reduced to fourteen by subsequent validation for consistent BRCA1 IRIF effects by siRNA-mediated knockdown of the kinase hits and increasing stringency criteria.

Materials and Methods

Cells: The human epithelial mammary gland adenocarcinoma MCF7 cell line was purchased from ATCC (HTB-22, Manassas, VA). Cells were cultured in Minimum essential medium (Eagle) with Earle's salts (Mediatech, Herndon, VA), containing 10% fetal bovine serum (FBS, Cambrex Bio Science, Rockland, ME), 50 U/ml each of penicillin and streptomycin (Mediatech), 2 mM L-glutamine (Mediatech), 1 mM pyruvate (Mediatech) and 1X nonessential amino acids (Mediatech) (complete MEM) at 37°C in a humidified, 5% CO₂-containing atmosphere.

Immunofluorescence Staining: MCF7 cells (5×10^4) were seeded on coverslips in complete MEM and incubated at 37°C in 5% CO₂ overnight (O/N). Prior to Protocols 1-3, cells were exposed to 20 Gy ionizing radiation (IR) and allowed to recover for 8h before staining. Prior to Protocol 4, cells were exposed to 10 Gy IR and allowed to recover for 6 h before staining.

Protocol 1: MCF7 cells were fixed in 3% paraformaldehyde (Electron Microscopy Sciences, Hatfield, PA) in PBS for 30 min on ice. Subsequently, cells were washed three times with PBS, and then permeabilized in 0.5% Triton X-100 (Fisher, Fair Lawn, NJ) in TBST-20 for 5 min at room temperature (RT). Following permeabilization, cells were washed three times with TBST-20 and then incubated with blocking solution (10% goat serum (Santa Cruz Biotechnology, Santa Cruz, CA) in TBST-20) for 1 h at RT. Afterward, cells were washed three times with TBST-20, and then primary anti-BRCA1 mouse monoclonal IgG1 antibody incubation (Calbiochem, Gibbstown, NJ) was O/N at 4°C (diluted 1:100 with 3% BSA, 1% goat serum, 0.1% Triton X-100 in TBST-20). The next day, cells were washed three times with TBST-20 prior to incubation with secondary AlexaFluor 488 goat anti-mouse IgG1 antibody (Molecular Probes/Invitrogen,

Carlsbad, CA) (diluted 1:400 with 3% BSA, 1% goat serum, 0.1% Triton X-100 in TBST-20) for 1 h at RT. Then, cells were washed three times with TBST-20 before the coverslips were mounted onto slides using Prolong Gold Antifade Reagent with DAPI (Molecular Probes/Invitrogen) and allowed to dry at RT for 24 h. All images were obtained using a 40X objective on the Nikon TE2000 microscope and processed using the MetaMorph program (Boyce Scientific, Gray Summit, MO, C. Vines laboratory).

Protocol 2: MCF7 cells were fixed in 3% paraformaldehyde/0.02% Triton X-100 in PBS for 10 min at RT. Afterward, cells were washed three times with PBS before permeabilization in 0.02% Triton X-100 in TBST-20 for 25 min at RT. Then after three washes with TBST-20, blocking solution (3% BSA, 5% goat serum, 0.02% Triton X-100 in TBST-20) incubation was for 90 min at RT. Subsequently, cells were washed three times before primary anti-BRCA1 mouse monoclonal IgG1 antibody (diluted 1:100 or 1:250 with 1% BSA, 1% goat serum, 0.02% Triton X-100 in TBST-20) incubation O/N at 4°C. The next day, following three washes with TBST-20, incubation with secondary AlexaFluor 488 goat anti-mouse IgG1 antibody (diluted 1:400 or 1:1000, respectively, with 1% BSA, 1% goat serum, 0.02% Triton X-100 in TBST-20) was for 1 h at RT. Finally, after the last three washes, coverslips were mounted onto slides with Prolong Gold Antifade Reagent with DAPI and allowed to dry at RT overnight. All images were obtained using a 40X objective on the Nikon TE2000 microscope and processed using the MetaMorph program.

Protocol 3 (Eckner et al., 1994): MCF7 cells were fixed in 3% paraformaldehyde/2% sucrose in PBS for 10 min at RT, washed twice with PBS, permeabilized in ice-cold Triton X-100 buffer

(50 mM NaCl, 3 mM MgCl₂, 200 mM sucrose, 10 mM HEPES pH=7.4, 0.5% Triton X-100) for 5 min, washed two more times with PBS, then incubated with blocking solution (5% goat serum and 0.5 µg/mL Human IgG (MP Biomedicals, Solon, OH) in PBS) at 37°C and 5% CO₂ for 20 min. There were no wash steps added between blocking and primary antibody. Subsequently, cells were incubated in primary anti-BRCA1 mouse monoclonal IgG1 antibody diluted 1:250 with PBS at 37°C and 5% CO₂ for 20 min, and then washed three times with PBS. Next, secondary AlexaFluor 488 goat anti-mouse IgG1 antibody was diluted 1:1000 and incubation was similar to that for primary. After another three washes with PBS, the coverslips were mounted onto slides using Prolong Gold Antifade Reagent with DAPI and allowed to dry at RT for 24 h. All images were obtained using a 40X objective on the Nikon TE2000 microscope and processed using the MetaMorph program.

Protocol 4: MCF7 cells were fixed in 4% paraformaldehyde/2% sucrose in PBS+0.1% glycerol (PBS-G) for 45 min at 4°C. Cells were then incubated with 0.1% NaBH₄ in PBS-G for 5 min at RT before they were washed three times with PBS-G and permeabilized in ice-cold Triton X-100 buffer (50 mM NaCl, 3 mM MgCl₂, 200 mM sucrose, 10 mM HEPES pH=7.4, 0.5% Triton X-100) for 5 min at RT. At this point, cells were washed three times with TBS+0.1% glycerol (TBS-G), then incubated with blocking solution (3% goat serum, 1% BSA, 0.1% Triton X-100 in TBS-G) overnight at 4°C. Subsequently, cells were incubated with primary anti-BRCA1 mouse monoclonal IgG1 antibody diluted 1:200 in blocking solution for 1 h at RT, washed three times with TBS-G, and then incubated with secondary AlexaFluor 488 goat anti-mouse IgG1 antibody diluted 1:1000 in blocking solution for 30 min at RT. Following another three washes with TBS-G, cells were incubated with 0.5 µg/ml DAPI for 5 min and then washed. Cells stained in the

Whatman 96-well glass bottom plate were stored in 100 μ l PBS-G. Cells stained on coverslips were mounted onto slides using Prolong Gold Antifade Reagent. Cells stained in the Nunc Lab-Tek II 4 well chamber slides (Rochester, NY) were mounted with a coverslip using Prolong Gold Antifade Reagent (Molecular Probes/Invitrogen) and allowed to dry at RT for 24 h. All images were either obtained using a 40X objective on the Nikon TE2000 microscope and processed using the MetaMorph program or obtained using a 40X objective on the iCys LSC and processed using its associated iCys cytometric analysis program (CompuCyte, Westwood, MA).

Effect of IR on BRCA1 IRIF formation: A BRCA1-specific antibody was used to stain MCF7 cells for BRCA1 IRIF following exposure to IR. Cells were exposed to 5, 10, and 20 Gy IR and fixed for analysis at 8 h post-IR. Cells were stained as described in Protocol 4. All images were obtained using a 40X objective on the Nikon TE2000 microscope and processed using the MetaMorph program.

Cell Cycle Analyses: Propidium iodide (PI) staining was done for cell cycle analysis by flow cytometry. MCF7 cells were subcultured in individual 60 mm dishes under indicated experimental conditions to a confluency of ~70-80% prior to fixation. MCF7 cells were trypsinized and 1×10^6 cells were fixed and permeabilized with 0.5 ml of 0.9% NaCl and 1.25 ml of 90% cold EtOH and then incubated for 30 min at RT. To stain, 0.5 ml of 50 μ g/ml PI was added. 50 μ l of 1 mg/ml RNase was added and then incubated at 37°C for 30 min before analysis. Samples were run using the BD LSR II for 10,000 cells and analyzed using the associated BD FACSDiva software (Becton, Dickinson and Company, Franklin Lakes, NJ). From the forward scatter vs. side scatter plot, a gate was established to include cells and exclude

debris. From the first gate, a second gate was established along a 45° angle to include all single cells. From there, a plot of area vs. cell count was generated and gated for sub-G₀/G₁, G₀/G₁, S, and G₂/M.

Effect of IR on cell cycle progression: The levels of IR investigated were 0, 2, 5, 10, and 20 Gy. At 0, 3, 6, 9, 12, 18, 24, 30, and 36 h post-IR, cells were processed for cell cycle analysis using the above described protocol.

Effect of cell synchronization on cell cycle progression: MCF7 cells were synchronized by serum starvation in complete MEM without FBS but supplemented with 0.05% BSA for 30 h and were processed 2, 4, 8, 18, 24, 30, 36, 42, 48, and 54 h following serum release in complete MEM with 20% for cell cycle analysis using the above described protocol.

Effect of combining cell synchronization and exposure to IR on cell cycle progression: MCF7 cells were synchronized by serum starvation for 30 h followed by serum release for 24 h, exposed to 20 Gy IR, and processed 0, 1, 2, 4, 6, 8, and 12 h post-IR. A matched control set of unsynchronized MCF7 cells was exposed to 20 Gy IR and processed 0, 1, 2, 4, 6, 8, and 12 h post-IR for cell cycle analysis.

Effect of combining siRNA transfection of Neg and BRCA1 siRNAs, cell synchronization, and exposure to IR on cell cycle progression: MCF7 cells were simultaneously transfected with either Neg (negative control) or BRCA1 siRNAs by chemical transfection with Lipofectamine RNAiMAX (Invitrogen) and cell synchronized by either serum starvation for 42 h followed by

serum release for 24 h or cultured first in complete MEM with reduced FBS (2% instead of 10%) and without antibiotics for 48 h and then complete MEM with 10% FBS and without antibiotics for 18 h. Cells were then exposed to 10 Gy IR and processed 0 and 24 h post-IR for cell cycle analysis.

siRNA Transfection Optimization:

Optimization with GAPDH siRNA and Ambion transfection reagents: A transfection method known as reverse transfection was used. MCF7 cells were trypsinized in 0.25% trypsin/2.21 mM EDTA in HBSS without sodium bicarbonate, calcium, and magnesium (Mediatech) and resuspended to a concentration of 1×10^5 cells per ml. The cells were then kept at 37°C while the transfection complexes were prepared. The first step in preparing the siRNA/transfection agent complexes was to dilute the transfection agent in OPTI-MEM I (Invitrogen) medium and incubate for 10 min at RT. Then the siRNA was diluted in OPTI-MEM I medium. After that, the diluted siRNA and diluted transfection agent were mixed, incubated at RT for 10 min, and dispensed into the wells of a clear 96-well plate. Finally, the MCF7 cells were mixed with the transfection complexes and incubated at 37°C for 48 h.

Both knockdown and cell viability were assessed using the KDAlert GAPDH Assay Kit (Ambion) per manufacturer's protocol. The culture medium was aspirated from the transfected cells. Then 200 μ l KDAlert Lysis Buffer was added to each sample well and incubated at 4°C for 20 min. 10 μ l of each cell lysate was then transferred to the wells of a black 96-well plate followed by 90 μ l of KDAlert Master Mix. Finally, the increase in fluorescence over a 4 minute interval of time for the samples was measured using the Victor 3V plate reader (Perkin Elmer, Waltham, MA) with an excitation wavelength at 560 nm and an emission wavelength at 590 nm.

The GAPDH activity was calculated by subtracting the fluorescence reading at t_0 from that at $t_4 \text{ min}$. The percent remaining gene expression was determined from the ratio of the fluorescence increase for samples transfected with GAPDH siRNA to the fluorescence increase for samples transfected with negative control (Neg) siRNA (Equation 1). The percent knockdown was calculated from the percent remaining gene expression (Equation 2). Relative cell viability was determined from GAPDH activity in negative control siRNA-transfected cells ($\Delta\text{fluorescence}_{\text{Neg}}$). A comparison of cell viability among the transfection agent volumes was made relative to the sample transfected with the lowest volume of transfection agent. The optimal balance factor (OBF) was calculated from relative cell viability and percent knockdown (Equation 3).

$$\text{Equation 1} \quad \% \text{ remaining expression} = (\Delta\text{fluorescence}_{\text{GAPDH}} / \Delta\text{fluorescence}_{\text{Neg}}) \times 100$$

$$\text{Equation 2} \quad \% \text{ knockdown} = 100 - \% \text{ remaining expression}$$

$$\text{Equation 3} \quad \text{OBF} = \Delta\text{fluorescence}_{\text{Neg}} \times \% \text{ knockdown}$$

In each experiment, positive and negative controls were run in triplicate for statistical analysis. The positive control was glyceraldehyde-3-phosphate dehydrogenase (GAPDH) siRNA and the negative control was a nontargeting, scrambled Neg siRNA. Other controls included a transfection agent-only control and a buffer-only control. To select a transfection agent and transfection agent volume, two transfection agents, siPORT Amine and siPORT NeoFX (Ambion, Foster City, CA), were evaluated in a 96-well plate at volumes of 0.15 μl , 0.3 μl , 0.6 μl , and 1.2 μl . A final siRNA concentration of 10 nM, incubation with the transfection complexes for 48 h, and a cell density of 8×10^3 MCF7 cells were used. If the GAPDH positive control siRNA was able to reduce GAPDH expression levels by $\geq 70\%$ with $\leq 15\%$ cell death, then optimization was complete. If not, then the amount of time that cells are exposed to

transfection complexes was evaluated. The transfection medium was replaced at 6, 12, and 24 h with fresh medium, and knockdown as well as cell viability was reevaluated 48 h following transfection. Again, if these new conditions were able to reduce GAPDH expression levels by $\geq 70\%$ with $\leq 15\%$ cell death, then optimization was complete. If not, then optimal siRNA quantity was determined. The amounts of siRNA evaluated were 1, 3, 10, and 30 nM final concentration. Again, if these new conditions were able to reduce GAPDH expression levels by $\geq 70\%$ with $\leq 15\%$ cell death, then optimization was complete. If not, then cell density was optimized. The cell densities evaluated were 8×10^3 and 4×10^3 .

Transfection efficiency was also assessed by microscopy using a FAM-labeled siRNA. The FAM-labeled siRNA was transfected using siPORT NeoFX in the same manner as described above and fluorescence was measured following the 488 laser excitation on an Olympus inverted fluorescence microscope (Olympus, Melville, NY) and processed using the Slidebook program (3i, Denver, CO).

Isolation of total RNA from cells: RNA was extracted per manufacturer's protocol using the RNeasy Plus RNA extraction kit (Qiagen, Valencia, CA). MCF7 cells were disrupted using Buffer RLT plus β -mercaptoethanol (10 μ l β -ME per 1 ml Buffer RLT). For $< 5 \times 10^6$ cells, 350 μ l of Buffer RLT was added. Each lysate was homogenized using a QIAshredder spin column and centrifuged using an Eppendorf 5415 D microcentrifuge (Westbury, New York) for 2 min at full speed (16,100xg). One volume or 350 μ l of 70% ethanol was added to the homogenized lysate and mixed by pipetting. The sample was then transferred to an RNeasy spin column and centrifuged for 15 s at ≥ 8000 xg. The flow-through was discarded. 700 μ l Buffer RW1 was added to the RNeasy spin column and centrifuged for 15 s at ≥ 8000 xg to wash the spin column

membrane. The flow-through was again discarded. 500 μ l Buffer RPE was then added to the RNeasy spin column and centrifuged for 15 s at $\geq 8000xg$ to wash the spin column membrane. The flow-through was again discarded. Another 500 μ l Buffer RPE was added to the RNeasy spin column and centrifuged for 2 min at $\geq 8000xg$. The RNeasy spin column was placed in a new 2 ml collection tube and centrifuged at full speed for 1 min to eliminate any possible carryover of Buffer RPE. The RNeasy spin column was then placed in a new 1.5 ml Eppendorf tube. The RNA was eluted with 30 μ l RNase-free water added directly to the spin column membrane and centrifuged for 1 min at $\geq 8000xg$. The eluate was then added to the RNeasy spin column membrane to concentrate the RNA further and centrifuged for 1 min at $\geq 8000xg$. The 260/280 ratio and concentration of each RNA sample were determined using an 8-channel NanoDrop 8000 spectrophotometer and its associated software ND-8000 v1.1.1 (Thermo Scientific, Wilmington, DE, P. Fields laboratory). RNA samples were reverse transcribed to cDNA immediately following extraction.

Quantitative real-time PCR (qRT-PCR): Complementary DNA (cDNA) was generated per manufacturer's protocol from 1000 ng extracted RNA in a 100 μ l volume using the High Capacity cDNA kit (Applied Biosystems, Foster City, CA). The 2x reverse transcription master mix prepared on ice (per 20- μ l reaction) was composed of 2 μ l 10X RT Buffer, 0.8 μ l 25X dNTP Mix (100 mM), 2.0 μ l 10X RT Random Primers, 1 μ l MultiScribe Reverse Transcriptase, and 4.2 μ l Nuclease-free H₂O. 10 μ l of RNA sample was mixed with 10 μ l of 2X RT master mix per 20- μ l reaction in a PCR tube. Reverse transcription of RNA to cDNA was performed in a GeneAmp PCR System 9700 thermal cycler (Applied Biosystems). The reverse transcription PCR program was run as follows: 25°C for 10 min, 37°C for 120 min, 85°C for 5 s, and 4°C for cDNA

samples were stored at -80°C until the qRT-PCR plate was ready to be set up. Gene expression of BRCA1 (Hs00173237_m1), GAPDH (Hs99999905_m1) and 18S (Hs99999901_s1) was detected using the TaqMan[®] Gene Expression assay kit (Applied Biosystems). Each PCR reaction was set up as follows: 9 μl cDNA + 10 μl TaqMan[®] Universal PCR Master Mix + 1 μl specific primer/probe set (BRCA1 or 18S) in a 96-well PCR plate. Controls for each set of experiments included the 18S housekeeping gene for normalization of C_t values to account for relative RNA amount, no cDNA control to assess specificity of the primer/probe set, and H₂O only to determine background of the instrument. Each sample was run in triplicate for statistical analysis. Each 20 μl reaction was run on the 7500 ABI real time PCR instrument (Applied Biosystems, P. Fields laboratory) with the following program: UNG incubation at 50°C for 2 min, AmpliTaq Gold activation at 95°C for 10 min followed by 40 PCR cycles of 95°C for 15 s to denature and 60°C for 1 min to anneal/extend. C_t values were obtained for each sample. Data analysis was carried out in Microsoft Excel. An average and standard error of the triplicate C_t values for each sample were calculated using the equation $C_{t\text{average}} = (C_{t1} + C_{t2} + \dots + C_{tn})/n$ and $C_{t\text{st error}} = C_{t\text{stdev}}/\text{sqrt}(n)$. Each averaged C_t value was then normalized to 18S (ΔC_t) and the corresponding standard error was calculated using the equation $\Delta C_t^{\text{st error}} = \text{sqrt}(C_{t\text{st error}}(18\text{s})^2 + C_{t\text{st error}}(\text{sample})^2)$. The ΔC_t value was further normalized to Neg siRNA, or the IRIF assay control ($\Delta\Delta C_t$) and the negative $\Delta\Delta C_t$ value was raised to the power of 2 to give relative remaining expression of the gene being investigated. The $\Delta C_t^{\text{st error}}$ was added to and subtracted from its corresponding $\Delta\Delta C_t$ and the negative resulting value was raised to the power of 2 to give the positive and negative standard error. The standard error for the average of replicate experiments was calculated using the equation adapted from Baker and Nissim, 1963: $e_3 = \text{sqrt}((1/(n(n-1))((n_1(n_1-1)e_1^2)+(n_2(n_2-1)e_2^2)+((n_1n_2)/n)(m_1-m_2)^2)))$, where e_3 refers to the new standard error,

n_1 and n_2 refer to the number of observations in the first and second group respectively, $n=n_1+n_2$, m_1 and m_2 refer to the mean in the first and second group respectively, and e_1 and e_2 refer to the standard error in the first and second group respectively. A t test was performed using GraphPad Prism 5 (GraphPad Software, Inc., La Jolla, CA) to determine whether the change in mRNA was statistically significant.

Isolation of total protein from cells: The medium was removed and the cells were washed 2x with PBS. Cells were scraped into ice-cold PBS and transferred to a microcentrifuge tube. The cells were then pelleted by centrifugation at 300xg for 5 min at 4°C. The supernatant was removed and the pellet was lysed in modified RIPA buffer (50 mM Tris base, 150 mM NaCl, 2 mM EDTA, 1% Triton X-100, 0.5% Na-deoxycholate, 0.1% SDS, 50 mM NaF, 5 mM Na_3VO_4 , 1X Sigma protease inhibitor cocktail) on ice for 30 min, vortexing occasionally. The cellular debris was then removed by centrifugation at 10,600xg for 30 min at 4°C. The supernatant containing the extracted proteins was collected and protein concentration was measured using the Bio-Rad Bradford protein assay. Reagent A' was made by adding 20 μl of Reagent S to each 1 ml of Reagent A. A standard curve was generated using BSA standards with concentrations of 0, 0.125, 0.25, 0.5, 0.75, 1, 1.5, and 2 mg/ml in triplicate. 5 μl of standards and samples were pipetted in triplicate into a 96-well plate. 25 μl of Reagent A' was added to each well using a multichannel pipette followed by 200 μl of Reagent B. The plate was mixed and incubated at RT for 15 min. The absorbance was then read at 750 nm in a Synergy microplate reader with associated Gen5 software (BioTek, Winooski, VT, S. Sittampalam laboratory). An average absorbance was calculated for each sample that was then normalized to its buffer control to eliminate background signal. The BSA standard curve was generated and a linear regression

analysis was done using GraphPad Prism 5 to interpolate the unknown baseline-corrected absorbance for each protein sample to a protein concentration.

Western blot analysis: 100 μ g of protein + 1X SDS-PAGE sample buffer (60 mM Tris-HCl pH=8.0, 2% w/v SDS, 4 mM EDTA, 10% v/v glycerol, 0.02% w/v bromophenol blue, 5% β -ME) per sample was loaded onto an 8% Tris-Glycine SDS-PAGE gel (Invitrogen). The proteins were separated by electrophoresis for 1.5 h at 125 V in a Tris-Glycine running buffer (25 mM Tris base, 192 mM glycine, 0.1% SDS). The proteins were then transferred onto PVDF membrane at 35 V O/N at 4°C in 8% transfer buffer (25 mM Tris base, 192 mM glycine, 20% v/v MeOH). The PVDF membrane was then blocked in 5% milk/PBS + 0.1% Tween-20 (PBS-T) for 1 h RT. The membrane was incubated with the primary antibody, anti-BRCA1 mouse mAb (Ab-1, Calbiochem), diluted 1:250 in 3% milk/PBS-T O/N at 4°C. Following incubation with the primary antibody, the blot was washed 1x15 min, 3x5 min in PBS-T at RT. The blot was then incubated with the secondary antibody, goat anti-mouse IgG, HRP-linked (GAM-HRP, Cell Signaling, Danvers, MA) diluted 1:5000 in 3% milk/PBS-T for 1 h at RT. To monitor equal protein loading, actin was detected using anti-actin (Chemicon/Millipore, Billerica, MA) at a 1:250,000 dilution in 5% milk/PBS-T for 1 h at RT. Following incubation with anti-actin, the blot was washed 1x15 min, 3x5 min in PBS-T at RT. The blot was then incubated with the secondary antibody, GAM-HRP, at 1:10,000 in 3% milk/PBS-T for 1h at RT. Prior to chemiluminescent detection the blots were washed 1x15 min, 3x5 min in PBS-T and 2x5 min in TBS. Chemiluminescence was detected using the SuperSignal West Femto kit (Pierce Biotechnology, Rockford, IL) and the UVP imaging center (Upland, CA). Densitometry was measured for each protein band using the UVP imaging center. To determine BRCA1 protein

expression following siRNA-mediated knockdown of BRCA1, the measured density for BRCA1 was normalized first to that of actin and then to that of the Neg siRNA control.

Transfection of siRNA by electroporation: A protocol optimized for MCF7 cells by Amaxa for their nucleofection system was used. Each nucleofection sample was prepared in a well of a 96-well round bottom plate by combining 4×10^5 MCF7 cells resuspended in 20 μ l of Cell Line 96-well Nucleofector Solution SE plus Supplement (Amaxa) and 2 μ l 1.25 μ M siRNA. 20 μ l of each sample was then transferred using a multichannel pipette to the Amaxa 96-well Nucleocuvette plate. The nucleofection process was completed using the Amaxa Nucleofector Device with 96-well Shuttle System, Nucleofector program 96-EN-130. 80 μ l of culture medium was added to each well of the Nucleocuvette plate before 25 μ l of the cells (1×10^5 cells) were transferred using a multichannel pipette to a Whatman 96-well glass bottom plate containing 175 μ l pre-warmed media and incubated at 37°C in a humidified, 5% CO₂-containing atmosphere. Additional culture medium was added 24 h after nucleofection to maintain cell viability.

Nucleofection conditions were kept constant between experiments to minimize variability. Both positive and negative controls for the nucleofection process and the functional foci formation assay were run in triplicate for statistical analysis. The positive control for the nucleofection process was a vector pmaxGFP and the negative controls included cells with DNA but without application of the program and cells without DNA with application of the program, which were used to monitor transfection efficiency. Transfection efficiency was assessed by microscopy using the vector pmaxGFP, which was transfected by electroporation in the same manner. Fluorescence was measured following the 488 laser excitation on an Olympus inverted fluorescence microscope (Olympus, Melville, NY) and processed using the Slidebook program.

The functional assay-specific positive and negative controls were BRCA1 and Neg siRNA, respectively. siRNA knockdown was assessed by qRT-PCR as described above.

Chemical transfection of siRNAs with RNAiMAX: For transfection in a 96-well plate, MCF7 cells (5×10^4) in 0.2 ml MEM with 2% FBS without antibiotics were added to each well containing 60 nM final siRNA concentration (12 μ l of 1.25 μ M siRNA diluted in 37 μ l OptiMEM) and 1 μ l RNAiMAX/ 5×10^4 cells (Invitrogen, Carlsbad, CA) previously incubated for 16 min at RT. For transfection in a 4-well chamber slide, MCF7 cells (9.75×10^5) in 0.7 ml medium with reduced FBS (2% instead of 10%) and without antibiotics were added to siRNA at a final concentration of 60 nM (42 μ l 1.25 μ M siRNA diluted in 133 μ l OptiMEM) previously incubated with 4 μ l RNAiMAX for 16 min at RT. The medium was replaced following 24 h incubation at 37°C, 5% CO₂ humidified atmosphere with complete medium without antibiotics and reduced FBS (2% instead of 10%) and again 24 h later with complete medium without antibiotics. Cells were exposed to 10 Gy IR 66 h following transfection and allowed to recover for 6 h. The positive and negative controls were BRCA1 and Neg siRNA, respectively. Transfection efficiency was assessed by flow cytometric analysis using the FAM-labeled siRNA on the BD FACSCalibur (Becton, Dickinson and Company, Franklin Lakes, NJ). The FAM-labeled siRNA was transfected using RNAiMAX in the same manner as described above. BRCA1 mRNA and protein levels were assessed by qRT-PCR and Western blot analysis, respectively, for siRNA-mediated knockdown of BRCA1 as described above.

Kinase siRNA Library and Plate Description: The *Silencer*® Human Kinase siRNA Library was purchased from Ambion (Austin, TX), containing 2157 unique siRNAs (0.25 nmol each)

targeting each of 719 kinase genes within a total of 27 96-well plates. The wells in column 12 of every 96-well plate were left empty for the negative assay-specific control siRNA (Neg, scrambled) and positive assay-specific control siRNA (BRCA1). The siRNAs were initially reconstituted to 5 μ M (mother plates) in RNase-free water (Ambion) and further diluted to a working concentration of 1.25 μ M (daughter plates) (HTS Laboratory).

Kinase siRNA Library Screen and Validation: The *Silencer*[®] Human Kinase siRNA Library was screened and validated using the following workflow: siRNA-mediated knockdown of a kinase by chemical transfection with RNAiMAX, exposure to 10 Gy IR 66 h post-transfection, staining using an anti-BRCA1 antibody for BRCA1 IRIF and DAPI for the nucleus, and data collection and analysis using the LSC. MCF7 cells were subcultured to a confluency of ~75-80% prior to siRNA transfection. siRNAs were introduced into MCF7 cells via chemical transfection with RNAiMAX as described above. The primary screen was completed in both the 96-well and 4-well format. The validation was completed in triplicate in 4 well chamber slides. Following 66 hour incubation, cells were exposed to 10 Gy of ionizing radiation, allowed to recover for 6 h, and then immunostained using Protocol 4 discussed previously. Finally, imaging and analysis of BRCA1 IRIF were performed using the CompuCyte LSC. For the primary screen, mean fluorescence intensities of DAPI and BRCA1 IRIF for one region with at least 36 images were measured. For the validation, mean fluorescence intensities of DAPI and BRCA1 IRIF for 6 regions with at least 36 images per region were collected on the LSC. BRCA1 IRIF mean fluorescence intensity was standardized to its corresponding DAPI mean fluorescence intensity to account for cell density for all siRNAs. Then the adjusted IRIF value for each kinase siRNA was compared to that of the Neg siRNA to yield a relative IRIF expression that was then

normalized to a value between the BRCA1 siRNA and Neg siRNA with the BRCA1 siRNA set at 0% and the Neg siRNA set at 100%.

Results and Discussion

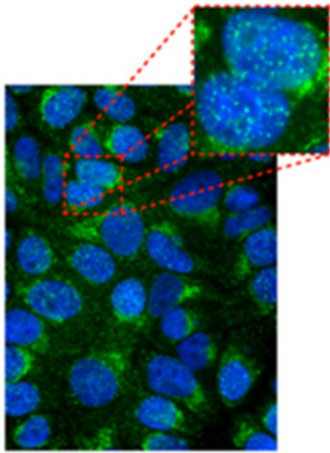
Studies to Optimize the BRCA1 Functional Assay

Immunofluorescence Staining: Preliminary experiments were performed to optimize the immunofluorescence staining protocol. The general protocol for intracellular staining involves fixation, permeabilization, blocking, primary antibody, secondary antibody, and counterstain for nuclei. Several protocols were employed to better understand the localization of BRCA1 staining. Protocol 1 yielded cells with greater polarized perinuclear compared to nuclear staining of BRCA1 (**Figure 1A**). This staining pattern suggested that the fixation and/or permeabilization step may have been too stringent. Triton X-100 is a detergent that is commonly used to improve antibody penetration by disrupting membranes, which is necessary for nuclear staining. It was one of several components evaluated to maximize BRCA1 detection. Different fixation and permeabilization reagents, primary and secondary antibody incubation conditions, as well as antibody choice and concentration play a role in the detection of localized BRCA1. Therefore, modifications were made to the protocol in an iterative manner, but the results still yielded similar staining characteristics (compare **Figure 1A** and **1B**). Further modifications were adapted from a protocol by Eckner et al, 1994 (Eckner et al., 1994) that added sucrose to the fixation to adjust for osmolarity and a pH buffered permeabilization that also adjusted for osmolarity. These changes yielded a predominantly nuclear staining (**Figure 1D**). Unfortunately, the signal to noise ratio was poor compared to the protocols that yielded the polarized perinuclear staining of BRCA1 despite lower primary and secondary antibody concentrations (compare **Figure 1D** with

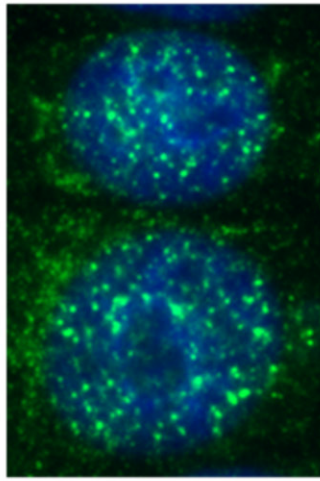
Figures 1A and 1B). The Eckner et al, 1994 protocol was further adjusted for incubation time and temperature, returned to a modified blocking reagent with detergent similar to Protocols 1 and 2, and added a treatment with NaBH₄ to help unmask antigens by reducing paraformaldehyde linkages. These changes improved the signal to noise ratio resulting in more distinct, punctate BRCA1 foci within the nucleus following DNA damage induced by IR (compare **Figure 1F** with **1A, 1B, and 1D**). As discussed in Chapter I, the presence of BRCA1 foci following exposure to IR indicates proper expression and localization of BRCA1 to sites of DNA damage. Finally, cells that have not been exposed to IR still stain for BRCA1 but in a more diffuse pattern (compare **Figure 1E and 1F**). The reagents and conditions established by Protocol 4 were kept constant for all subsequent staining of BRCA1 IRIF.

To determine the dose of IR that provides robust, punctate BRCA1 foci, MCF7 cells were exposed to varying doses of IR and stained with a BRCA1-specific antibody. Exposure to 10 and 20 Gy IR showed a greater percentage of cells with increased numbers of BRCA1 foci compared to 5 Gy (compare **Figures 2B and 2C** with **2A**). However, there was greater non-specific staining at 20 Gy than at 10 Gy (compare **Figure 2B and 2C**). Therefore, subsequent exposure to 10 Gy IR was selected for the primary screen of the kinase siRNA library.

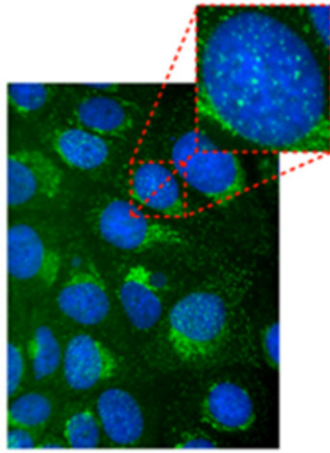
Before the arrival of the LSC, all immunostaining steps were performed on coverslips. Each coverslip was seeded with 5×10^4 MCF7 cells and immunostained following exposure to IR. With the arrival of the LSC, all immunostaining steps were performed in Whatman 96-well glass bottom plates. Conditions and protocols were maintained in the transition. Microscopy was used as a measure of readout because altered phenotypes with loss-of-function assays can be easily



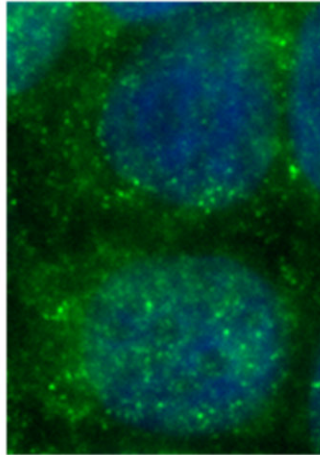
C



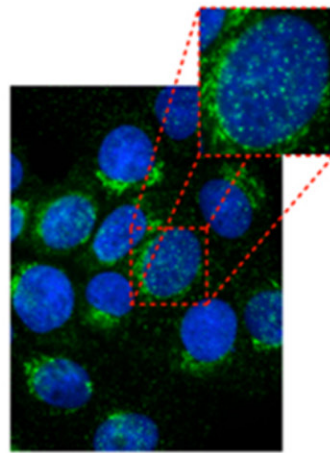
F



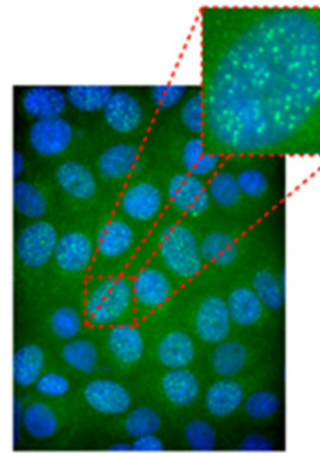
B



E



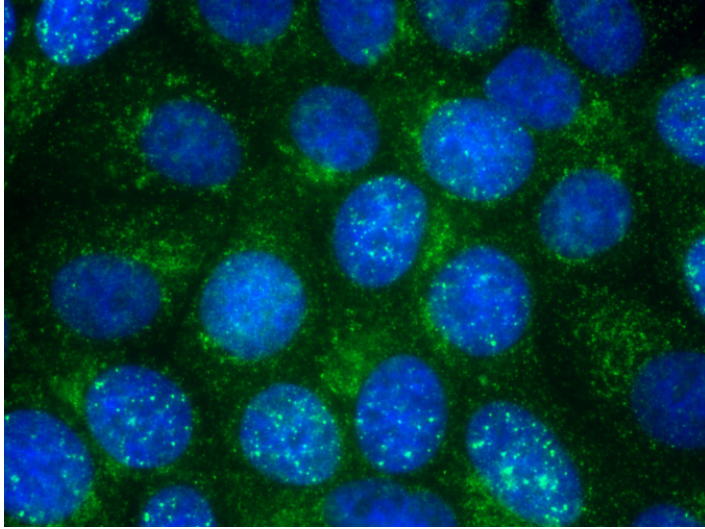
A



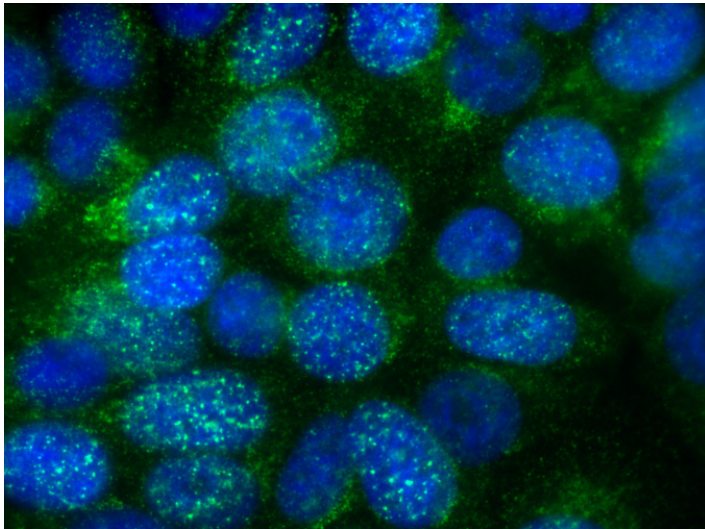
D

Figure 1: Staining optimization for BRCA1 IRIF following IR. All panels are a representative image of staining in MCF7 cells by the indicated protocol, exposure to IR, 1° anti-BRCA1 antibody dilution, and 2° AlexaFluor 488 goat anti-mouse IgG1 antibody dilution. BRCA1 is the green signal for IRIF formation and DAPI is the blue counterstain for the nucleus. Panel A used Protocol 1, 20 Gy IR, 1° antibody dilution of 1:100, and 2° antibody dilution of 1:100. Panel B used Protocol 2, 20 Gy IR, 1° antibody dilution of 1:100, and 2° antibody dilution of 1:400. Panel C used Protocol 2, 20 Gy IR, 1° antibody dilution of 1:250, and 2° antibody dilution of 1:1000. Panel D used Protocol 3, 20 Gy IR, 1° antibody dilution of 1:250 and 2° antibody dilution of 1:1000. Panel E used Protocol 4, unirradiated, 1° antibody dilution of 1:200 and 2° antibody dilution of 1:1000. Panel F used Protocol 4, 10 Gy IR, 1° antibody dilution of 1:200 and 2° antibody dilution of 1:1000.

A.



B.



C.

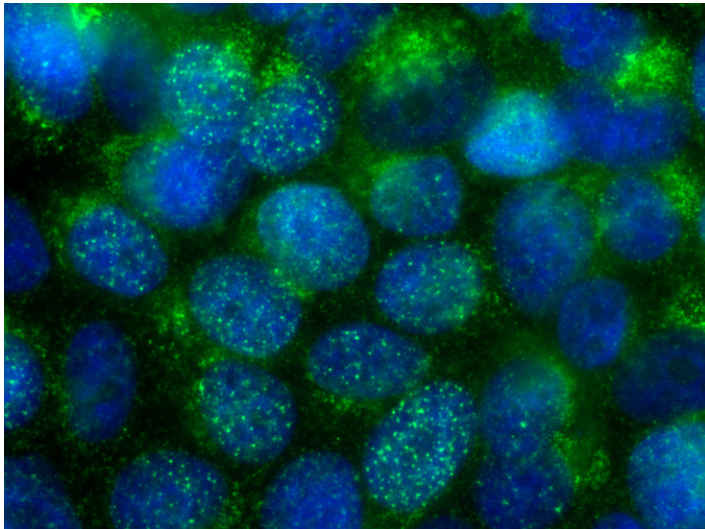


Figure 2: Effect of IR on BRCA1 IRIF formation. MCF7 cells were exposed to 5, 10, and 20 Gy IR and stained for BRCA1 (green) and counterstained with DAPI for the nucleus (blue) 8 h post-IR. Panel A shows a representative image of BRCA1 IRIF formation following exposure to 5 Gy IR. Panel B shows a representative image of BRCA1 IRIF formation following exposure to 10 Gy IR. Panel C shows a representative image of BRCA1 IRIF formation following exposure to 20 Gy IR.

visualized by immunofluorescence. With the LSC, parameters could be defined to collect for specific information concerning the IRIF formation.

An alternative approach that can be used to quantify foci is fluorescence resonance energy transfer (FRET) by flow cytometry. The basis for this approach involves the intentional excitation of one fluorochrome whose emission spectrum overlaps with the excitation spectrum of a second fluorochrome. The energy transfer that occurs will lead to the excitation of the second fluorochrome and the resulting emission can be measured. This approach would enable quantification of foci formation based on two proteins that are localized within the foci, which can facilitate investigation of the colocalization of BRCA1 with another interacting protein from one of the various macrocomplexes discussed in the Introduction chapter to assess a specific function. However, this transfer will only occur if the two fluorochromes are positioned within a certain distance of each other.

Cell Cycle Analyses: As discussed previously, exposure to IR leads to DSBs in the DNA. A network of proteins involved in the DNA damage checkpoint, including BRCA1, will recognize these abnormalities and initiate a signal cascade to elicit a cellular response. This cellular response includes activation of cell cycle checkpoints to stall progression to the next cell cycle phase as well as localization of repair proteins to these sites of damage. Preventing progression of the cell cycle ensures that a cell with a modification in its DNA does not have the capacity to undergo division and maintain the mutation until it can be repaired. But if the damage cannot be repaired, then the cell will undergo apoptosis, or programmed cell death, to ensure the integrity of the DNA. Thus, it is important to explore the effect of varying levels of IR on cell cycle progression as well as the effect of IR on BRCA1 IRIF formation. The goal was to define the cell

cycle profile of MCF7 cells to maximize the number of cells progressing through S, G₂ and M phases of the cell cycle to produce a robust BRCA1 IRIF signal.

To determine the effect of IR on cell cycle progression, increasing doses of IR were used. The levels of IR investigated were 0, 2, 5, 10, and 20 Gy. At the indicated times post-IR, cells were processed for cell cycle analysis. Cells that have not been exposed to IR show a fairly consistent ratio of cells in G₀/G₁ and S+G₂/M phases for all time points investigated (**Figure 3A**). As the level of IR increased, cells seemed to accumulate in S+G₂/M for longer periods of time, suggesting that cells were halted from progressing through the cell cycle to allow for repair and that a longer time for repair was needed with increasing IR dose (**Figures 3B-3E**). Approximately 30 DSBs per cell per Gy IR are believed to be produced (Iliakis, 1991; Stenerlow et al., 2003). Because BRCA1 foci are present during the S and G₂/M phases of cell cycle (Scully et al., 1997) and at most about 40% of unsynchronized cells are in S and G₂/M (**Figure 3**), cell synchronization was evaluated.

To determine when to stain for BRCA1 IRIF to maximize cell cycle progression of cells to S and G₂/M phases, both the time point following serum release to expose cells to IR and the time point following exposure to IR was determined. To determine the time point at which to expose cells to IR following serum release, MCF7 cells were synchronized by serum starvation for 30 h and then processed at the indicated time points for cell cycle analysis. Maximal % of cells in S and G₂/M occurred 24 h following serum release (**Figure 4**). To determine the time point at which to stain for BRCA1 IRIF, MCF7 cells were synchronized by serum starvation for 30 h followed by serum release for 24 h (as determined by the previous set of experiments). Cells were exposed to 20 Gy IR and then processed for cell cycle analysis. MCF7 cells were also left unsynchronized, exposed to 20 Gy IR, and processed for cell cycle analysis at the same time

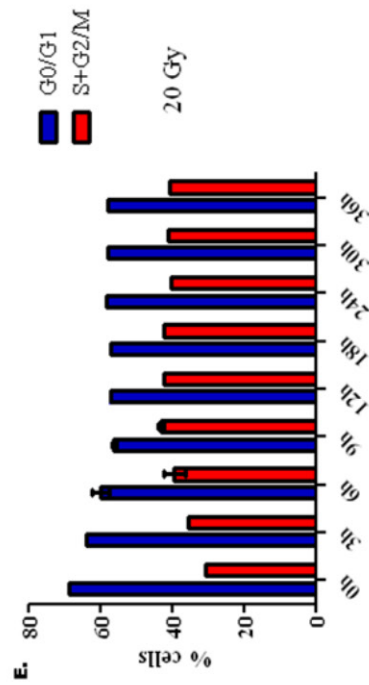
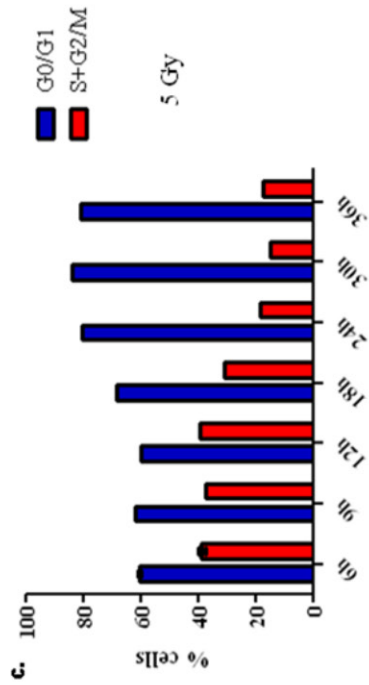
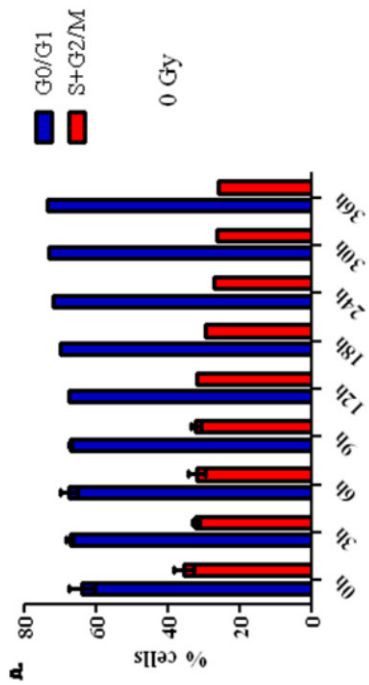
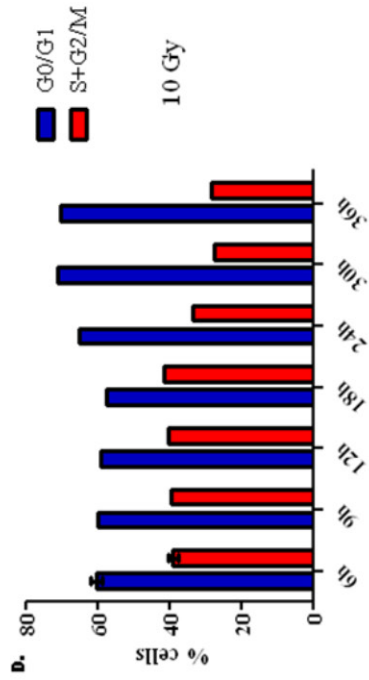
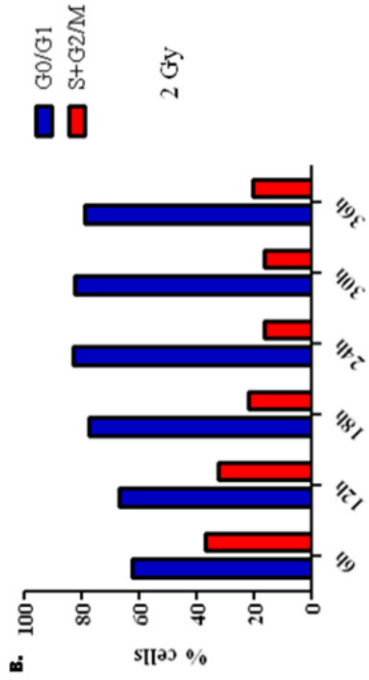


Figure 3: Cell cycle analysis to determine the dose of IR and time post-IR to stain for BRCA1 IRIF. MCF7 cells were exposed to varying doses of IR and allowed to recover for the indicated time points before cells were processed for cell cycle analysis with propidium iodide. Panel A = unirradiated cell, Panel B = 2 Gy IR, Panel C = 5 Gy IR, Panel D = 10 Gy IR, and Panel E = 20 Gy IR.

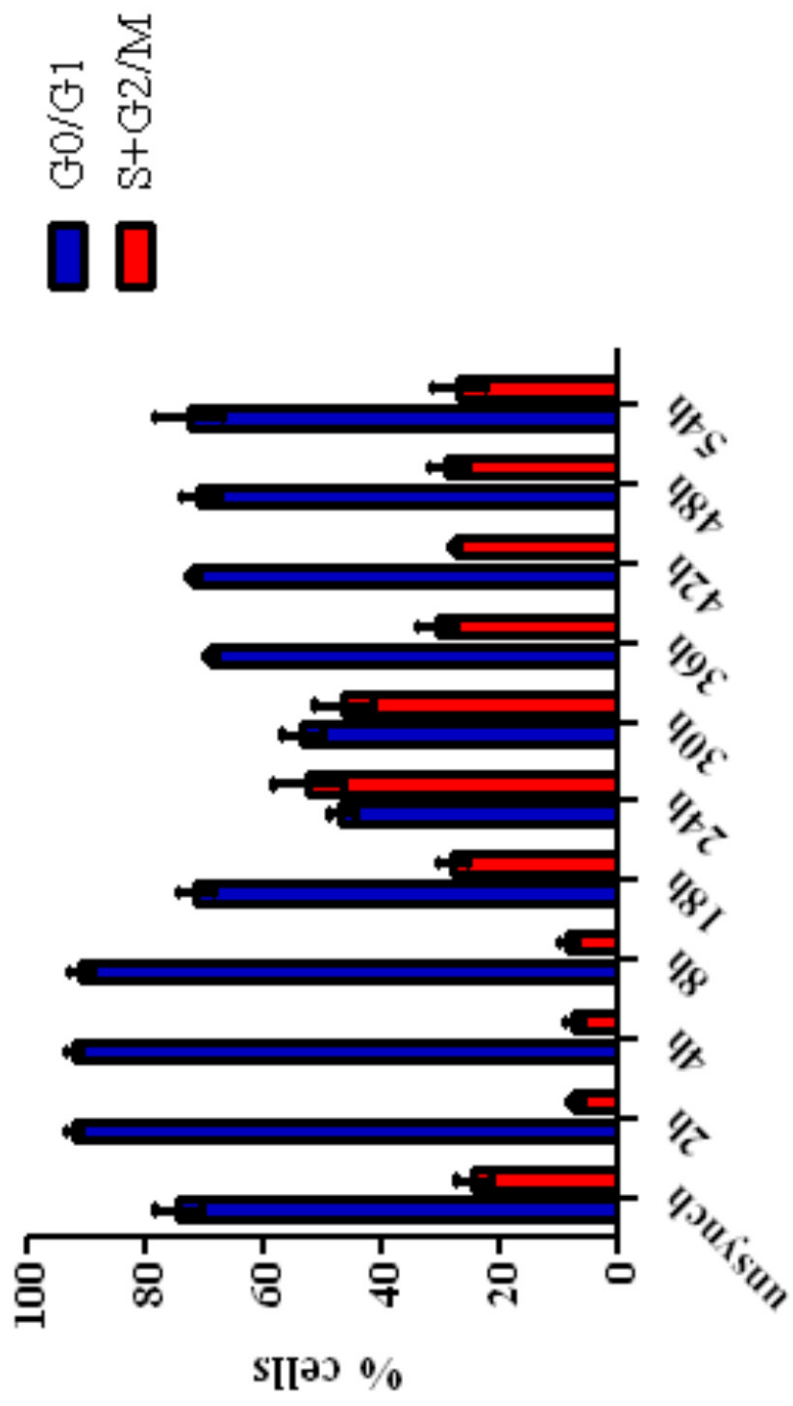


Figure 4: Cell cycle analysis to determine the time point following serum release to expose cells to IR. MCF7 cells were synchronized by serum starvation for 30 h and were processed at the indicated time points following serum release for cell cycle analysis with propidium iodide to determine the time point at which to expose cells to IR.

points or comparison. Cell synchronization enhanced the percent of cells in S and G₂/M phases of cell cycle (**Figure 5**). Based on BRCA1 foci kinetics and appearance during the S+G₂/M phases of cell cycle (Schlegel et al., 2006), the 6 h time point was chosen for all subsequent analyses.

Once siRNA transfection parameters were optimized (to be discussed), cell cycle analysis to determine the effect of Neg and BRCA1 siRNAs following cell synchronization and exposure to IR was completed. MCF7 cells were simultaneously transfected with either Neg or BRCA1 siRNAs by chemical transfection with RNAiMAX (Invitrogen) and then cell synchronized by one of two methods. Cell synchronization by serum starvation for 42 h followed by serum release for 24 h had been previously characterized. However, when these cells were stained for BRCA1 IRIF, few cells remained at the end of the staining process and those that remained did not exhibit robust BRCA1 IRIF formation (**Figure 6A**). Therefore, a modified synchronization protocol was employed using culture medium with reduced FBS (2% instead of 10%) and without antibiotics for 48 h followed by complete MEM with 10% FBS and without antibiotics for 18 h. Cells were subsequently exposed to 10 Gy IR and stained 6 h post-IR. This semisynchronization process proved more successful when stained for BRCA1 IRIF (compare **Figure 6B** and **6A**). Cell cycle analysis comparing the two synchronization methods yielded similar profiles (**Figure 7**). The modified semisynchronization method was maintained for all subsequent experiments because it demonstrated more robust BRCA1 IRIF staining with similar percentages of cells in S and G₂/M. Additionally, the semisynchronization of cells can maximize the number of cells transfected with siRNA (to be discussed) as well as cell cycle progression of cells to S and G₂/M compared to unsynchronized (compare **Figure 7A** and **5A**). As discussed

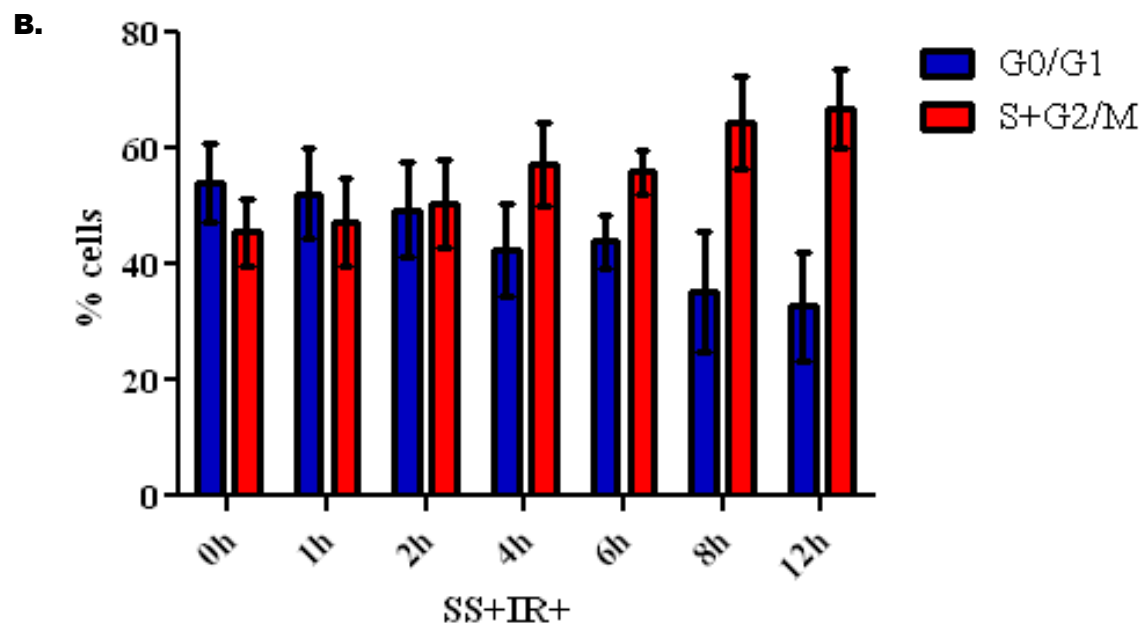
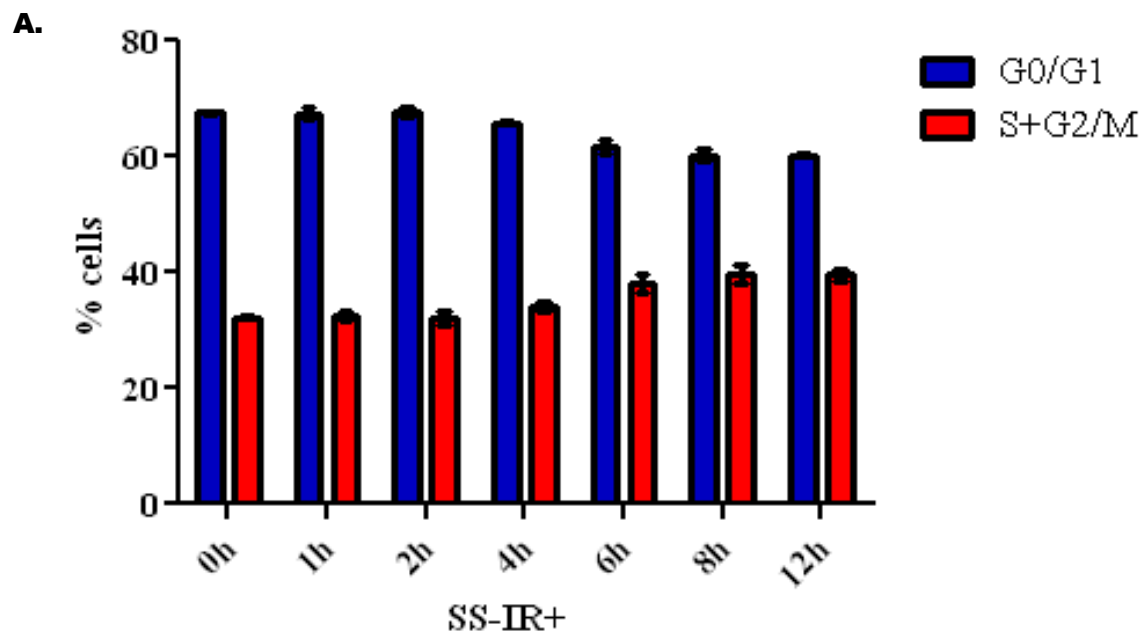
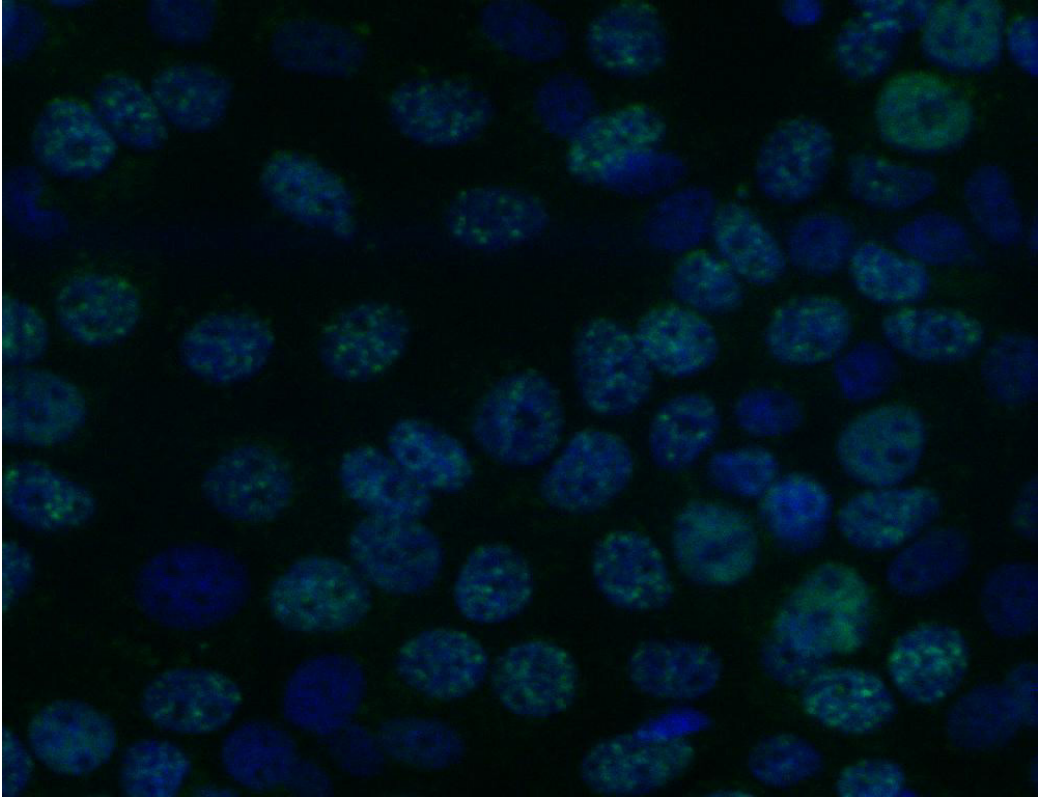


Figure 5: Cell cycle analysis to determine the time point following serum release and exposure to IR to stain for BRCA1 IRIF. MCF7 cells were either left unsynchronized (Panel A) or synchronized by serum starvation using complete MEM without FBS but supplemented with 0.05% BSA for 42 h followed by serum release in complete MEM with 20% FBS for 24 h (Panel B). Both populations were then exposed to 20 Gy IR and processed at the indicated time points post-IR for cell cycle analysis with propidium iodide to determine the time point at which to stain for BRCA1 IRIF. SS- = unsynchronized, SS+ = synchronized, and IR+ = irradiated.

A.



B.

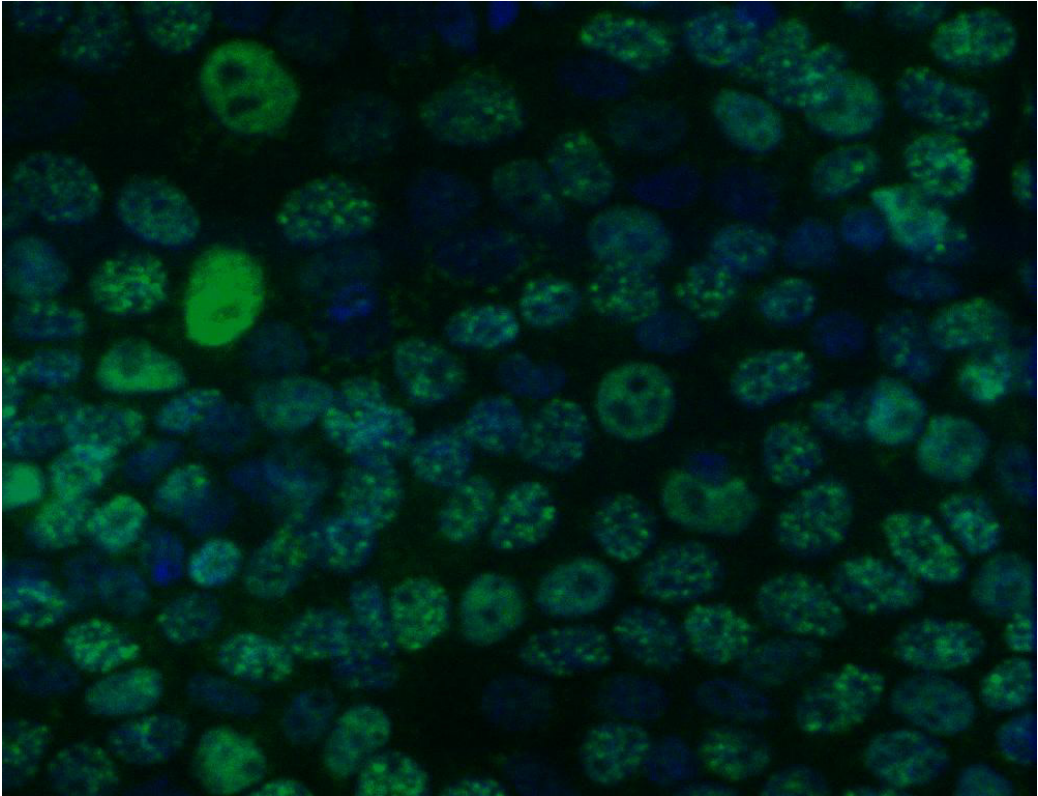


Figure 6: Comparison of BRCA1 IRIF formation in synchronized vs. semisynchronized MCF7 cells. MCF7 cells were either synchronized by serum starvation using complete MEM without FBS but supplemented with 0.05% BSA for 42 h followed by serum release in complete MEM with 20% FBS for 24 h (Panel A) or semisynchronized using culture medium with reduced FBS (2% instead of 10%) and without antibiotics for 48 h followed by complete MEM with 10% FBS and without antibiotics for 18 h (Panel B). Both populations were then exposed to 10 Gy IR and stained 6 h post-IR using anti-BRCA1 (green) and DAPI (blue).

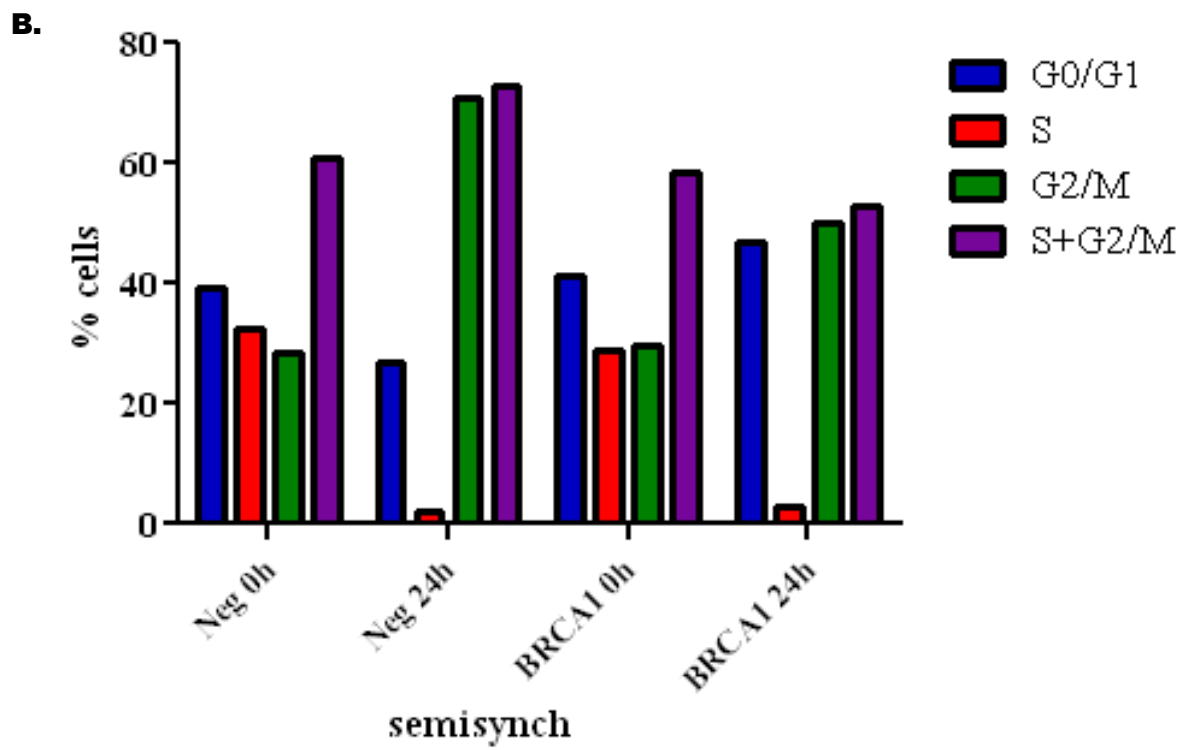
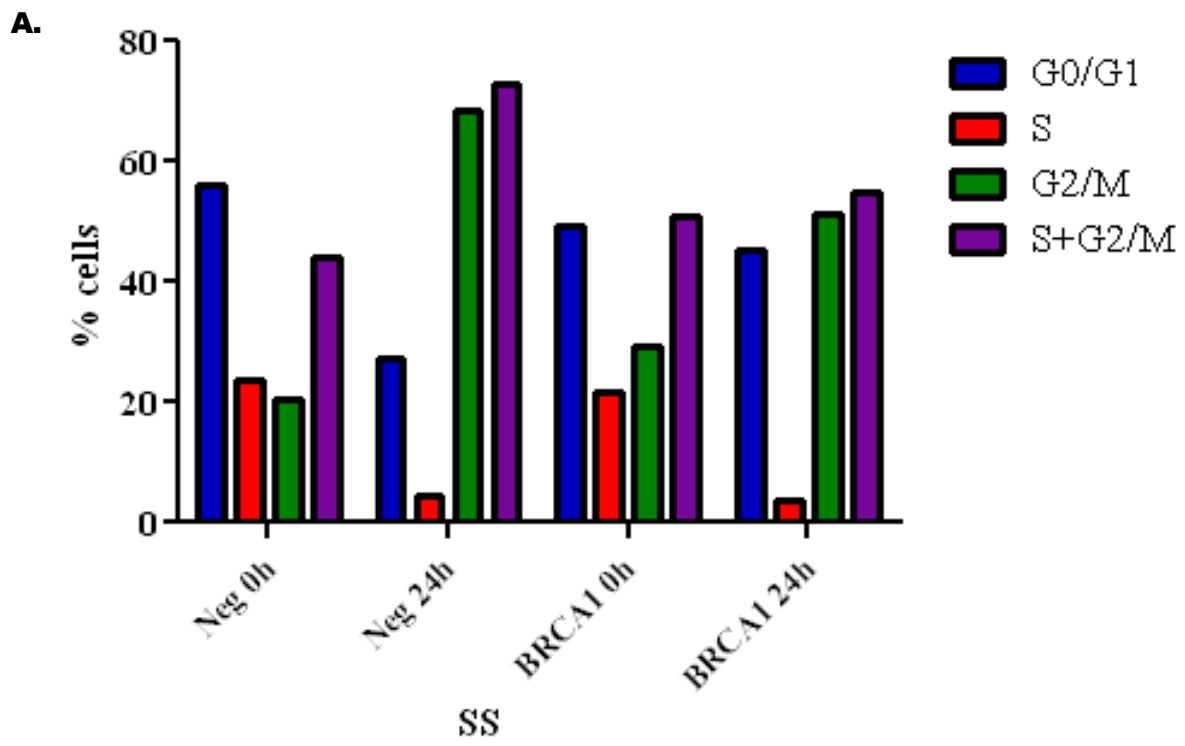


Figure 7: Analysis to determine the effect of Neg and BRCA1 siRNAs following cell synchronization and exposure to IR on cell cycle. MCF7 cells were either synchronized by serum starvation using complete MEM without FBS but supplemented with 0.05% BSA for 30 h followed by serum release in complete MEM with 20% FBS for 24 h (Panel A) or semisynchronized using culture medium with reduced FBS (2% instead of 10%) and without antibiotics for 48 h followed by complete MEM with 10% FBS and without antibiotics for 18 h (Panel B). Both populations were then exposed to 10 Gy IR and allowed to recover for the indicated time points before cells were processed for cell cycle analysis with propidium iodide.

previously, BRCA1 expression levels are dependent on the cell cycle; it is low in G₀/G₁, is induced at the G₁/S interface, and is increased throughout S and G₂/M (Chen et al., 1996). BRCA1 phosphorylation state also changes throughout the cell cycle as well in response to DNA damage (Thomas et al., 1997). Based on these observations, BRCA1 IRIF formation is dependent on both BRCA1 expression and phosphorylation.

siRNA Transfection Optimization: Experiments were performed to define the optimal transfection parameters in a 96-well plate format. The goal was to optimize these conditions to maximize specific gene knockdown and minimize transfection-associated toxicity in MCF7 cells. Conditions evaluated that affect transfection efficiency include choice of transfection agent, transfection agent volume, exposure to transfection agent, siRNA quantity, and cell density. Once these conditions were determined, they were kept constant between experiments to minimize variability.

A method known as reverse transfection was used to introduce siRNAs into cells. Cells are transfected with siRNA/transfection agent complexes as they adhere to a plate after trypsinization. This method bypasses the pre-plating step 24 h prior to transfection, thus saving valuable time. Initially, a GAPDH siRNA was used as the positive control. GAPDH is a housekeeping gene whose activity is not involved in DNA damage repair. Thus knockdown of its activity did not affect the study, but could be used as a measure of siRNA efficiency. A nontargeting Neg siRNA was used as the negative control. It is a scrambled sequence that has no significant homology to the human, mouse, or rat genome, so it should have no effect on GAPDH. Other controls used included a transfection agent-only control to identify the effects of

transfection agent alone on the cells and a buffer-only control to identify the effects of mock transfection on the cells.

The KDAlert GAPDH Assay Kit was recommended by Ambion as a more cost- and time-effective means of assessing siRNA delivery efficiency compared to qRT-PCR. This fluorescence-based assay was capable of determining both GAPDH siRNA-induced knockdown and transfection induced cytotoxicity. GAPDH siRNA-induced knockdown was determined by comparing GAPDH enzymatic activity (as measured by the conversion of NAD^+ to NADH by GAPDH in the presence of phosphate and its substrate glyceraldehyde-3-phosphate) in cells transfected with GAPDH siRNA to those transfected with a negative control siRNA. Data interpretation was provided per manufacturer's protocol. The optimal balance factor (OBF) was a way to describe and select for the parameter(s) that yield the greatest knockdown with the least effect on GAPDH activity of the Neg siRNA (Equation 3). Each new parameter tested used the conditions with the highest OBF from the previous optimization step. This method was used to determine the optimized combination of parameters for siRNA knockdown.

Chemical transfection of siRNA into MCF7 cells initially proved inefficient. Parameters evaluated to optimize knockdown using siPORT NeoFX (Ambion) included transfection agent volume, siRNA concentration, and amount of time for efficient knockdown. The conditions were tested in a 96-well plate, using 8×10^3 MCF7 cells/well with a validated GAPDH siRNA and Neg control siRNA. The GAPDH enzyme activity was assessed using the KDAlert GAPDH Assay Kit (Ambion). The rationale was that decreased GAPDH mRNA would result in decreased GAPDH enzyme, so when the reaction substrates were added, the measured activity would be lower in cells transfected with the GAPDH siRNA. However, no combination of parameters with the GAPDH siRNA was able to reduce the expression levels by $\geq 70\%$ compared to the Neg siRNA

(**Table 1**). Other transfection agents were also evaluated but yielded poor knockdown when assessed by either GAPDH activity or qRT-PCR (**Table 2**).

A FAM-labeled siRNA was then used to assess transfection efficiency by chemical transfection with siPORT NeoFX as described previously. The goal of this study was to determine whether the poor knockdown observed was a consequence of the inability of the transfection agent:siRNA complexes to enter the cell or a failure of the complexes to act on the mRNA target. The only difference between the control well and the experimental well was addition of the FAM-labeled siRNA to the experimental well. A blue laser 488 nm was used to measure the FAM fluorescent signal and images were taken using a 40X objective on a Nikon inverted fluorescence microscope. The transfection agent:siRNA complexes do not appear to cross the membrane (**Figure 8**). Fluorescence was mostly observed outside the cells, suggesting that the poor knockdown observed was a consequence of the inability of siRNA to enter the cells by siPORT NeoFX.

Another method of transfection called electroporation was explored. In contrast to the chemical transfection of siRNAs, transfection of siRNAs using electroporation proved more successful. Similar combinations of parameters were assessed to enable a direct comparison of the two techniques. Nucleofection involved the delivery of an electrical pulse to induce uptake of the siRNAs, which required that the process occur within a specially formulated buffer with a greater number of cells to ensure survival. GAPDH enzyme activity was again measured following electroporation with GAPDH and Neg control siRNAs. The conditions were tested in a 96-well plate, using 1×10^5 MCF7 cells/well with a validated GAPDH siRNA and Neg control siRNA (Ambion). The GAPDH enzyme activity was assessed using the KDAlert GAPDH Assay Kit (Ambion). Knockdown of GAPDH activity improved over time and approached the

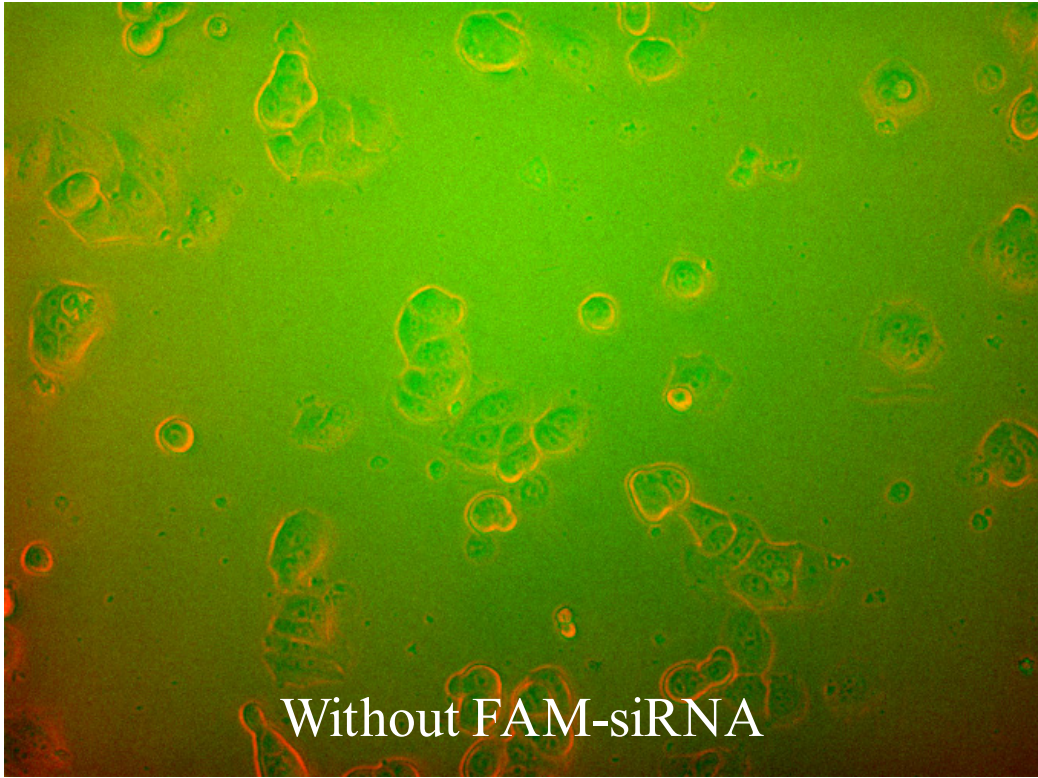
siPORT NeoFX Volume (µl)			Final siRNA Concentration (nM)				Percent Remaining Expression		
	0.3	0.6	1.0	1	10	30	48 h	72 h	
	X			X			83.8 ± 34.1%	92.4 ± 19.3%	
	X				X		87.3 ± 33.6%	94.0 ± 12.8%	
	X					X	91.1 ± 37.1%	95.1 ± 23.2%	
		X		X			89.5 ± 33.7%	84.4 ± 18.2%	
		X			X		81.0 ± 29.1%	79.8 ± 12.8%	
		X				X	83.1 ± 35.5%	88.1 ± 28.7%	
			X	X			93.4 ± 33.4%	91.0 ± 17.6%	
			X		X		84.4 ± 39.4%	78.6 ± 20.9%	
			X			X	79.6 ± 38.6%	77.9 ± 14.8%	

Table 1: Representative data of siRNA-mediated knockdown by chemical transfection with siPORT NeoFX. Either Neg or GAPDH siRNAs (Ambion) at the indicated final siRNA concentrations were introduced into 8×10^3 MCF7 cells/well in a 96-well plate using siPORT NeoFX (Ambion) at the indicated volumes. The medium was changed 24 h after transfection and analysis was completed using the KDaIert GAPDH Assay Kit (enzymatic reaction, Ambion) at the indicated times. The Neg siRNA served as a control for GAPDH activity.

Transfection Agent	Transfection Agent Volume (µl)	Final siRNA Concentration (nM)	Percent Remaining Expression
siPORT Amine	0.15	10	113.1 ± 21.9%
siPORT Amine	0.3	10	109.2 ± 26.1%
siPORT Amine	0.6	10	69.6 ± 32.1%
siPORT Amine	1.2	10	59.9 ± 19.7%
XtremeGENE	0.2	22	77.4 ± 31.3%
		67	104.4 ± 26.6%
		133	77.8 ± 7.8%
XtremeGENE	0.8	22	114.0 ± 47.8%
		67	92.3 ± 20.3%
		133	78.2 ± 24.3%
XtremeGENE	2	22	64.8 ± 18.2%
		67	52.4 ± 7.6%
		133	64.7 ± 17.7%
Lipofectamine 2000	0.5	100	69.7 ± 2.2%

Table 2: Representative data of siRNA-mediated knockdown by chemical transfection with siPORT Amine (Ambion), XtremeGENE (Roche), and Lipofectamine 2000 (Invitrogen). Either Neg or GAPDH siRNAs (Ambion) at the indicated final siRNA concentrations were introduced into 8×10^3 MCF7 cells/well in a 96-well plate using siPORT Amine or 1×10^4 MCF7 cells/well in a 96-well plate using XtremeGENE at the indicated volumes. Either Neg or BRCA1 siRNAs (Ambion) at the indicated final siRNA concentration were introduced into 1×10^4 MCF7 cells/well in a 96-well plate using Lipofectamine 2000 at the indicated volume. The medium was changed 24 h after transfection and analysis was completed 48 h after transfection using either the KDatert GAPDH Assay Kit (enzymatic reaction, Ambion) for siPORT Amine and XtremeGENE or qRT-PCR for Lipofectamine 2000. The Neg siRNA served as a control for either GAPDH activity or BRCA1 expression.

A.



B.

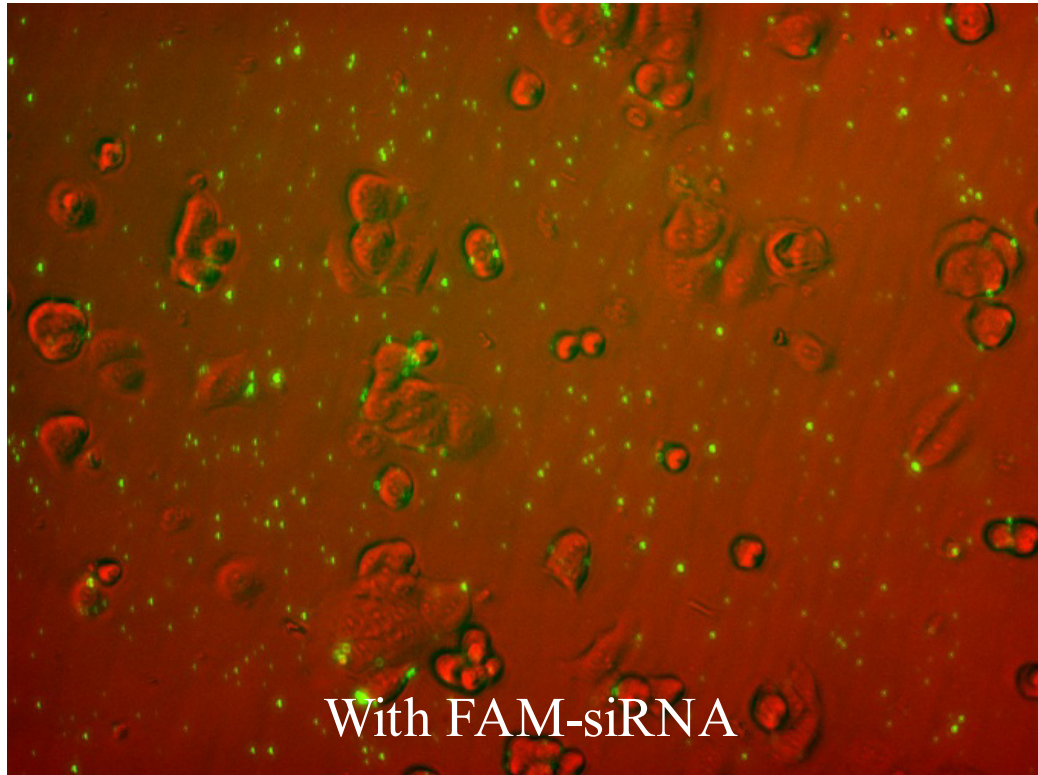


Figure 8: A FAM-labeled siRNA (green) was used to monitor transfection efficiency by chemical transfection with siPORT NeoFX. Panel A shows cells that were treated with siPORT NeoFX transfection agent alone. Panel B shows cells that were treated with FAM-siRNA:siPORT NeoFX transfection agent complexes. Images were taken on a Nikon inverted fluorescence microscope, 40X.

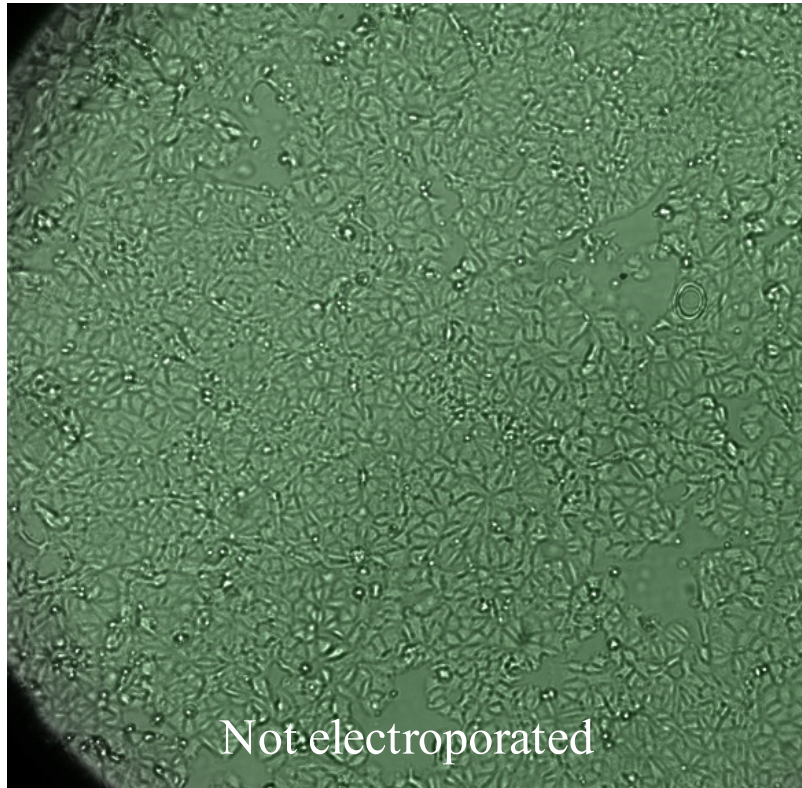
recommended percent remaining expression of $\leq 30\%$ with all siRNA concentrations tested (**Table 3**). A 72 hour analysis time point was selected for subsequent experiments to ensure sufficient knockdown of target mRNA. Efficient knockdown was corroborated using a vector pmaxGFP to monitor transfection efficiency. The only difference between the control well and the experimental well was the delivery of an electrical pulse to the experimental well. A blue laser 488 nm was used to measure the GFP fluorescent signal and images were taken using a 10X objective on the Olympus inverted fluorescence microscope. The majority of electroporated cells appear to express pmaxGFP (**Figure 9**), indicating improved transfection efficiency compared to chemical transfection. Transfection efficiency was $\geq 80\%$ after 24 h as measured on the BD FACSCalibur (data not shown). Similar success in knockdown of GAPDH mRNA was demonstrated using qRT-PCR 72 h following electroporation with a GAPDH siRNA according to the protocol described above (**Figure 10**). Knockdown of BRCA1 mRNA was also demonstrated using qRT-PCR 72 h following electroporation with a BRCA1 siRNA (**Figure 11**).

A differential BRCA1 IRIF phenotype has been demonstrated in cells electroporated with Neg siRNA compared to BRCA1 siRNA. Following nucleofection, cells were incubated for 66 h before being exposed to 10 Gy IR. Cells were allowed to recover for 6 h and then were immunostained with an anti-BRCA1 antibody for BRCA1 IRIF and DAPI for the nucleus. A blue laser 488 nm was used to measure the BRCA1 fluorescence signal while a violet laser 405 nm was used to measure the DAPI fluorescence signal. Cells were then imaged using a 40X objective on the Olympus inverted fluorescence microscope. Both BRCA1 fluorescence intensity and number of IRIF are greatly diminished as a result of siRNA-mediated knockdown of BRCA1 following transfection by electroporation compared to the Neg control (**Figure 12**). However, there was a significant difference in cell morphology and numbers when comparing cells minus

Final siRNA Concentration (nM)				Percent Remaining Expression			
1	10	30	50	24 h	48 h	72 h	
X				57.8 ± 21.0%	45.4 ± 16.4%	30.6 ± 15.8%	
	X			71.0 ± 13.6%	45.6 ± 13.6%	33.4 ± 11.3%	
		X		70.3 ± 23.4%	41.0 ± 7.4%	32.3 ± 17.0%	
			X	67.4 ± 23.0%	38.0 ± 16.8%	23.6 ± 10.0%	

Table 3: Representative data of siRNA-mediated knockdown following transfection by electroporation. Either Neg or GAPDH siRNAs (Ambion) at the indicated final siRNA concentrations were introduced into 1×10^5 MCF7 cells/well in a 96-well plate using the Nucleofector 96-well Shuttle System, Program 96-EN-130 (Amaxa). The medium was changed 24 h after transfection and analysis was completed using Ambion's KDalet GAPDH Assay Kit (enzymatic reaction, Ambion) at the indicated times. The Neg siRNA served as a control for GAPDH activity.

A.



B.

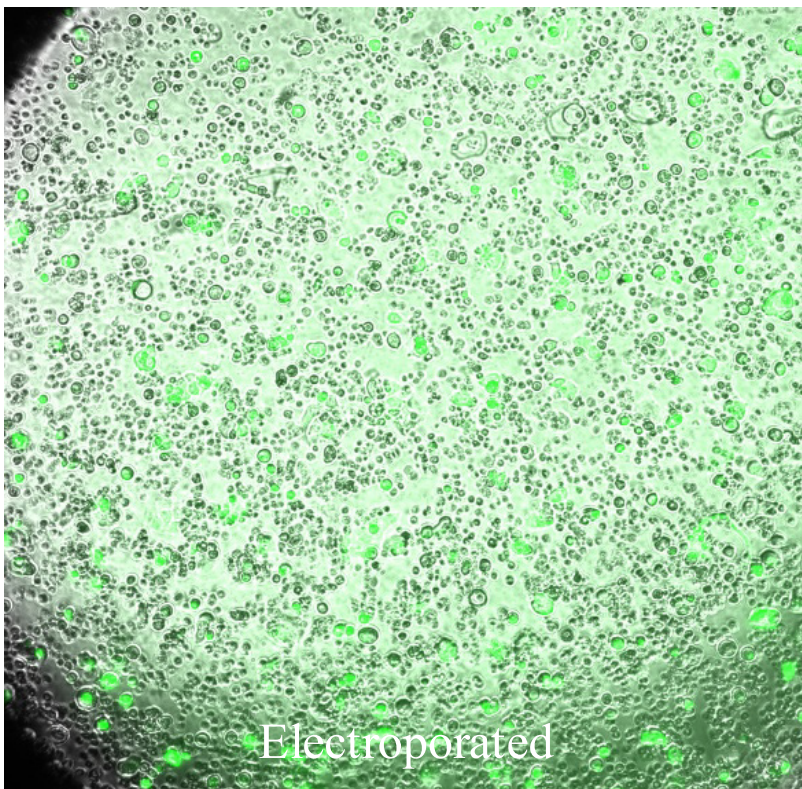


Figure 9: A vector pmaxGFP (green) was used to monitor transfection efficiency following transfection by electroporation. Panel A shows cells with pmaxGFP that were not pulsed in the Amaxa Nucleofector system. Panel B shows cells with pmaxGFP that were pulsed in the Amaxa Nucleofector system. Images were taken on an Olympus inverted fluorescence microscope, 10X.

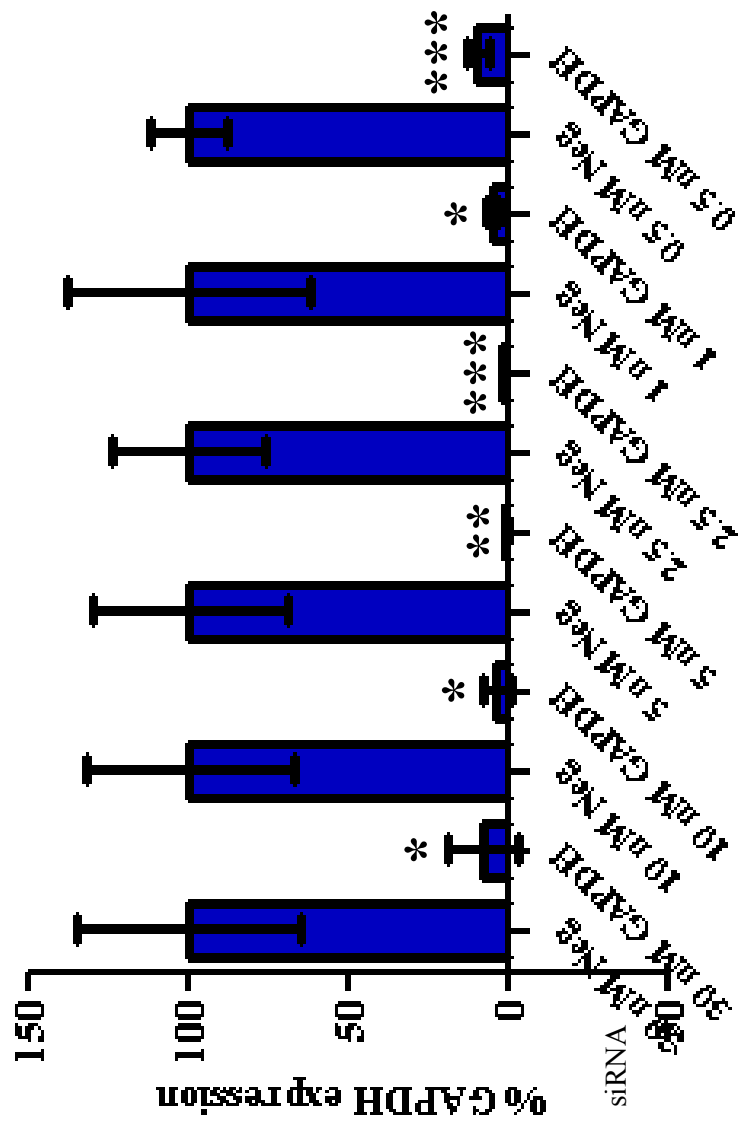


Figure 10: Analysis of GAPDH mRNA levels by qRT-PCR following transfection by electroporation. Either Neg or GAPDH siRNAs (Ambion) at the indicated final siRNA concentrations were introduced into 1×10^5 MCF7 cells/ well in a 96-well plate using the Nucleofector 96-well Shuttle System, Program 96-EN-130 (Amaxa). The medium was changed 24 h after transfection and analysis was completed 48 h post-transfection. Data are presented as an average of the siRNA \pm standard error (n=3 for 5, 2.5, and 1 nM; n=2 for 30, 10, and 0.5 nM). * denotes $P \leq 0.0315$, ** denotes $P = 0.0037$, *** denotes $P \leq 0.0005$. The Neg siRNA served as a control for GAPDH expression.

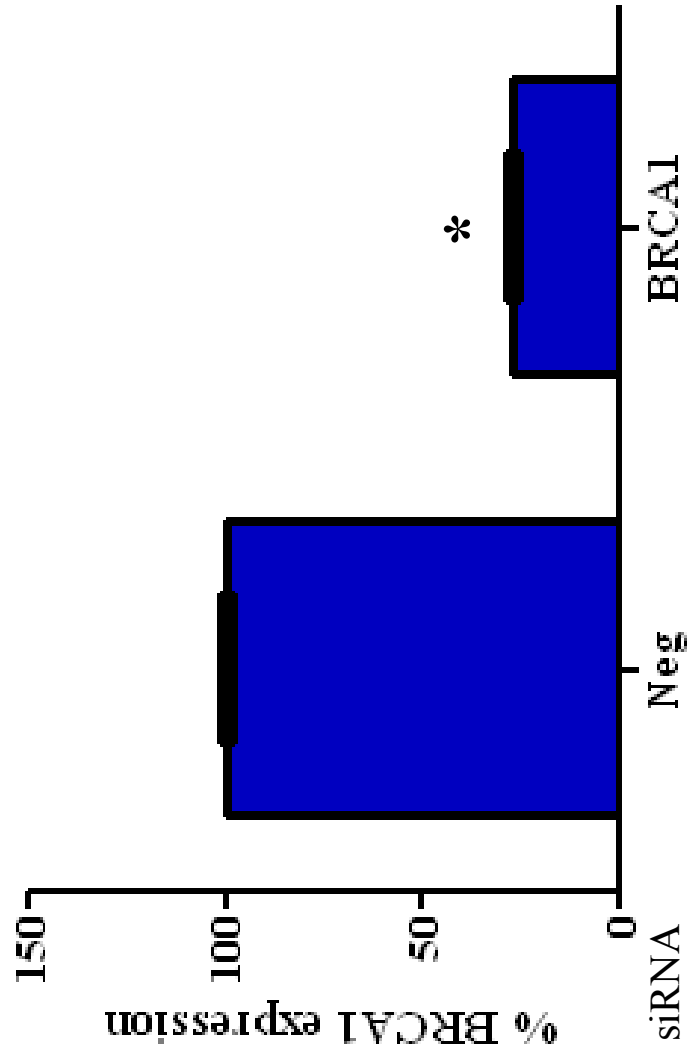
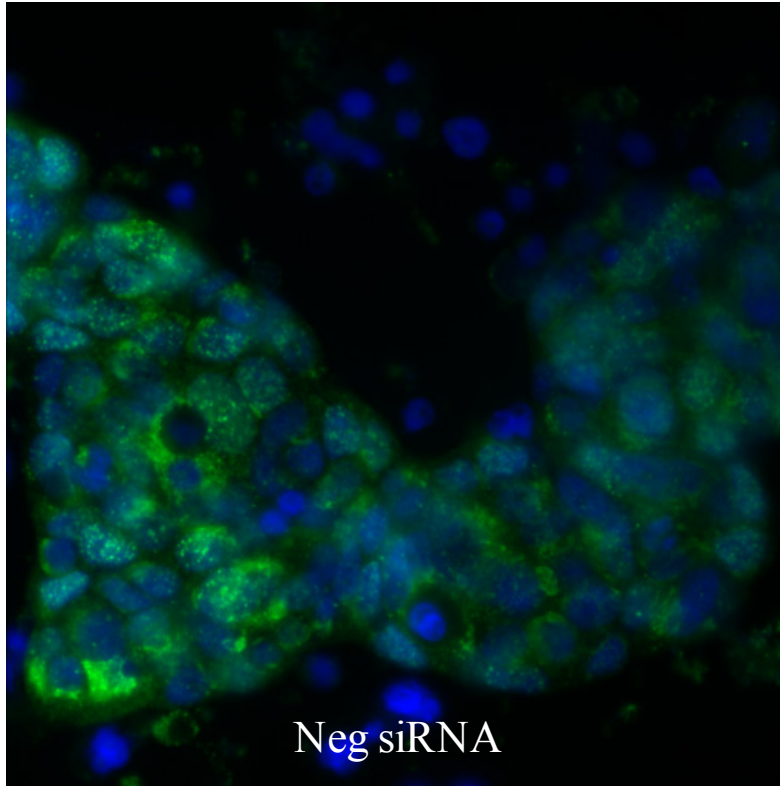


Figure 11: Analysis of BRCA1 mRNA levels by qRT-PCR following transfection by electroporation. Either Neg or BRCA1 siRNAs (Ambion) at 10 nM final siRNA concentration were introduced into 1×10^5 MCF7 cells/ well in a 96-well plate using the Nucleofector 96-well Shuttle System, Program 96-EN-130 (Amaxa). The medium was changed 24 h after transfection and analysis was completed 48 h post-transfection. Data are presented as an average of the siRNA \pm standard error (n=5). * denotes $P < 0.0001$. The Neg siRNA served as a control for BRCA1 expression.

A.



B.

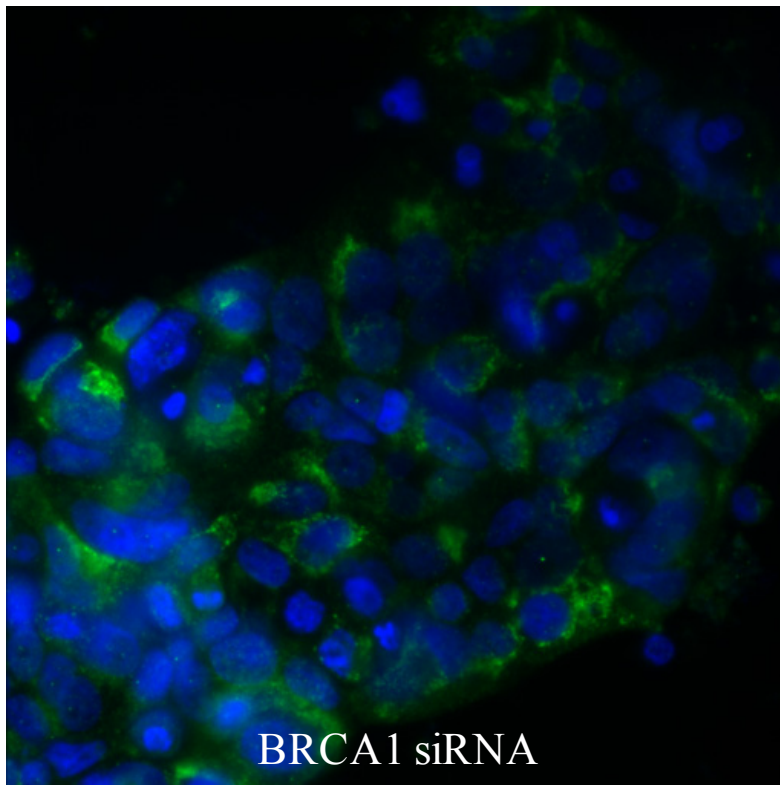


Figure 12: Representative fluorescence images of MCF7 cells following transfection by electroporation. Either Neg (Panel A) or BRCA1 (Panel B) siRNAs (Ambion) at 10 nM final siRNA concentration were introduced into 1×10^5 MCF7 cells/ well in a 96-well plate using the Nucleofector 96-well Shuttle System, Program 96-EN-130 (Amaxa). The medium was changed 24 h after transfection and analysis was completed 72 h post-transfection. Cells were then exposed to 10 Gy IR, allowed to recover for 6 h, and then immunostained with an anti-BRCA1 antibody (green) for BRCA1 IRIF and counterstained with DAPI for the nucleus (blue).

siRNA that underwent the nucleofection program with cells minus siRNA that were not electroporated. MCF7 cells are epithelial and they spread as they adhere to a surface; however, following the nucleofection program, the cells tended to remain balled up and were prone to be washed away during the staining process. Therefore, the optimization of parameters for chemical transfection was revisited.

Chemical transfection of siRNAs in MCF7 cells with the Lipofectamine RNAiMAX (Invitrogen, Carlsbad, CA) transfection reagent provided the greatest success. Transfection conditions that have consistently resulted in $\geq 70\%$ knockdown were 60 nM final siRNA concentration, 1 μ l RNAiMAX/ 5×10^4 cells, incubation of siRNA and transfection reagent for 16 min at RT, and 72 h incubation at 37°C, 5% CO₂ humidified atmosphere prior to analysis. The medium was replaced after 24 h incubation with complete medium without antibiotics and reduced FBS (2% instead of 10%) and again 24 h later with complete medium without antibiotics. Cells were exposed to 10 Gy IR 66 h following transfection and allowed to recover for 6 h. Following reverse transfection with BRCA1 siRNA (assay-specific positive control) and RNAiMAX, BRCA1 mRNA and protein levels were considerably reduced compared to the Neg siRNA (assay-specific negative control) (**Figures 13 and 14**). In addition, these conditions resulted in diminished BRCA1 IRIF formation (**Figure 15**). These data suggest that BRCA1 siRNA leads to knockdown of BRCA1 mRNA levels and subsequent reduction of BRCA1 protein levels such that significantly fewer BRCA1 IRIF form at sites of DSBs following exposure to ionizing radiation. Results from these studies defined the appropriate parameters for the functional BRCA1 assay and provided a baseline for comparison with BRCA1 mRNA and protein levels following siRNA knockdown of a potential regulator of BRCA1 expression.

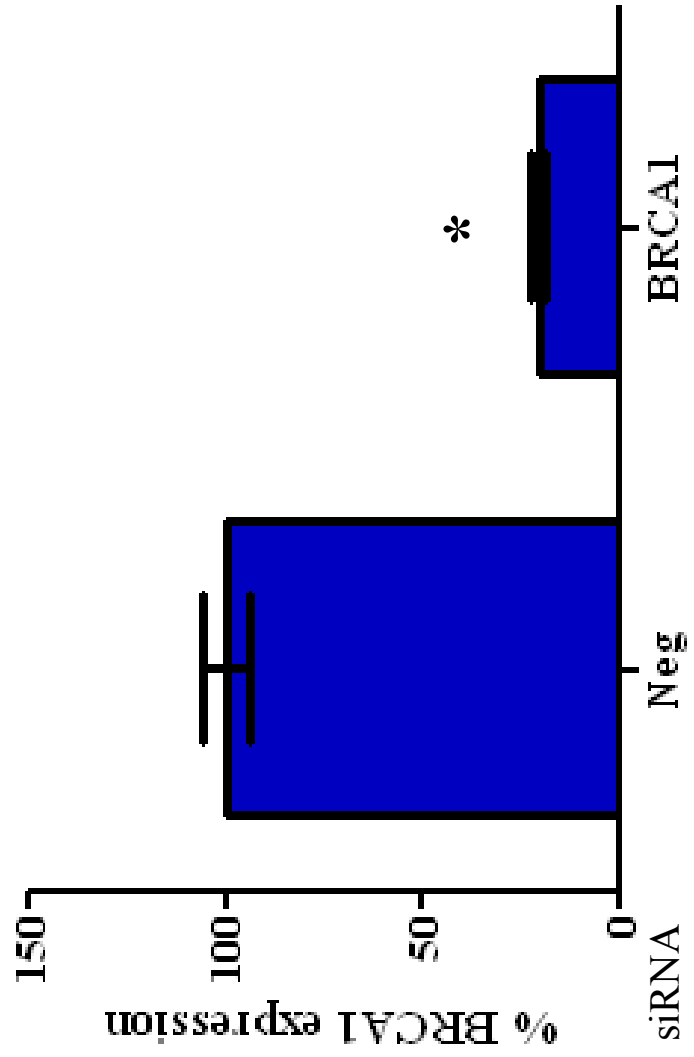
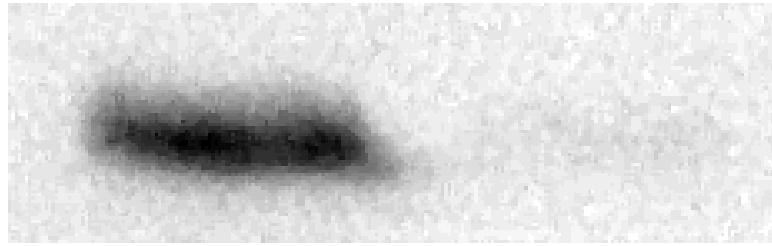


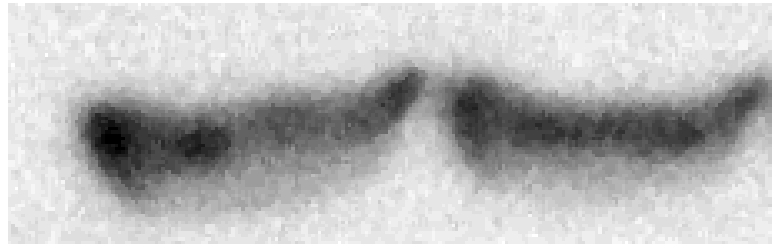
Figure 13: Analysis of BRCA1 mRNA levels by qRT-PCR following chemical transfection with RNAiMAX. Either Neg or BRCA1 siRNAs (Ambion) at 60 nM final siRNA concentration were introduced into 5×10^4 MCF7 cells/well in a 96-well plate using 1 μ l RNAiMAX (Invitrogen)/ 5×10^4 cells. siRNA:RNAiMAX complexes were incubated for 16 min prior to addition of cells. Analysis was completed 48 h post-transfection. Data are presented as an average of the siRNA \pm standard error (n=3). * denotes $P < 0.0001$.

A.

WB: BRCA1
220 kDa



WB: Actin
42 kDa



siRNA

Neg

BRCA1

B.

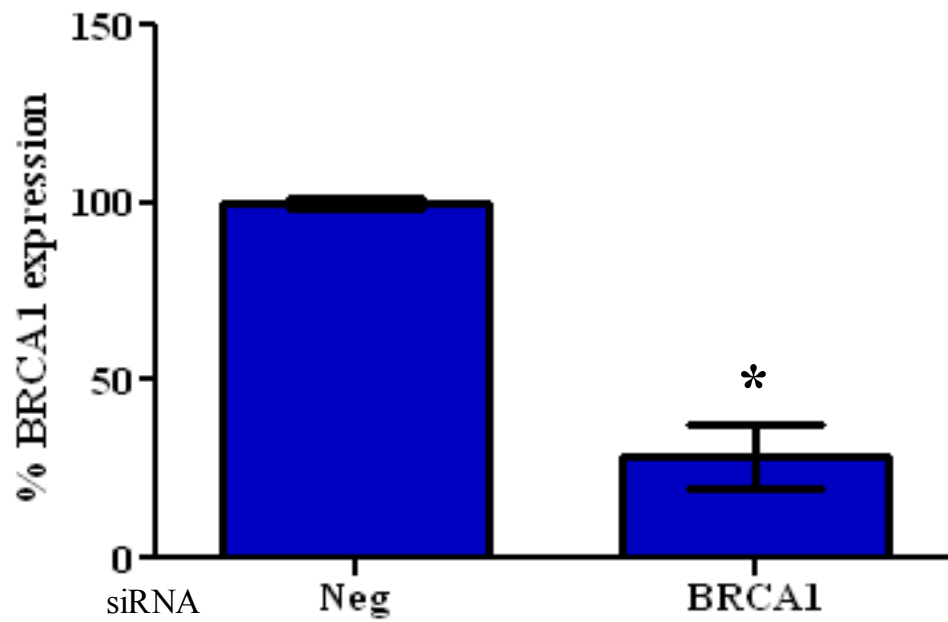
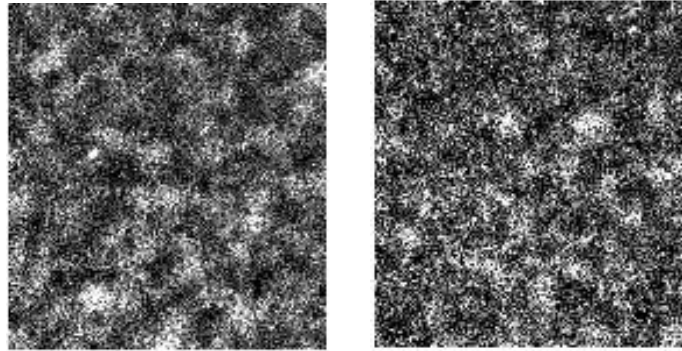


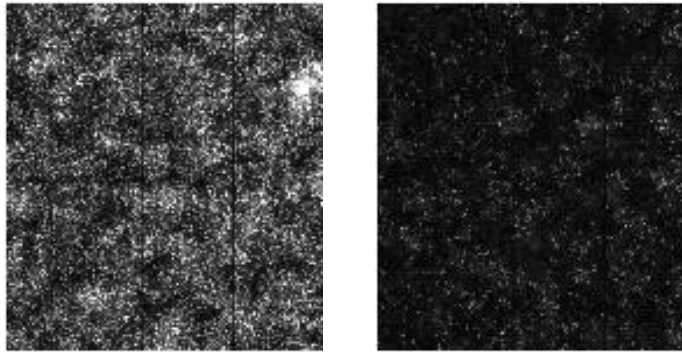
Figure 14: Analysis of BRCA1 protein levels by Western blot following chemical transfection with RNAiMAX. Either Neg or BRCA1 siRNAs (Ambion) at 60 nM final siRNA concentration were introduced into 5×10^4 MCF7 cells/well in a 96-well plate using 1 μ l RNAiMAX (Invitrogen)/ 5×10^4 cells. siRNA:RNAiMAX complexes were incubated for 16 min prior to addition of cells. Analysis was completed 72 h post-transfection. Panel A is representative Western blots for BRCA1 and actin (served as loading control) following siRNA-mediated knockdown of BRCA1 and Panel B shows densitometry for the indicated samples. Data are presented as an average of the siRNA \pm standard error (n=10). * denotes $P < 0.0001$.

A.

DAPI



BRCA1



siRNA

Neg

BRCA1

B.

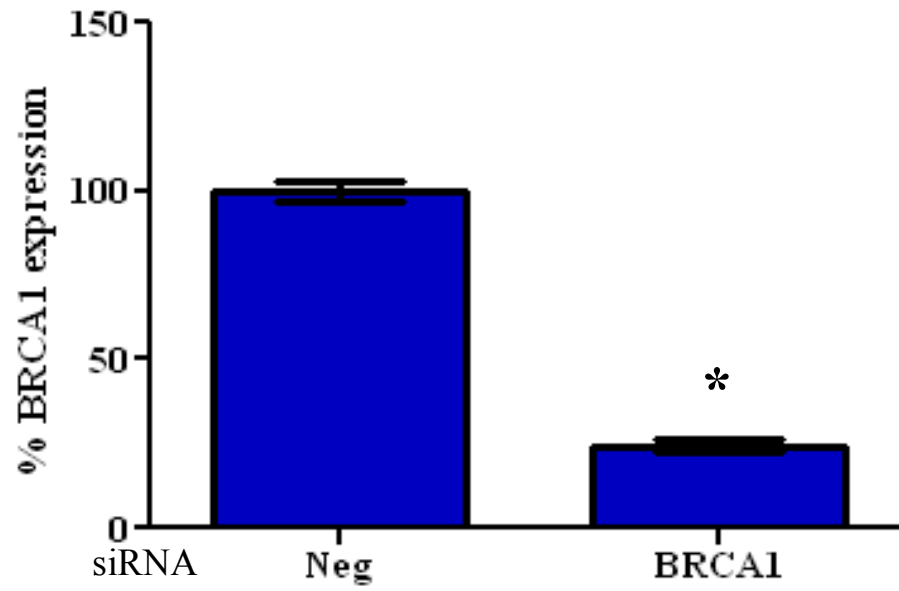


Figure 15: Analysis of BRCA1 IRIF formation by the LSC following chemical transfection with RNAiMAX. Either Neg or BRCA1 siRNAs (Ambion) at 60 nM final siRNA concentration were introduced into 5×10^4 MCF7 cells/well in a 96-well plate using 1 μ l RNAiMAX (Invitrogen)/ 5×10^4 cells. siRNA:RNAiMAX complexes were incubated for 16 min prior to addition of cells. Analysis was completed 72 h post-transfection. Cells were exposed to 10 Gy IR and stained with anti-BRCA1 antibody for BRCA1 IRIF and DAPI for the nucleus. Panel A shows representative images obtained using the LSC. Panel B shows relative BRCA1 expression for the Neg and BRCA1 siRNAs. Data are presented as an average of the siRNA \pm standard error (n=14). * denotes $P < 0.0001$.

RNAi technology is a powerful genetic tool that can selectively knockdown the expression of one gene by targeting its mRNA for degradation. The rationale for using chemically synthesized siRNA is their specificity for the target mRNA. In addition, they are commercially available for the entire genome or for select gene families. They were designed using a stringent algorithm to ensure specificity and many have been validated for gene knockdown. They can be easily taken up by MCF7 cells using the established chemical transfection protocol. Finally, siRNAs provide the ability to evaluate the effect of one gene's knockdown on BRCA1's ability to form IRIF in a timely manner.

Kinase siRNA Library Screen and Validation: The rationale for developing the functional BRCA1 assay together with RNAi technology is that ionizing radiation-induced foci formation can be easily visualized and any disturbances to foci formation may be due to dysregulation at any point of BRCA1 gene expression or activity. The effect of siRNAs targeting kinases was evaluated because there could be signal transduction pathways involving kinases that are activated and result in regulation of BRCA1 expression or kinases that are involved in phosphorylating BRCA1 and inducing its activity. This approach may prove instrumental in gaining a better understanding of the regulation of BRCA1 expression and function because downstream effects can be assessed from the potential dysregulation introduced into a cell-based system with a siRNA targeting a kinase that may be necessary for BRCA1 IRIF formation and DNA damage repair.

Once experimental parameters for the BRCA1 functional assay were optimized, a *Silencer*® Kinase siRNA Library from Ambion was screened. Using the ability of BRCA1 to form IRIF following the siRNA-mediated knockdown of kinases and induction of DNA damage

(**Figure 16A**), potential kinase regulators of BRCA1 expression and function could be identified. If knockdown of a kinase resulted in decreased BRCA1 foci formation, then that kinase was identified as a potential positive regulator of BRCA1 because its presence promotes foci formation while its absence inhibits foci formation. Likewise, if knockdown of a kinase resulted in increased BRCA1 foci formation, then that kinase was identified as a potential negative regulator of BRCA1 since its presence inhibits foci formation while its absence promotes foci formation (**Figure 16B**).

Three different siRNAs for each kinase were examined for BRCA1 IRIF formation 72 h following reverse transfection with RNAiMAX. The three different siRNAs were tested individually by plating in the same position in three separate 96-well plates rather than pooled to avoid siRNA interactions with each other that may diminish knockdown and enhance off-target effects since a greater total siRNA quantity may be necessary for sufficient knockdown. Foci formation was visualized by staining MCF7 cells with anti-BRCA1 and AlexaFluor 488 antibodies. DAPI was included in the staining protocol to visualize the nucleus. Images of BRCA1 and DAPI staining were taken by the Compucyte LSC and relative BRCA1 IRIF expression was determined for each kinase siRNA (**Figure 17**). The red box in **Figure 17B** is an example of a potential positive regulator of BRCA1 because siRNA-mediated knockdown of the kinase resulted in a BRCA1 IRIF phenotype similar to that of the BRCA1 siRNA suggesting that the presence of the kinase promotes BRCA1 IRIF formation. The blue and green boxes in **Figure 17B** are examples of the Neg and BRCA1 control siRNAs, respectively that established the dynamic range of the assay. Data from all kinase siRNAs screened were graphed in order of lowest IRIF expression to highest IRIF expression without regard to specific kinase siRNA with the relative IRIF expression of the Neg siRNA set at 100% and that of the BRCA1 siRNA set at

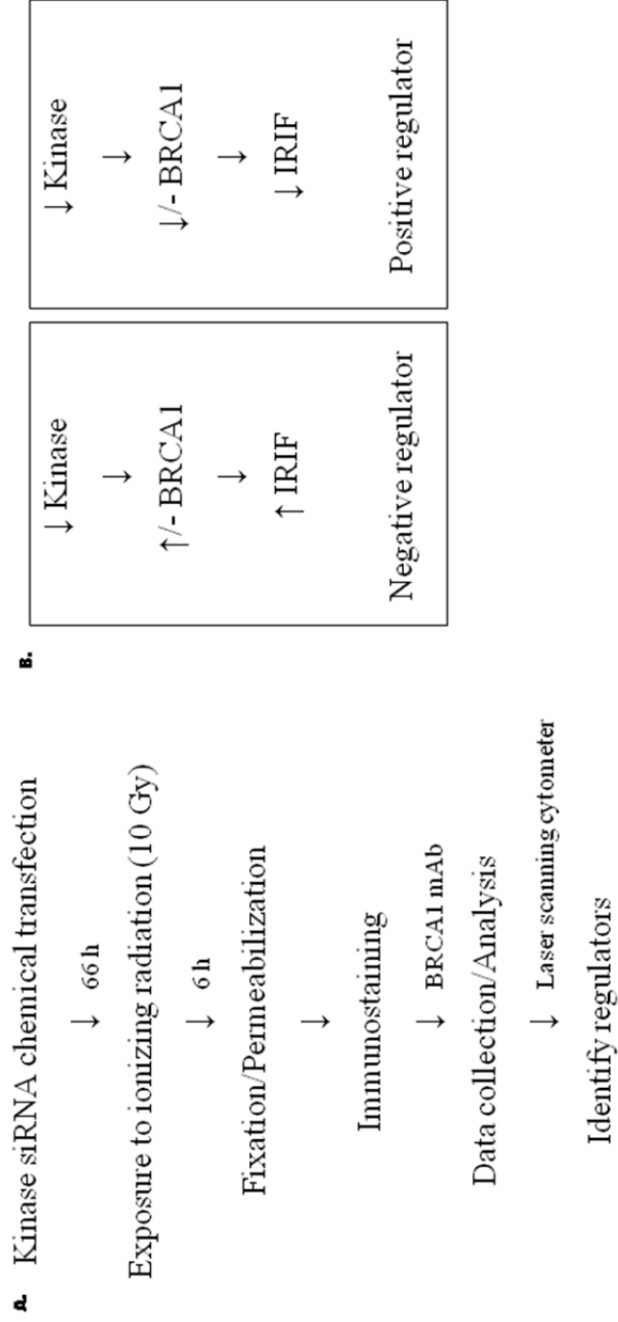
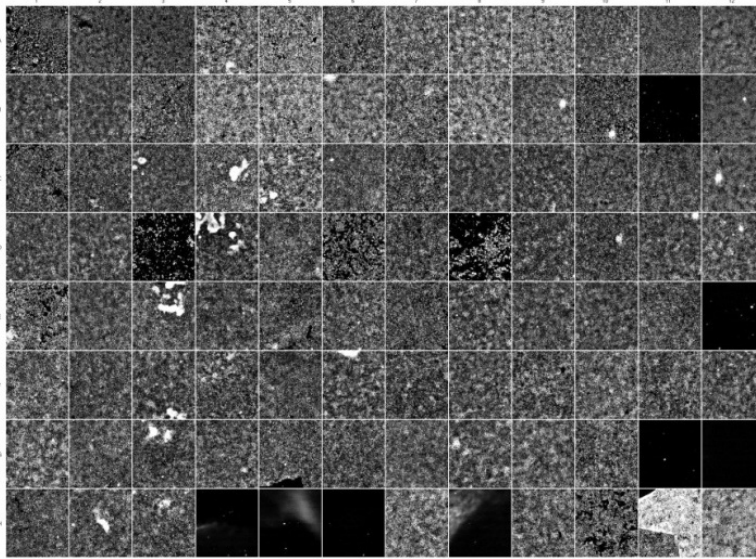


Figure 16: BRCA1 functional assay workflow and analysis of potential kinase regulators. Panel A depicts the BRCA1 functional assay workflow used to identify potential kinase regulators using BRCA1 IRIF formation as the readout following siRNA-mediated knockdown of a kinase and exposure to IR. Panel B shows the rationale for identifying potential kinase regulators. For example, if knockdown of a kinase resulted in decreased BRCA1 foci formation, then that kinase was identified as a potential positive regulator of BRCA1 because its presence promotes foci formation while its absence inhibits foci formation.

A. DAPI



B. BRCA1

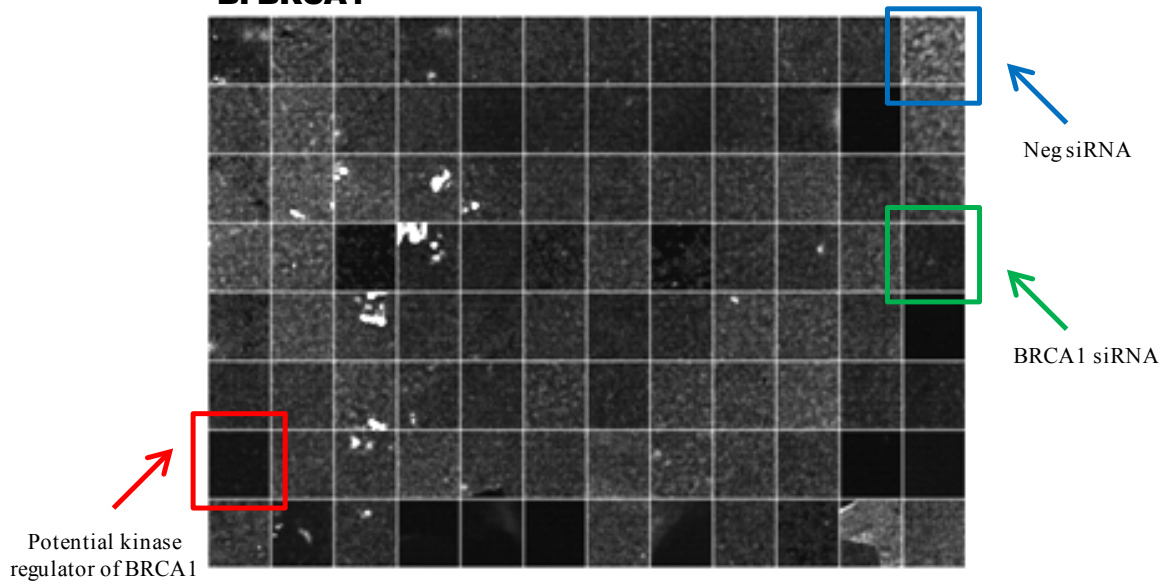


Figure 17: Representative data from the kinase siRNA library screen. Three different siRNAs for each kinase (in three separate 96-well plates) were evaluated in MCF7 cells for BRCA1 IRIF formation 72 h following reverse transfection with RNAiMAX. Panel A shows an example of the images collected from a 96-well plate for DAPI counterstain of the nucleus. Panel B shows an example of the corresponding images collected from the same plate for BRCA1 IRIF. Red box in panel B is an example of a potential kinase regulator of BRCA1. Blue and green boxes in panel B are examples of the Neg and BRCA1 siRNAs, respectively, that established the dynamic range of the functional assay.

0% (**Figure 18**). At least two of the three siRNAs targeting a specific kinase must alter IRIF expression by 2-fold or greater change in standard error from the Neg siRNA to be considered for further validation. A total of thirty-two kinases fulfilled this criteria and were selected for validation (green box in **Figure 18**, **Table 4**). A few kinases exhibited similar and even further diminished BRCA1 IRIF expression compared to that of the BRCA1 siRNA (red box in **Figure 18**); however, they did not validate when the IRIF assay was repeated in triplicate. Additionally, a few kinase siRNAs resulted in a higher IRIF expression with greater than 2-fold change in standard error compared to the Neg control siRNA (blue box in **Figure 18**), but when all three siRNAs for that kinase were analyzed, they did not fulfill the criteria. The primary screen was also able to identify ATM as a kinase regulator of BRCA1, suggesting that the BRCA1 functional assay has the potential to identify other novel kinases. ATM affects BRCA1 at the post-translational level by phosphorylation following exposure to IR (Cortez et al., 1999). The design of this foci formation assay was more conducive to identifying diminishment of BRCA1 IRIF expression of statistical significance than enhancement of BRCA1 IRIF expression.

As the primary screen progressed, more and more wells of each subsequent 96-well plate showed little or no cells by the end of the staining process. Therefore, the screening format was switched to a larger 4-well chamber slide format to minimize loss of cells, which appeared to correct the situation. It was suggested that this phenomenon may be due to mycoplasma contamination, so cells were discarded and another stock of MCF7 cells was used. The conditions of the siRNA transfection with RNAiMAX in the 4-well chamber slide format were scaled-up by a factor of 4 to mirror the conditions for the 96-well plate format. MCF7 cells (9.75×10^5) in 0.7 ml medium with reduced FBS (2% instead of 10%) and without antibiotics were added to siRNA at a final concentration of 60 nM (42 μ l 1.25 μ M siRNA diluted in 133 μ l

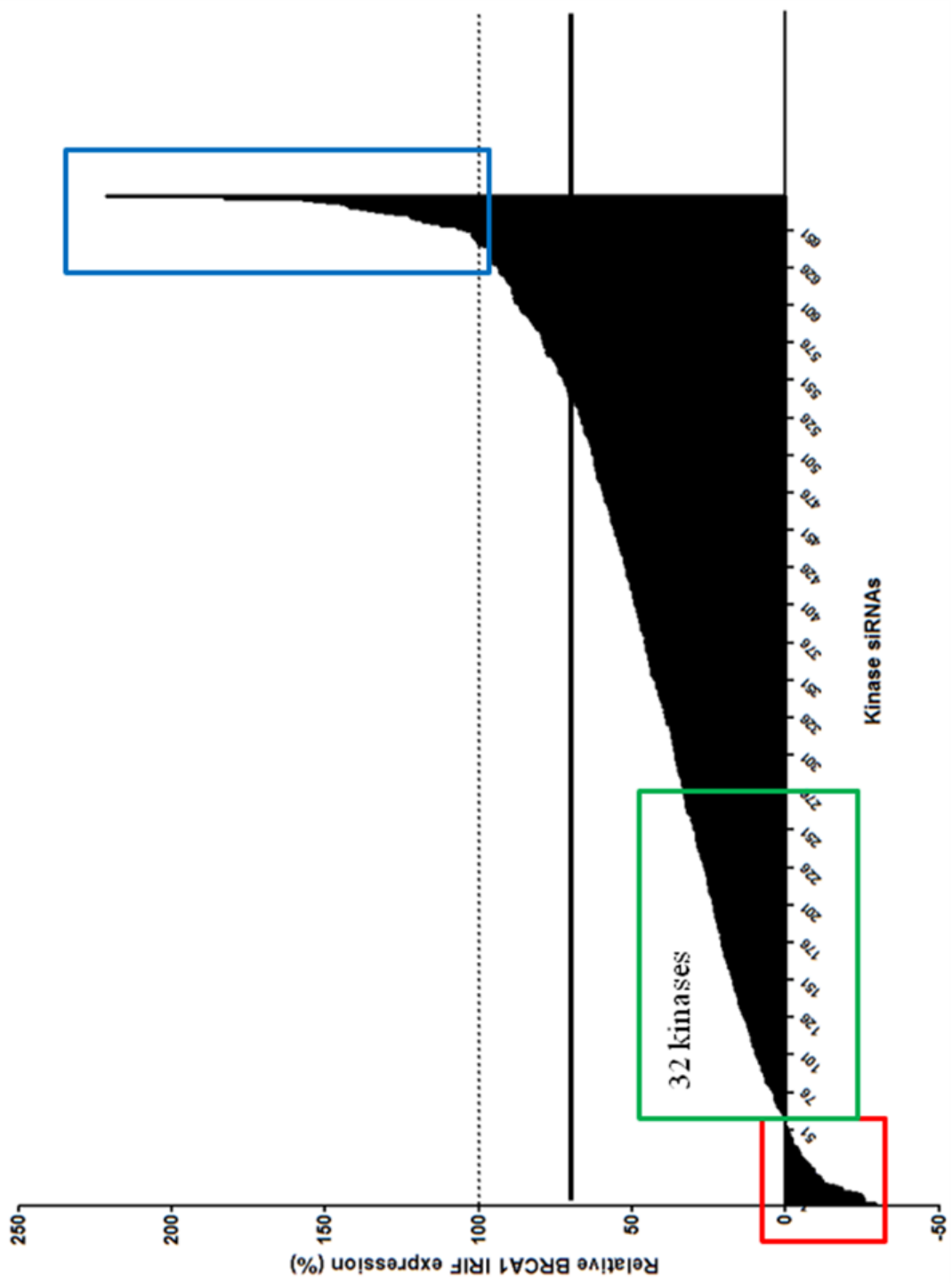


Figure 18: Effect of siRNA-mediated knockdown of kinases from the Ambion *Silencer*[®] Kinase siRNA Library on BRCA1 IRIF formation. Three different siRNAs for each kinase (in three separate 96-well plates) were examined in MCF7 cells for BRCA1 IRIF formation 72 h following reverse transfection with RNAiMAX. The mean fluorescence intensity of BRCA1 was normalized to that of DAPI and then compared to the assay-specific controls, Neg (set as 100%) and BRCA1 (set as 0%). Data from all kinase siRNAs screened are graphed in order of lowest IRIF expression to highest IRIF expression. Red and blue boxes include kinases that exhibited even further diminished BRCA1 IRIF expression compared to that of the BRCA1 siRNA and kinases that resulted in a higher IRIF expression compared to that of the Neg siRNA, respectively; however, they either did not validate or fulfill the selection criteria. Green box includes kinases that met the following criteria: At least two of the three siRNAs must yield normalized values with greater than 2-fold standard error change compared to the Neg control (black line) to be further validated.

Kinase hits that alter BRCA1 IRIF formation selected for primary validation

ACVRL1 = activin A receptor type II-like 1	MAP2K2 = mitogen-activated protein kinase kinase 2
AK1 = adenylylate kinase 1	MAP2K3 = mitogen-activated protein kinase kinase 3
AMHR2 = anti-Mullerian hormone receptor, type II	MAP2K5 = mitogen-activated protein kinase kinase 5
AXL = AXL receptor tyrosine kinase	MAP2K6 = mitogen-activated protein kinase kinase 6
BLK = B lymphoid tyrosine kinase	MAP3K1 = mitogen-activated protein kinase kinase kinase 1
BMX = BMX non-receptor tyrosine kinase	MAP3K6 = mitogen-activated protein kinase kinase kinase 6
CDK3 = cyclin-dependent kinase 3	MAP3K10 = mitogen-activated protein kinase kinase kinase 10
CKM = creatine kinase, muscle	MAP4K5 = mitogen-activated protein kinase kinase kinase kinase 5
CKMT1B = creatine kinase, mitochondrial 1B	MAPK4 = mitogen-activated protein kinase 4
DMPK = dystrophin myotonic-protein kinase	MAPK7 = mitogen-activated protein kinase 7
DOK1 = docking protein 1, 62 kDa	MAPKAPK2 = mitogen-activated protein kinase-activated protein kinase 2
EPHA4 = EPH receptor A4	PIK4CA = phosphatidylinositol 4-kinase, catalytic, alpha polypeptide
EPHB6 = EPH receptor B6	PLK3 = polo-like kinase 3 (Drosophila)
FGFR2 = fibroblast growth factor receptor 2	PLXNA1 = plexin A1
HCK = hemopoietic cell kinase	PLXNA2 = plexin A2
HK3 = hexokinase 3 (white cell)	PLXNB1 = plexin B1

Table 4: List of 32 kinase hits identified from the kinase siRNA library. These 32 kinases met the criteria that at least two of the three siRNAs targeting each kinase must yield normalized values with greater than 2-fold standard error change compared to the Neg control siRNA to be further validated.

OptiMEM) previously incubated with 4 μ l RNAiMAX for 16 min at RT. Kinase siRNAs continued to be evaluated in this manner.

Potential kinase regulators were validated by repeating the siRNA transfection and foci formation assay in triplicate for statistical analysis. Validation of the thirty-two kinases selected from the primary screen was completed in Nunc Lab-Tek 4-well chamber slides so that more regions per kinase siRNA could be imaged. The conditions of the siRNA transfection were kept the same with a final siRNA concentration of 60 nM, 1 μ l RNAiMAX/ 5×10^4 cells, incubation of siRNA and RNAiMAX for 16 min at RT, and analysis 72 h post-transfection. Mean fluorescence intensities of BRCA1 IRIF and DAPI for 6 regions with at least 36 images per region were collected on the LSC. Again, BRCA1 IRIF mean fluorescence intensity was standardized to its corresponding DAPI mean fluorescence intensity to account for cell density for all siRNAs. Then the adjusted IRIF value for each kinase siRNA was compared to that of the Neg siRNA to yield a relative IRIF expression that was then normalized to a value between the BRCA1 siRNA and Neg siRNA with the BRCA1 siRNA set at 0% and the Neg siRNA set at 100%. The criteria set to select kinases for further characterization was that at least two of the three siRNAs targeting each kinase in triplicate must yield a 2-fold or greater standard error change compared to the Neg siRNA. A total of fourteen kinases were found to meet the criteria (**Figures 19-21, red boxes**).

The proposed experimental approach is dependent on the interplay of kinases and BRCA1 that exist within the cell line used, which may be a representative finding or unique to that cell line. For example, decreased expression of BRCA1 has been found in high grade ductal carcinomas, which are often estrogen receptor and progesterone receptor negative, while MCF7 cells express both (Hall et al., 1990; Tang et al., 2006; Wilson et al., 1999). MCF7 cells are luminal and are representative of estrogen receptor positive breast cancers. Also, microarray

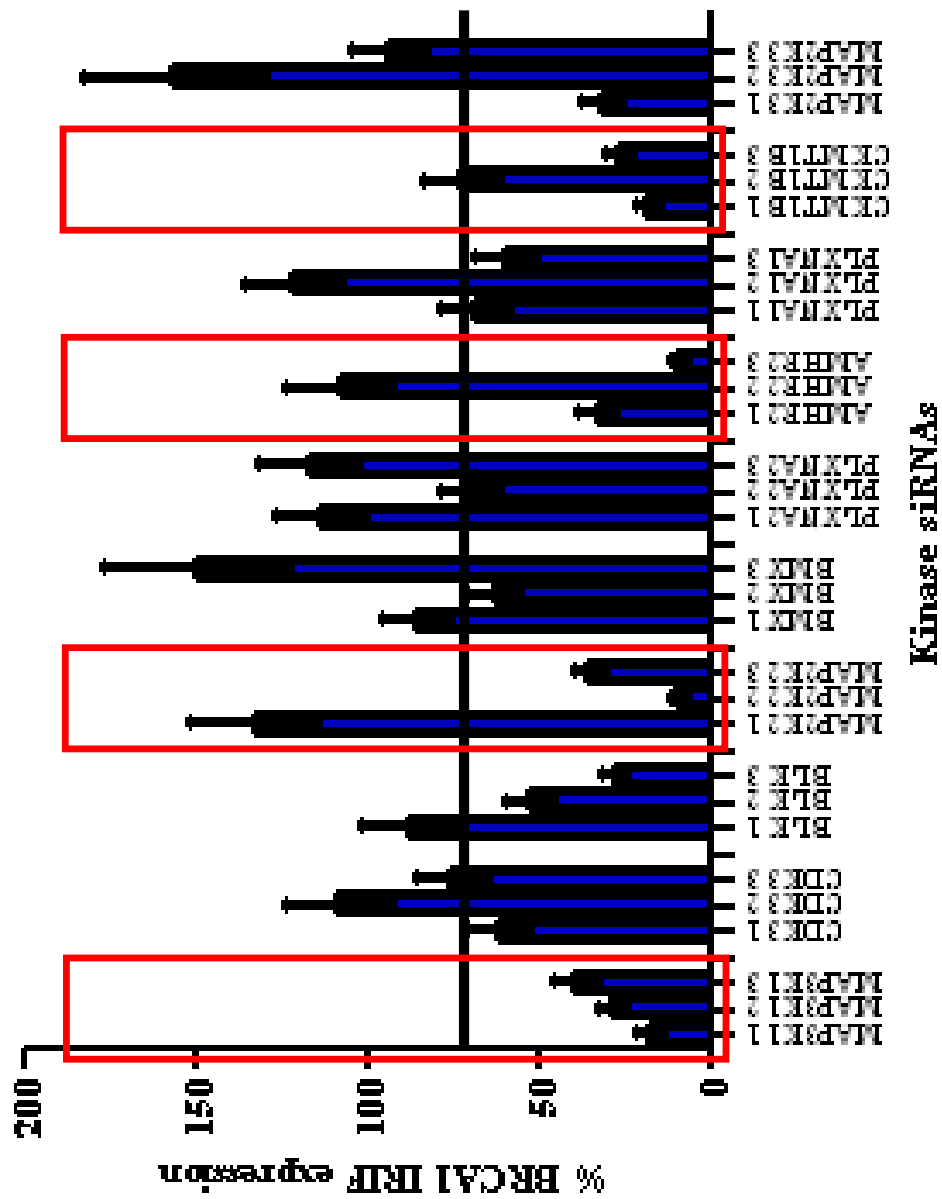


Figure 19: BRCA1 IRIF formation analysis performed in triplicate with three siRNAs targeting the indicated putative kinase regulator – set 1. Kinase siRNAs were introduced into MCF7 cells by chemical transfection with RNAiMAX as previously described. After 72 h, cells were exposed to 10 Gy IR and stained with an anti-BRCA1 antibody for BRCA1 IRIF and counterstained with DAPI for the nucleus. The mean fluorescence intensity of BRCA1 was normalized to that of DAPI and then compared to the assay-specific controls, Neg (set as 100%) and BRCA1 (set as 0%). Relative BRCA1 IRIF expression is presented as an average of the three replicates \pm standard error for each siRNA. Criteria: At least two of the three siRNAs in triplicate must yield normalized values with greater than 2-fold standard error change compared to the Neg control to be further validated. Red boxes indicate kinase siRNAs that fulfilled the criteria.

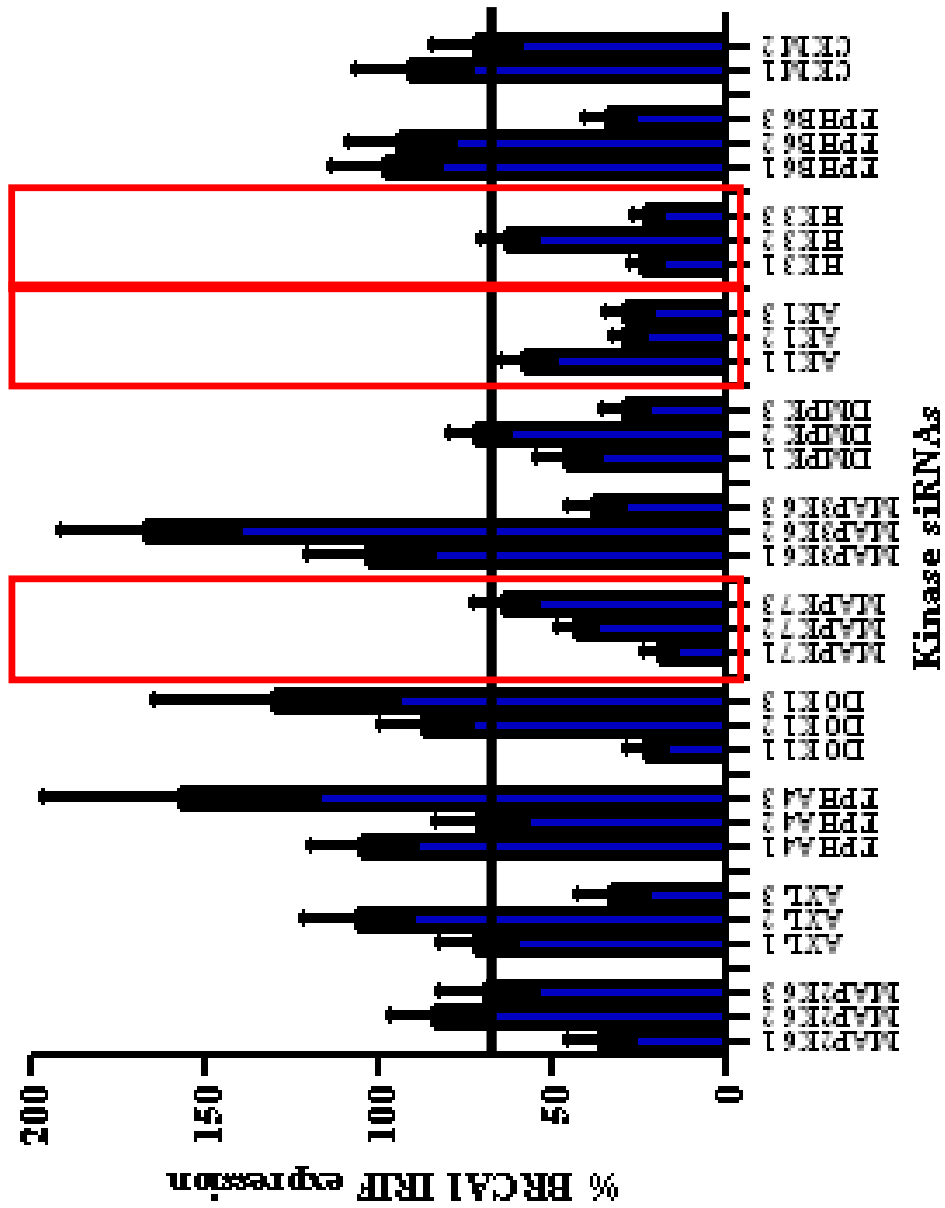


Figure 20: BRCA1 IRIF formation analysis performed in triplicate with three siRNAs targeting the indicated putative kinase regulator – set 2. Kinase siRNAs were introduced into MCF7 cells by chemical transfection with RNAiMAX as previously described. After 72 h, cells were exposed to 10 Gy IR and stained with an anti-BRCA1 antibody for BRCA1 IRIF and counterstained with DAPI for the nucleus. The mean fluorescence intensity of BRCA1 was normalized to that of DAPI and then compared to the assay-specific controls, Neg (set as 100%) and BRCA1 (set as 0%). Relative BRCA1 IRIF expression is presented as an average of the three replicates \pm standard error for each siRNA. Criteria: At least two of the three siRNAs in triplicate must yield normalized values with greater than 2-fold standard error change compared to the Neg control to be further validated. Red boxes indicate kinase siRNAs that fulfilled the criteria.

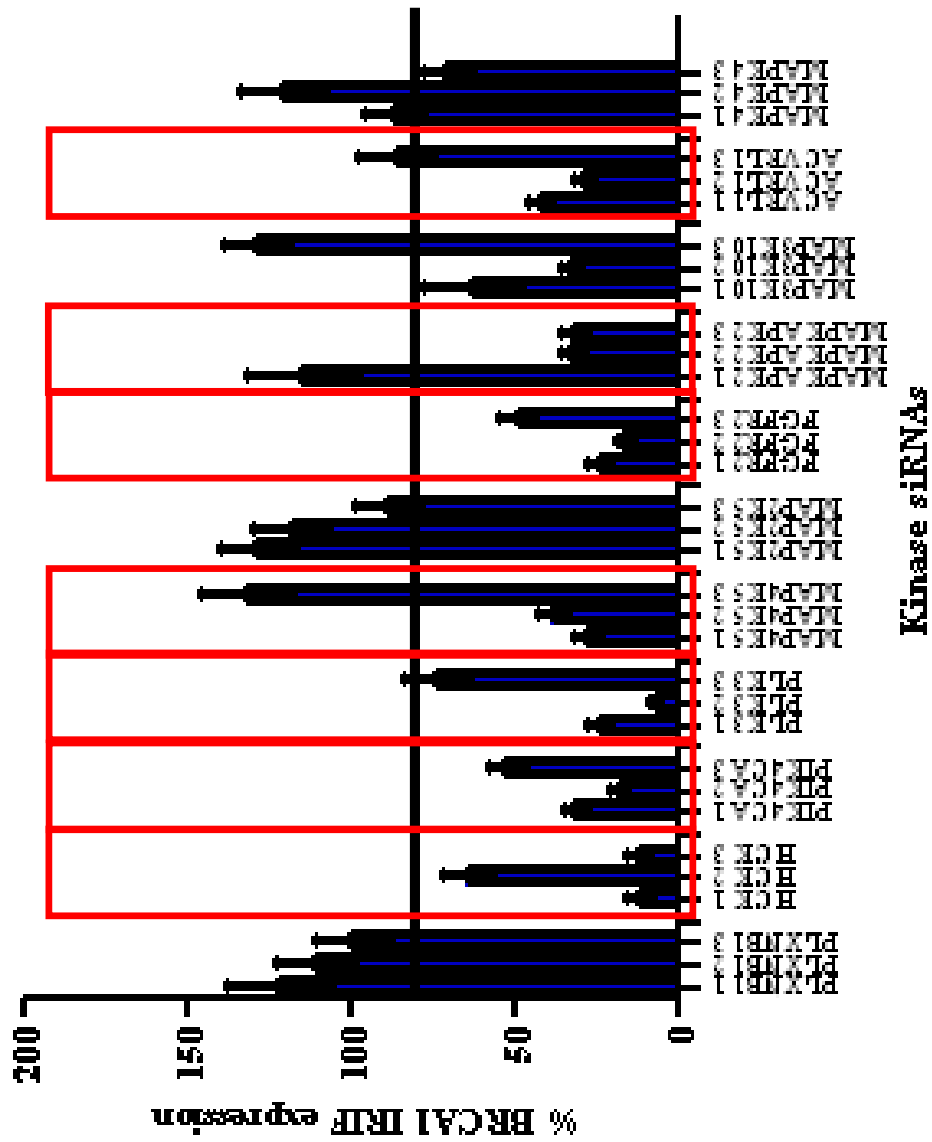


Figure 21: BRCA1 IRIF formation analysis performed in triplicate with three siRNAs targeting the indicated putative kinase regulator – set 3. Kinase siRNAs were introduced into MCF7 cells by chemical transfection with RNAiMAX as previously described. After 72 h, cells were exposed to 10 Gy IR and stained with an anti-BRCA1 antibody for BRCA1 IRIF and counterstained with DAPI for the nucleus. The mean fluorescence intensity of BRCA1 was normalized to that of DAPI and then compared to the assay-specific controls, Neg (set as 100%) and BRCA1 (set as 0%). Relative BRCA1 IRIF expression is presented as an average of the three replicates \pm standard error for each siRNA. Criteria: At least two of the three siRNAs in triplicate must yield normalized values with greater than 2-fold standard error change compared to the Neg control to be further validated. Red boxes indicate kinase siRNAs that fulfilled the criteria.

studies have shown that the gene expression profile differs between estrogen receptor positive and negative breast cancers (Perou et al., 2000). Therefore, the utility of this functional approach would be enhanced by the use of other cell lines that represent the major types of invasive breast cancer, including luminal (MCF7), basal-like (MDA-MB-231), HER2+ (SK-BR-3), and normal breast-like (HMEC) (Sorlie et al., 2003) to delineate common pathways.

Since the nature of the experimental approach precludes the optimization of every siRNA in the kinase library, one of three outcomes are possible: 1) the intended effect of optimal knockdown with minimal cytotoxicity, 2) off-target effects and/or enhanced cytotoxicity, or 3) insufficient knockdown. However, preemptive measures have been taken to minimize false positives and false negatives. For example, siRNAs against GAPDH and BRCA1 were used to establish the experimental parameters and were chosen based on several criteria including their abundance in the cell, mRNA and protein half-life, and relevance to the assay (Blagosklonny et al., 1999; Lekas et al., 2000; Saunus et al., 2007). By most accounts, the two were at opposite ends of the spectrum, so conditions that prove successful for both will likely work for targets that fall in between. In addition, by using individual rather than pooled siRNAs, it is possible to ascribe the observed effects to a particular siRNA and to define a concentration that allows sufficient knockdown without inducing off-target effects. Finally, subsequent validation will help confirm those kinases that influence BRCA1 expression and function.

Although the siRNAs in the kinase library were designed using a stringent algorithm to ensure specificity and those that have been validated for gene knockdown are included, they may not sufficiently affect the target kinase to levels that impact BRCA1 expression and function. An alternative may be to evaluate pharmacologic inhibitors of kinases on BRCA1 expression and

function. Protein kinase inhibitor libraries are commercially available from several companies, including EMD Biosciences.

Staining using an anti-BRCA1 antibody whose epitope is within the N terminus may detect not only IRIF with DNA damage repair but also other parallel cellular processes that require BRCA1, including transcription-coupled repair. Perhaps colocalization with γ H2AX, an early marker of DNA damage (Paull et al., 2000), or use of a phospho-specific BRCA1 antibody will more accurately identify the foci of interest.

Although the LSC enables high content analysis and minimizes the subjectivity inherent in manually imaging and counting foci, there are certain limitations that must be considered. For example, the software controlling the microscope cannot be programmed to image near the periphery of a well. Additionally, it is unable to contour cells at the edge of the image field and it has difficulty distinguishing apposed cells.

Inherent redundancies in signaling pathways may exclude detection of certain kinases, which is unfortunate but not entirely ineffectual. The ultimate goal is to effectively translate our understanding of various cellular processes and pathways into a potent combination therapy that is both targeted and safe. Polygenic influences suggest a critical role for that pathway but a difficult task to dissect.

Another approach to validating the potential regulatory kinases is to assess whether exogenous expression of the kinase will restore (or inhibit) BRCA1 IRIF formation in a cell line deficient for that kinase. This can also be done using a cell line that has been transduced with an shRNA-encoding lentiviral vector for stable silencing of kinase expression.

Ranking of Lead Kinases: Each set of three kinase siRNAs was evaluated based on the criteria that at least two of the three siRNAs targeting each kinase in triplicate must yield a 2-fold or greater standard error change compared to the Neg control siRNA. Of the fourteen kinases that met the criteria, four kinases had two siRNAs that dramatically diminished BRCA1 IRIF expression and one siRNA that appeared to have no effect on BRCA1 IRIF expression. In those cases, that siRNA was excluded from further calculations. These fourteen lead kinases were ranked based on an average of the relative BRCA1 IRIF expressions of the siRNAs targeting each kinase. They are presented from the least relative BRCA1 IRIF intensity to the greatest relative BRCA1 IRIF intensity (**Figure 22**).

Conclusions

The BRCA1 functional assay workflow was developed and optimized to evaluate siRNAs from a kinase siRNA library to identify novel kinases that impact the ability of BRCA1 to form IRIF following exposure to 10 Gy IR. Immunofluorescence parameters were optimized for visualization of distinct, punctate BRCA1 IRIF in the nucleus with an anti-BRCA1 antibody following exposure to IR. Cell cycle analyses of unsynchronized and synchronized MCF7 cells were conducted to establish a cell cycle profile that was used to determine time points for exposure to IR and fixation/permeabilization for immunostaining. Optimization of siRNA transfection conditions established that chemical transfection with RNAiMAX proved most successful in MCF7 cells. Following the primary screen and validation, fourteen lead kinases have consistently demonstrated diminished BRCA1 IRIF formation following siRNA-mediated knockdown and exposure to IR. MAP3K1, HCK, FGFR2, PIK4CA, and PLK3 were selected for further evaluation because they were the top five kinases where all three siRNAs effectively

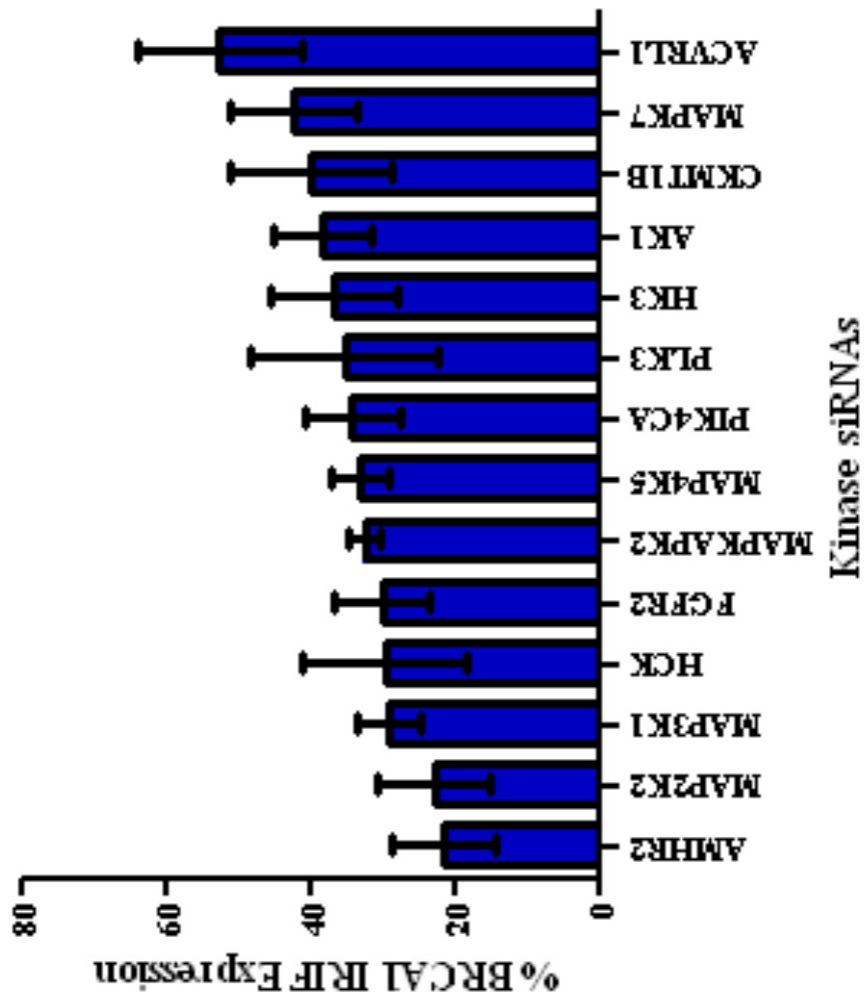


Figure 22: BRCA1 IRIF formation analysis performed in triplicate with three siRNAs targeting the indicated putative kinase regulator – combined analysis. Relative BRCA1 IRIF expression presented as an average of the three siRNAs \pm standard error. Criteria: At least two of the three siRNAs in triplicate must yield normalized values with greater than 2-fold standard error change compared to the Neg control to be further validated. The fourteen lead kinases that met the above criteria are ranked in order of increasing BRCA1 IRIF expression.

diminished BRCA1 IRIF formation. Subsequent secondary validation and characterization will be performed to determine whether the kinase regulates BRCA1 at the transcriptional level or post-translational level and how siRNA-mediated knockdown of these kinases will affect DSB repair and the ability of a cell to proliferate following DNA damage.

CHAPTER III

EVALUATE THE EFFECT OF siRNA-MEDIATED KNOCKDOWN OF LEAD KINASES ON BRCA1 mRNA LEVELS AS WELL AS ON BOTH TARGET AND BRCA1 PROTEIN LEVELS

Introduction

Validation of the regulatory kinases identified from the primary BRCA1 assay will help determine the extent of siRNA-mediated knockdown of the target protein as well as whether the changes in foci formation were due to a difference in BRCA1 expression or a DNA damage response defect. mRNA levels for BRCA1 following siRNA-mediated knockdown of MAP3K1, HCK, FGFR2, PIK4CA, and PLK3 were evaluated by qRT-PCR. These kinases were selected because all three siRNAs targeting the kinase decreased BRCA1 IRIF levels at least 2-fold or greater standard error change compared to the Neg control siRNA and they exhibited the least relative BRCA1 IRIF intensity. Protein levels for MAP3K1, HCK, and FGFR2 as well as the corresponding levels of BRCA1 following siRNA-mediated knockdown of these three kinases were evaluated by Western blot analysis. If BRCA1 mRNA and protein levels from MCF7 cells following siRNA treatment are different from that of the control, this will indicate an effect of the kinase on BRCA1 expression. If there is no change in either mRNA or protein in siRNA transfected cells compared to control, then it would suggest a DNA damage response defect.

Materials and Methods

Chemical Transfection of siRNAs with RNAiMAX: MCF7 cells (9.75×10^5) in 3.9 ml MEM with 2% FBS without antibiotics were added to each well of a 6-well plate containing 60 nM final

siRNA concentration (240 μ l of 1.25 μ M siRNA diluted in 760 μ l OptiMEM) and 23 μ l RNAiMAX (Invitrogen, Carlsbad, CA) previously incubated for 16 min at room temperature (RT). The medium was replaced following 24h incubation at 37°C, 5% CO₂ humidified atmosphere with complete medium without antibiotics and reduced FBS (2% instead of 10%) and again 24h later with complete medium without antibiotics. Cells were either exposed to 10 Gy ionizing radiation 66h following transfection and allowed to recover for 6h or left unirradiated before processing for RNA and protein.

Isolation of Total RNA from Cells: RNA was extracted per manufacturer's protocol using the RNeasy Plus RNA extraction kit (Qiagen, Valencia, CA). MCF7 cells were disrupted using Buffer RLT + β -mercaptoethanol (10 μ l β -ME per 1 ml Buffer RLT). For $< 5 \times 10^6$ cells, 350 μ l of Buffer RLT was added. Each lysate was homogenized using a QIAshredder spin column and centrifuged using an Eppendorf 5415 D microcentrifuge (Westbury, New York) for 2 min at full speed (16,100xg). One volume or 350 μ l of 70% ethanol was added to the homogenized lysate and mixed by pipetting. The sample was then transferred to an RNeasy spin column and centrifuged for 15 s \approx 8000xg. The flow-through was discarded. 700 μ l Buffer RW1 was added to the RNeasy spin column and centrifuged for 15 s \approx 8000xg to wash the spin column membrane. The flow-through was again discarded. 500 μ l Buffer RPE was then added to the RNeasy spin column and centrifuged for 15 s \approx 8000xg to wash the spin column membrane. The flow-through was again discarded. Another 500 μ l Buffer RPE was added to the RNeasy spin column and centrifuged for 2 min \approx 8000xg. The RNeasy spin column was placed in a new 2 ml collection tube and centrifuged at full speed for 1 min to eliminate any possible carryover of Buffer RPE. The RNeasy spin column was then placed in a new 1.5 ml Eppendorf

tube. The RNA was eluted with 30 μ l RNase-free water added directly to the spin column membrane and centrifuged for 1 min at \geq 8000xg. The eluate was then added to the RNeasy spin column membrane to concentrate the RNA further and centrifuged for 1 min at 8000xg. The 260/280 ratio and concentration of each RNA sample were determined using an 8-channel NanoDrop 8000 spectrophotometer and its associated software ND-8000 v1.1.1 (Thermo Scientific, Wilmington, DE, P. Fields laboratory). RNA samples were reverse transcribed to cDNA immediately following extraction.

Quantitative Real-Time PCR (qRT-PCR): Complementary DNA (cDNA) was generated per manufacturer's protocol from 1000 ng extracted RNA in a 100 μ l volume using the High Capacity cDNA kit (Applied Biosystems, Foster City, CA). The 2x reverse transcription master mix prepared on ice (per 20- μ l reaction) was composed of 2 μ l 10X RT Buffer, 0.8 μ l 25X dNTP Mix (100 mM), 2.0 μ l 10X RT Random Primers, 1 μ l MultiScribe Reverse Transcriptase, and 4.2 μ l Nuclease-free H₂O. 10 μ l of RNA sample was mixed with 10 μ l of 2X RT master mix per 20- μ l reaction in a PCR tube. Reverse transcription of RNA to cDNA was performed in a GeneAmp PCR System 9700 thermal cycler (Applied Biosystems). The reverse transcription PCR program was run as follows: 25°C for 10 min, 37°C for 120 min, 85°C for 5 s, and 4°C for ∞ . cDNA samples were stored at -80°C until the qRT-PCR plate was ready to be set up. Gene expression of BRCA1 (Hs00173237_m1), HCK (Hs00176654_m1) and 18S (Hs99999901_s1) was detected using the TaqMan[®] Gene Expression assay kit (Applied Biosystems). Each PCR reaction was set up as follows: 9 μ l cDNA + 10 μ l TaqMan[®] Universal PCR Master Mix + 1 μ l specific primer/probe set (BRCA1, HCK or 18S) in a 96-well PCR plate. Controls for each set of experiments included the 18S housekeeping gene for normalization of C_t values to account for

relative RNA amount, no cDNA control to assess specificity of the primer/probe set, and H₂O only to determine background of the instrument. Each sample was run in triplicate for statistical analysis. Each 20 µl reaction was run on the 7500 ABI real time PCR instrument with the following program: UNG incubation at 50°C for 2 min, AmpliTaq Gold activation at 95°C for 10 min followed by 40 PCR cycles of 95°C for 15 s to denature and 60°C for 1 min to anneal/extend (Applied Biosystems, P. Fields laboratory). Ct values were obtained for each sample. Data analysis was carried out in Microsoft Excel. An average and standard error of the triplicate Ct values for each sample were calculated using the equation $Ct_{\text{average}} = (Ct_1 + Ct_2 + \dots + Ct_n)/n$ and $Ct_{\text{st error}} = Ct_{\text{stdev}}/\sqrt{n}$. Each averaged Ct value was then normalized to 18S (ΔCt) and the corresponding standard error was calculated using the equation $\Delta Ct^{\text{st error}} = \sqrt{(Ct_{\text{st error (18s)}})^2 + Ct_{\text{st error (sample)}}^2}$. The ΔCt value was further normalized to Neg siRNA, or the IRIF assay control ($\Delta\Delta Ct$) and the negative $\Delta\Delta Ct$ value was raised to the power of 2 to give relative remaining expression of the gene being investigated. The $\Delta Ct^{\text{st error}}$ was added to and subtracted from its corresponding $\Delta\Delta Ct$ and the negative resulting value was raised to the power of 2 to give the positive and negative standard error. The standard error for the average of replicate experiments was calculated using the equation adapted from Baker and Nissim, 1963: $e_3 = \sqrt{((1/(n(n-1))((n_1(n_1-1)e_1^2)+(n_2(n_2-1)e_2^2)+((n_1n_2)/n)(m_1-m_2)^2)))}$, where e_3 refers to the new standard error, n_1 and n_2 refer to the number of observations in the first and second group respectively, $n=n_1+n_2$, m_1 and m_2 refer to the mean in the first and second group respectively, and e_1 and e_2 refer to the standard error in the first and second group respectively. A t test was performed using GraphPad Prism 5 to determine whether the change in mRNA was statistically significant.

Isolation of Total Protein from Cells: The medium was removed and the cells were washed 2x with PBS. Cells were scraped into ice-cold PBS and transferred to a microcentrifuge tube. The cells were then pelleted by centrifugation at 300xg for 5 min at 4°C. The supernatant was removed and the pellet was lysed in modified RIPA buffer (50 mM Tris base, 150 mM NaCl, 2 mM EDTA, 1% Triton X-100, 0.5% Na-deoxycholate, 0.1% SDS, 50 mM NaF, 5 mM Na₃VO₄, 1X Sigma protease inhibitor cocktail) on ice for 30 min, vortexing occasionally. The cellular debris was then removed by centrifugation at 10,600xg for 30 min at 4°C. The supernatant containing the extracted proteins was collected and protein concentration was measured using the Bio-Rad Bradford protein assay. Reagent A' was made by adding 20 µl of Reagent S to each 1 ml of Reagent A. A standard curve was generated using BSA standards with concentrations of 0, 0.125, 0.25, 0.5, 0.75, 1, 1.5, and 2 mg/ml in triplicate. 5 µl of standards and samples were pipetted in triplicate into a 96-well plate. 25 µl of Reagent A' was added to each well using a multichannel pipette followed by 200 µl of Reagent B. The plate was mixed and incubated at RT for 15 min. The absorbance was then read at 750 nm in a Synergy microplate reader with associated Gen5 software (BioTek, Winooski, VT, S. Sittampalam laboratory). An average absorbance was calculated for each sample that was then normalized to its buffer control to eliminate background signal. The BSA standard curve was generated and a linear regression analysis was done using GraphPad Prism 5 to interpolate the unknown baseline-corrected absorbance for each protein sample to a protein concentration.

Western Blot Analysis: 50 µg of protein + 1X SDS-PAGE sample buffer (60 mM Tris-HCl pH=8.0, 2% w/v SDS, 4 mM EDTA, 10% v/v glycerol, 0.02% w/v bromophenol blue, 5% β-ME) per sample was loaded onto a 4-20% Tris-Glycine SDS-PAGE gel (Invitrogen). The

proteins were separated by electrophoresis for 1.5 h at 200 V in a Tris-Glycine running buffer (25 mM Tris base, 192 mM glycine, 0.1% SDS). The proteins were then transferred onto PVDF membrane for 2.5 h at 35 V in 8% transfer buffer (25 mM Tris base, 192 mM glycine, 20% v/v MeOH). The PVDF membrane was then blocked in 5% milk/TBS (25 mM Tris pH 8.0, 135 mM NaCl, 2.5 mM KCl) + 0.1% Tween-20 (TBS-T) for 1 h RT. The membrane was incubated with primary antibody diluted in TBS-T + 0.01% sodium azide (anti-BRCA1 mouse mAb (Ab-1, Calbiochem) at a 1:250 dilution, anti-MEK kinase-1 rabbit pAb (MAP3K1, C-22, Santa Cruz Biotechnology) at a 1:250 dilution, anti-HCK rabbit pAb (N-30, Santa Cruz Biotechnology) at a 1:250 dilution) overnight at 4°C. To monitor equal protein loading, actin was detected using anti-actin mouse mAb (Chemicon/Millipore, Billerica, MA) at a 1:250,000 dilution in TBS-T + 0.01% sodium azide overnight at 4°C. Following incubation with the primary antibody, the blot was washed 1x15 min, 3x5 min in TBS-T at RT. The blot was then incubated with the secondary antibody diluted in TBS-T (goat anti-mouse IgG, HRP-linked (GAM-HRP, Cell Signaling, Danvers, MA) at 1:5,000 for BRCA1; goat anti-rabbit IgG, HRP-linked (Cell Signaling) at 1:5000 for MAP3K1 and HCK; and GAM-HRP at 1:10,000 for actin) for 1 h at RT. Prior to chemiluminescent detection the blots were washed 1x15 min, 3x5 min in TBS-T and 2x5 min in TBS. Chemiluminescence was detected using the SuperSignal West Femto kit (Pierce Biotechnology, Rockford, IL) and the UVP imaging center (Upland, CA). Densitometry was measured for each protein band using the UVP imaging center. To determine protein expression for the protein of interest following siRNA-mediated knockdown of a kinase, the measured density for the protein of interest was normalized first to that of actin and then to that of the Neg siRNA control.

Results and Discussion

Effect of siRNA-mediated knockdown of lead kinases on BRCA1 mRNA levels: mRNA levels of BRCA1 were evaluated using qRT-PCR analysis. siRNA-mediated knockdown of MAP3K1, HCK, FGFR2, PI4KA, and PLK3 was achieved by chemical transfection using RNAiMAX and the same three siRNAs for each kinase from the primary screen and validation. RNA was extracted and reverse transcribed using commercially available kits per manufacturer's protocol. Established TaqMan[®] primer/probe sets for BRCA1 and 18S were used to assess RNA expression. Results from the three siRNAs for each kinase were averaged for each experimental set and then averaged across replicate data sets and are graphed as percent BRCA1 mRNA expression \pm standard error (**Figure 1**). BRCA1 mRNA expression for Neg siRNA was set at 100%. BRCA1 mRNA expression following siRNA-mediated knockdown of BRCA1 demonstrated effective knockdown of BRCA1 mRNA expression. siRNA-mediated knockdown of HCK and PLK3 showed a modest decrease in BRCA1 mRNA levels, suggesting that both HCK and PLK3 may play a role in regulating BRCA1 expression at the transcriptional level. In contrast, siRNA-mediated knockdown of MAP3K1, FGFR2, and PI4KA maintained BRCA1 mRNA levels similar to the Neg control siRNA, suggesting that MAP3K1, FGFR2, and PI4KA does not regulate BRCA1 expression at the transcriptional level. The extent of knockdown of each of the target kinases has not been quantified at the mRNA level, except HCK (discussed below). Further qRT-PCR studies should be done to establish the extent of knockdown of each of the target kinases. Based on microarray data from Oncomine (www.oncomine.org, Compendia Bioscience, Ann Arbor, MI), MCF7 cells appear to express MAP3K1, HCK, and FGFR2.

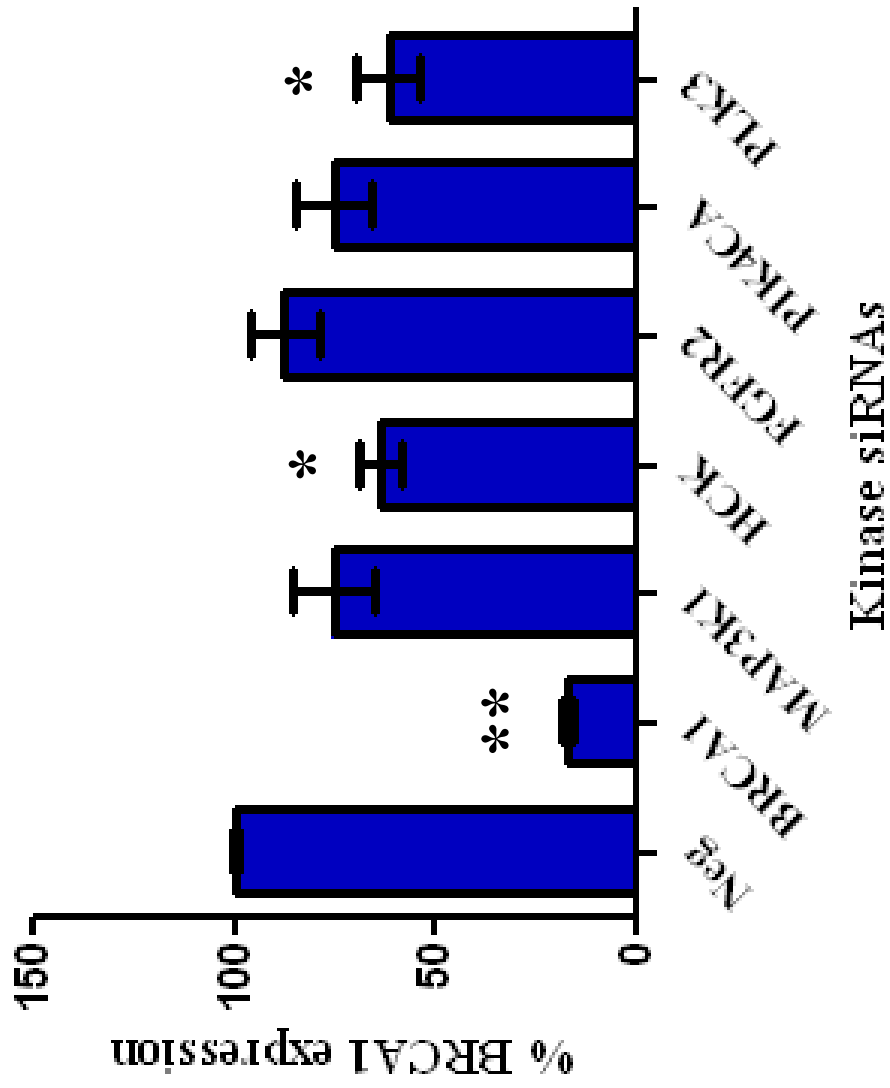
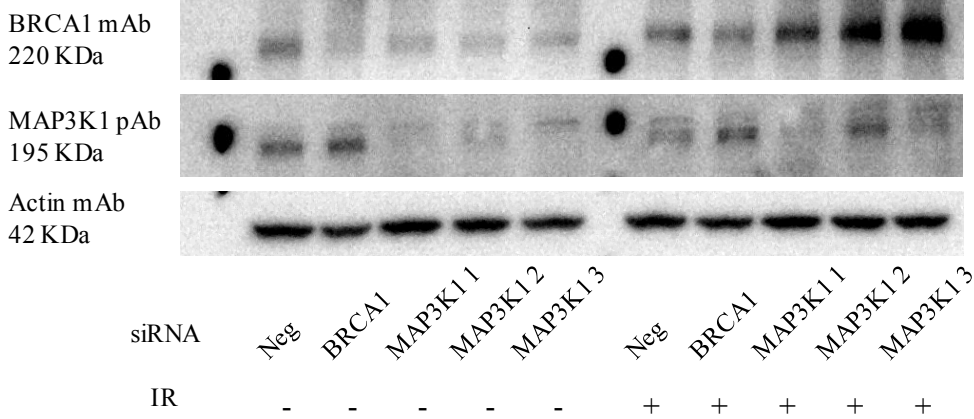


Figure 1: Effect of siRNA-mediated knockdown of kinases on BRCA1 mRNA levels. BRCA1 RNA analysis by qRT-PCR in MCF7 cells 72 h following reverse transfection with RNAiMAX and either Neg, BRCA1, or three individual siRNAs targeting the indicated putative kinase regulator. Data are presented as an average of the three siRNAs \pm standard error (n=3). * denotes P 0.0125, ** denotes P < 0.0001.

Effect of siRNA-mediated knockdown of lead kinases on BRCA1 and target protein levels:

Protein levels of BRCA1 and target proteins were evaluated using Western blot analysis. siRNA-mediated knockdown of MAP3K1, FGFR2, and HCK was achieved by chemical transfection using RNAiMAX and the same three siRNAs for each kinase from the primary screen and validation. Samples were either irradiated with 10 Gy IR and allowed to recover for 6 h or left unirradiated. Protein was extracted, separated by electrophoresis, and detected using antibodies for BRCA1, target kinase, and actin (loading control) to assess protein expression. Results from the three siRNAs for each kinase are graphed as percent protein expression \pm standard error. Both BRCA1 and target kinase protein expression for Neg siRNA was set at 100%. As expected, BRCA1 protein levels are decreased following siRNA-mediated knockdown of BRCA1. Preliminary results from siRNA-mediated knockdown of MAP3K1 show more robust knockdown of MAP3K1 protein with a concomitant decrease in BRCA1 protein for all three siRNAs in nonIR samples compared to IR samples, suggesting that MAP3K1 affects BRCA1 expression at the protein level (**Figure 2**). Both BRCA1 and MAP3K1 protein expression are higher in IR samples compared to nonIR samples, suggesting that BRCA1 and MAP3K1 protein expression may be induced by IR. Additionally, MAP3K1 knockdown appears to increase BRCA1 protein expression in IR samples, which would seem contradictory to the diminished BRCA1 IRIF expression. However, replicate analyses of siRNA-mediated knockdown of MAP3K1 are needed for statistical significance. FGFR2 protein expression is significantly diminished with siRNA-mediated knockdown of at least two of the three FGFR2 siRNAs and a concomitant decrease in BRCA1 protein expression is observed (**Figure 3**). siRNA-mediated knockdown of BRCA1 leads to a decrease in FGFR2 protein expression, suggesting that BRCA1 may positively regulate FGFR2. siRNA-mediated knockdown of HCK leads to moderately

A.



B.

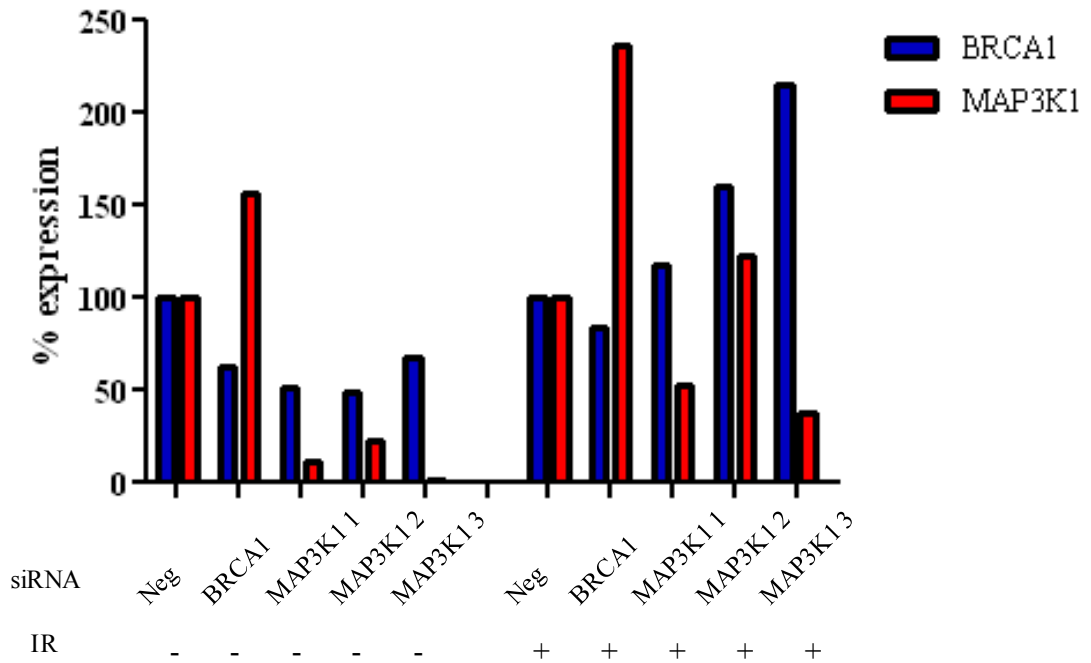
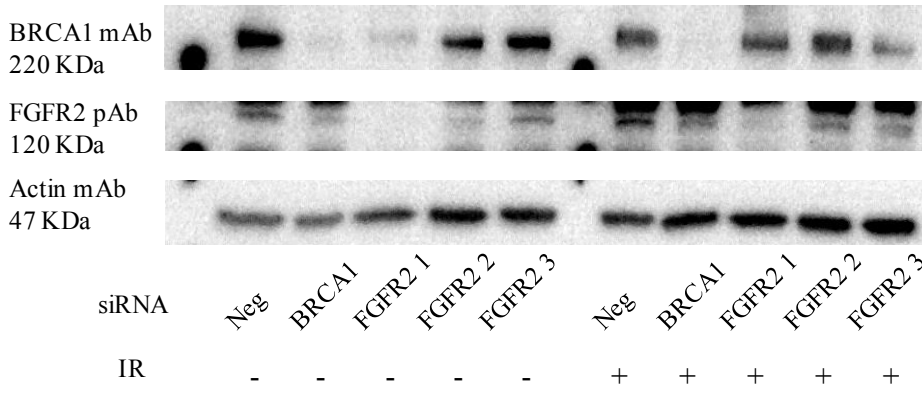


Figure 2: Effect of siRNA-mediated knockdown of MAP3K1 on BRCA1 protein levels. Protein analysis by Western blot in MCF7 cells 72 h following reverse transfection with RNAiMAX and either Neg, BRCA1, or three individual siRNAs targeting the indicated putative kinase regulator and then either left unirradiated or irradiated with 10 Gy of ionizing radiation. Panel A is representative Western blots for BRCA1, MAP3K1 and actin (served as loading control) following siRNA-mediated knockdown of MAP3K1 and Panel B shows the respective densitometry of each sample (n = 1).

A.



B.

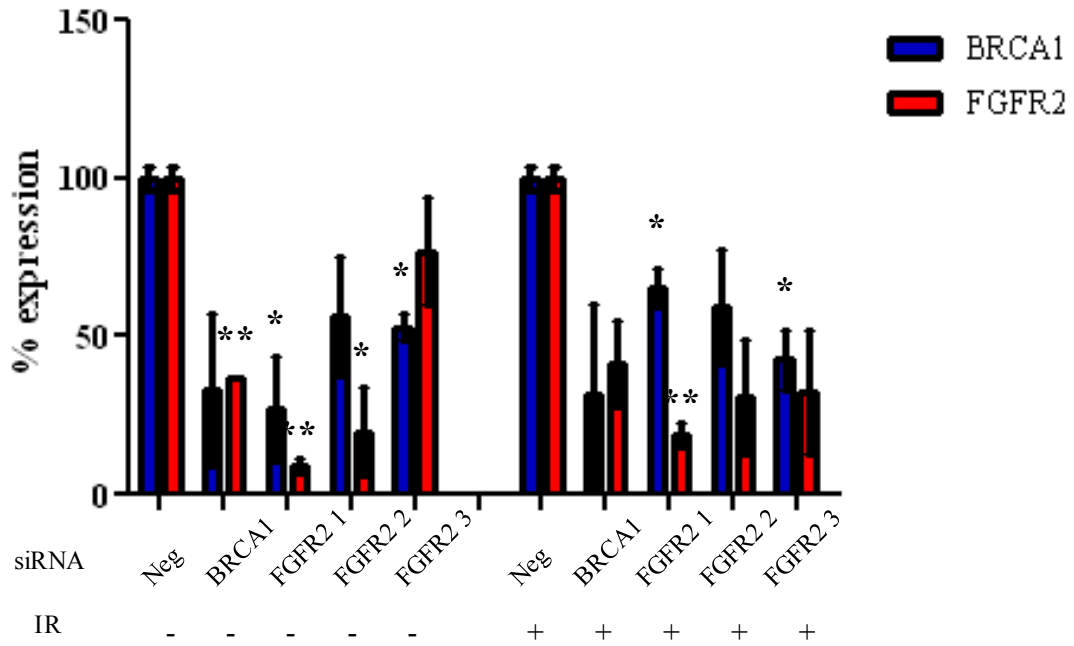


Figure 3: Effect of siRNA-mediated knockdown of FGFR2 on BRCA1 protein levels. Protein analysis by Western blot in MCF7 cells 72 h following reverse transfection with RNAiMAX and either Neg, BRCA1, or three individual siRNAs targeting the indicated putative kinase regulator and then either left unirradiated or irradiated with 10 Gy of ionizing radiation. Panel A is representative Western blots for BRCA1, FGFR2 and actin (served as loading control) following siRNA-mediated knockdown of FGFR2 and Panel B shows the respective densitometry of each sample (n = 2, presented as average values \pm standard error). * denotes $P \leq 0.0498$, ** denotes $P \leq 0.0042$.

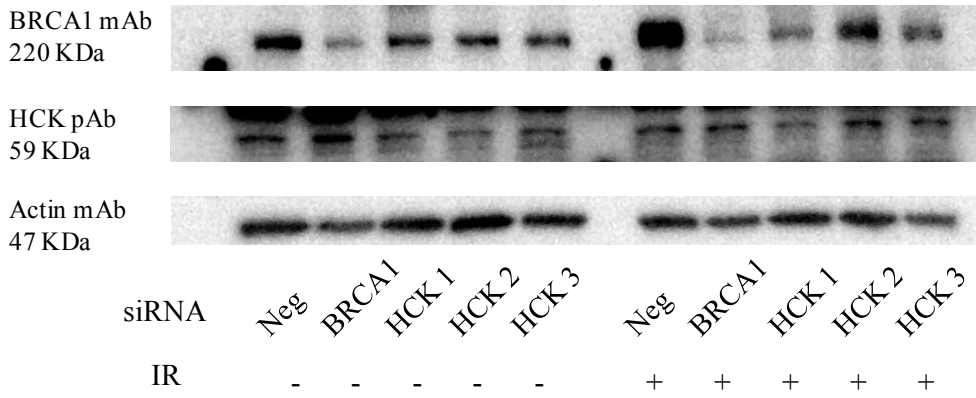
diminished HCK protein expression for both nonIR and IR samples (**Figure 4**). This effect is not due to poorly functioning siRNAs since HCK mRNA levels following siRNA-mediated knockdown of HCK are very low (**Figure 5**), suggesting that the HCK protein may be very stable. However, BRCA1 protein expression is reduced when HCK protein expression is decreased, suggesting that HCK affects BRCA1 expression at the protein level.

Conclusions

Secondary validation of kinase hits identified from the primary screen utilized qRT-PCR to assess for mRNA levels of BRCA1 and Western blot analysis to assess for protein levels of the target kinase and BRCA1. Neither siRNA-mediated knockdown of MAP3K1 nor FGFR2 appear to affect BRCA1 mRNA expression, but both affect BRCA1 protein expression, possibly suggesting that they are involved in a pathway that affects either translation efficiency of BRCA1 protein or BRCA1 protein stability. Additionally, BRCA1 appears to positively regulate FGFR2 expression. This could be possible because BRCA1 has been shown to be a component of the RNA polymerase II holoenzyme to modulate the expression of downstream genes (Scully et al., 1997). Alternatively, BRCA1 may physically interact with FGFR2 to regulate its signaling in a manner similar to JAK-STAT3 signaling (Gao et al., 2001). siRNA-mediated knockdown of HCK impacts BRCA1 mRNA expression to a lesser degree than BRCA1 protein expression, suggesting that the effects of regulation are greater at the protein level.

Western blot analysis to assess for target protein expression following siRNA-mediated knockdown of a kinase has proven more difficult because of the lack of antibodies with high sensitivity and specificity. Alternative approaches need to be explored to determine whether siRNA-mediated knockdown of a kinase has occurred. One method to improve the sensitivity

A.



B.

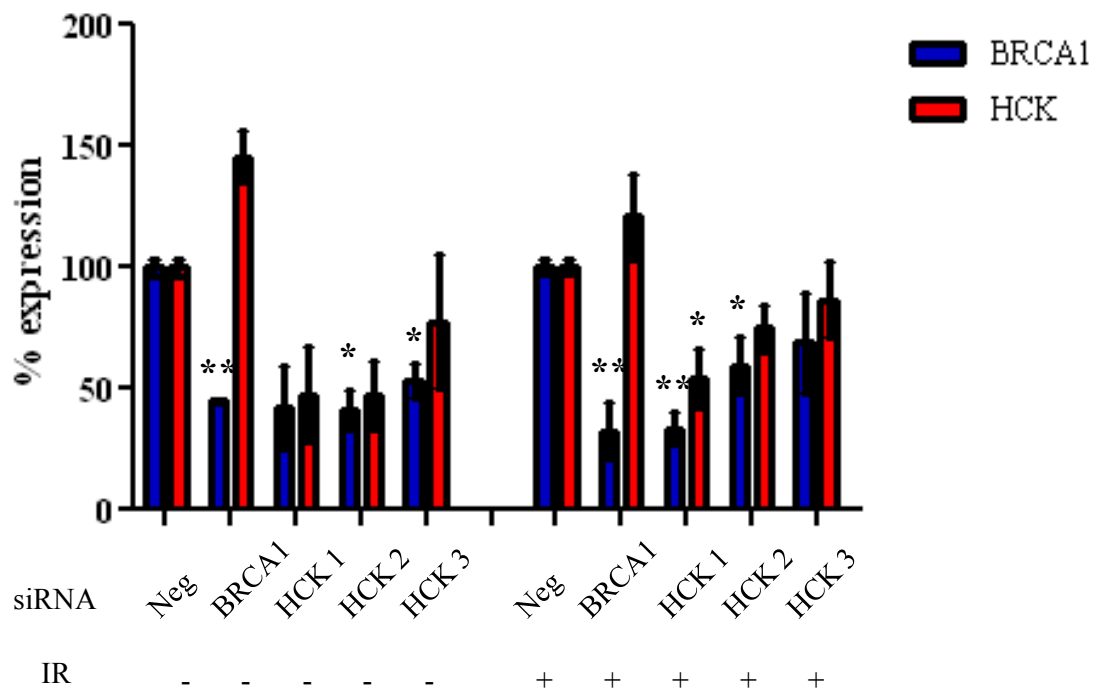


Figure 4: Effect of siRNA-mediated knockdown of HCK on BRCA1 protein levels. Protein analysis by Western blot in MCF7 cells 72 h following reverse transfection with RNAiMAX and either Neg, BRCA1, or three individual siRNAs targeting the indicated putative kinase regulator and then either left unirradiated or irradiated with 10 Gy of ionizing radiation. Panel A is representative Western blots for BRCA1, HCK and actin (served as loading control) following siRNA-mediated knockdown of HCK and Panel B shows the respective densitometry of each sample (n = 2 for nonIR, n = 3 for IR presented as average values \pm standard error). * denotes $P \leq 0.0278$, ** denotes $P \leq 0.005$.

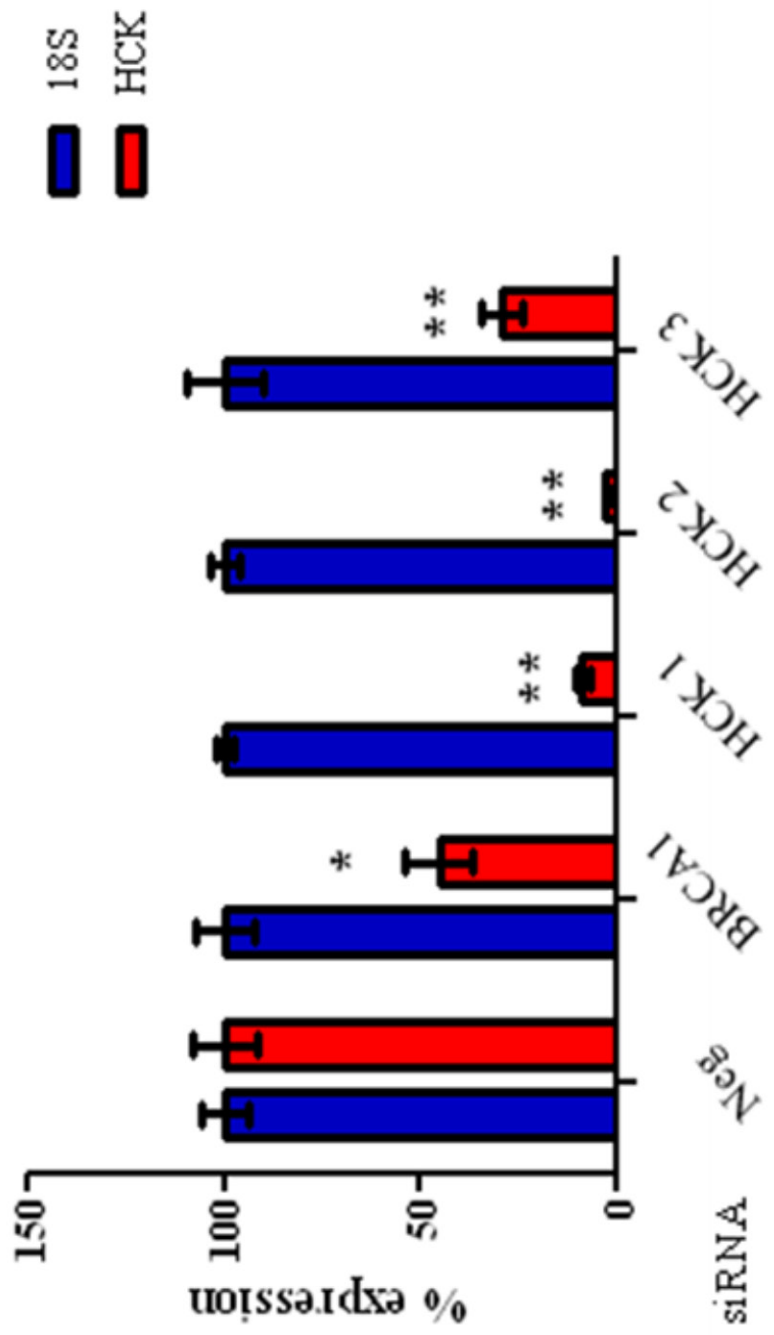


Figure 5: Validation of siRNA-mediated knockdown of HCK siRNAs. HCK RNA analysis by qRT-PCR in MCF7 cells 72 h following reverse transfection with RNAiMAX and either Neg, BRCA1, or three individual siRNAs targeting the indicated putative kinase regulator. Data presented as relative HCK expression \pm standard error (n=3). * denotes P ** denotes P < 0.0001.

and specificity of available antibodies is incubation with a biotinylated secondary antibody followed by streptavidin-conjugated tertiary antibody. Additionally, attempts to use these antibodies for immunofluorescence to assess for target kinase knockdown using staining conditions for BRCA1 have proven difficult as well. However, optimization of staining conditions for each individual antibody may help resolve this issue.

CHAPTER IV

EVALUATE THE EFFECT OF KINASE KNOCKDOWN ON THE ABILITY OF CELLS TO RESPOND TO DNA DAMAGE

Introduction

Kinases play a significant role in the regulation of cellular responses within various signaling pathways, such as DNA damage repair and cell cycle checkpoints. For example, the protein kinase A (PKA) pathway plays a role in the constitutive expression of BRCA1 via CREB (Ghosh et al., 2008). Furthermore, dysregulation of kinases, such as those in the PI3K, EGFR, and ErbB2 pathways, is prevalent in many cancers, including breast cancer (Bader et al., 2005; Nicholson et al., 2001). Additionally, mutations in ATM and CHK2 lead to increased breast cancer susceptibility (Ahmed and Rahman, 2006; Weischer et al., 2007). As mentioned in the Introduction, both ATM and CHK2 are involved in the phosphorylation of BRCA1 to mediate DSB repair (Cortez et al., 1999; Zhang et al., 2004). As the signaling pathways that connect these kinases to BRCA1 expression and function are being elucidated, bioinformatics suggest other potential kinase involvement in the regulation of BRCA1 expression and function. There are regulatory elements within the BRCA1 promoter that have been shown to bind specific transcription factors (Atlas et al., 2001; Atlas et al., 2000; Baker et al., 2003; Gilbert et al., 2010; Jeffy et al., 2005), but events upstream involving kinases have not yet been fully described. Additionally, there are phosphorylation sites in BRCA1 that do not have an associated kinase. DNA damage repair is a critical BRCA1 function in maintaining genomic stability and preventing tumorigenesis (Jasin, 2002; Khanna and Jackson, 2001; van Gent et al., 2001). The role of BRCA1 in the DNA damage pathway provided a model for our cell-based functional

assay to identify kinase regulators of BRCA1 expression and function from a kinase siRNA library screen. Fourteen kinases have been identified and validated where the associated siRNAs consistently diminished BRCA1 IRIF formation following exposure to IR. Previous chapters have outlined the process by which these kinases were identified and validated. This chapter evaluates the effect of siRNA-mediated knockdown of these kinases on the ability of cells to repair DNA damage and continue to survive. DSBs are generated with IR and can be repaired by either the error-free homologous recombination (HR) or the error-prone non-homologous end-joining (NHEJ). Studies involving the colocalization of BRCA1 and Rad51, an important component in HR, within nuclear foci suggest that BRCA1 is involved in HR (Baumann et al., 1996; Scully et al., 1997). Additionally, BRCA1 has been shown to interact with MRN, which participates in both HR and NHEJ, to form nuclear foci that are distinct from Rad51 (Zhong et al., 1999). The efficiency of repair of both mechanisms was evaluated using an established DSB repair assay that involves the use of an I-SceI repair reporter plasmid (DR-GFP) and an I-SceI expression plasmid (pCBASce) (Nakanishi et al., 2005) (We thank Maria Jasin, PhD at Memorial Sloan-Kettering Cancer Center for providing these plasmids). A clonogenic survival assay was used to measure the ability of a single cell to proliferate and form a colony of at least 50 cells following chemical transfection of the Neg, BRCA1, and kinase siRNAs and treatment with IR. Findings from the repair assay demonstrated the cell repair capacity by HDR and NHEJ while the clonogenic assay demonstrated the role of siRNA-mediated knockdown of the kinase in determining sensitivity to IR.

Materials and Methods

DSB Repair Assay: The repair assay involved the use of an I-SceI repair reporter plasmid (DR-GFP) and an I-SceI expression plasmid (pCBASce). MCF7 and HeLa (immortal cell line derived from cervical cancer cells) cells were transfected with DR-GFP DNA by electroporation (4 µg DNA into 4×10^5 cells) and selected in puromycin (15 µg/ml for MCF7 cells and 2 µg/ml for HeLa cells) for 3 weeks at 37°C in 5% CO₂. To test the effect of siRNA-mediated knockdown of a kinase on HR and NHEJ, DR-GFP-expressing MCF7 or HeLa cells were transfected with siRNA targeting the kinase regulator by chemical transfection with RNAiMAX as previously described in Chapter 2. The same three siRNAs for each kinase from the primary screen and secondary validation were evaluated. After 48 hours, these cells were transfected with either I-SceI expression plasmid pCBASce or mock vector pCAGGS by electroporation (4 µg DNA into 4×10^5 cells) using the using the Nucleofector 96-well Shuttle System, Program 96-EN-130 (Amaxa) as previously described in Chapter 2. To determine the amount of repair by HR, the percentage of GFP+ cells was quantitated by flow cytometric analysis on the Becton Dickinson FACS Calibur 3 days after electroporation. An average % GFP+ cells was calculated and a t test was performed using GraphPad Prism 5 (GraphPad Software) to determine whether the change in % GFP+ cells was statistically significant.

Genomic DNA was isolated 3 days after electroporation using the DNeasy Blood and Tissue Kit from Qiagen and used as the template for PCR with the following primers: DRGFP-F, 5'-CTGCTAACCATGTTCATGCC-3'; DRGFP-R, 5'-AAGTCGTGCTGCTTATGTG-3'. PCR conditions were 1 cycle for 1 min at 94°C for initial denaturation; 35 cycles for 20 s at 94°C for denaturation, then 40 s at 54°C for annealing, and 40 s at 72°C for extension; and 1 cycle for 7 min at 72°C for final extension. PCR products were purified using the QIAquick PCR

Purification Kit (Qiagen) and then digested with I-SceI (described below). The products by digest with I-SceI were purified using the QIAquick PCR Purification Kit (Qiagen) and then a half volume of the products was digested with BcgI (described below). The products by digest with both I-SceI and BcgI were purified using the QIAquick PCR Purification Kit (Qiagen) and then the products digested with I-SceI alone and both I-SceI and BcgI were separated on a 1.2% agarose gel in 1X TAE (40 mM Tris-acetate, 1 mM EDTA). The gel was stained with ethidium bromide and the ethidium signals were quantified using the UVP imaging center.

Extraction of Genomic DNA: gDNA was extracted using the DNeasy Blood and Tissue Kit (Qiagen). Cells were centrifuged for 5 min at 300xg in an Eppendorf 5415 D microcentrifuge (Westbury, New York). The pellet was resuspended in 200 μ l PBS. 20 μ l proteinase K and 4 μ l RNase A (100 mg/ml) were then added and incubated for 2 min at RT. 200 μ l Buffer AL was added, mixed thoroughly by vortexing and incubated at 56°C for 10 min. 200 μ l ethanol was then added to each sample and mixed thoroughly by vortexing. The mixture was transferred to a DNeasy Mini spin column and centrifuged at \geq 6000xg for 1 min. Flow-through and collection tube were discarded. 500 μ l Buffer AW1 was then added and centrifuged for 1 min at \geq 6000xg. Again the flow-through and collection tube were discarded. 500 μ l Buffer AW2 was added and centrifuged for 3 min at full speed (16,100xg) dry the DNeasy membrane. Flow-through and collection tube were discarded. The DNeasy Mini spin column was placed in a 1.5 ml Eppendorf tube, 100 μ l Buffer AE was pipetted directly onto the DNeasy membrane, incubated at RT for 1 min, and then centrifuged for 1 min at \geq 6000xg to elute the DNA.

I-SceI and BcgI Restriction Enzyme Digest: The amplified fragment of DSB repair products was digested with 10 units of I-SceI (2 μ l of 5,000 units/ml) (New England BioLabs, Ipswich, MA) in 5 μ l NEBuffer I-SceI (10X) plus 0.5 μ l of BSA (100X) in a total reaction volume of 50 μ l for 16 h at 37°C and then heat inactivated at 65°C for 20 min. A half volume of the products was then digested with 20 units of BcgI (10 μ l of 2,000 units/ml) (New England BioLabs) in 10 μ l NEBuffer 3 (10X) supplemented with 20 μ M S-adenosylmethionine (SAM) (2 μ l of 1 mM SAM) in a total reaction volume of 100 μ l for 4 h at 37°C and then heat inactivated at 65°C for 20 min.

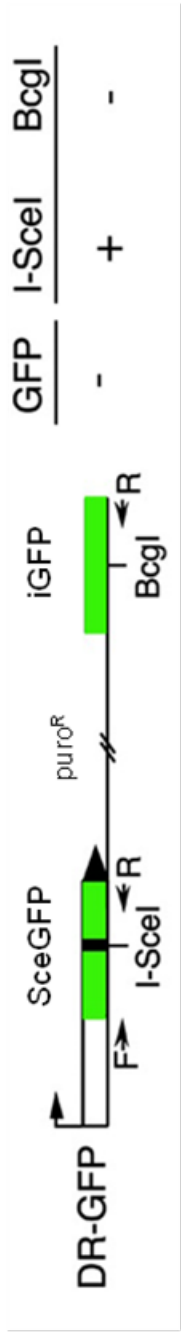
Purification of PCR Products: PCR products were purified using the QIAquick PCR Purification Kit (Qiagen). 5 volumes of Buffer PB were added to 1 volume of the PCR sample and mixed. The sample was transferred to a QIAquick spin column and centrifuged for 1 min at full speed (16,100xg). Flow-through was discarded. 750 μ l Buffer PE was added to wash the QIAquick spin column membrane and centrifuged for 1 min at full speed (16,100xg). Flow-through was again discarded. The column was centrifuged for an additional 1 min to remove residual Buffer PE. The QIAquick column was then placed in a 1.5 ml Eppendorf tube and the DNA was eluted by adding 30 μ l Buffer EB, letting the column stand for 1 min, and then centrifuging for 1 min at full speed (16,100xg).

Clonogenic Assay: The protocol for reverse transfection of MCF7 cells with RNAiMAX and kinase siRNAs was described in Chapter 2. Twenty-four hours post-transfection, cells were trypsinized, passed through a 40 μ m strainer, and counted using the ViCell (Beckman Coulter, Brea, CA). 3,000 viable cells were plated per dish in the desired number of 60 mm dishes (6

dishes per siRNA to assess for dose-dependent response to IR) and incubated at 37°C in 5% CO₂. The next day, cells were irradiated with 0, 1, 2, 4, 6, or 8 Gy of IR from a ¹³⁷Cs source and incubated at 37°C in 5% CO₂ for 10 days. The media was not changed during those 10 days. After 10 days, the medium was aspirated from each dish. Cells were washed once with PBS and then fixed with 100% methanol for 5 min at RT. The methanol was aspirated from each dish and the methanol fixation was repeated. The methanol was aspirated and the dishes were allowed to dry at RT. Colonies were stained with 2 ml of 1% crystal violet (in ddH₂O) for 5 min at RT then washed twice with ddH₂O and allowed to dry at RT. Each dish was then imaged upside-down on the white table (Coomassie setting) of the UVP (Upland, CA) imaging center. Each TIF file was opened in ImageJ (public domain, Java-based image processing program developed at the National Institutes of Health) and converted to an 8-bit grayscale image. Threshold was set equally for each image and the “Analyze Particles” program was used. Relative survival was calculated in Excel by comparing the number of colonies at 1, 2, 4, 6, and 8 Gy to the number of colonies at 0 Gy for each siRNA. Percent survival was plotted in GraphPad Prism 5 (GraphPad Software, San Diego, CA) and a t test was employed to determine statistical significance.

Results and Discussion

DSB Repair Assay to Assess DNA Repair Capacity: MCF7 and HeLa cell lines were established with an integrated copy of the DR-GFP reporter plasmid, which is composed of two inactive alleles of GFP, SceGFP and iGFP, separated by a puromycin resistance marker with various cleavage sites for Sall, HindIII, I-SceI, and BcgI (**Figure 1**). The SceGFP contains the 18-bp recognition site for the I-SceI endonuclease. Transfection by electroporation of the I-SceI expression vector pCBASce leads to expression of the I-SceI endonuclease, which generates a



+ endonuclease = DSB

Resolution by

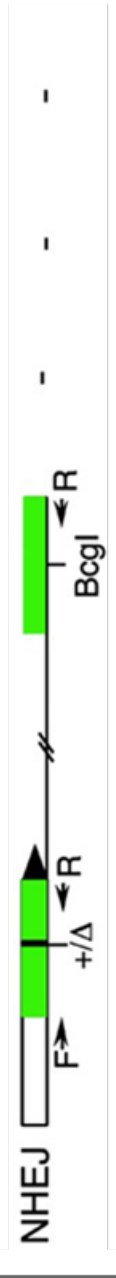
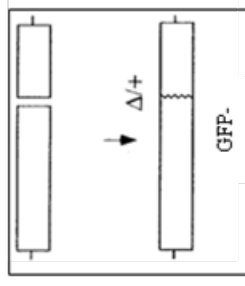
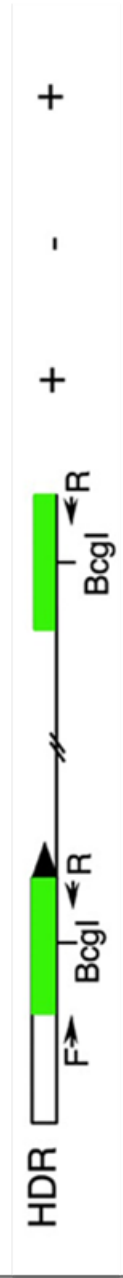
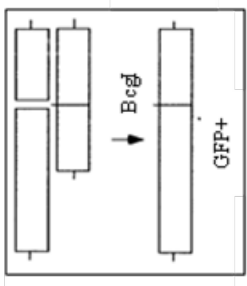


Figure 1: Schematic of the DR-GFP reporter plasmid and DSB repair mechanisms. The DR-GFP reporter plasmid is composed of two inactive alleles of GFP, SceGFP and iGFP, separated by a puromycin resistance marker with I-SceI and BcgI cleavage sites. It is stably integrated at a random chromosomal locus in HeLa cells. Expression of the I-SceI endonuclease generates a DSB at the I-SceI site in the SceGFP gene. The DSB can be repaired by either HDR or NHEJ. HDR is an error-free mechanism of repair in which the broken ends use a homologous sequence elsewhere in the genome as a template to mediate repair synthesis while NHEJ is an error-prone mechanism of repair that modifies and rejoins the ends. Repair of the DSB by HDR is directed by the homologous downstream iGFP repeat to restore an intact GFP with loss of the I-SceI site and introduction of a BcgI site. Repair of the DSB by NHEJ also results in loss of the I-SceI site but does not produce a functional GFP or a BcgI site (Johnson and Jasin, 2001; Nakanishi et al., 2005).

DSB at the I-SceI site in the SceGFP gene. The DSB can be repaired by either homology-directed repair (HDR) or non-homologous end joining (NHEJ). HDR is an error-free mechanism of repair in which the broken ends use a homologous sequence elsewhere in the genome as a template to mediate repair synthesis while NHEJ is an error-prone mechanism of repair that modifies and rejoins the ends (Shrivastav et al., 2008) (**Figure 1**). Repair of the DSB by HDR is directed by the homologous downstream iGFP repeat to restore an intact GFP with loss of the I-SceI site and introduction of a BcgI site. Repair by HDR can be directly assessed by flow cytometric analysis for GFP⁺ cells. Repair of the DSB by NHEJ also results in loss of the I-SceI site but does not produce a functional GFP or a BcgI site. Total repair capacity can be assessed by digest of PCR-amplified repair products with I-SceI alone. The contribution of repair by NHEJ can be directly assessed by digest of PCR-amplified repair products with both I-SceI and BcgI.

To determine whether the identified kinases play a role in HDR and NHEJ, siRNA-mediated knockdown of MAP3K1, FGFR2, and HCK in HeLa cells stably expressing the DR-GFP reporter plasmid was performed by chemical transfection as previously described. After 48 h, these siRNA-treated cells were transfected by electroporation with either the I-SceI expression vector pCBASce (+I-SceI) or the mock control vector pCAGGS (-I-SceI) using the Amaxa nucleofection system as previously described. Following an additional 72 h, each sample was split for either flow cytometric analysis or digest of PCR-amplified repair products with I-SceI alone or I-SceI and BcgI (**Figure 2**).

Repair by HDR was more robust in HeLa cells ($26.7 \pm 0.3\%$ GFP⁺ cells) compared to MCF7 cells (0.84% GFP⁺ cells) (**Figure 3**), so subsequent repair analyses were completed in HeLa cells. HeLa cells have frequently been used to study BRCA1 expression and function and

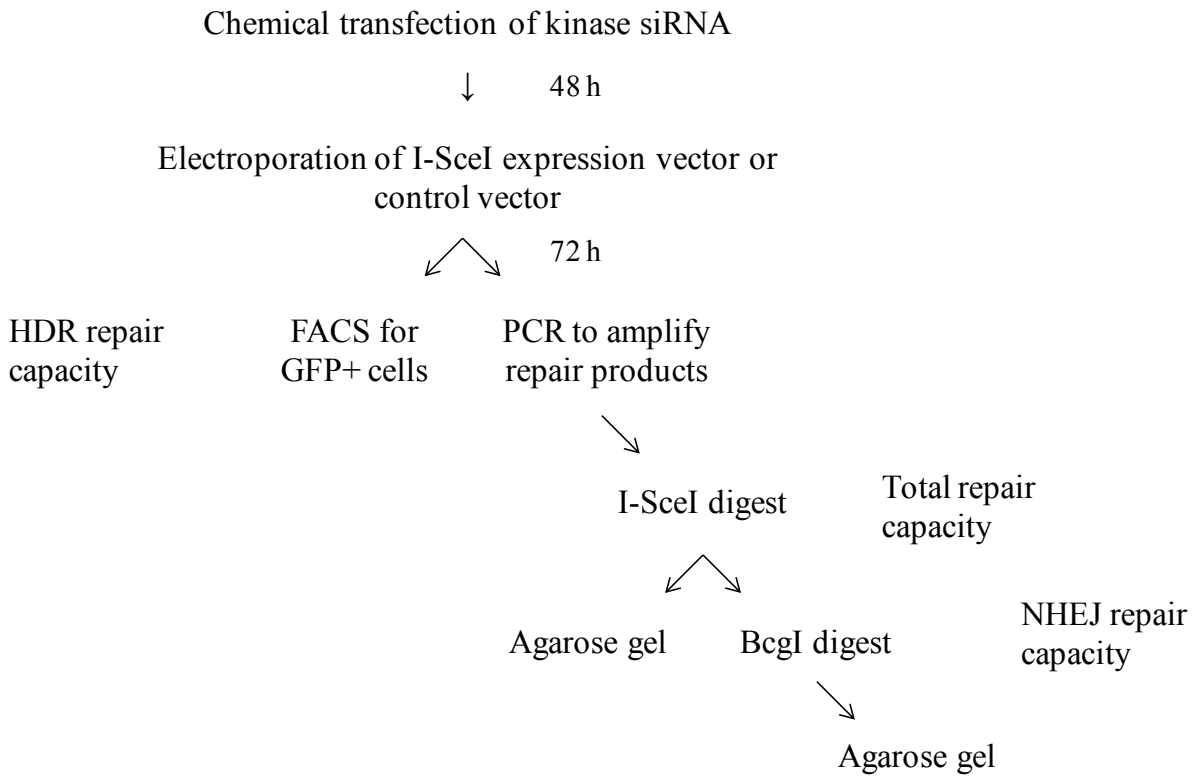


Figure 2: Schematic of the DSB repair assay workflow. Following chemical transfection of kinase siRNA and electroporation of either I-SceI expression vector or control vector, each sample was split for either flow cytometric analysis or I-SceI and BcgI digests of PCR-amplified repair products. Digest of PCR-amplified repair products with I-SceI alone represents total repair capacity. Digest of PCR-amplified repair products with both I-SceI and BcgI indicates the contribution to total repair by NHEJ. Flow cytometric analysis for GFP+ cells shows repair of DSB by HDR.

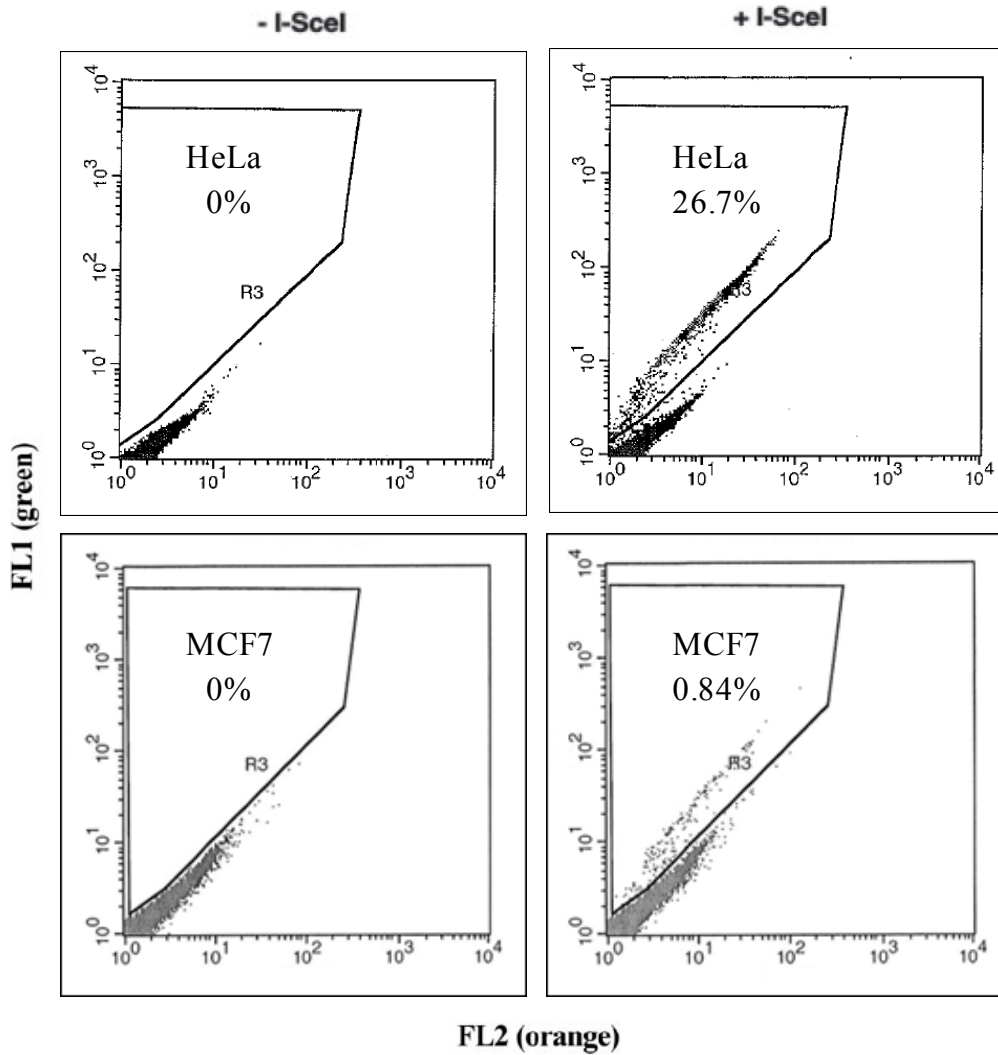


Figure 3: Efficiency of HDR in HeLa cells compared to MCF7 cells. A representative flow cytometric analysis is shown for HDR events comparing HeLa and MCF7 cells following cleavage of the I-SceI endonuclease site within the SceGFP portion of the GFP gene and subsequent repair by HDR directed by the downstream iGFP portion of the GFP gene. The GFP+ population shifts greenward to separate from the GFP- population.

have proven easier to use experimentally. The expression of each of the target kinases has not been quantified at the protein level in HeLa cells, so further Western blot analysis should be done to establish the extent of knockdown of each of the target kinases. Based on microarray data from Oncomine (www.oncomine.org, Compendia Bioscience, Ann Arbor, MI), HeLa cells appear to express BRCA1, MAP3K1, HCK, and FGFR2.

To determine total repair capacity and the contribution of repair by NHEJ, DSB repair products were analyzed using the described PCR assay. The genomic region surrounding the I-SceI site after expression of I-SceI endonuclease was amplified with PCR primers that included DSB repair products from both HDR and NHEJ. Two bands can be visualized by ethidium bromide-stained agarose gel electrophoresis when the PCR-amplified DSB repair products are digested by either I-SceI alone or I-SceI and BcgI. The 0.65-kb band represents the uncut fraction while the 0.5-kb band represents the cut fraction. The percentage uncut is the ratio of the 0.65-kb band density to the total band density (0.65-kb + 0.5-kb band densities). To determine how much of the amplified fragment underwent repair (total repair), the DSB repair products were cleaved with I-SceI alone. The uncut fraction represents total repaired products, which would remain uncut by digest with I-SceI because expression of the I-SceI endonuclease produces a DSB that is subsequently repaired with loss of the I-SceI cleavage site. The uncut fraction following digest with BcgI again represents repair by NHEJ because BcgI cleaves repair products from HDR. To determine how much of the amplified fragment underwent NHEJ, the DSB repair products were cleaved with both I-SceI and BcgI. NHEJ repair products are resistant to both digest with I-SceI and BcgI because expression of the I-SceI endonuclease results in cleavage at the I-SceI restriction site, thereby eliminating the I-SceI restriction site, and repair by NHEJ does not create a BcgI restriction site like repair by HDR. The cut fraction could represent

cells that were not successfully transfected by electroporation with pCBASce and therefore would be cleaved by digest with I-SceI. Another explanation could be that cells unable to repair by any mechanism may undergo apoptosis resulting in a greater contribution of the cut fraction to the total fraction.

Initially, the effect of siRNA-mediated knockdown of BRCA1 on DNA repair capacity was evaluated. The control siRNA used for comparison was Neg siRNA. The repair assay-specific control for the I-SceI expression vector (+I-SceI) was the mock vector pCAGGS (-I-SceI). In -I-SceI cells with Neg siRNA, the amplified fragment was completely cleaved by digest with I-SceI because no I-SceI endonuclease was expressed and the I-SceI cleavage site was left intact (**Figures 4-6**). The same outcome was observed when the amplified fragment was digested with BcgI (**Figures 7-9**). Digest with BcgI of -I-SceI cells should have no effect on the percentage uncut because there was neither expression of the I-SceI endonuclease nor generation of a DSB, so no repair was initiated and no BcgI site was introduced. This was confirmed by flow cytometric analysis of -I-SceI cells with Neg, BRCA1, MAP3K1, FGFR2, and HCK siRNAs where few if any GFP⁺ cells were detected (**Figures 10-12**). The +I-SceI cells with Neg siRNA established the baseline for total repair and repair by NHEJ. There were $63.9 \pm 3.0\%$ of repair products uncut by I-SceI (**Figures 4-6**) and $41.8 \pm 4.7\%$ of repair products uncut by I-SceI and BcgI (**Figures 7-9**). The amplified fragment was digestible with BcgI because the percentage uncut was less when the amplified fragment was digested with both I-SceI and BcgI ($41.8 \pm 4.7\%$) compared to when the amplified fragment was digested with I-SceI alone ($63.9 \pm 3.0\%$), suggesting a contribution of the homologous repair product (i.e., cleavable by BcgI) to total repair. This was confirmed by flow cytometric analysis for GFP⁺ cells, which resulted in approximately $26.7 \pm 0.3\%$ GFP⁺ cells (**Figures 10-12**). Conversely, in +I-SceI cells with

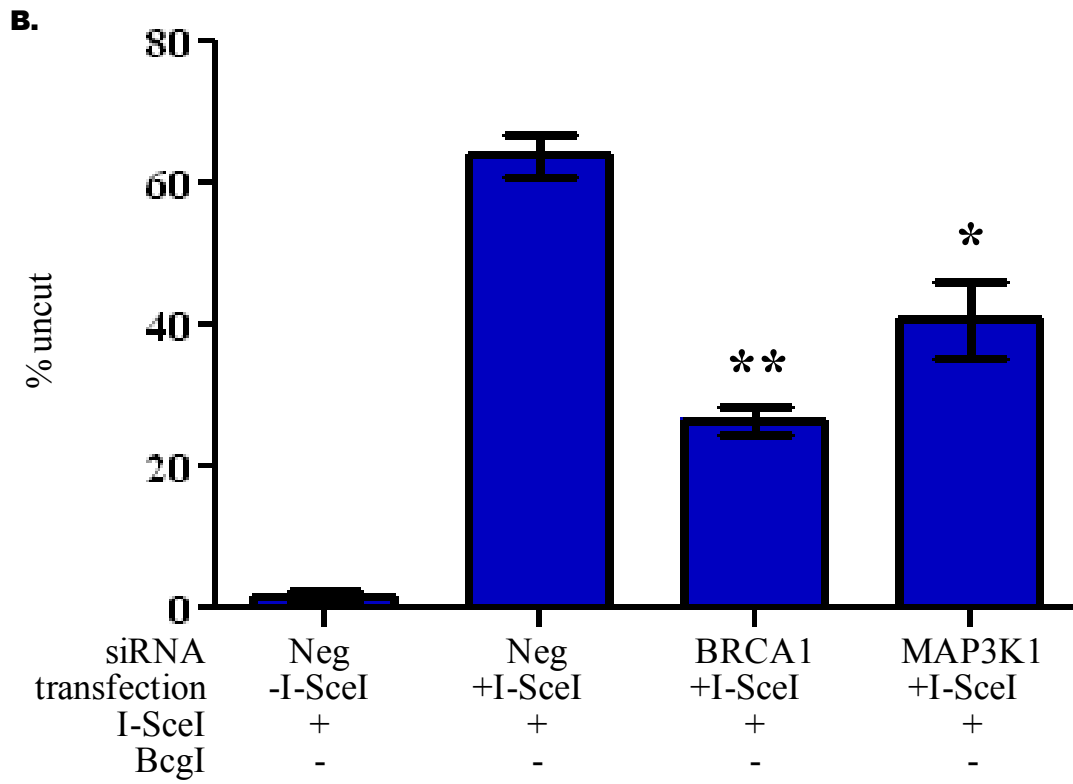
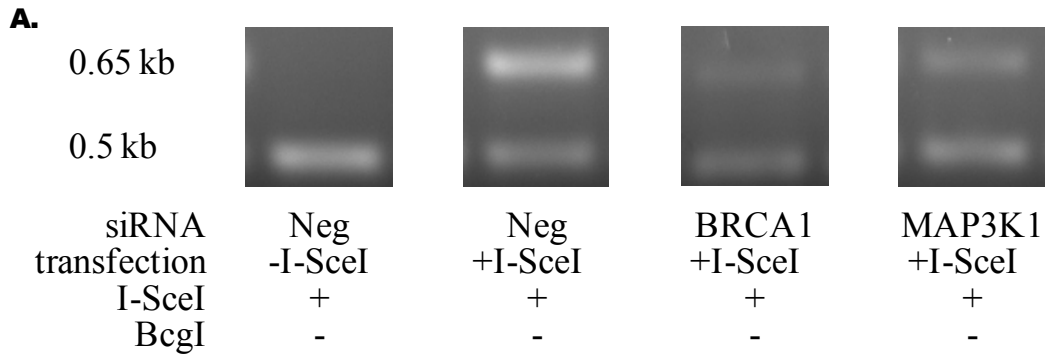


Figure 4: HeLa cells with stably integrated DR-GFP have decreased total repair capacity following siRNA-mediated knockdown of MAP3K1. Repair assay in HeLa cells first transfected by chemical transfection with RNaiMAX and either Neg, BRCA1, or three individual siRNAs targeting MAP3K1 and then transfected by electroporation with either mock vector pCAGGS (-I-SceI) or I-SceI expression vector pCBASce (+I-SceI). Panel A depicts representative images of the amplified products digested with I-SceI alone. Panel B quantifies the PCR results from cells transfected with the I-SceI expression vector and digested with I-SceI alone following siRNA-mediated knockdown of MAP3K1. Data are presented as an average of three siRNAs \pm standard error (n=2). * denotes $P = 0.0221$, ** denotes $P = 0.0005$.

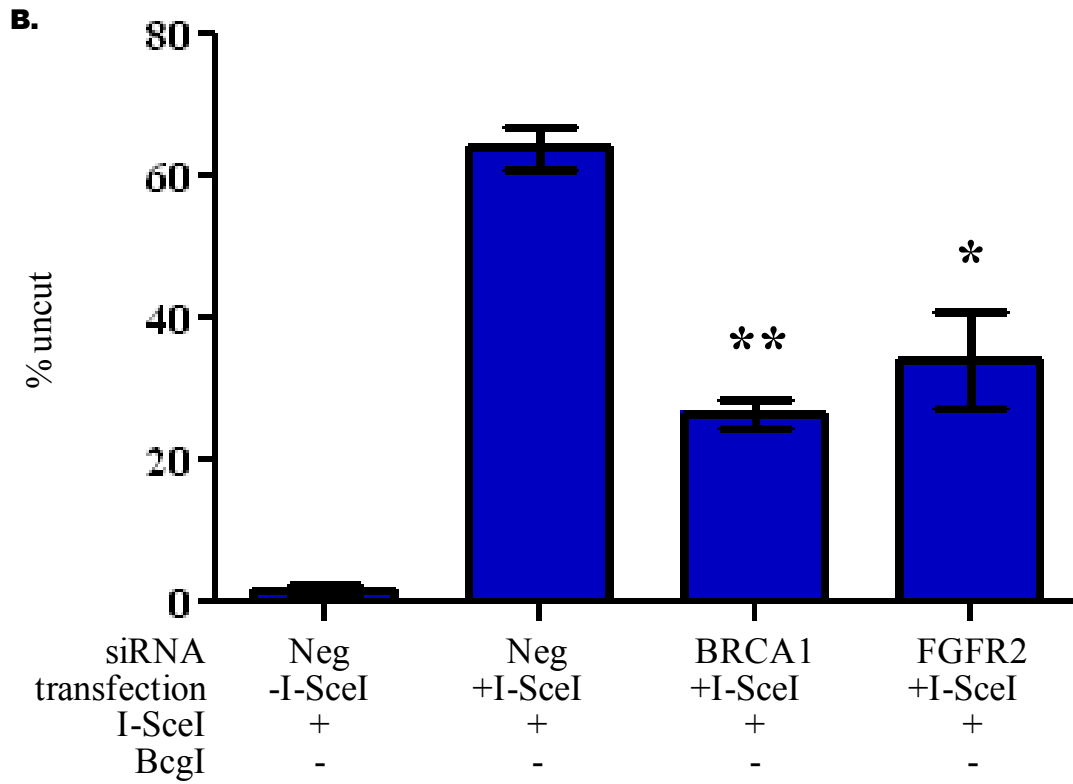
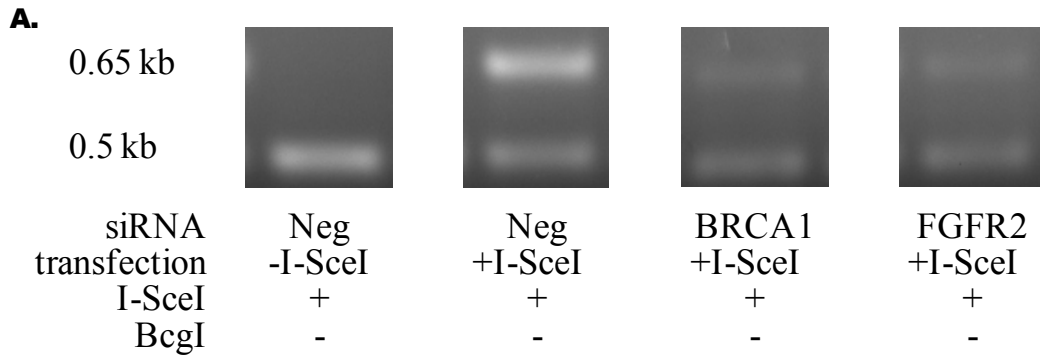


Figure 5: HeLa cells with stably integrated DR-GFP have decreased total repair capacity following siRNA-mediated knockdown of FGFR2. Repair assay in HeLa cells first transfected by chemical transfection with RNaiMAX and either Neg, BRCA1, or three individual siRNAs targeting FGFR2 and then transfected by electroporation with either mock vector pCAGGS (-I-SceI) or I-SceI expression vector pCBASce (+I-SceI). Panel A depicts representative images of the amplified products digested with I-SceI alone. Panel B quantifies the PCR results from cells transfected with the I-SceI expression vector and digested with I-SceI alone following siRNA-mediated knockdown of FGFR2. Data are presented as an average of three siRNAs \pm standard error (n=2). * denotes $P = 0.0230$, ** denotes $P = 0.0005$.

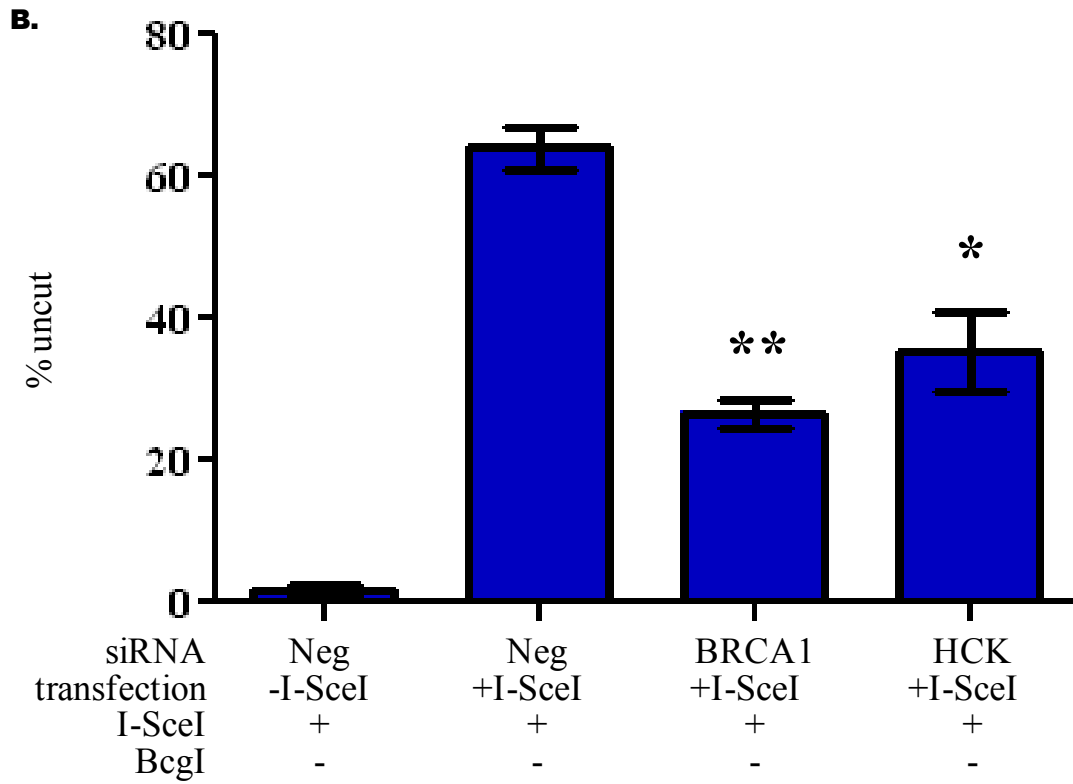
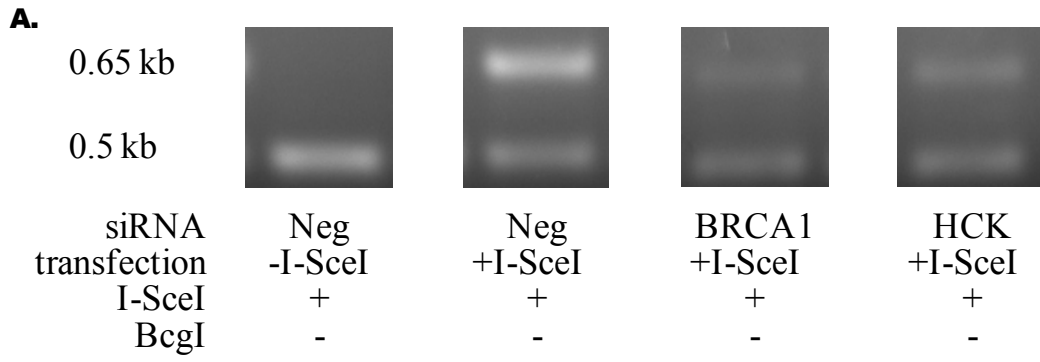


Figure 6: HeLa cells with stably integrated DR-GFP have decreased total repair capacity following siRNA-mediated knockdown of HCK. Repair assay in HeLa cells first transfected by chemical transfection with RNaiMAX and either Neg, BRCA1, or three individual siRNAs targeting HCK and then transfected by electroporation with either mock vector pCAGGS (-I-SceI) or I-SceI expression vector pCBASce (+I-SceI). Panel A depicts representative images of the amplified products digested with I-SceI alone. Panel B quantifies the PCR results from cells transfected with the I-SceI expression vector and digested with I-SceI alone following siRNA-mediated knockdown of HCK. Data are presented as an average of three siRNAs \pm standard error (n=2). * denotes $P = 0.0101$, ** denotes $P = 0.0005$.

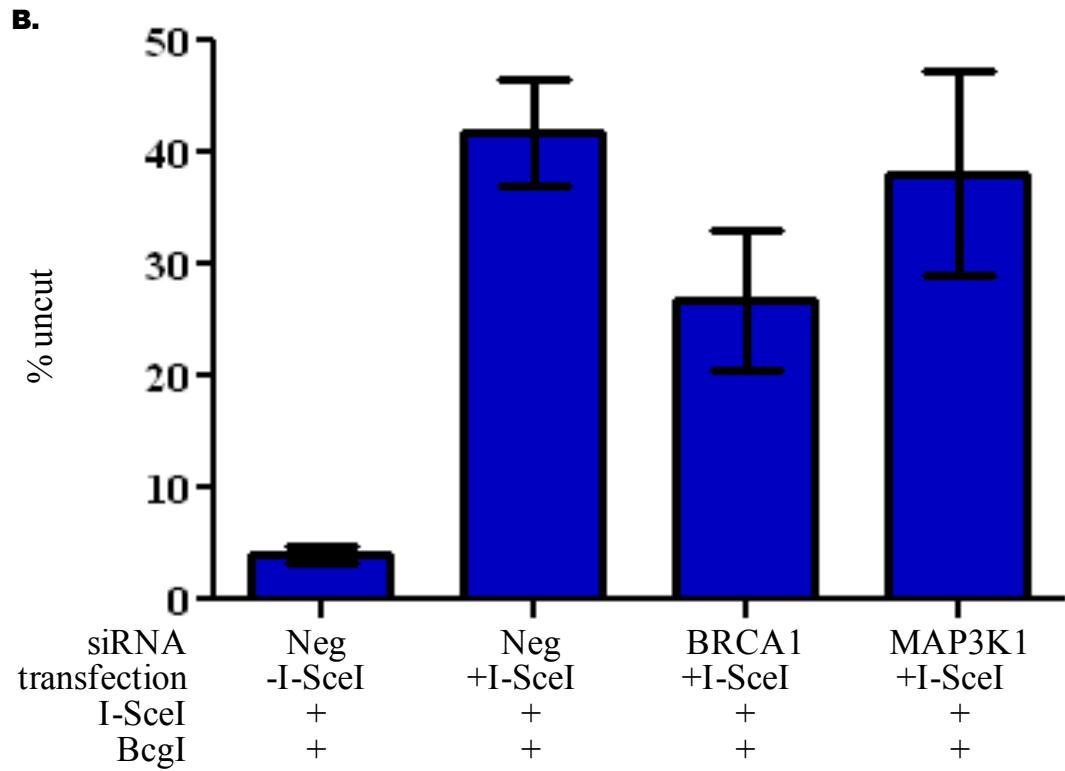
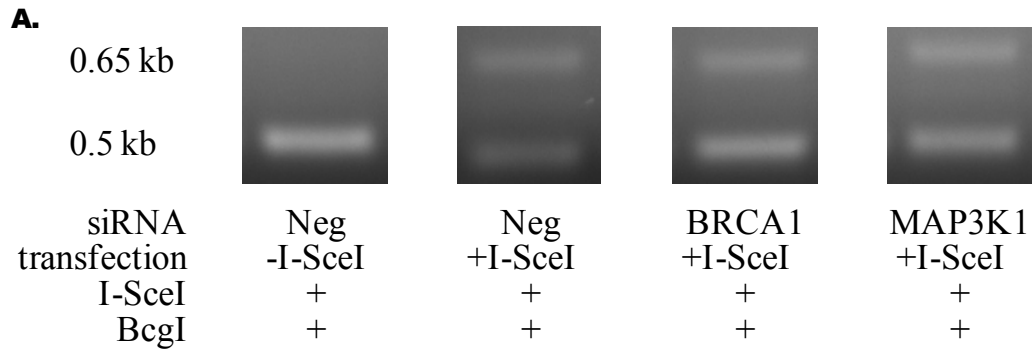


Figure 7: HeLa cells with stably integrated DR-GFP have normal levels of NHEJ following siRNA-mediated knockdown of MAP3K1. Repair assay in HeLa cells first transfected by chemical transfection with RNaiMAX and either Neg, BRCA1, or three individual siRNAs targeting MAP3K1 and then transfected by electroporation with either mock vector pCAGGS (-I-SceI) or I-SceI expression vector pCBASce (+I-SceI). Panel A depicts representative images of the amplified products digested with I-SceI and BcgI. Panel C quantifies the PCR results from cells transfected with the I-SceI expression vector and digested with I-SceI and BcgI following siRNA-mediated knockdown of MAP3K1. Data are presented as an average of three siRNAs \pm standard error (n=2).

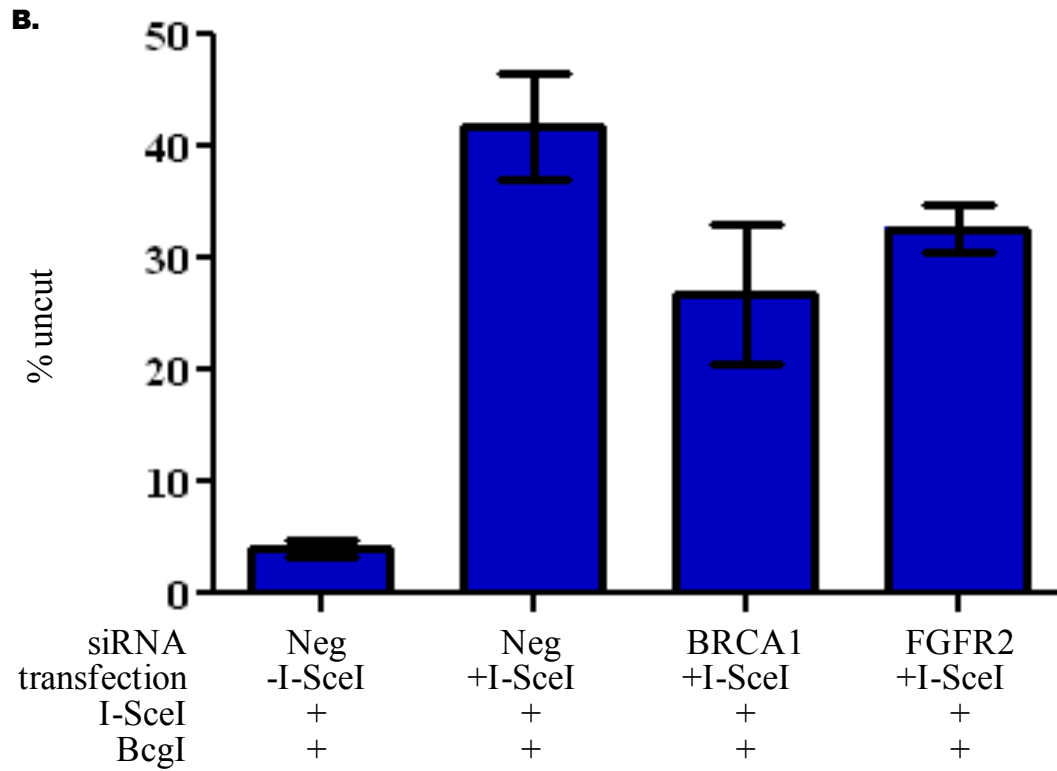
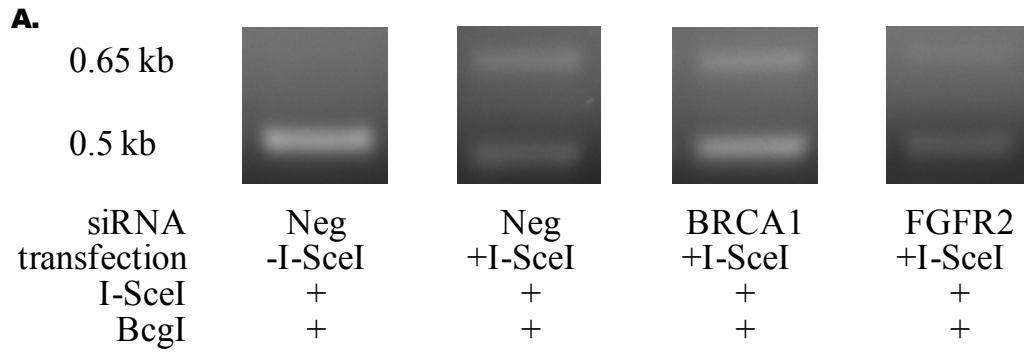


Figure 8: HeLa cells with stably integrated DR-GFP have normal levels of NHEJ following siRNA-mediated knockdown of FGFR2. Repair assay in HeLa cells first transfected by chemical transfection with RNaiMAX and either Neg, BRCA1, or three individual siRNAs targeting FGFR2 and then transfected by electroporation with either mock vector pCAGGS (-I-SceI) or I-SceI expression vector pCBASce (+I-SceI). Panel A depicts representative images of the amplified products digested with I-SceI and BcgI. Panel C quantifies the PCR results from cells transfected with the I-SceI expression vector and digested with I-SceI and BcgI following siRNA-mediated knockdown of FGFR2. Data are presented as an average of three siRNAs \pm standard error (n=2).

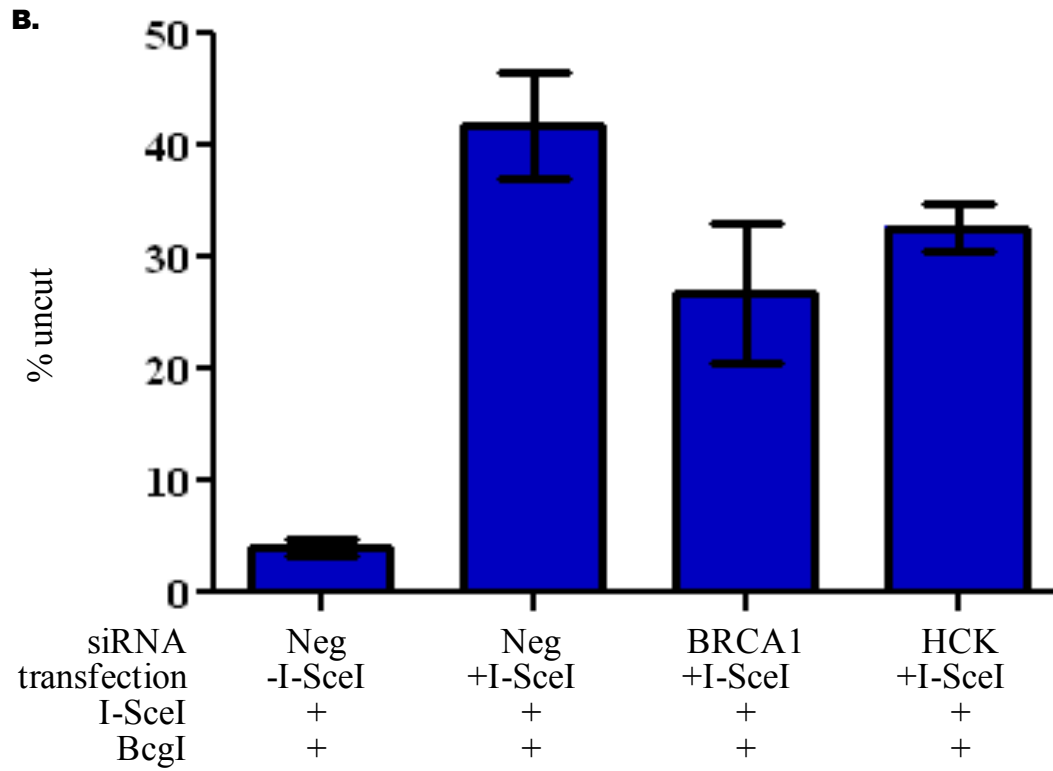
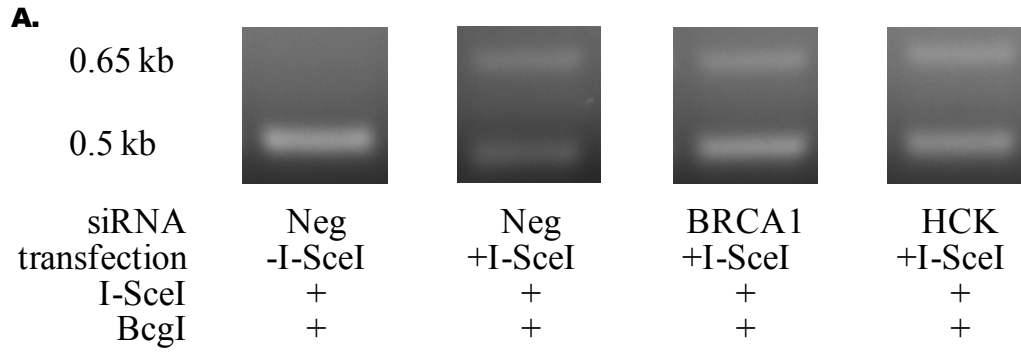


Figure 9: HeLa cells with stably integrated DR-GFP have normal levels of NHEJ following siRNA-mediated knockdown of HCK. Repair assay in HeLa cells first transfected by chemical transfection with RNaiMAX and either Neg, BRCA1, or three individual siRNAs targeting HCK and then transfected by electroporation with either mock vector pCAGGS (-I-SceI) or I-SceI expression vector pCBASce (+I-SceI). Panel A depicts representative images of the amplified products digested with I-SceI and BcgI. Panel C quantifies the PCR results from cells transfected with the I-SceI expression vector and digested with I-SceI and BcgI following siRNA-mediated knockdown of HCK. Data are presented as an average of three siRNAs \pm standard error (n=2).

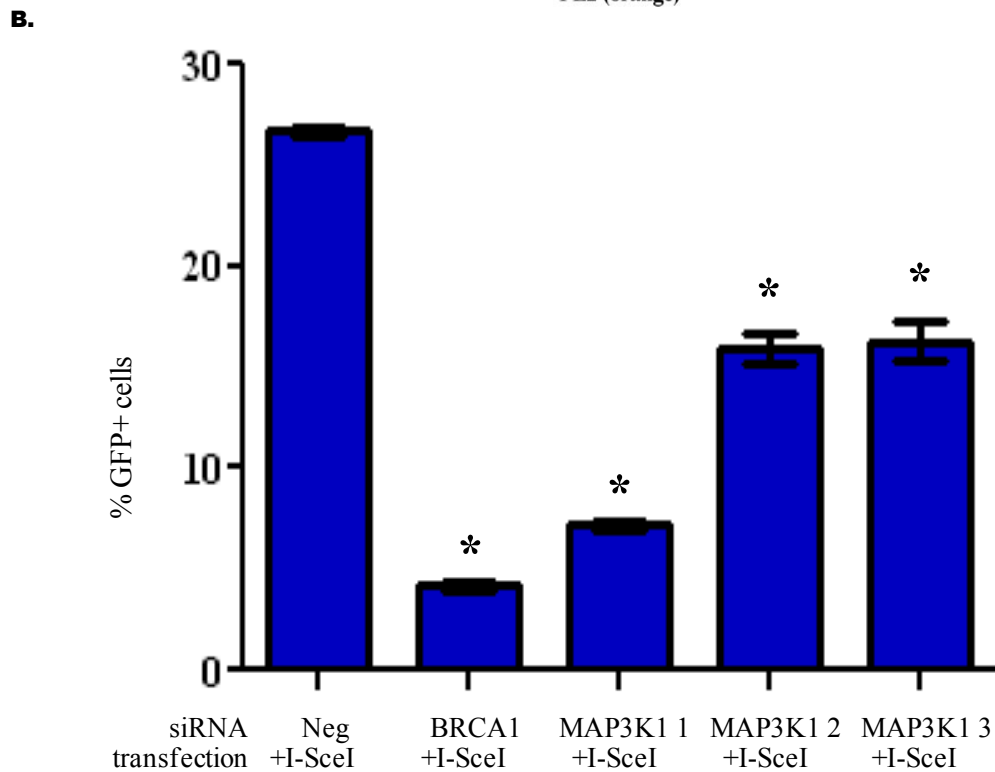
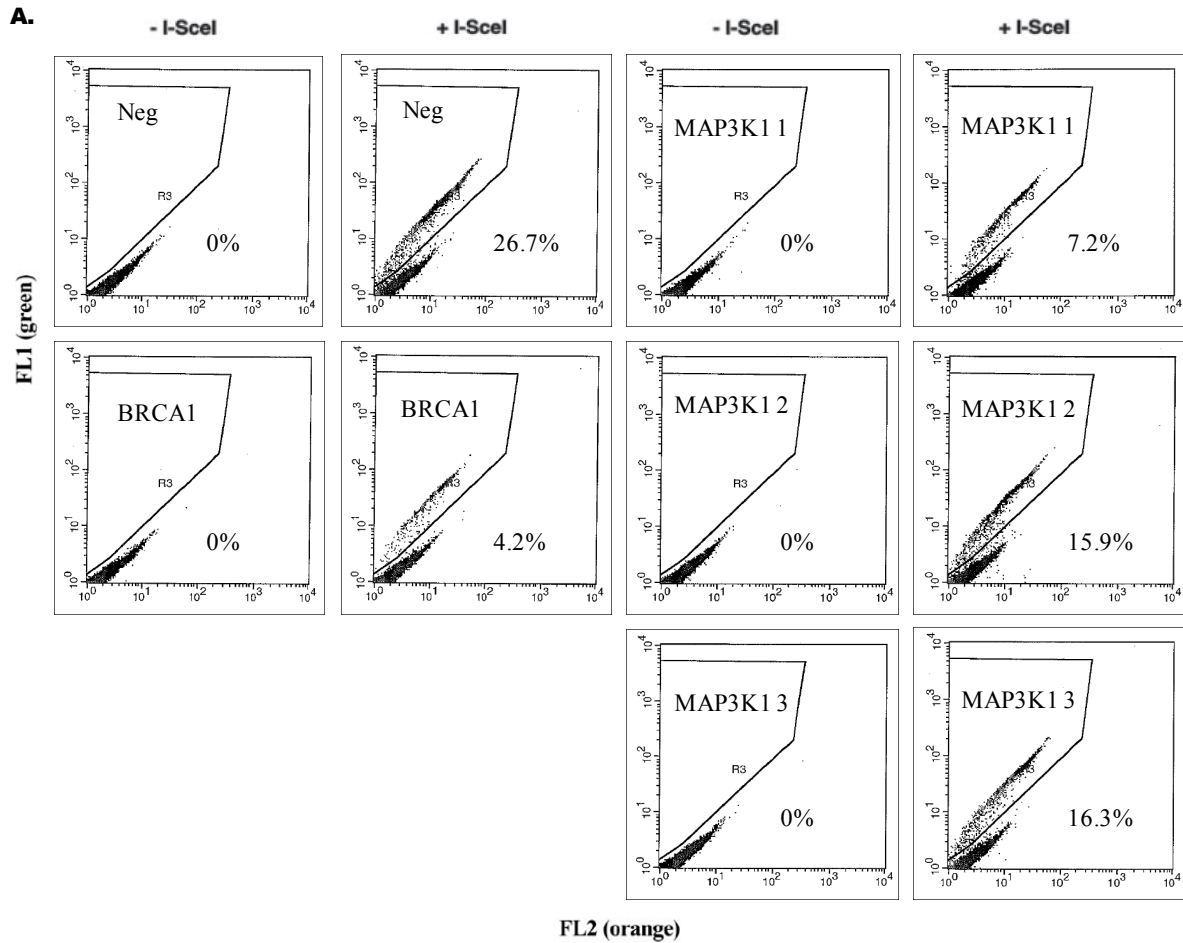


Figure 10: HDR is compromised in HeLa cells stably expressing DR-GFP following siRNA-mediated knockdown of MAP3K1 and expression of the I-SceI expression vector. Repair assay in HeLa cells first transfected by chemical transfection with RNaiMAX and either Neg, BRCA1, or three individual siRNAs targeting MAP3K1 and then transfected by electroporation with either mock vector pCAGGS (-I-SceI) or I-SceI expression vector pCBASce (+I-SceI). Panel A shows a representative flow cytometric analysis for HDR events following cleavage of the I-SceI endonuclease site within the SceGFP portion of the GFP gene and subsequent repair by HDR directed by the downstream iGFP portion of the GFP gene. The GFP⁺ population shifts greenward to separate from the GFP⁻ population. Panel B quantifies results from Panel A as average percent GFP⁺ cells \pm standard error (n=2). * denotes $P < 0.0001$.

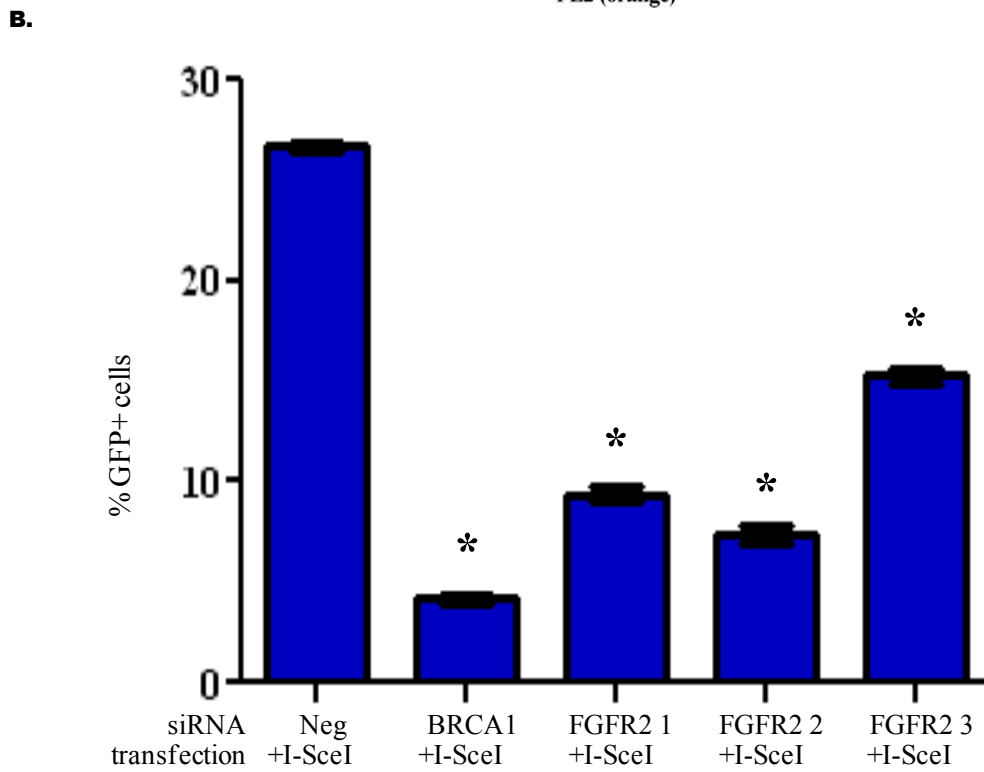
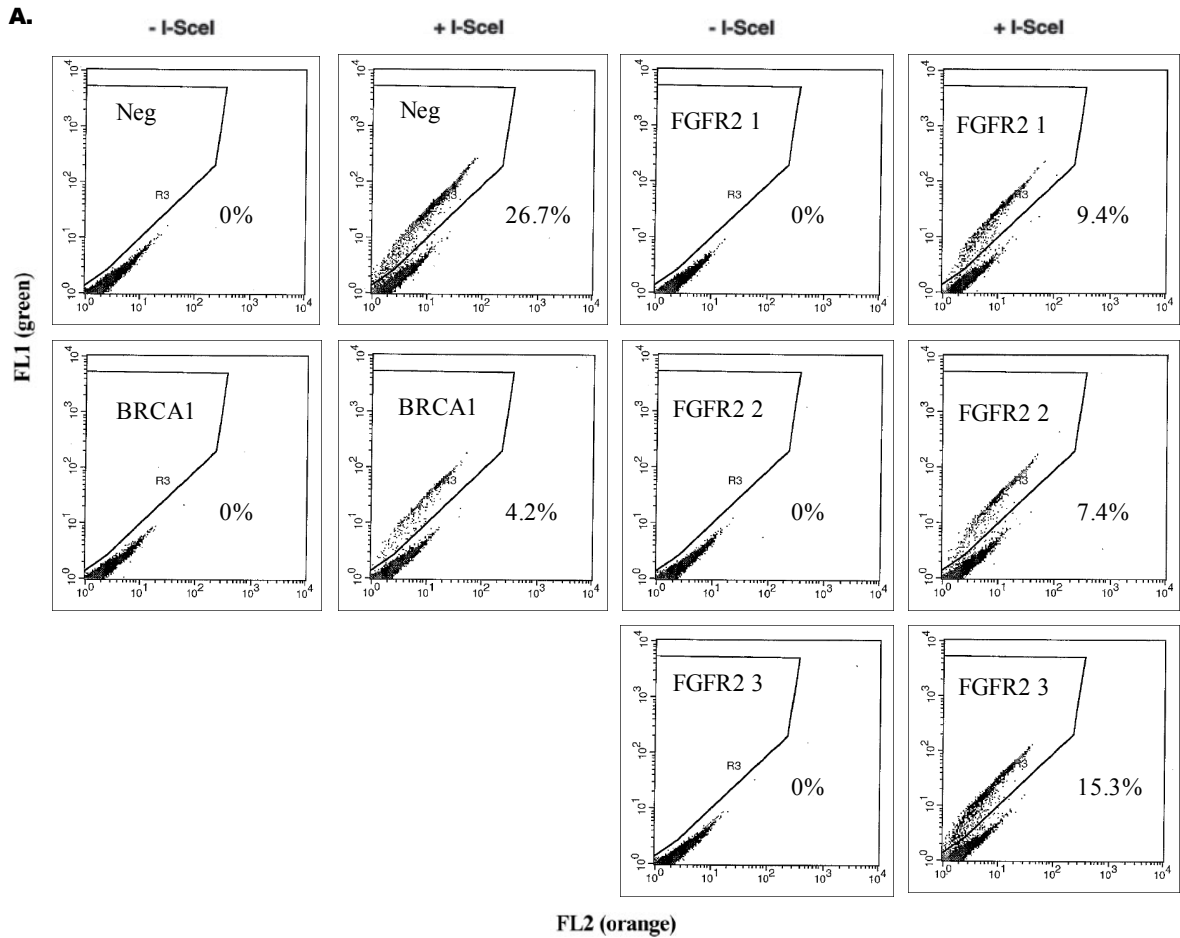


Figure 11: HDR is compromised in HeLa cells stably expressing DR-GFP following siRNA-mediated knockdown of FGFR2 and expression of the I-SceI expression vector. Repair assay in HeLa cells first transfected by chemical transfection with RNaiMAX and either Neg, BRCA1, or three individual siRNAs targeting FGFR2 and then transfected by electroporation with either mock vector pCAGGS (-I-SceI) or I-SceI expression vector pCBASce (+I-SceI). Panel A shows a representative flow cytometric analysis for HDR events following cleavage of the I-SceI endonuclease site within the SceGFP portion of the GFP gene and subsequent repair by HDR directed by the downstream iGFP portion of the GFP gene. The GFP⁺ population shifts greenward to separate from the GFP⁻ population. Panel B quantifies results from Panel A as average percent GFP⁺ cells \pm standard error (n=2). * denotes $P < 0.0001$.

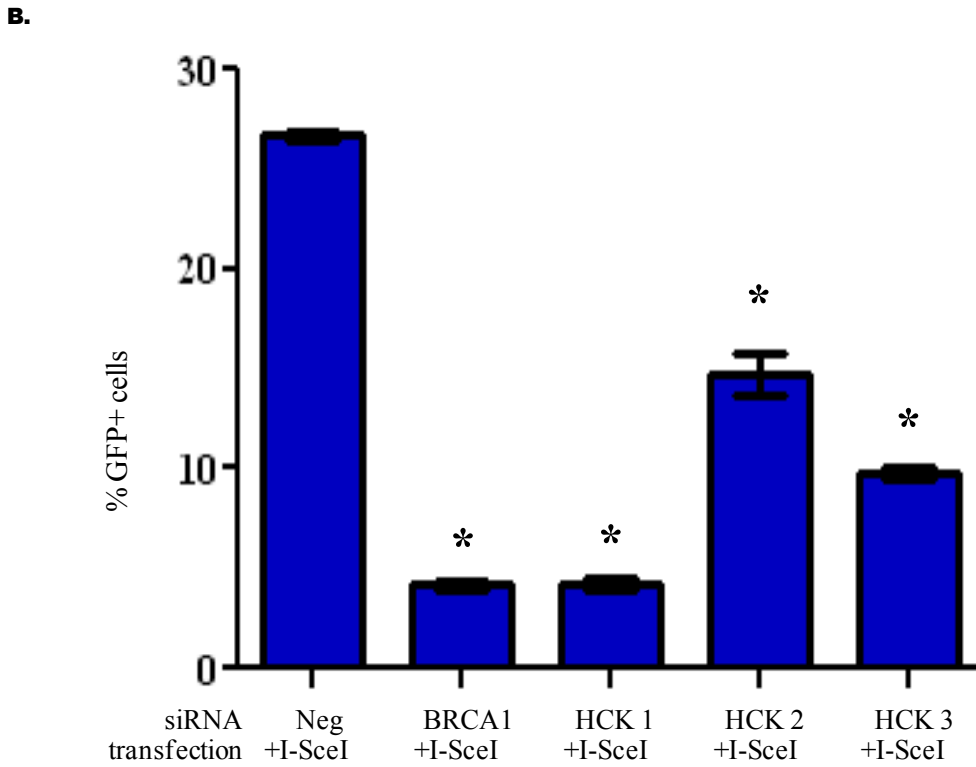
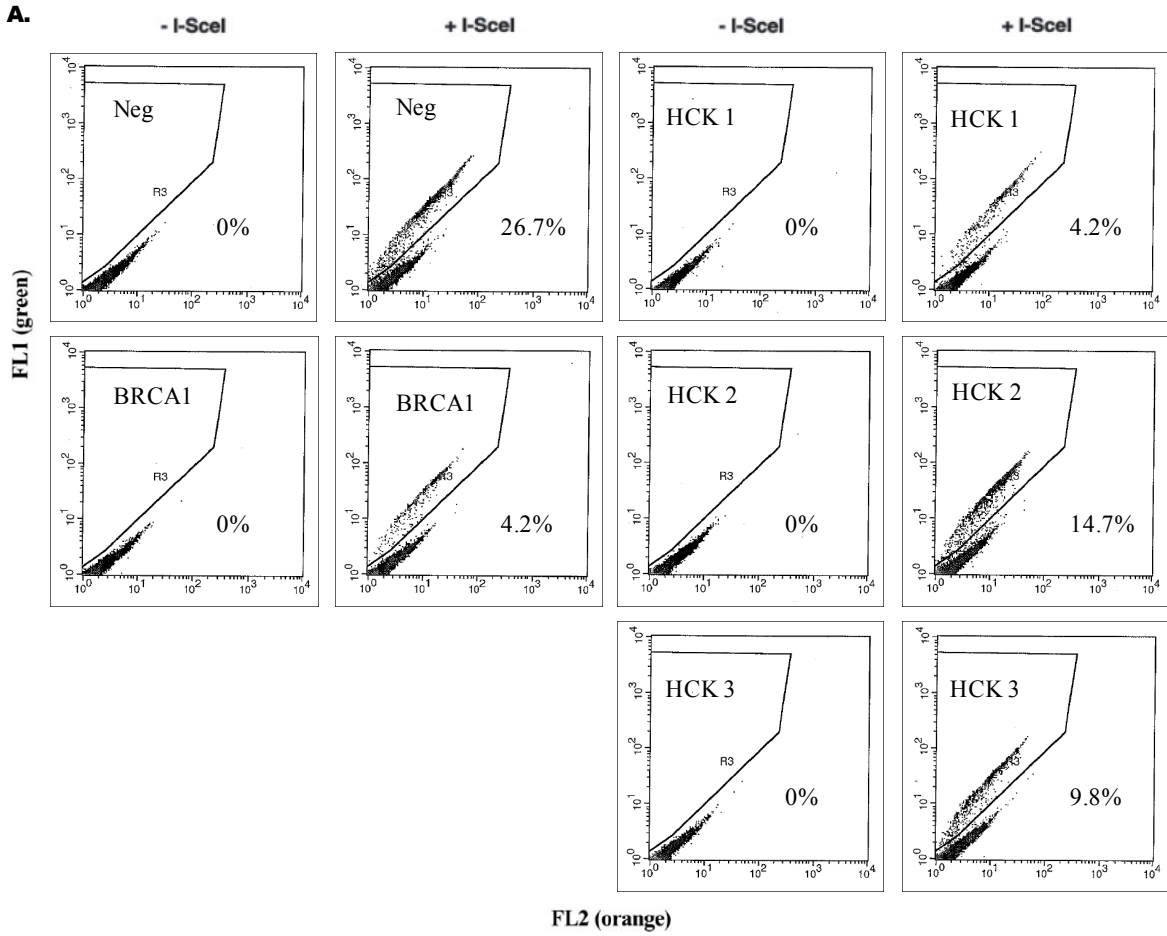


Figure 12: HDR is compromised in HeLa cells stably expressing DR-GFP following siRNA-mediated knockdown of HCK and expression of the I-SceI expression vector. Repair assay in HeLa cells first transfected by chemical transfection with RNaiMAX and either Neg, BRCA1, or three individual siRNAs targeting HCK and then transfected by electroporation with either mock vector pCAGGS (-I-SceI) or I-SceI expression vector pCBASce (+I-SceI). Panel A shows a representative flow cytometric analysis for HDR events following cleavage of the I-SceI endonuclease site within the SceGFP portion of the GFP gene and subsequent repair by HDR directed by the downstream iGFP portion of the GFP gene. The GFP⁺ population shifts greenward to separate from the GFP⁻ population. Panel B quantifies results from Panel A as average percent GFP⁺ cells \pm standard error (n=2). * denotes $P < 0.0001$.

BRCA1 siRNA, there was a lower amount of repair products uncut by I-SceI ($26.6 \pm 2.0\%$ compared to $63.9 \pm 3.0\%$) (**Figures 5-7**). The amount of repair products uncut by I-SceI and BcgI was $26.7 \pm 6.3\%$ (**Figures 8-10**), suggesting that the repair products were a result of repair by NHEJ and that repair by NHEJ was not affected because the percentage uncut following digest with I-SceI and BcgI was similar to the percentage uncut following digest with I-SceI alone. This indirectly proposed that the decrease in total repair products was due to a decrease in repair by HDR, which was confirmed by flow cytometric analysis. The +I-SceI cells with BRCA1 siRNA resulted in $4.2 \pm 0.2\%$ GFP+ cells, about a 6.4-fold decrease in GFP+ cells compared the +I-SceI cells with Neg siRNA (**Figures 11-13**). These results show that the role of BRCA1 is critical in HDR.

Three kinases, MAP3K1, FGFR2, and HCK, were evaluated using the DSB repair assay. The same three siRNAs for each kinase from both the primary screen and secondary validation were used. The Neg siRNA served as the negative control and the BRCA1 siRNA served as the positive control. The mock vector pCAGGS (-I-SceI) served as the control for the I-SceI expression vector pCBASce (+I-SceI) in the DSB repair assay. In +I-SceI cells with MAP3K1, FGFR2, and HCK siRNAs, there was a lower amount of repair products uncut by I-SceI ($40.7 \pm 5.2\%$ for MAP3K1, $34.1 \pm 6.9\%$ for FGFR2, and $35.4 \pm 5.5\%$ for HCK compared to $63.9 \pm 3.0\%$ for Neg), analogous to that of BRCA1 siRNA (**Figure 5-7**). The amount of repair products uncut by I-SceI and BcgI was $38.1 \pm 9.1\%$ for MAP3K1, $31.3 \pm 5.3\%$ for FGFR2, and $32.6 \pm 2.1\%$ for HCK (**Figures 8-10**), suggesting that the repair products were a result of repair by NHEJ and that repair by NHEJ was not affected because the percentage uncut following digest with I-SceI and BcgI was similar to the percentage uncut following digest with I-SceI alone, which was also the case with BRCA1 siRNA. The contribution of HDR to total repair was confirmed by flow

cytometric analysis. The +I-SceI cells with each of the three MAP3K1 siRNAs resulted in $7.2 \pm 0.2\%$, $15.9 \pm 0.8\%$, and $16.3 \pm 0.9\%$ GFP+ cells (**Figure 10**). The average % GFP+ cells of the three MAP3K1 siRNAs was $13.5 \pm 1.1\%$, about a 2-fold decrease in GFP+ cells compared to the Neg control siRNA. Similar results were obtained for FGFR2 and HCK. The +I-SceI cells with each of the three FGFR2 siRNAs resulted in $9.4 \pm 0.3\%$, $7.4 \pm 0.4\%$, and $15.3 \pm 0.4\%$ GFP+ cells (**Figure 11**). The average % GFP+ cells of the three FGFR2 siRNAs was $10.9 \pm 0.9\%$. The +I-SceI cells with each of the three HCK siRNAs resulted in $4.2 \pm 0.3\%$, $14.7 \pm 1.1\%$, and $9.8 \pm 0.3\%$ GFP+ cells (**Figure 12**). The average % GFP+ cells of the three HCK siRNAs was $10.7 \pm 1.1\%$, about a 2.5-fold decrease in GFP+ cells compared to the Neg control siRNA. These results show that MAP3K1, FGFR2, and HCK play a role in HDR.

HR and NHEJ analysis using the DR-GFP system provided valuable information regarding the nature and capacity of repair; however, it is labor-intensive and time-consuming. An alternative approach to evaluating the effect of regulatory kinase knockdown on repair of DSBs may be a kinetics study to monitor the disappearance of γ H2AX foci following transfection of kinase siRNA by chemical transfection and exposure to 10 Gy IR. H2AX is quickly phosphorylated (γ H2AX) at sites of DSBs and is believed to be retained until the damage is repaired. Therefore, if cells exhibit higher numbers of γ H2AX foci compared to control at the same time point, it indicates that DSB repair is impaired. Likewise, if the cells exhibit lower numbers of γ H2AX compared to control at the same time point, it indicates that DSB repair is augmented. However, this method cannot distinguish repair by HR or NHEJ.

Clonogenic Assay to Assess Sensitivity to Ionizing Radiation: To determine whether siRNA-mediated knockdown of the kinases alters the ability of cells to form colonies, the clonogenic

assay was used to assess cell survival following exposure to IR (**Figure 13**). As the dose of IR was increased, the percent of cells able to form colonies diminished, which indicated that fewer cells were able to repair the damage and continue proliferating. When a cell is exposed to IR, SSBs and DSBs are generated. Increasing the dose of IR increases the number of DSBs generated because a sufficient number of SSBs occur in the same region to generate a DSB. Cells that were transfected by chemical transfection with Neg siRNA set the baseline for comparison at each of the IR doses. Cells that were transfected with BRCA1 siRNA demonstrated a statistically significant decrease in the percent of cells able to form colonies at 2, 4, and 6 Gy. Similar results were seen with siRNA-mediated knockdown of HCK (**Figure 14**). Preliminary results with siRNA-mediated knockdown of MAP3K1 and FGFR2 do not appear to affect survival following exposure to increasing doses of IR (**Figures 15 and 16**), but more replicates will need to be done to assess statistical significance.

DNA damage sensors such as BASC and DNA-PK recognize these regions of damage and initiate a cascade of events that recruit mediators such as BRCA1 to sites of damage, which then acts as a central scaffold to facilitate the localization of effectors such as MRN to remove DNA from the 5' end of the break in a process called resection and Rad51 to direct strand invasion of the overhanging 3' end into a homologous chromosome in the case of HDR (Baumann et al., 1996; Bekker-Jensen et al., 2006; Wang et al., 2000; Zhong et al., 1999). The DNA damage pathway also activates cell cycle checkpoints (Iliakis et al., 2003; Zhou and Elledge, 2000) to ensure that a cell with a modification in its DNA does not undergo division until it can be repaired. And if the damage cannot be repaired, then the cell undergoes apoptosis, or programmed cell death, to ensure the integrity of the DNA. Cells that were transfected with Neg siRNA have functional BRCA1 and therefore an intact DNA damage repair pathway. These

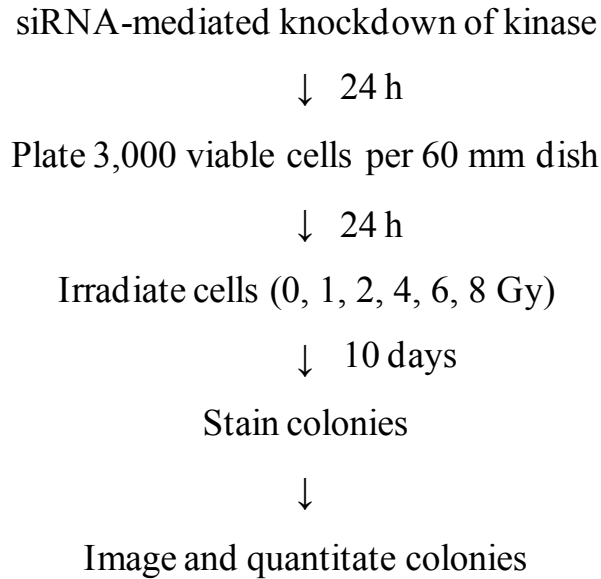


Figure 13: Schematic of the clonogenic assay workflow. Twenty-four hours following reverse transfection of MCF7 cells with RNAiMAX and either Neg, BRCA1, or kinase siRNAs, cells were trypsinized and counted before 3,000 viable cells were plated per 60 mm dish for a total of six dishes per siRNA. The six dishes correspond to the six different doses of IR to which the cells were exposed 24 h after plating. After 10 days of incubation, colonies were stained, imaged, and quantified.

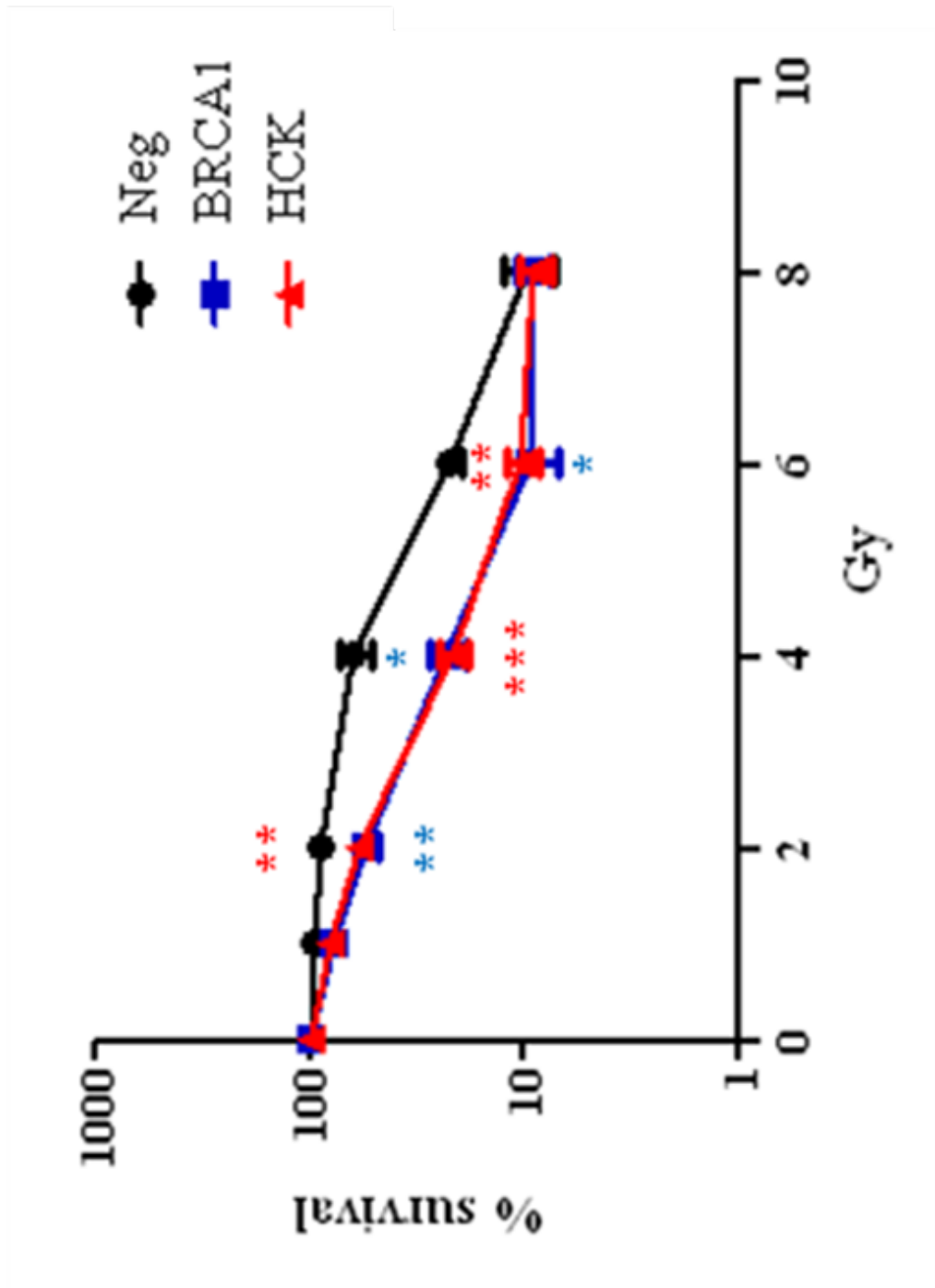


Figure 14: Knockdown of HCK sensitizes cells to ionizing radiation to a level similar to that of BRCA1. Clonogenic assay in MCF7 cells following reverse transfection with RNaiMAX and either Neg, BRCA1, or three individual siRNAs targeting HCK. Data are presented as an average of three HCK siRNAs \pm standard error (n=3). * denotes $P \leq 0.0190$, ** denotes $P \leq 0.0097$, *** denotes $P = 0.0006$.

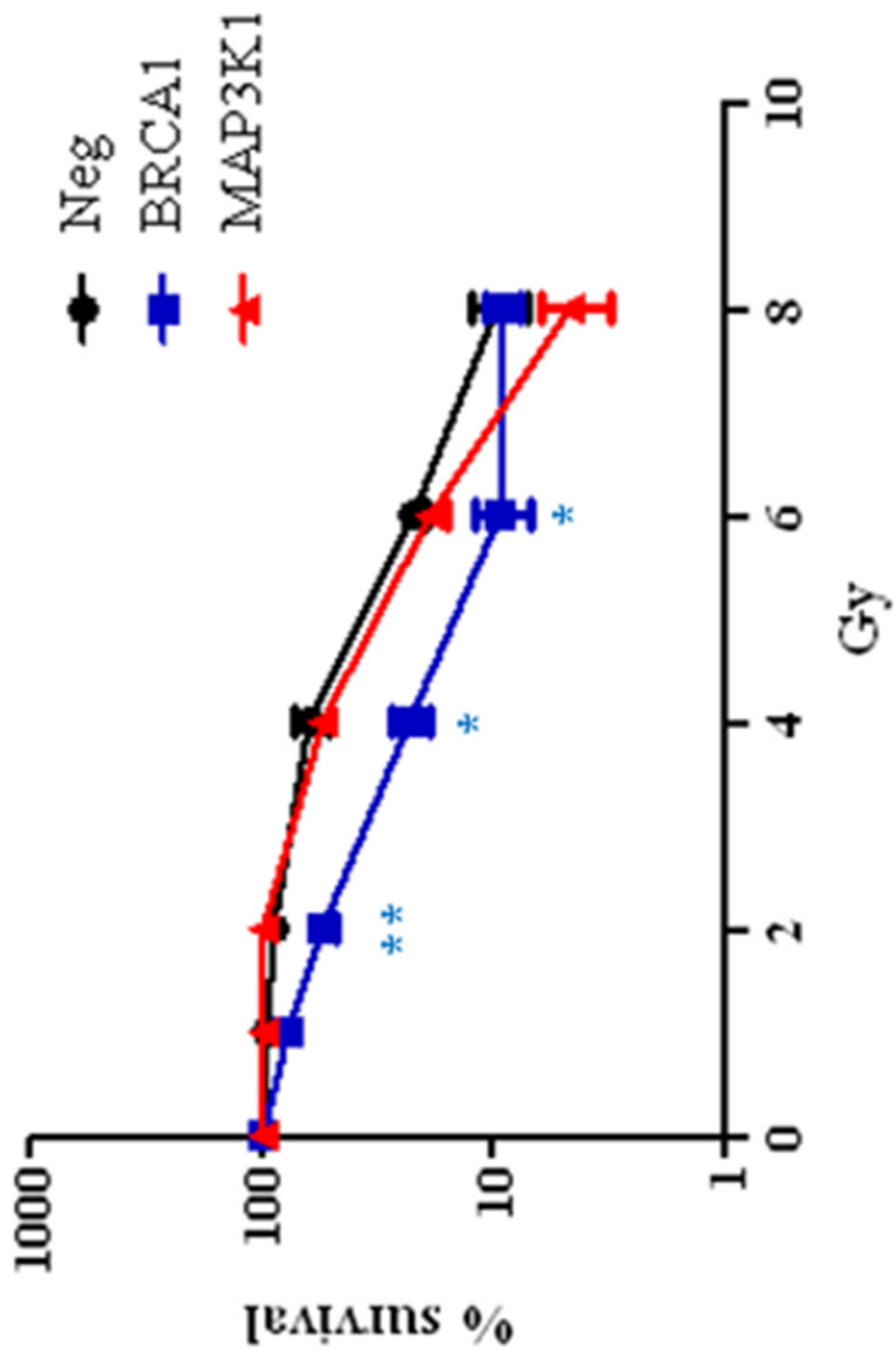


Figure 15: Knockdown of MAP3K1 does not sensitize cells to ionizing radiation. Clonogenic assay in MCF7 cells following reverse transfection with RNaiMAX and either Neg, BRCA1, or three individual siRNAs targeting MAP3K1. Data are presented as an average of three MAP3K1 siRNAs \pm standard error (n=1). * denotes $P \leq 0.0190$, ** denotes $P \leq 0.0097$.

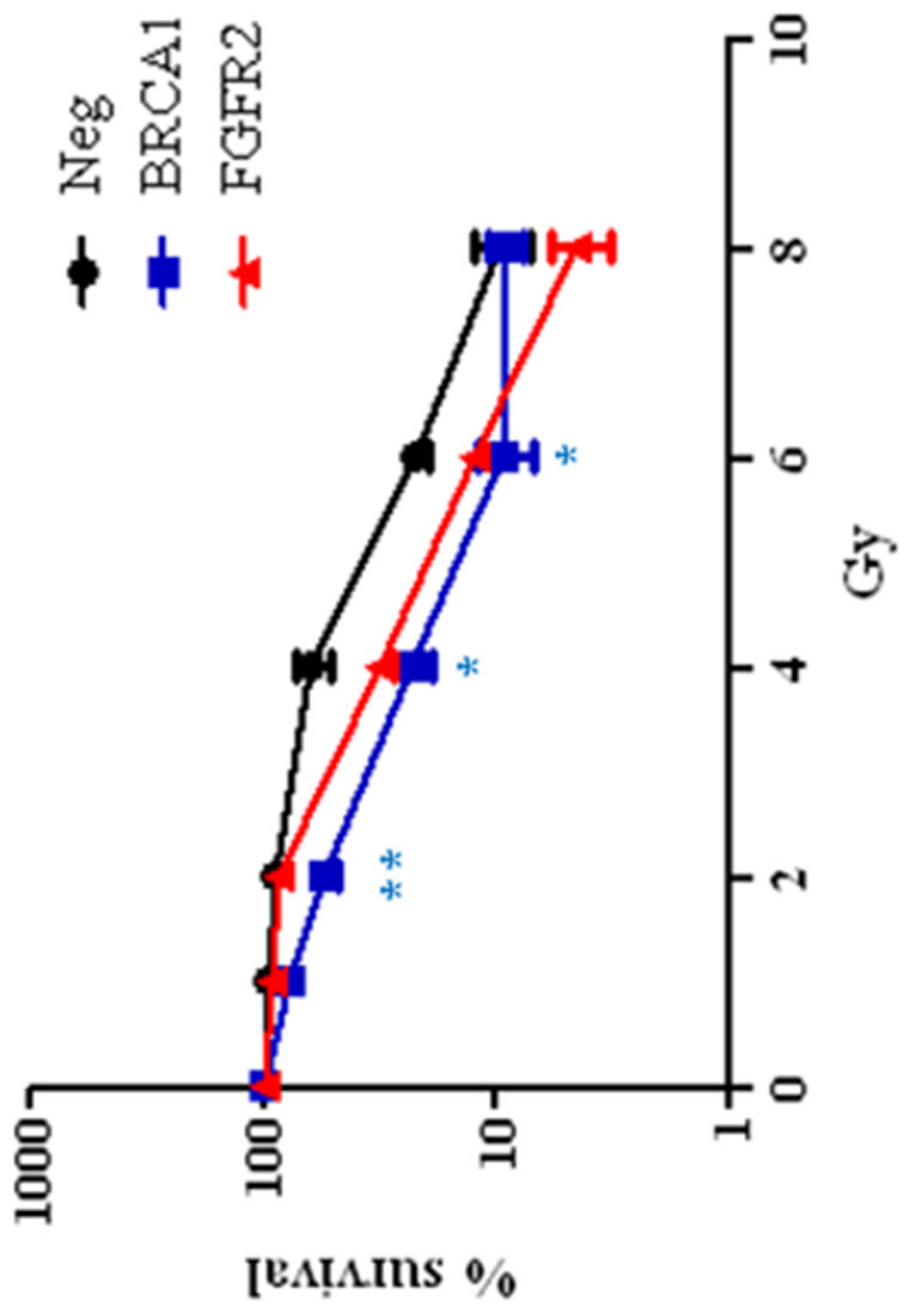


Figure 16: Knockdown of FGFR2 does not sensitize cells to ionizing radiation. Clonogenic assay in MCF7 cells following reverse transfection with RNaiMAX and either Neg, BRCA1, or three individual siRNAs targeting FGFR2. Data are presented as an average of three FGFR2 siRNAs \pm standard error (n=1). * denotes $P \leq 0.0190$, ** denotes $P \leq 0.0097$.

cells are more capable of repairing the damage, which alleviates the arrest in cell cycle progression and allows the cells to continue proliferating to form colonies. Cells that were transfected with either BRCA1 siRNA, which diminishes expression of BRCA1 protein and subsequent participation in the DNA damage pathway, or kinase siRNAs, which either diminish the ability of BRCA1 to be expressed or to function in the DNA damage pathway, are more likely to be maintained in a cell cycle arrest or to have received the signal to undergo apoptosis and therefore cannot continue proliferating to form colonies.

Since single cells were plated at such a low density, the ability of each cell to form colonies was more easily distinguished. Each colony generated had a defined border that was not impacted by any neighboring colonies. The images were taken using the UVP imaging system under the same parameters of positioning, magnification, and exposure time. Use of the ImageJ software to differentiate and count the number of colonies based on the same signal threshold values as well as range of size and circularity of colonies eliminated the subjective nature of counting colonies.

Conclusions

siRNA-mediated knockdown of MAP3K1, HCK, and FGFR2 diminished the ability of BRCA1 to facilitate repair of DSBs by HDR as shown by the results of the repair assay. Only siRNA-mediated knockdown of HCK sensitized the cells to increasing doses of IR, which prevented the cells from proliferating to form colonies as seen by the results of the clonogenic assay.

CHAPTER V

SIGNIFICANCE AND PERSPECTIVE

Potential Role of Lead Kinases in Regulating BRCA1 Expression and Function

The primary screen identified thirty-two potential kinase regulators of BRCA1 expression and function, of which fourteen kinases were validated. siRNA-mediated knockdown of these fourteen kinases consistently demonstrated significant diminishment of BRCA1 IRIF formation following exposure to IR. Of the fourteen kinases, siRNA-mediated knockdown of MAP3K1, HCK, FGFR2, PIK4CA, and PLK3 were assessed for their effect on BRCA1 mRNA levels. siRNA-mediated knockdown of MAP3K1, HCK, and FGFR2 were also assessed for their effect on BRCA1 and target kinase protein levels. The effect of kinase siRNA-mediated knockdown on BRCA1 mRNA and protein levels can help determine the level at which BRCA1 is regulated. Additionally, siRNA-mediated knockdown of MAP3K1, HCK, and FGFR2 were further characterized for their ability to repair DNA damage using a DSB repair assay and their ability to proliferate following DNA damage induced by IR using a clonogenic assay. Each of these lead kinases can serve as a starting point to evaluate whether its role in existing pathways affects BRCA1. siRNAs can be used to selectively target each step of the identified pathway to determine whether knockdown of that component will recapitulate the phenotype previously observed with an siRNA targeting the kinase. A better understanding of the molecular mechanism involving the regulatory kinase and BRCA1 will provide a framework for further analysis of therapeutic targets that can restore BRCA1 expression and tumor suppressor function.

FGFR2 is a member of the fibroblast growth factor receptor family that activates the PLC γ , PI3K/AKT, and MAPK pathways (Dailey et al., 2005). MAP3K1 is a serine/threonine

kinase involved in the MAP kinase cascades that include ERK1/2, JNK/SAPK, and p38 pathways (Pearson et al., 2001). Additionally, both FGFR2 and MAP3K1 were discovered using genome-wide association studies of SNPs to increase susceptibility to breast cancer (Easton et al., 2007; Hunter et al., 2007). siRNA-mediated knockdown of both FGFR2 and MAP3K1 resulted in significant diminishment of BRCA1 IRIF formation without affecting BRCA1 mRNA levels. Preliminary results from siRNA-mediated knockdown of MAP3K1 suggest that MAP3K1 affects BRCA1 at the protein level and that both MAP3K1 and BRCA1 expression are induced following IR. More replicates are needed of BRCA1 protein levels following siRNA-mediated knockdown of MAP3K1 for statistical significance. siRNA-mediated knockdown of FGFR2 decreased BRCA1 protein levels. Using Ingenuity Pathway Analysis (Ingenuity Systems, Redwood City, CA), FGFR2 has been shown to interact with Grb2, an adaptor protein that links cell surface growth factor receptors to the Ras signaling pathway (Lu et al., 2003). Additionally, the SH3 domain of Grb2 has been shown to associate with the proline-rich domain of MAP3K1 (Pomerance et al., 1998). It has also been shown that there is a feedback regulatory loop between ERK1/2 and BRCA1 where BRCA1 regulates ERK1/2 activation following exposure to IR and ERK1/2 is required for induction of BRCA1 protein post-IR by inhibiting the proteasomal degradation of BRCA1 (Yan et al., 2008). By decreasing FGFR2 and MAP3K1, it is possible that ERK1/2 activation is impaired, which leads to proteasomal degradation of BRCA1 following exposure to IR. Decreased BRCA1 protein levels lead to decreased BRCA1 IRIF formation and diminished repair capacity by HR as demonstrated by these studies.

HCK is a member of the Src family of protein tyrosine kinases that was first shown to be expressed in cells of the myeloid and B-lymphoid lineage and then found to be involved in maintaining pluripotency of embryonic stem cells (Ernst et al., 1994; Meyn et al., 2005; Quintrell

et al., 1987; Ziegler et al., 1987). HCK exists as two isoforms (p61 and p59 in humans) due to alternative translational start sites (Lock et al., 1991). HCK, like other Src family kinases, possesses a tyrosine kinase catalytic domain as well as a Src-homology 2 (SH2) domain (binds phosphorylated tyrosine residues) and a Src-homology 3 (SH3) domain (binds proline-rich domains) that mediate intramolecular and intermolecular interactions important in signal transduction (Pawson, 1995; Sicheri et al., 1997) (**Figure 1**). HCK may have an indirect effect on BRCA1 expression by transducing signals from surface receptors through internal signaling pathways to the nucleus. HCK has been shown to localize to the nucleus (Paliwal et al., 2007), so it may also be possible that HCK can directly interact with BRCA1 to affect its function. It is possible that HCK may regulate BRCA1 function in a kinase-dependent or independent manner. siRNA-mediated knockdown of HCK decreased BRCA1 mRNA levels, but this decrease does not completely account for the reduction seen with either BRCA1 protein or BRCA1 IRIF formation. Potentially, this could be due to the role of HCK in activating STAT3 and/or STAT5 (Klejman et al., 2002; Schreiner et al., 2002). STAT3 has been shown to induce cyclins D2 and D3, which binds to CDK4 and CDK6 to mediate early to late G₁ transition, as well as cyclin A, which binds to CDK2 to mediate the G₁ to S phase transition (Fukada et al., 1998). Additionally, STAT3 is involved in downregulation of CDK inhibitors p21 and p27 (Fukada et al., 1998). STAT5 has been shown to participate in an enhancer complex with Sp1 to induce cyclin D2 (Martino et al., 2001). Cyclin-CDK complex formation may be affected by siRNA-mediated knockdown of HCK and thus prevent Rb phosphorylation and release of E2F (Weinberg, 1995). The Rb-E2F complex has been shown to repress BRCA1 expression (Wang et al., 2000). Since both BRCA1 expression and phosphorylation are affected by cell cycle (Chen et al., 1996; Gudas et al., 1996; Thomas et al., 1997), the change in BRCA1 mRNA levels following siRNA-

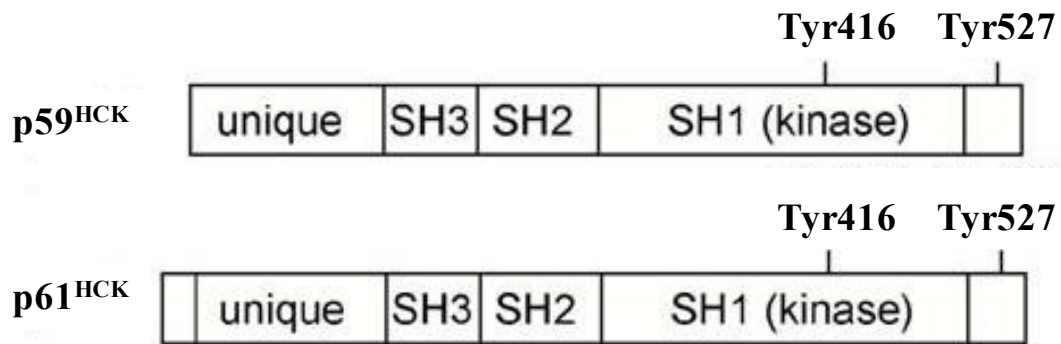


Figure 1: Schematic of the two isoforms of HCK. HCK exists as two isoforms due to alternative translational start sites. HCK contains a tyrosine kinase catalytic domain as well as a Src-homology 2 (SH2) domain that binds phosphorylated tyrosine residues and a Src-homology 3 (SH3) domain that binds proline-rich domains. Tyr527 is involved in an inhibitory intramolecular interaction with the SH2 domain while Tyr416 is involved in HCK activation (adapted from Hong et al., 2007).

mediated knockdown of HCK may be due to cell cycle alterations. To determine whether siRNA-mediated knockdown of HCK alters cell cycle, analysis by PI staining can be used to determine changes in the ratio of cells in G₀/G₁, S, and G₂/M phases. Additionally, WB analysis of phosphorylated STAT3, phosphorylated STAT5, and cyclin D2 in siRNA-mediated knockdown of HCK can be compared to that of Neg control siRNA. Finally, the *BRCA1* promoter can be isolated by PCR and cloned upstream of the luciferase reporter (BRCA1-luc wt). A BRCA1-luc with mutations in the E2F sites would also be generated (BRCA1-luc E2F-). Cells would be transfected with either BRCA1-luc wt or BRCA1-luc E2F- to assess the effect of siRNA-mediated knockdown of HCK compared to that of the Neg control siRNA on the regulation of the *BRCA1* promoter by the Rb-E2F pathway.

siRNA-mediated knockdown of HCK led to decreased BRCA1 protein levels as well as decreased BRCA1 IRIF formation; however, a greater reduction in BRCA1 IRIF formation was noted than would be reflected by the change in BRCA1 protein levels. Additionally, siRNA-mediated knockdown of HCK reduced DNA repair capacity by HR and led to radiosensitivity similar to siRNA-mediated knockdown of BRCA1. These results have demonstrated that HCK impacts BRCA1 in a complex manner. A link between reduced expression of HCK and reduced PI3K/AKT activity has been shown (Podar et al., 2004; Sagan et al., 2008). Additionally, reduced AKT activity led to radiosensitivity by impairing DNA repair in glioblastoma cells (Kao et al., 2007). Finally, phosphorylation of BRCA1 by AKT has been demonstrated in breast cancer cells (Altiok et al., 1999). These results suggest a potential pathway for post-translational regulation of BRCA1 by HCK via the PI3K/AKT pathway. WB analysis of phosphorylated AKT compared to total AKT following siRNA-mediated knockdown of HCK would determine whether HCK acts through the PI3K/AKT pathway. BRCA1 IRIF formation following siRNA-

mediated knockdown of AKT and exposure to IR would determine whether AKT plays a role in the localization of BRCA1 to DSBs. Interestingly, AKT1 has been shown to inhibit BRCA1 IRIF formation as well as DNA repair in breast cancer cells by inducing cytoplasmic retention of BRCA1; however, DNA repair does not appear to depend on AKT phosphorylation of BRCA1 (Plo et al., 2008). Another group has shown a novel AKT phosphorylation site in BRCA1 at S694 that promotes nuclear localization of BRCA1 and increases total BRCA1 protein expression by preventing proteasomal degradation (Nelson et al., 2010). Various experimental conditions differ between our studies, so it would be interesting to see whether our system would demonstrate this phenomenon. AKT has also been shown to activate CHK2, which affects both HR and NHEJ repair by BRCA1 (Anai et al., 2005; Zhang et al., 2004; Zhuang et al., 2006). WB analysis of phosphorylated CHK2 compared to total CHK2 following siRNA-mediated knockdown of HCK would determine whether HCK impacts BRCA1 and DNA damage repair via CHK2. One confounding observation was that HCK protein levels are not diminished anywhere near the level HCK mRNA levels are decreased. This suggests that either HCK protein is very stable and requires more time before the siRNA-mediated knockdown manifests at the protein level or the HCK polyclonal antibody may not be specific to HCK and may be reacting with other members of the Src family of protein tyrosine kinases that possess similar epitopes. HCK protein stability can be assessed by treating cells with cycloheximide to inhibit protein synthesis in a time-course experiment followed by Western blot of the cell lysates for HCK to establish protein half-life. Another method to assess protein stability is with metabolic labeling of cells with ³⁵S-methionine in a pulse-chase assay. Cells incorporate the radioactively labeled amino acid into newly synthesized protein during the pulse phase. At various time points following the labeling, total protein can be extracted, immunoprecipitated for HCK, and SDS-

PAGE-separated. The ³⁵S-labeled HCK can be visualized by autoradiography to determine its decay over time while Western blot analysis for HCK can be used to determine total HCK protein expression. Additionally, other HCK antibodies can be evaluated, including monoclonal antibodies that do not cross-react with other Src family kinases such as Lyn and Fyn.

Significance and Future Directions

A screening assay has been developed that provides an opportunity to investigate BRCA1 function with a genomic approach. A better understanding of the regulation of BRCA1 expression and function can identify new druggable targets in the development of either a novel prevention or therapeutic agent for breast cancer patients. Expression of BRCA1 in non-cancer cells has been shown to have a protective effect against tumor development (Hoshino et al., 2007), so the ability to modulate BRCA1 expression and function to normal levels would help prevent breast cancer. Tumors that lack functional BRCA1 tend to be of a basal-like phenotype, which is characterized by more undifferentiated tumors with an aggressive clinical behavior, resistance to chemotherapy, and increased risk of metastasis (Sorlie et al., 2001; Turner and Reis-Filho, 2006; Turner et al., 2007). Basal-like breast cancers (BLBCs) are almost uniformly triple-negative, meaning they lack ER, PR, and ErbB2/HER2; therefore, they do not respond to anti-estrogen or anti-HER2 therapies like that of luminal-type or HER2-overexpressing tumors, respectively. Conversely, tumors with functional BRCA1 are predominantly of the luminal type and are associated with more differentiated tumors that exhibit a more indolent clinical behavior, responsiveness to endocrine therapies, and improved survival (Yang et al., 2001). Therefore, the ability to modulate the expression of BRCA1 would enable differentiation of BLBCs to a more luminal phenotype. The critical role of BRCA1 in DNA damage repair maintains genomic

stability and prevents tumorigenesis. Likewise, recent studies of human breast and ovarian cancers in *BRCA1* and *BRCA2* mutation carriers have shown reversion mutations that restore the *BRCA1* and *BRCA2* reading frame, which enables resistance to agents that induce DSBs (Ashworth, 2008; Swisher et al., 2008). It would be interesting to test whether these resistant cells can be re-sensitized following downregulation of MAP3K1, HCK, or FGFR2.

Future directions include assessing BRCA1 mRNA levels as well as BRCA1 and target kinase protein levels for the remaining lead kinases. Repair capacity and sensitivity to IR will also be assessed for these remaining lead kinases. To identify whether the kinases directly affect BRCA1, they can be further characterized using co-immunoprecipitation and an *in vitro* kinase assay. Cell extracts can be immunoprecipitated with an anti-BRCA1 antibody followed by immunoblotting with an anti-kinase antibody. The anti-BRCA1 antibody will pull down BRCA1 and anything that is bound to it and the anti-kinase antibody will identify whether the interacting protein is the kinase. Likewise, cell extracts can be immunoprecipitated with an anti-kinase antibody and immunoblotted with an anti-BRCA1 antibody. The reverse setup will identify whether BRCA1 is bound to the isolated kinase. Demonstrating interaction both ways reinforces this relationship between BRCA1 and the kinase. For the *in vitro* kinase assay, a recombinant active kinase can be incubated with ^{32}P -ATP and a recombinant BRCA1 in kinase buffer. Proteins can be separated by SDS-PAGE, and phosphorylation visualized by autoradiography. BRCA1 should be phosphorylated if it is a kinase substrate. It is possible that the interaction between the kinase and BRCA1 may either be too weak or too transient to be identified by immunoprecipitation. An alternative approach would be the label transfer assay. The kinase can be derivatized with the labeled cross-linking agent Sulfo-SBED (Pierce), which will transfer a biotin component to any interacting protein after the linkage is cleaved. The interacting protein

can be detected using streptavidin-HRP chemiluminescent substrates. Pathways can also be determined either using bioinformatics or arrays of siRNAs or kinase inhibitors targeting various pathways involving the lead kinase. The purpose of using siRNAs or kinase inhibitors against each step of the identified pathway is to establish a spatiotemporal relationship connecting BRCA1 to signaling components upstream, including the regulatory kinase. Assuming a linear signaling pathway, knockdown of any component in a pathway that ultimately affects BRCA1 will recapitulate the BRCA1 IRIF phenotype previously observed with an siRNA targeting the kinase. The *in vitro* work to establish the relationship between the lead kinases and BRCA1 is important to better understand the basic biology as well as functional effects and consequences. *In vivo* studies with animal models are equally important to understanding the complexities of regulation in the context of an organism. For example, lentiviral-based knockdown of HCK or adenoviral-based overexpression of HCK in various cell lines that represent the major types of invasive breast cancer, including luminal (MCF7), basal-like (MDA-MB-231), HER2+ (SK-BR-3), and normal breast-like (HMEC) (Sorlie et al., 2003) can be used for intraductal injection into cleared mammary fat pads of virgin female SCID-beige mice to assess for tumor formation and growth in the mammary ducts as well as progression of invasion into the surrounding stroma (Behbod et al., 2009). Additionally, a knockout mouse model of HCK (Lowell et al., 1994) can be used to evaluate mammary tumor formation following exposure to the carcinogen DMBA.

Perspective

The development of the BRCA1 functional assay coupled with siRNA-mediated knockdown was able to identify novel kinase regulators of BRCA1 expression and function. For example, knockdown of HCK decreases BRCA1 mRNA expression, leading to decreased

BRCA1 protein expression and inability to localize to sites of DSBs following exposure to IR. The functional effect was then defective HR and the functional consequence was increased radiosensitivity and decreased cell survival following exposure to IR. The identification of these kinase regulators provides new avenues of research to better understand the pathogenesis of sporadic breast cancers expressing low levels of BRCA1. Additionally, the functional assay can be used to screen for a variety of gene classes to identify other potential regulators of BRCA1 expression and function.

REFERENCES

- Abbott, D. W., Thompson, M. E., Robinson-Benion, C., Tomlinson, G., Jensen, R. A. and Holt, J. T.** (1999). BRCA1 expression restores radiation resistance in BRCA1-defective cancer cells through enhancement of transcription-coupled DNA repair. *J Biol Chem* **274**, 18808-12.
- Ahmed, M. and Rahman, N.** (2006). ATM and breast cancer susceptibility. *Oncogene* **25**, 5906-11.
- Altioik, S., Batt, D., Altioik, N., Papautsky, A., Downward, J., Roberts, T. M. and Avraham, H.** (1999). Heregulin induces phosphorylation of BRCA1 through phosphatidylinositol 3-Kinase/AKT in breast cancer cells. *J Biol Chem* **274**, 32274-8.
- Anai, M., Shojima, N., Katagiri, H., Ogihara, T., Sakoda, H., Onishi, Y., Ono, H., Fujishiro, M., Fukushima, Y., Horike, N. et al.** (2005). A novel protein kinase B (PKB)/AKT-binding protein enhances PKB kinase activity and regulates DNA synthesis. *J Biol Chem* **280**, 18525-35.
- Anderson, S. F., Schlegel, B. P., Nakajima, T., Wolpin, E. S. and Parvin, J. D.** (1998). BRCA1 protein is linked to the RNA polymerase II holoenzyme complex via RNA helicase A. *Nat Genet* **19**, 254-6.
- Aprelikova, O. N., Fang, B. S., Meissner, E. G., Cotter, S., Campbell, M., Kuthiala, A., Bessho, M., Jensen, R. A. and Liu, E. T.** (1999). BRCA1-associated growth arrest is RB-dependent. *Proc Natl Acad Sci U S A* **96**, 11866-71.
- Arizti, P., Fang, L., Park, I., Yin, Y., Solomon, E., Ouchi, T., Aaronson, S. A. and Lee, S. W.** (2000). Tumor suppressor p53 is required to modulate BRCA1 expression. *Mol Cell Biol* **20**, 7450-9.
- Ashworth, A.** (2008). Drug resistance caused by reversion mutation. *Cancer Res* **68**, 10021-3.

Atalay, A., Crook, T., Ozturk, M. and Yulug, I. G. (2002). Identification of genes induced by BRCA1 in breast cancer cells. *Biochem Biophys Res Commun* **299**, 839-46.

Atlas, E., Stramwasser, M. and Mueller, C. R. (2001). A CREB site in the BRCA1 proximal promoter acts as a constitutive transcriptional element. *Oncogene* **20**, 7110-4.

Atlas, E., Stramwasser, M., Whiskin, K. and Mueller, C. R. (2000). GA-binding protein alpha/beta is a critical regulator of the BRCA1 promoter. *Oncogene* **19**, 1933-40.

Au, W. W. and Henderson, B. R. (2007). Identification of sequences that target BRCA1 to nuclear foci following alkylative DNA damage. *Cell Signal* **19**, 1879-92.

Bader, A. G., Kang, S., Zhao, L. and Vogt, P. K. (2005). Oncogenic PI3K deregulates transcription and translation. *Nat Rev Cancer* **5**, 921-9.

Baer, R. and Ludwig, T. (2002). The BRCA1/BARD1 heterodimer, a tumor suppressor complex with ubiquitin E3 ligase activity. *Curr Opin Genet Dev* **12**, 86-91.

Baker, K. M., Wei, G., Schaffner, A. E. and Ostrowski, M. C. (2003). Ets-2 and components of mammalian SWI/SNF form a repressor complex that negatively regulates the BRCA1 promoter. *J Biol Chem* **278**, 17876-84.

Baldassarre, G., Battista, S., Belletti, B., Thakur, S., Pentimalli, F., Trapasso, F., Fedele, M., Pierantoni, G., Croce, C. M. and Fusco, A. (2003). Negative regulation of BRCA1 gene expression by HMGA1 proteins accounts for the reduced BRCA1 protein levels in sporadic breast carcinoma. *Mol Cell Biol* **23**, 2225-38.

Bartel, D. P. (2004). MicroRNAs: genomics, biogenesis, mechanism, and function. *Cell* **116**, 281-97.

Baumann, P., Benson, F. E. and West, S. C. (1996). Human Rad51 protein promotes ATP-dependent homologous pairing and strand transfer reactions in vitro. *Cell* **87**, 757-66.

Beger, C., Pierce, L. N., Kruger, M., Marcusson, E. G., Robbins, J. M., Welsh, P., Welch, P. J., Welte, K., King, M. C., Barber, J. R. et al. (2001). Identification of Id4 as a regulator of BRCA1 expression by using a ribozyme-library-based inverse genomics approach. *Proc Natl Acad Sci U S A* **98**, 130-5.

Behbod, F., Kittrell, F. S., LaMarca, H., Edwards, D., Kerbawy, S., Heestand, J. C., Young, E., Mukhopadhyay, P., Yeh, H. W., Allred, D. C. et al. (2009). An intraductal human-in-mouse transplantation model mimics the subtypes of ductal carcinoma in situ. *Breast Cancer Res* **11**, R66.

Bekker-Jensen, S., Lukas, C., Kitagawa, R., Melander, F., Kastan, M. B., Bartek, J. and Lukas, J. (2006). Spatial organization of the mammalian genome surveillance machinery in response to DNA strand breaks. *J Cell Biol* **173**, 195-206.

Bernstein, E., Caudy, A. A., Hammond, S. M. and Hannon, G. J. (2001). Role for a bidentate ribonuclease in the initiation step of RNA interference. *Nature* **409**, 363-6.

Blagosklonny, M. V., An, W. G., Melillo, G., Nguyen, P., Trepel, J. B. and Neckers, L. M. (1999). Regulation of BRCA1 by protein degradation. *Oncogene* **18**, 6460-8.

Blom, N., Gammeltoft, S. and Brunak, S. (1999). Sequence and structure-based prediction of eukaryotic protein phosphorylation sites. *J Mol Biol* **294**, 1351-62.

Bochar, D. A., Wang, L., Beniya, H., Kinev, A., Xue, Y., Lane, W. S., Wang, W., Kashanchi, F. and Shiekhattar, R. (2000). BRCA1 is associated with a human SWI/SNF-related complex: linking chromatin remodeling to breast cancer. *Cell* **102**, 257-65.

Budhram-Mahadeo, V., Ndisang, D., Ward, T., Weber, B. L. and Latchman, D. S. (1999). The Brn-3b POU family transcription factor represses expression of the BRCA-1 anti-oncogene in breast cancer cells. *Oncogene* **18**, 6684-91.

Cantor, S. B., Bell, D. W., Ganesan, S., Kass, E. M., Drapkin, R., Grossman, S., Wahrer, D. C., Sgroi, D. C., Lane, W. S., Haber, D. A. et al. (2001). BACH1, a novel helicase-like protein, interacts directly with BRCA1 and contributes to its DNA repair function. *Cell* **105**, 149-60.

Cao, L., Xu, X., Bunting, S. F., Liu, J., Wang, R. H., Cao, L. L., Wu, J. J., Peng, T. N., Chen, J., Nussenzweig, A. et al. (2009). A selective requirement for 53BP1 in the biological response to genomic instability induced by Brca1 deficiency. *Mol Cell* **35**, 534-41.

Catteau, A., Harris, W. H., Xu, C. F. and Solomon, E. (1999). Methylation of the BRCA1 promoter region in sporadic breast and ovarian cancer: correlation with disease characteristics. *Oncogene* **18**, 1957-65.

Chai, Y. L., Cui, J., Shao, N., Shyam, E., Reddy, P. and Rao, V. N. (1999). The second BRCT domain of BRCA1 proteins interacts with p53 and stimulates transcription from the p21WAF1/CIP1 promoter. *Oncogene* **18**, 263-8.

Chen, C. F., Li, S., Chen, Y., Chen, P. L., Sharp, Z. D. and Lee, W. H. (1996a). The nuclear localization sequences of the BRCA1 protein interact with the importin-alpha subunit of the nuclear transport signal receptor. *J Biol Chem* **271**, 32863-8.

Chen, L., Nievera, C. J., Lee, A. Y. and Wu, X. (2008). Cell cycle-dependent complex formation of BRCA1.CtIP.MRN is important for DNA double-strand break repair. *J Biol Chem* **283**, 7713-20.

Chen, X., Arciero, C. A., Wang, C., Broccoli, D. and Godwin, A. K. (2006). BRCC36 is essential for ionizing radiation-induced BRCA1 phosphorylation and nuclear foci formation. *Cancer Res* **66**, 5039-46.

Chen, Y., Farmer, A. A., Chen, C. F., Jones, D. C., Chen, P. L. and Lee, W. H. (1996b). BRCA1 is a 220-kDa nuclear phosphoprotein that is expressed and phosphorylated in a cell cycle-dependent manner. *Cancer Res* **56**, 3168-72.

Choudhury, A. D., Xu, H. and Baer, R. (2004). Ubiquitination and proteasomal degradation of the BRCA1 tumor suppressor is regulated during cell cycle progression. *J Biol Chem* **279**, 33909-18.

Cortez, D., Wang, Y., Qin, J. and Elledge, S. J. (1999). Requirement of ATM-dependent phosphorylation of brca1 in the DNA damage response to double-strand breaks. *Science* **286**, 1162-6.

Dailey, L., Ambrosetti, D., Mansukhani, A. and Basilico, C. (2005). Mechanisms underlying differential responses to FGF signaling. *Cytokine Growth Factor Rev* **16**, 233-47.

Deng, C. X. and Brodie, S. G. (2000). Roles of BRCA1 and its interacting proteins. *Bioessays* **22**, 728-37.

Deng, C. X. and Scott, F. (2000). Role of the tumor suppressor gene Brca1 in genetic stability and mammary gland tumor formation. *Oncogene* **19**, 1059-64.

Dimitrov, S., Brennerova, M. and Forejt, J. (2001). Expression profiles and intergenic structure of head-to-head oriented Brca1 and Nbr1 genes. *Gene* **262**, 89-98.

Easton, D. F., Bishop, D. T., Ford, D. and Crockford, G. P. (1993). Genetic linkage analysis in familial breast and ovarian cancer: results from 214 families. The Breast Cancer Linkage Consortium. *Am J Hum Genet* **52**, 678-701.

Easton, D. F. Pooley, K. A. Dunning, A. M. Pharoah, P. D. Thompson, D. Ballinger, D. G. Struewing, J. P. Morrison, J. Field, H. Luben, R. et al. (2007). Genome-wide association study identifies novel breast cancer susceptibility loci. *Nature* **447**, 1087-93.

Echeverri, C. J. and Perrimon, N. (2006). High-throughput RNAi screening in cultured cells: a user's guide. *Nat Rev Genet* **7**, 373-84.

Eckner, R., Ewen, M. E., Newsome, D., Gerdes, M., DeCaprio, J. A., Lawrence, J. B. and Livingston, D. M. (1994). Molecular cloning and functional analysis of the adenovirus E1A-associated 300-kD protein (p300) reveals a protein with properties of a transcriptional adaptor. *Genes Dev* **8**, 869-84.

Ernst, M., Gearing, D. P. and Dunn, A. R. (1994). Functional and biochemical association of Hck with the LIF/IL-6 receptor signal transducing subunit gp130 in embryonic stem cells. *EMBO J* **13**, 1574-84.

Fabbro, M., Rodriguez, J. A., Baer, R. and Henderson, B. R. (2002). BARD1 induces BRCA1 intranuclear foci formation by increasing RING-dependent BRCA1 nuclear import and inhibiting BRCA1 nuclear export. *J Biol Chem* **277**, 21315-24.

Feng, L., Huang, J. and Chen, J. (2009). MERIT40 facilitates BRCA1 localization and DNA damage repair. *Genes Dev* **23**, 719-28.

Fire, A., Xu, S., Montgomery, M. K., Kostas, S. A., Driver, S. E. and Mello, C. C. (1998). Potent and specific genetic interference by double-stranded RNA in *Caenorhabditis elegans*. *Nature* **391**, 806-11.

Fukada, T., Ohtani, T., Yoshida, Y., Shirogane, T., Nishida, K., Nakajima, K., Hibi, M. and Hirano, T. (1998). STAT3 orchestrates contradictory signals in cytokine-induced G1 to S cell-cycle transition. *EMBO J* **17**, 6670-7.

Galanty, Y., Belotserkovskaya, R., Coates, J., Polo, S., Miller, K. M. and Jackson, S. P. (2009). Mammalian SUMO E3-ligases PIAS1 and PIAS4 promote responses to DNA double-strand breaks. *Nature* **462**, 935-9.

Gao, B., Shen, X., Kunos, G., Meng, Q., Goldberg, I. D., Rosen, E. M. and Fan, S. (2001). Constitutive activation of JAK-STAT3 signaling by BRCA1 in human prostate cancer cells. *FEBS Lett* **488**, 179-84.

Ghosh, S., Lu, Y. and Hu, Y. (2008). A Role of CREB in BRCA1 Constitutive Promoter Activity and Aromatase Basal Expression. *Int J Biomed Sci* **4**, 260-265.

Gilbert, P. M., Mouw, J. K., Unger, M. A., Lakins, J. N., Gbegnon, M. K., Clemmer, V. B., Benezra, M., Licht, J. D., Boudreau, N. J., Tsai, K. K. et al. (2010). HOXA9 regulates BRCA1 expression to modulate human breast tumor phenotype. *J Clin Invest* **120**, 1535-50.

Gravel, S., Chapman, J. R., Magill, C. and Jackson, S. P. (2008). DNA helicases Sgs1 and BLM promote DNA double-strand break resection. *Genes Dev* **22**, 2767-72.

Greenberg, R. A., Sobhian, B., Pathania, S., Cantor, S. B., Nakatani, Y. and Livingston, D. M. (2006). Multifactorial contributions to an acute DNA damage response by BRCA1/BARD1-containing complexes. *Genes Dev* **20**, 34-46.

Gudas, J. M., Li, T., Nguyen, H., Jensen, D., Rauscher, F. J., 3rd and Cowan, K. H. (1996). Cell cycle regulation of BRCA1 messenger RNA in human breast epithelial cells. *Cell Growth Differ* **7**, 717-23.

Hall, J. M., Lee, M. K., Newman, B., Morrow, J. E., Anderson, L. A., Huey, B. and King, M. C. (1990). Linkage of early-onset familial breast cancer to chromosome 17q21. *Science* **250**, 1684-9.

Hall, R. E., Lee, C. S., Alexander, I. E., Shine, J., Clarke, C. L. and Sutherland, R. L. (1990). Steroid hormone receptor gene expression in human breast cancer cells: inverse relationship between oestrogen and glucocorticoid receptor messenger RNA levels. *Int J Cancer* **46**, 1081-7.

Hammond, S. M., Bernstein, E., Beach, D. and Hannon, G. J. (2000). An RNA-directed nuclease mediates post-transcriptional gene silencing in *Drosophila* cells. *Nature* **404**, 293-6.

Hannon, G. J. and Rossi, J. J. (2004). Unlocking the potential of the human genome with RNA interference. *Nature* **431**, 371-8.

Harkin, D. P., Bean, J. M., Miklos, D., Song, Y. H., Truong, V. B., Englert, C., Christians, F. C., Ellisen, L. W., Maheswaran, S., Oliner, J. D. et al. (1999). Induction of GADD45 and JNK/SAPK-dependent apoptosis following inducible expression of BRCA1. *Cell* **97**, 575-86.

Hinton, C. V., Fitzgerald, L. D. and Thompson, M. E. (2007). Phosphatidylinositol 3-kinase/Akt signaling enhances nuclear localization and transcriptional activity of BRCA1. *Exp Cell Res* **313**, 1735-44.

Hong, H., Kitaura, J., Xiao, W., Horejsi, V., Ra, C., Lowell, C. A., Kawakami, Y. and Kawakami, T. (2007). The Src family kinase Hck regulates mast cell activation by suppressing an inhibitory Src family kinase Lyn. *Blood* **110**, 2511-9.

Hoshino, A., Yee, C. J., Campbell, M., Woltjer, R. L., Townsend, R. L., van der Meer, R., Shyr, Y., Holt, J. T., Moses, H. L. and Jensen, R. A. (2007). Effects of BRCA1 transgene expression on murine mammary gland development and mutagen-induced mammary neoplasia. *Int J Biol Sci* **3**, 281-91.

Houvras, Y., Benezra, M., Zhang, H., Manfredi, J. J., Weber, B. L. and Licht, J. D. (2000). BRCA1 physically and functionally interacts with ATF1. *J Biol Chem* **275**, 36230-7.

Hsu, L. C. and White, R. L. (1998). BRCA1 is associated with the centrosome during mitosis. *Proc Natl Acad Sci U S A* **95**, 12983-8.

Hunter, D. J., Kraft, P., Jacobs, K. B., Cox, D. G., Yeager, M., Hankinson, S. E., Wacholder, S., Wang, Z., Welch, R., Hutchinson, A. et al. (2007). A genome-wide association

study identifies alleles in FGFR2 associated with risk of sporadic postmenopausal breast cancer. *Nat Genet* **39**, 870-4.

Iliakis, G. (1991). The role of DNA double strand breaks in ionizing radiation-induced killing of eukaryotic cells. *Bioessays* **13**, 641-8.

Iliakis, G., Wang, Y., Guan, J. and Wang, H. (2003). DNA damage checkpoint control in cells exposed to ionizing radiation. *Oncogene* **22**, 5834-47.

Jasin, M. (2002). Homologous repair of DNA damage and tumorigenesis: the BRCA connection. *Oncogene* **21**, 8981-93.

Jeffy, B. D., Hockings, J. K., Kemp, M. Q., Morgan, S. S., Hager, J. A., Beliakoff, J., Whitesell, L. J., Bowden, G. T. and Romagnolo, D. F. (2005). An estrogen receptor-alpha/p300 complex activates the BRCA-1 promoter at an AP-1 site that binds Jun/Fos transcription factors: repressive effects of p53 on BRCA-1 transcription. *Neoplasia* **7**, 873-82.

Jensen, D. E., Proctor, M., Marquis, S. T., Gardner, H. P., Ha, S. I., Chodosh, L. A., Ishov, A. M., Tommerup, N., Vissing, H., Sekido, Y. et al. (1998). BAP1: a novel ubiquitin hydrolase which binds to the BRCA1 RING finger and enhances BRCA1-mediated cell growth suppression. *Oncogene* **16**, 1097-112.

Jensen, R. A., Thompson, M. E., Jetton, T. L., Szabo, C. I., van der Meer, R., Helou, B., Tronick, S. R., Page, D. L., King, M. C. and Holt, J. T. (1996). BRCA1 is secreted and exhibits properties of a granin. *Nat Genet* **12**, 303-8.

Johnson, R. D. and Jasin, M. (2001). Double-strand-break-induced homologous recombination in mammalian cells. *Biochem Soc Trans* **29**, 196-201.

Kao, G. D., Jiang, Z., Fernandes, A. M., Gupta, A. K. and Maity, A. (2007). Inhibition of phosphatidylinositol-3-OH kinase/Akt signaling impairs DNA repair in glioblastoma cells following ionizing radiation. *J Biol Chem* **282**, 21206-12.

Kehn, K., Berro, R., Alhaj, A., Bottazzi, M. E., Yeh, W. I., Klase, Z., Van Duyne, R., Fu, S. and Kashanchi, F. (2007). Functional consequences of cyclin D1/BRCA1 interaction in breast cancer cells. *Oncogene* **26**, 5060-9.

Khanna, K. K. and Jackson, S. P. (2001). DNA double-strand breaks: signaling, repair and the cancer connection. *Nat Genet* **27**, 247-54.

Kim, H., Chen, J. and Yu, X. (2007a). Ubiquitin-binding protein RAP80 mediates BRCA1-dependent DNA damage response. *Science* **316**, 1202-5.

Kim, H., Huang, J. and Chen, J. (2007b). CCDC98 is a BRCA1-BRCT domain-binding protein involved in the DNA damage response. *Nat Struct Mol Biol* **14**, 710-5.

Klejman, A., Schreiner, S. J., Nieborowska-Skorska, M., Slupianek, A., Wilson, M., Smithgall, T. E. and Skorski, T. (2002). The Src family kinase Hck couples BCR/ABL to STAT5 activation in myeloid leukemia cells. *EMBO J* **21**, 5766-74.

Lacroix, M. and Leclercq, G. (2004). Relevance of breast cancer cell lines as models for breast tumours: an update. *Breast Cancer Res Treat* **83**, 249-89.

Lee, Y., Ahn, C., Han, J., Choi, H., Kim, J., Yim, J., Lee, J., Provost, P., Radmark, O., Kim, S. et al. (2003). The nuclear RNase III Drosha initiates microRNA processing. *Nature* **425**, 415-9.

Lee, Y., Jeon, K., Lee, J. T., Kim, S. and Kim, V. N. (2002). MicroRNA maturation: stepwise processing and subcellular localization. *EMBO J* **21**, 4663-70.

Lekas, P., Tin, K. L., Lee, C. and Prokipcak, R. D. (2000). The human cytochrome P450 1A1 mRNA is rapidly degraded in HepG2 cells. *Arch Biochem Biophys* **384**, 311-8.

Liu, S., Ginestier, C., Charafe-Jauffret, E., Foco, H., Kleer, C. G., Merajver, S. D., Dontu, G. and Wicha, M. S. (2008). BRCA1 regulates human mammary stem/progenitor cell fate. *Proc Natl Acad Sci U S A* **105**, 1680-5.

Liu, Z., Wu, J. and Yu, X. (2007). CCDC98 targets BRCA1 to DNA damage sites. *Nat Struct Mol Biol* **14**, 716-20.

Lock, P., Ralph, S., Stanley, E., Boulet, I., Ramsay, R. and Dunn, A. R. (1991). Two isoforms of murine hck, generated by utilization of alternative translational initiation codons, exhibit different patterns of subcellular localization. *Mol Cell Biol* **11**, 4363-70.

Lou, Z., Chini, C. C., Minter-Dykhouse, K. and Chen, J. (2003). Mediator of DNA damage checkpoint protein 1 regulates BRCA1 localization and phosphorylation in DNA damage checkpoint control. *J Biol Chem* **278**, 13599-602.

Lowell, C. A., Soriano, P. and Varmus, H. E. (1994). Functional overlap in the src gene family: inactivation of hck and fgr impairs natural immunity. *Genes Dev* **8**, 387-98.

Lu, M., Conzen, S. D., Cole, C. N. and Arrick, B. A. (1996). Characterization of functional messenger RNA splice variants of BRCA1 expressed in nonmalignant and tumor-derived breast cells. *Cancer Res* **56**, 4578-81.

Lu, Y., Pan, Z. Z., Devaux, Y. and Ray, P. (2003). p21-activated protein kinase 4 (PAK4) interacts with the keratinocyte growth factor receptor and participates in keratinocyte growth factor-mediated inhibition of oxidant-induced cell death. *J Biol Chem* **278**, 10374-80.

Lund, E., Guttinger, S., Calado, A., Dahlberg, J. E. and Kutay, U. (2004). Nuclear export of microRNA precursors. *Science* **303**, 95-8.

Mancini, D. N., Rodenhiser, D. I., Ainsworth, P. J., O'Malley, F. P., Singh, S. M., Xing, W. and Archer, T. K. (1998). CpG methylation within the 5' regulatory region of the BRCA1 gene is tumor specific and includes a putative CREB binding site. *Oncogene* **16**, 1161-9.

Martin, S. A., Lord, C. J. and Ashworth, A. (2008). DNA repair deficiency as a therapeutic target in cancer. *Curr Opin Genet Dev* **18**, 80-6.

Martino, A., Holmes, J. H. t., Lord, J. D., Moon, J. J. and Nelson, B. H. (2001). Stat5 and Sp1 regulate transcription of the cyclin D2 gene in response to IL-2. *J Immunol* **166**, 1723-9.

Matsuoka, S., Ballif, B. A., Smogorzewska, A., McDonald, E. R., 3rd, Hurov, K. E., Luo, J., Bakalarski, C. E., Zhao, Z., Solimini, N., Lerenthal, Y. et al. (2007). ATM and ATR substrate analysis reveals extensive protein networks responsive to DNA damage. *Science* **316**, 1160-6.

McCoy, M. L., Mueller, C. R. and Roskelley, C. D. (2003). The role of the breast cancer susceptibility gene 1 (BRCA1) in sporadic epithelial ovarian cancer. *Reprod Biol Endocrinol* **1**, 72.

McEachern, K. A., Archey, W. B., Douville, K. and Arrick, B. A. (2003). BRCA1 splice variants exhibit overlapping and distinct transcriptional transactivation activities. *J Cell Biochem* **89**, 120-32.

Meyn, M. A., 3rd, Schreiner, S. J., Dumitrescu, T. P., Nau, G. J. and Smithgall, T. E. (2005). SRC family kinase activity is required for murine embryonic stem cell growth and differentiation. *Mol Pharmacol* **68**, 1320-30.

Miki, Y., Swensen, J., Shattuck-Eidens, D., Futreal, P. A., Harshman, K., Tavtigian, S., Liu, Q., Cochran, C., Bennett, L. M., Ding, W. et al. (1994). A strong candidate for the breast and ovarian cancer susceptibility gene BRCA1. *Science* **266**, 66-71.

Moffat, J. and Sabatini, D. M. (2006). Building mammalian signalling pathways with RNAi screens. *Nat Rev Mol Cell Biol* **7**, 177-87.

Morris, J. R., Boutell, C., Keppler, M., Densham, R., Weekes, D., Alamshah, A., Butler, L., Galanty, Y., Pangon, L., Kiuchi, T. et al. (2009). The SUMO modification pathway is involved in the BRCA1 response to genotoxic stress. *Nature* **462**, 886-90.

Mueller, C. R. and Roskelley, C. D. (2003). Regulation of BRCA1 expression and its relationship to sporadic breast cancer. *Breast Cancer Res* **5**, 45-52.

Nakanishi, K., Yang, Y. G., Pierce, A. J., Taniguchi, T., Digweed, M., D'Andrea, A. D., Wang, Z. Q. and Jasin, M. (2005). Human Fanconi anemia monoubiquitination pathway promotes homologous DNA repair. *Proc Natl Acad Sci U S A* **102**, 1110-5.

Napoli, C., Lemieux, C. and Jorgensen, R. (1990). Introduction of a Chimeric Chalcone Synthase Gene into Petunia Results in Reversible Co-Suppression of Homologous Genes in trans. *Plant Cell* **2**, 279-289.

Nelson, A. C., Lyons, T. R., Young, C. D., Hansen, K. C., Anderson, S. M. and Holt, J. T. (2010). AKT regulates BRCA1 stability in response to hormone signaling. *Mol Cell Endocrinol* **319**, 129-42.

Nicholson, R. I., Gee, J. M. and Harper, M. E. (2001). EGFR and cancer prognosis. *Eur J Cancer* **37 Suppl 4**, S9-15.

Nimonkar, A. V., Ozsoy, A. Z., Genschel, J., Modrich, P. and Kowalczykowski, S. C. (2008). Human exonuclease 1 and BLM helicase interact to resect DNA and initiate DNA repair. *Proc Natl Acad Sci U S A* **105**, 16906-11.

Oberley, M. J., Inman, D. R. and Farnham, P. J. (2003). E2F6 negatively regulates BRCA1 in human cancer cells without methylation of histone H3 on lysine 9. *J Biol Chem* **278**, 42466-76.

- Okada, S. and Ouchi, T.** (2003). Cell cycle differences in DNA damage-induced BRCA1 phosphorylation affect its subcellular localization. *J Biol Chem* **278**, 2015-20.
- Olsen, J. V., Blagoev, B., Gnad, F., Macek, B., Kumar, C., Mortensen, P. and Mann, M.** (2006). Global, in vivo, and site-specific phosphorylation dynamics in signaling networks. *Cell* **127**, 635-48.
- Orban, T. I. and Olah, E.** (2003). Emerging roles of BRCA1 alternative splicing. *Mol Pathol* **56**, 191-7.
- Ouchi, M., Fujiuchi, N., Sasai, K., Katayama, H., Minamishima, Y. A., Ongusaha, P. P., Deng, C., Sen, S., Lee, S. W. and Ouchi, T.** (2004). BRCA1 phosphorylation by Aurora-A in the regulation of G2 to M transition. *J Biol Chem* **279**, 19643-8.
- Ouchi, T., Lee, S. W., Ouchi, M., Aaronson, S. A. and Horvath, C. M.** (2000). Collaboration of signal transducer and activator of transcription 1 (STAT1) and BRCA1 in differential regulation of IFN-gamma target genes. *Proc Natl Acad Sci U S A* **97**, 5208-13.
- Paliwal, P., Radha, V. and Swarup, G.** (2007). Regulation of p73 by Hck through kinase-dependent and independent mechanisms. *BMC Mol Biol* **8**, 45.
- Pao, G. M., Janknecht, R., Ruffner, H., Hunter, T. and Verma, I. M.** (2000). CBP/p300 interact with and function as transcriptional coactivators of BRCA1. *Proc Natl Acad Sci U S A* **97**, 1020-5.
- Paull, T. T., Rogakou, E. P., Yamazaki, V., Kirchgessner, C. U., Gellert, M. and Bonner, W. M.** (2000). A critical role for histone H2AX in recruitment of repair factors to nuclear foci after DNA damage. *Curr Biol* **10**, 886-95.
- Pawson, T.** (1995). Protein modules and signalling networks. *Nature* **373**, 573-80.

Pearson, G., Robinson, F., Beers Gibson, T., Xu, B. E., Karandikar, M., Berman, K. and Cobb, M. H. (2001). Mitogen-activated protein (MAP) kinase pathways: regulation and physiological functions. *Endocr Rev* **22**, 153-83.

Perou, C. M., Sorlie, T., Eisen, M. B., van de Rijn, M., Jeffrey, S. S., Rees, C. A., Pollack, J. R., Ross, D. T., Johnsen, H., Akslen, L. A. et al. (2000). Molecular portraits of human breast tumours. *Nature* **406**, 747-52.

Plo, I., Laulier, C., Gauthier, L., Lebrun, F., Calvo, F. and Lopez, B. S. (2008). AKT1 inhibits homologous recombination by inducing cytoplasmic retention of BRCA1 and RAD51. *Cancer Res* **68**, 9404-12.

Podar, K., Mostoslavsky, G., Sattler, M., Tai, Y. T., Hayashi, T., Catley, L. P., Hideshima, T., Mulligan, R. C., Chauhan, D. and Anderson, K. C. (2004). Critical role for hematopoietic cell kinase (Hck)-mediated phosphorylation of Gab1 and Gab2 docking proteins in interleukin 6-induced proliferation and survival of multiple myeloma cells. *J Biol Chem* **279**, 21658-65.

Polanowska, J., Martin, J. S., Garcia-Muse, T., Petalcorin, M. I. and Boulton, S. J. (2006). A conserved pathway to activate BRCA1-dependent ubiquitylation at DNA damage sites. *EMBO J* **25**, 2178-88.

Pomerance, M., Multon, M. C., Parker, F., Venot, C., Blondeau, J. P., Tocque, B. and Schweighoffer, F. (1998). Grb2 interaction with MEK-kinase 1 is involved in regulation of Jun-kinase activities in response to epidermal growth factor. *J Biol Chem* **273**, 24301-4.

Quintrell, N., Lebo, R., Varmus, H., Bishop, J. M., Pettenati, M. J., Le Beau, M. M., Diaz, M. O. and Rowley, J. D. (1987). Identification of a human gene (HCK) that encodes a protein-tyrosine kinase and is expressed in hemopoietic cells. *Mol Cell Biol* **7**, 2267-75.

Rao, V. N., Shao, N., Ahmad, M. and Reddy, E. S. (1996). Antisense RNA to the putative tumor suppressor gene BRCA1 transforms mouse fibroblasts. *Oncogene* **12**, 523-8.

Rice, J. C., Massey-Brown, K. S. and Futscher, B. W. (1998). Aberrant methylation of the BRCA1 CpG island promoter is associated with decreased BRCA1 mRNA in sporadic breast cancer cells. *Oncogene* **17**, 1807-12.

Rosen, E. M., Fan, S., Pestell, R. G. and Goldberg, I. D. (2003). BRCA1 gene in breast cancer. *J Cell Physiol* **196**, 19-41.

Ruffner, H., Jiang, W., Craig, A. G., Hunter, T. and Verma, I. M. (1999). BRCA1 is phosphorylated at serine 1497 in vivo at a cyclin-dependent kinase 2 phosphorylation site. *Mol Cell Biol* **19**, 4843-54.

Sagan, D., Eckardt-Schupp, F. and Eichholtz-Wirth, H. (2008). Reduced expression of SRC family kinases decreases PI3K activity in NBS1-/- lymphoblasts. *Biochem Biophys Res Commun* **377**, 181-6.

Satterwhite, D. J., Matsunami, N. and White, R. L. (2000). TGF-beta1 inhibits BRCA1 expression through a pathway that requires pRb. *Biochem Biophys Res Commun* **276**, 686-92.

Saunus, J. M., Edwards, S. L., French, J. D., Smart, C. E. and Brown, M. A. (2007). Regulation of BRCA1 messenger RNA stability in human epithelial cell lines and during cell cycle progression. *FEBS Lett* **581**, 3435-42.

Schlegel, B. P., Jodelka, F. M. and Nunez, R. (2006). BRCA1 promotes induction of ssDNA by ionizing radiation. *Cancer Res* **66**, 5181-9.

Schreiner, S. J., Schiavone, A. P. and Smithgall, T. E. (2002). Activation of STAT3 by the Src family kinase Hck requires a functional SH3 domain. *J Biol Chem* **277**, 45680-7.

Scully, R., Anderson, S. F., Chao, D. M., Wei, W., Ye, L., Young, R. A., Livingston, D. M. and Parvin, J. D. (1997a). BRCA1 is a component of the RNA polymerase II holoenzyme. *Proc Natl Acad Sci U S A* **94**, 5605-10.

Scully, R., Chen, J., Ochs, R. L., Keegan, K., Hoekstra, M., Feunteun, J. and Livingston, D. M. (1997b). Dynamic changes of BRCA1 subnuclear location and phosphorylation state are initiated by DNA damage. *Cell* **90**, 425-35.

Scully, R., Chen, J., Plug, A., Xiao, Y., Weaver, D., Feunteun, J., Ashley, T. and Livingston, D. M. (1997c). Association of BRCA1 with Rad51 in mitotic and meiotic cells. *Cell* **88**, 265-75.

Shao, G., Lilli, D. R., Patterson-Fortin, J., Coleman, K. A., Morrissey, D. E. and Greenberg, R. A. (2009a). The Rap80-BRCC36 de-ubiquitinating enzyme complex antagonizes RNF8-Ubc13-dependent ubiquitination events at DNA double strand breaks. *Proc Natl Acad Sci U S A* **106**, 3166-71.

Shao, G., Patterson-Fortin, J., Messick, T. E., Feng, D., Shanbhag, N., Wang, Y. and Greenberg, R. A. (2009b). MERIT40 controls BRCA1-Rap80 complex integrity and recruitment to DNA double-strand breaks. *Genes Dev* **23**, 740-54.

Shao, N., Chai, Y. L., Shyam, E., Reddy, P. and Rao, V. N. (1996). Induction of apoptosis by the tumor suppressor protein BRCA1. *Oncogene* **13**, 1-7.

Shrivastav, M., De Haro, L. P. and Nickoloff, J. A. (2008). Regulation of DNA double-strand break repair pathway choice. *Cell Res* **18**, 134-47.

Sicheri, F., Moarefi, I. and Kuriyan, J. (1997). Crystal structure of the Src family tyrosine kinase Hck. *Nature* **385**, 602-9.

Signori, E., Bagni, C., Papa, S., Primerano, B., Rinaldi, M., Amaldi, F. and Fazio, V. M. (2001). A somatic mutation in the 5'UTR of BRCA1 gene in sporadic breast cancer causes down-modulation of translation efficiency. *Oncogene* **20**, 4596-600.

Snouwaert, J. N., Gowen, L. C., Latour, A. M., Mohn, A. R., Xiao, A., DiBiase, L. and Koller, B. H. (1999). BRCA1 deficient embryonic stem cells display a decreased homologous recombination frequency and an increased frequency of non-homologous recombination that is corrected by expression of a *brca1* transgene. *Oncogene* **18**, 7900-7.

Sobhian, B., Shao, G., Lilli, D. R., Culhane, A. C., Moreau, L. A., Xia, B., Livingston, D. M. and Greenberg, R. A. (2007). RAP80 targets BRCA1 to specific ubiquitin structures at DNA damage sites. *Science* **316**, 1198-202.

Sorlie, T., Perou, C. M., Tibshirani, R., Aas, T., Geisler, S., Johnsen, H., Hastie, T., Eisen, M. B., van de Rijn, M., Jeffrey, S. S. et al. (2001). Gene expression patterns of breast carcinomas distinguish tumor subclasses with clinical implications. *Proc Natl Acad Sci U S A* **98**, 10869-74.

Sorlie, T., Tibshirani, R., Parker, J., Hastie, T., Marron, J. S., Nobel, A., Deng, S., Johnsen, H., Pesich, R., Geisler, S. et al. (2003). Repeated observation of breast tumor subtypes in independent gene expression data sets. *Proc Natl Acad Sci U S A* **100**, 8418-23.

Starita, L. M. and Parvin, J. D. (2003). The multiple nuclear functions of BRCA1: transcription, ubiquitination and DNA repair. *Curr Opin Cell Biol* **15**, 345-50.

Stenerlow, B., Karlsson, K. H., Cooper, B. and Rydberg, B. (2003). Measurement of prompt DNA double-strand breaks in mammalian cells without including heat-labile sites: results for cells deficient in nonhomologous end joining. *Radiat Res* **159**, 502-10.

Stiff, T., O'Driscoll, M., Rief, N., Iwabuchi, K., Lobrich, M. and Jeggo, P. A. (2004). ATM and DNA-PK function redundantly to phosphorylate H2AX after exposure to ionizing radiation. *Cancer Res* **64**, 2390-6.

Stucki, M., Clapperton, J. A., Mohammad, D., Yaffe, M. B., Smerdon, S. J. and Jackson, S. P. (2005). MDC1 directly binds phosphorylated histone H2AX to regulate cellular responses to DNA double-strand breaks. *Cell* **123**, 1213-26.

Suen, T. C. and Goss, P. E. (2001). Identification of a novel transcriptional repressor element located in the first intron of the human BRCA1 gene. *Oncogene* **20**, 440-50.

Swisher, E. M., Sakai, W., Karlan, B. Y., Wurz, K., Urban, N. and Taniguchi, T. (2008). Secondary BRCA1 mutations in BRCA1-mutated ovarian carcinomas with platinum resistance. *Cancer Res* **68**, 2581-6.

Sy, S. M., Huen, M. S. and Chen, J. (2009). PALB2 is an integral component of the BRCA complex required for homologous recombination repair. *Proc Natl Acad Sci U S A* **106**, 7155-60.

Tang, P., Wang, X., Schiffhauer, L., Wang, J., Bourne, P., Yang, Q., Quinn, A. and Hajdu, S. (2006). Expression patterns of ER-alpha, PR, HER-2/neu, and EGFR in different cell origin subtypes of high grade and non-high grade ductal carcinoma in situ. *Ann Clin Lab Sci* **36**, 137-43.

Thakur, S., Zhang, H. B., Peng, Y., Le, H., Carroll, B., Ward, T., Yao, J., Farid, L. M., Couch, F. J., Wilson, R. B. et al. (1997). Localization of BRCA1 and a splice variant identifies the nuclear localization signal. *Mol Cell Biol* **17**, 444-52.

Thomas, J. E., Smith, M., Tonkinson, J. L., Rubinfeld, B. and Polakis, P. (1997). Induction of phosphorylation on BRCA1 during the cell cycle and after DNA damage. *Cell Growth Differ* **8**, 801-9.

Thompson, L. H. and Schild, D. (2002). Recombinational DNA repair and human disease. *Mutat Res* **509**, 49-78.

Thompson, M. E., Jensen, R. A., Obermiller, P. S., Page, D. L. and Holt, J. T. (1995). Decreased expression of BRCA1 accelerates growth and is often present during sporadic breast cancer progression. *Nat Genet* **9**, 444-50.

Tibbetts, R. S., Cortez, D., Brumbaugh, K. M., Scully, R., Livingston, D., Elledge, S. J. and Abraham, R. T. (2000). Functional interactions between BRCA1 and the checkpoint kinase ATR during genotoxic stress. *Genes Dev* **14**, 2989-3002.

Tomlinson, G. E., Chen, T. T., Stastny, V. A., Virmani, A. K., Spillman, M. A., Tonk, V., Blum, J. L., Schneider, N. R., Wistuba, II, Shay, J. W. et al. (1998). Characterization of a breast cancer cell line derived from a germ-line BRCA1 mutation carrier. *Cancer Res* **58**, 3237-42.

Turner, N. C. and Reis-Filho, J. S. (2006). Basal-like breast cancer and the BRCA1 phenotype. *Oncogene* **25**, 5846-53.

Turner, N. C., Reis-Filho, J. S., Russell, A. M., Springall, R. J., Ryder, K., Steele, D., Savage, K., Gillett, C. E., Schmitt, F. C., Ashworth, A. et al. (2007). BRCA1 dysfunction in sporadic basal-like breast cancer. *Oncogene* **26**, 2126-32.

van Gent, D. C., Hoeijmakers, J. H. and Kanaar, R. (2001). Chromosomal stability and the DNA double-stranded break connection. *Nat Rev Genet* **2**, 196-206.

Vaughn, J. P., Davis, P. L., Jarboe, M. D., Huper, G., Evans, A. C., Wiseman, R. W., Berchuck, A., Iglehart, J. D., Futreal, P. A. and Marks, J. R. (1996). BRCA1 expression is induced before DNA synthesis in both normal and tumor-derived breast cells. *Cell Growth Differ* **7**, 711-5.

- Wang, A., Schneider-Broussard, R., Kumar, A. P., MacLeod, M. C. and Johnson, D. G.** (2000a). Regulation of BRCA1 expression by the Rb-E2F pathway. *J Biol Chem* **275**, 4532-6.
- Wang, B. and Elledge, S. J.** (2007). Ubc13/Rnf8 ubiquitin ligases control foci formation of the Rap80/Abraxas/Brcal/Brc36 complex in response to DNA damage. *Proc Natl Acad Sci U S A* **104**, 20759-63.
- Wang, B., Hurov, K., Hofmann, K. and Elledge, S. J.** (2009). NBA1, a new player in the Brcal A complex, is required for DNA damage resistance and checkpoint control. *Genes Dev* **23**, 729-39.
- Wang, B., Matsuoka, S., Ballif, B. A., Zhang, D., Smogorzewska, A., Gygi, S. P. and Elledge, S. J.** (2007). Abraxas and RAP80 form a BRCA1 protein complex required for the DNA damage response. *Science* **316**, 1194-8.
- Wang, B., Matsuoka, S., Carpenter, P. B. and Elledge, S. J.** (2002). 53BP1, a mediator of the DNA damage checkpoint. *Science* **298**, 1435-8.
- Wang, H., Shao, N., Ding, Q. M., Cui, J., Reddy, E. S. and Rao, V. N.** (1997). BRCA1 proteins are transported to the nucleus in the absence of serum and splice variants BRCA1a, BRCA1b are tyrosine phosphoproteins that associate with E2F, cyclins and cyclin dependent kinases. *Oncogene* **15**, 143-57.
- Wang, Q., Zhang, H., Kajino, K. and Greene, M. I.** (1998). BRCA1 binds c-Myc and inhibits its transcriptional and transforming activity in cells. *Oncogene* **17**, 1939-48.
- Wang, W.** (2007). Emergence of a DNA-damage response network consisting of Fanconi anaemia and BRCA proteins. *Nat Rev Genet* **8**, 735-48.

Wang, Y., Cortez, D., Yazdi, P., Neff, N., Elledge, S. J. and Qin, J. (2000b). BASC, a super complex of BRCA1-associated proteins involved in the recognition and repair of aberrant DNA structures. *Genes Dev* **14**, 927-39.

Wardrop, S. L. and Brown, M. A. (2005). Identification of two evolutionarily conserved and functional regulatory elements in intron 2 of the human BRCA1 gene. *Genomics* **86**, 316-28.

Weber, B. L., Abel, K. J., Brody, L. C., Flejter, W. L., Chandrasekharappa, S. C., Couch, F. J., Merajver, S. D. and Collins, F. S. (1994). Familial breast cancer. Approaching the isolation of a susceptibility gene. *Cancer* **74**, 1013-20.

Weinberg, R. A. (1995). The retinoblastoma protein and cell cycle control. *Cell* **81**, 323-30.

Weischer, M., Bojesen, S. E., Tybjaerg-Hansen, A., Axelsson, C. K. and Nordestgaard, B. G. (2007). Increased risk of breast cancer associated with CHEK2*1100delC. *J Clin Oncol* **25**, 57-63.

Welsh, P. L., Owens, K. N. and King, M. C. (2000). Insights into the functions of BRCA1 and BRCA2. *Trends Genet* **16**, 69-74.

Wilson, C. A., Ramos, L., Villasenor, M. R., Anders, K. H., Press, M. F., Clarke, K., Karlan, B., Chen, J. J., Scully, R., Livingston, D. et al. (1999). Localization of human BRCA1 and its loss in high-grade, non-inherited breast carcinomas. *Nat Genet* **21**, 236-40.

Wu, L. C., Wang, Z. W., Tsan, J. T., Spillman, M. A., Phung, A., Xu, X. L., Yang, M. C., Hwang, L. Y., Bowcock, A. M. and Baer, R. (1996). Identification of a RING protein that can interact in vivo with the BRCA1 gene product. *Nat Genet* **14**, 430-40.

Xu, B., Kim, S. and Kastan, M. B. (2001). Involvement of Brca1 in S-phase and G(2)-phase checkpoints after ionizing irradiation. *Mol Cell Biol* **21**, 3445-50.

- Xu, B., O'Donnell, A. H., Kim, S. T. and Kastan, M. B.** (2002). Phosphorylation of serine 1387 in Brca1 is specifically required for the Atm-mediated S-phase checkpoint after ionizing irradiation. *Cancer Res* **62**, 4588-91.
- Xu, C. F., Brown, M. A., Chambers, J. A., Griffiths, B., Nicolai, H. and Solomon, E.** (1995). Distinct transcription start sites generate two forms of BRCA1 mRNA. *Hum Mol Genet* **4**, 2259-64.
- Xu, C. F., Chambers, J. A. and Solomon, E.** (1997). Complex regulation of the BRCA1 gene. *J Biol Chem* **272**, 20994-7.
- Xu, C. F. and Solomon, E.** (1996). Mutations of the BRCA1 gene in human cancer. *Semin Cancer Biol* **7**, 33-40.
- Xu, X., Wagner, K. U., Larson, D., Weaver, Z., Li, C., Ried, T., Hennighausen, L., Wynshaw-Boris, A. and Deng, C. X.** (1999). Conditional mutation of Brca1 in mammary epithelial cells results in blunted ductal morphogenesis and tumour formation. *Nat Genet* **22**, 37-43.
- Yan, J., Kim, Y. S., Yang, X. P., Li, L. P., Liao, G., Xia, F. and Jetten, A. M.** (2007). The ubiquitin-interacting motif containing protein RAP80 interacts with BRCA1 and functions in DNA damage repair response. *Cancer Res* **67**, 6647-56.
- Yan, Y., Black, C. P., Cao, P. T., Haferbier, J. L., Kolb, R. H., Spieker, R. S., Ristow, A. M. and Cowan, K. H.** (2008). Gamma-irradiation-induced DNA damage checkpoint activation involves feedback regulation between extracellular signal-regulated kinase 1/2 and BRCA1. *Cancer Res* **68**, 5113-21.

Yang, Q., Sakurai, T., Mori, I., Yoshimura, G., Nakamura, M., Nakamura, Y., Suzuma, T., Tamaki, T., Umemura, T. and Kakudo, K. (2001). Prognostic significance of BRCA1 expression in Japanese sporadic breast carcinomas. *Cancer* **92**, 54-60.

Yarden, R. I. and Brody, L. C. (1999). BRCA1 interacts with components of the histone deacetylase complex. *Proc Natl Acad Sci U S A* **96**, 4983-8.

Yarden, R. I., Pardo-Reoyo, S., Sgagias, M., Cowan, K. H. and Brody, L. C. (2002). BRCA1 regulates the G2/M checkpoint by activating Chk1 kinase upon DNA damage. *Nat Genet* **30**, 285-9.

Yi, R., Qin, Y., Macara, I. G. and Cullen, B. R. (2003). Exportin-5 mediates the nuclear export of pre-microRNAs and short hairpin RNAs. *Genes Dev* **17**, 3011-6.

Yu, X., Wu, L. C., Bowcock, A. M., Aronheim, A. and Baer, R. (1998). The C-terminal (BRCT) domains of BRCA1 interact in vivo with CtIP, a protein implicated in the CtBP pathway of transcriptional repression. *J Biol Chem* **273**, 25388-92.

Yun, M. H. and Hiom, K. (2009). CtIP-BRCA1 modulates the choice of DNA double-strand-break repair pathway throughout the cell cycle. *Nature* **459**, 460-3.

Zhang, F., Ma, J., Wu, J., Ye, L., Cai, H., Xia, B. and Yu, X. (2009). PALB2 links BRCA1 and BRCA2 in the DNA-damage response. *Curr Biol* **19**, 524-9.

Zhang, J., Willers, H., Feng, Z., Ghosh, J. C., Kim, S., Weaver, D. T., Chung, J. H., Powell, S. N. and Xia, F. (2004). Chk2 phosphorylation of BRCA1 regulates DNA double-strand break repair. *Mol Cell Biol* **24**, 708-18.

Zheng, L., Pan, H., Li, S., Flesken-Nikitin, A., Chen, P. L., Boyer, T. G. and Lee, W. H. (2000). Sequence-specific transcriptional corepressor function for BRCA1 through a novel zinc finger protein, ZBRK1. *Mol Cell* **6**, 757-68.

- Zhong, Q., Boyer, T. G., Chen, P. L. and Lee, W. H.** (2002). Deficient nonhomologous end-joining activity in cell-free extracts from Brca1-null fibroblasts. *Cancer Res* **62**, 3966-70.
- Zhong, Q., Chen, C. F., Li, S., Chen, Y., Wang, C. C., Xiao, J., Chen, P. L., Sharp, Z. D. and Lee, W. H.** (1999). Association of BRCA1 with the hRad50-hMre11-p95 complex and the DNA damage response. *Science* **285**, 747-50.
- Zhou, B. B. and Elledge, S. J.** (2000). The DNA damage response: putting checkpoints in perspective. *Nature* **408**, 433-9.
- Zhuang, J., Zhang, J., Willers, H., Wang, H., Chung, J. H., van Gent, D. C., Hallahan, D. E., Powell, S. N. and Xia, F.** (2006). Checkpoint kinase 2-mediated phosphorylation of BRCA1 regulates the fidelity of nonhomologous end-joining. *Cancer Res* **66**, 1401-8.
- Ziegler, S. F., Marth, J. D., Lewis, D. B. and Perlmutter, R. M.** (1987). Novel protein-tyrosine kinase gene (hck) preferentially expressed in cells of hematopoietic origin. *Mol Cell Biol* **7**, 2276-85.

CURRICULUM VITAE

WENJIA WANG

4803 HORTON ST
MISSION, KS 66202-1729
(316) 461-5428
wwang@kumc.edu

EDUCATION

M.D. Medicine and Surgery In Progress
School of Medicine
University of Kansas Medical Center
Kansas City, KS

USMLE Step 1 completed June 13, 2006

Ph.D. Pathology and Oncology 1/06 – 7/10
Department of Pathology & Laboratory Medicine
University of Kansas Medical Center
Kansas City, KS

Dissertation: *Identification and Characterization of Novel Kinases that Regulate BRCA1 Expression and Function*

Mentor: Roy A. Jensen, M.D.
Professor, Pathology & Laboratory Medicine
Director, University of Kansas Cancer Center
University of Kansas Medical Center

Ph.D. Comprehensive Exam completed April 21, 2008

Ph.D. Defense completed July 15, 2010

B.S. Biochemistry 8/00 – 8/04
Department of Molecular Biosciences
University of Kansas
Lawrence, KS

Thesis: *Determination of Diphenhydramine Delivery to the Skin and Muscle Following Intravenous Injection Utilizing In Vivo Microdialysis*

Mentor: Craig E. Lunte, Ph.D.
Professor, Chemistry
University of Kansas

CURRENT RESEARCH INTERESTS

Identifying novel kinases involved in BRCA1-associated breast cancers.

Defining the role of identified kinases in the regulation of BRCA1 expression and function.

Developing targeted therapy against newly established molecular targets in sporadic breast cancers.

RESEARCH EXPERIENCE

Graduate Research 1/06 – Present
Laboratory of Roy A. Jensen, M.D.
Department of Pathology & Laboratory Medicine
University of Kansas Medical Center
Kansas City, KS

Research Experience 6/04 – 12/05
Laboratory of Linheng Li, Ph.D.
Investigator & Adjunct Faculty
Stowers Institute for Medical Research
Kansas City, MO

Undergraduate Research 1/02 – 5/04
Laboratory of Craig. E. Lunte, Ph.D.
Department of Chemistry
University of Kansas
Lawrence, KS

TEACHING EXPERIENCE

Facilitator Clinical Skills Small Groups* 10/06 – Present
School of Medicine
University of Kansas Medical Center
Kansas City, KS

*Select sessions: Drug Allergy
Gastroenteritis
Sepsis

Tutor School of Medicine Tutoring Program 8/06 – 5/07
University of Kansas School of Medicine
Kansas City, KS

Facilitator Mary Dunkin's Best MedPrep 1/05 – Present
MCAT Preparation Program
Lawrence, KS

Tutor KUAC Strategic Tutoring Program 8/03 – 5/04
University of Kansas
Lawrence, KS

CLINICAL EXPERIENCE

Clinical Continuity	M.D./Ph.D. Program Mark Cohen, M.D., Ph.D. University of Kansas Medical Center Kansas City, KS	Fall 2008
Preceptorship	Internal Medicine Courtney Rhudy, M.D. University of Kansas Medical Center Kansas City, KS	8/05 – 5/06
Preceptorship	Family Medicine John Bernard, M.D. Cotton O'Neil Clinic Topeka, KS	8/04 – 5/05
Student Physician Social Services	JayDoc Free Clinic Kansas City, KS	8/04 – 5/06

PUBLICATIONS

R.A. Jensen, L.M. Harlan-Williams, **W. Wang**, and S.R. Stecklein: *Basic Cancer Biology and Immunology*. Principles and Practice of Fertility Preservation, Donnez and Kim, Cambridge University Press, 2011 (In Press).

POSTERS AND PRESENTATIONS

W. Wang, L.M. Harlan-Williams, and R.A. Jensen: *Identification and characterization of novel kinases that regulate BRCA1 expression and function*.

Annual Meeting

American Association for Cancer Research

Washington, D.C.

April, 2010

S.R. Stecklein, L.M. Harlan-Williams, **W. Wang**, J.D. Eskew, V. Chaguturu, and R.A. Jensen: *Inhibition of Hsp90 induces BRCA1 degradation and hypersensitivity to ionizing radiation*.

Annual Meeting

American Association for Cancer Research

Washington, D.C.

April, 2010

L.M. Harlan-Williams, J. Overton, S.R. Stecklein, **W. Wang**, and R.A. Jensen: *Identification and characterization of small molecule activators of BRCA1 Expression*.
Annual Meeting
American Association for Cancer Research
Washington, D.C.
April, 2010

W. Wang, L.M. Harlan-Williams, and R.A. Jensen: *Identification and Characterization of HCK on BRCA1 Expression and Function*.
Student Research Forum
University of Kansas Medical Center
Kansas City, KS
April, 2010

W. Wang, L.M. Harlan-Williams, and R.A. Jensen: *Identification and Characterization of Novel Kinases that Regulate BRCA1 Expression and Function*.
Cancer Research Symposium
The University of Kansas Cancer Center
Kansas City, KS
November, 2009

L.M. Harlan-Williams, J. Overton, S.R. Stecklein, **W. Wang**, and R.A. Jensen: *Small Molecule Activators of BRCA1 Expression*.
Cancer Research Symposium
The University of Kansas Cancer Center
Kansas City, KS
November, 2009

M. Ortega, J. Jacob, **W. Wang**, Y. Feng, J. Vivian, and P. Fields: *Histone Methylation via DOT1L Recruits BRCA1 to Sites of DNA Damage*.
Postdoc Research Forum
University of Kansas Medical Center
Kansas City, KS
April, 2009

W. Wang, L.M. Harlan-Williams, and R.A. Jensen: *Analysis of Kinases on BRCA1 Expression and Function*.
Annual Meeting
American Association for Cancer Research
Denver, CO
April, 2009

W. Wang, L.M. Harlan-Williams, and R.A. Jensen: *Analysis of Kinases on BRCA1 Expression and Function.*

Cancer Research Symposium
Kansas Masonic Cancer Research Institute
University of Kansas Medical Center
Kansas City, KS
November, 2008

W. Wang, L.M. Harlan-Williams, and R.A. Jensen: *Functional Approach to Identifying Regulatory Kinases of BRCA1 Expression and Function.*

Student Research Forum
University of Kansas Medical Center
Kansas City, KS
April, 2008

W. Wang, L.M. Harlan-Williams, and R.A. Jensen: *Functional Approach to Understanding the Regulation of BRCA1 Expression.*

Cancer Research Symposium
Kansas Masonic Cancer Research Institute
University of Kansas Medical Center
Kansas City, KS
December, 2007

W. Wang, L.M. Harlan-Williams, and R.A. Jensen: *Developing a functional assay to understand the regulatory mechanism of BRCA1 expression.*

Student Research Forum
University of Kansas Medical Center
Kansas City, KS
April, 2007

“Determination of Diphenhydramine Delivery to the Dermis and Muscle Following Intravenous Injection Utilizing *In Vivo* Microdialysis”

W. Wang and C.E. Lunte
Undergraduate Research Presentation
Honors Program
University of Kansas
Lawrence, KS, May 2004

7th Annual Undergraduate Research Symposium
University of Kansas
Lawrence, KS, March 2004

K-BRIN Second Annual Student Symposium
Kansas State University
Manhattan, KS, January 2004

1st Kansas IDeA Biomedical Focus Group Symposium
University of Kansas
Lawrence, KS, November 2003

Research Experience for Undergraduates (REU) Summer Program Presentation
University of Kansas
Lawrence, KS, August 2003

6th Annual KU Undergraduate Research Symposium
University of Kansas
Lawrence, KS, March 2003

American Chemical Society (ACS) Undergraduate Symposium
University of Kansas
Lawrence, KS, October 2002

Research Experience for Undergraduates (REU) Summer Program Presentation
University of Kansas
Lawrence, KS, August 2002

LEADERSHIP

Planning Committee	M.D./Ph.D. Student Council Annual Retreat Committee University of Kansas Medical Center Kansas City, KS	8/09 – 7/10
Committee Chair	Student Research Forum Speaker Committee University of Kansas Medical Center Kansas City, KS	8/09 – 4/10
Committee Chair	Student Research Forum Budget Expense Committee University of Kansas Medical Center Kansas City, KS	8/08 – 4/09
Committee Chair	Student Research Forum Program Book Committee University of Kansas Medical Center Kansas City, KS	1/08 – 4/08
Vice President	M.D./Ph.D. Student Council University of Kansas Medical Center Kansas City, KS	6/07 – 5/08

Committee Co-Chair	Student Research Forum Workshop Committee University of Kansas Medical Center Kansas City, KS	8/06 – 4/07
Treasurer	Student Governing Council University of Kansas Medical Center Kansas City, KS	8/06 – 5/07
Treasurer	Asian American Medical Students Association University of Kansas Medical Center Kansas City, KS	8/06 – 5/07
Co-President	Care for Kids University of Kansas Medical Center Kansas City, KS	8/05 – 5/06
Co-Chair	KUMC Street Fair University of Kansas Medical Center Kansas City, KS	8/05 – 5/06
Representative	Honored Council Board Director of Outreach University of Kansas Lawrence, KS	8/03 – 5/04
Secretary	Golden Key International Honor Society University of Kansas Lawrence, KS	8/03 – 5/04
Representative	Selections Committee for General Chemistry Lab Director University of Kansas Lawrence, KS	Fall 2002
Representative	Student Senate University Affairs Committee University of Kansas Lawrence, KS	8/00 – 5/01

HONORS AND AWARDS

Student Travel Award	University of Kansas Cancer Center University of Kansas Medical Center Kansas City, KS	2008
----------------------	--	------

Student Research Fellowship	University of Kansas Cancer Center University of Kansas Medical Center Kansas City, KS	2008
Excellence in Research Award	University of Kansas Cancer Center University of Kansas Medical Center Kansas City, KS	2007
Max Barlow Book Award for Physical Chemistry	University of Kansas Lawrence, KS	2004
College of Liberal Arts and Sciences Merit Scholarship	University of Kansas Lawrence, KS	2003
Lance S. Foster Outstanding Junior in Biology Award	University of Kansas Lawrence, KS	2003
KU Undergraduate Research Award	University of Kansas Lawrence, KS	2003
Kansas Biomedical Research Infrastructure Network Scholarship	University of Kansas Lawrence, KS	2003
Golden Key International Honor Society	University of Kansas Lawrence, KS	2002 – 2004
University Honors Program	University of Kansas Lawrence, KS	2000 – 2004
Dean's Honor Roll	University of Kansas Lawrence, KS	2000 – 2004
Watkins-Berger Scholar	University of Kansas Lawrence, KS	2000 – 2004

S E R V I C E

Volunteer	KUMC Street Fair University of Kansas Medical Center Kansas City, KS	April 2009
Volunteer	Brain Discovery Fair Society for Neuroscience KC Chapter University of Kansas Medical Center Kansas City, KS	March 2009

YouthFriends E-mentor	Wyandotte High School Kansas City, KS	Fall 2008
Volunteer	KUMC Street Fair University of Kansas Medical Center Kansas City, KS	April 2008
Volunteer	KUMC Street Fair University of Kansas Medical Center Kansas City, KS	April 2007
Volunteer (Moderator)	Student Research Forum University of Kansas Medical Center Kansas City, KS	April 2007
Volunteer (Photography)	Student Research Forum University of Kansas Medical Center Kansas City, KS	April 2006
YouthFriends E-mentor	Bonner Springs High School Bonner Springs, KS	10/05 – present
Volunteer	KUMC Street Fair University of Kansas Medical Center Kansas City, KS	April 2005
Student Physician Social Services	JayDoc Free Clinic Kansas City, KS	8/04 – 5/06
YouthFriends Tutor	Rosedale Middle School Kansas City, KS	8/04 – 5/05
Volunteer	KUMC Kids University of Kansas Medical Center Kansas City, KS	8/04 – 5/05

PROFESSIONAL AFFILIATIONS

American Association for Cancer Research
American Medical Association
American Medical Student Association
American Physician Scientist Association
American College of Physicians
Kansas Medical Society